UNCOVERING ATP INTERACTORS AND SIGNALING MECHANISMS IN INFLAMMATION AND WOUND HEALING

By

Mark Joseph Jelcic

A Dissertation

Presented to the Faculty of the Louis V. Gerstner, Jr.

Graduate School of Biomedical Sciences,

Memorial Sloan Kettering Cancer Center

in Partial Fulfillment of the Requirements for the Degree of

Doctor of Philosophy

New York, NY

May, 2020

Philipp Niethammer, PhD
Dissertation Mentor

Date

For Mom, Dad, Greg, Alex, and Isabella

ABSTRACT

ATP is an important energy metabolite and allosteric signal in health and disease. ATP-interacting signaling proteins, such as P2 receptors, control inflammation, cell death and migration, and wound healing. However, identification of novel non-catalytic ATP-binding sites in proteins remains challenging, and our current inventory of ATP-controlled pathways is likely incomplete. Here, we develop and verify *mipATP* as a minimally invasive photoaffinity probe for ATP-interacting proteins. Unlike previous ATP baits, the compact N^6 functionalization of mipATP enables efficient target enrichment by UV-crosslinking and subsequent conjugation to reporter tags by “click” chemistry. The additions are sterically minimal, allowing mipATP to completely retain the calcium signaling responses of native ATP *in vitro* and *in vivo*. In three orthogonal proteomic screens, mipATP specifically enriched for known nucleotide binders in A549 cell membrane fractions. In addition, it robustly retrieved previously unknown, putative ATP interactors, such as the FAS receptor, CD44, and various membrane transporters of the SLC family. Thus, mipATP is a promising new tool to identify allosteric ATP sites in the proteome.

Injury-induced dysfunction of epithelial barriers in zebrafish larvae leads to a drop in interstitial osmotic pressure that stimulates non-lytic ATP release at injury sites. Extracellular ATP then initiates rapid wound closure through activation of basal epithelial cell migration through an unclear mechanism. Here, we evaluate the role of known ATP signaling mechanisms in zebrafish wound closure using intravital fluorescence microscopy. Comprehensive functional genetic screening

and pharmacological profiling do not make a strong case for a characterized P2 receptor subtype as the essential mediator of basal epithelial cell migration, suggesting the existence of a yet to be identified ATP receptor. MipATP activates the unidentified receptor, indicating that future chemical proteomic profiling of zebrafish cell membranes may uncover the receptor of interest.

Besides the epithelium, it is unclear whether additional tissues detect damage by sensing osmotically secreted ATP in zebrafish. Using intravital fluorescence microscopy we find that osmotic cues from the environment initiate rapid vasodilation near injury sites through G protein-coupled receptor (GPCR) stimulated nitric oxide (NO) signaling. Interstitial ATP is able to rescue vasodilation through extracellular hydrolysis and subsequent activation of the adenosine A_{2B} receptor (Adora2b) in the absence of an osmotic gradient. A_{2B} genetic disruption did not perturb osmotically triggered vasodilation, suggesting that non-lytic ATP secretion is not required or is coupled with other osmotically triggered signals to redundantly regulate vascular tone upon injury.

BIOGRAPHICAL SKETCH

Mark was born to Tereza and Vitorino Jelcic on December 16th, 1986 in New York, NY. Shortly before he was born, Mark's family moved to Little Neck, NY where he would spend his childhood. Mark graduated from Great Neck South High School in 2005 and soon after moved to Boston, MA to attend Boston University (BU). In 2007, Mark transferred to New York University (NYU) where he eventually graduated with a Bachelor of Arts in Biochemistry in 2009. While at NYU, Mark began his scientific training in the laboratory of Dr. Jane Carlton, PhD. During his time in the Carlton lab, Mark assisted Dr. Shehre-Banoo Malik, PhD in investigating new genetic markers to improve phylogenetic resolution of parasitic parabasalids and their relatives. After graduating, Mark took a research technician position in the lab of Dr. Brian Dynlacht, PhD at the NYU Langone Medical Center (NYULMC). At NYULMC, Mark investigated the role of the E3 ubiquitin ligase RNF11 in transforming growth factor β (TGFβ) signaling and the regulation of the atypical Mitogen-activated protein kinase (MAPK) ERK3 under the guidance of Dr. Irma Sánchez. In 2013, Mark joined the Louis V. Gerstner Jr. Graduate School of Biomedical Sciences at Memorial Sloan Kettering Cancer Center. In 2014, Mark began his doctoral training under the mentorship of Dr. Philipp Niethammer.

ACKNOWLEDGEMENTS

First, I want to thank my mentor Dr. Philipp Niethammer for his support throughout my PhD and for providing me the freedom to explore my interests and take responsibility of my projects. Our conversations have greatly assisted in my development to think critically and creatively about science.

I want to thank all the past and present members of the Niethammer lab for their help and comments throughout the years. I want to especially thank Dr. Balázs Enyedi and Dr. Will Gault for their mentorship and support during my first two years in the lab. Also, a special thank you to Dr. King Lam Hui for his help in developing the tools to investigate and analyze calcium signals in cells and zebrafish larvae. Thank you to Dr. Gary Gerlach, Dr. Cong Huang, Dr. Michelina Stoddard, Zhouyang (Joe) Shen, Dr. Yanan Ma, and Anushka Katikaneni for all our insightful conversations on science and for making the lab a great place to work.

Thank you to Dr. Minkui Luo, Dr. Ke Wang, and Dr. Xiaochuan Cai for synthesizing the ATP probe (mipATP) that made this work possible. Additional thanks to all the past and present members of the Luo lab for their technical advice.

I want to express my gratitude to the members of my PhD committee, Dr. Richard White, Dr. Yueming Li, and Dr. Alan Hall for their excellent critical advice throughout my PhD. Thank you to all the past and present members of the White lab for providing reagents and protocols throughout the years.

Thank you to my classmates Ivan Cohen, Hannah Wise, Yun-Han (Hannah) Huang, Brian Joseph, James Keith, Michael Langberg, Brandon Nemieboka,

Grant Robinson, Brian Santich, Ryan Smith, George Vaisey, and Zeda Zhang for their friendship throughout these past years.

I would like to thank all the past and present members of the GSK graduate school particularly Dr. Ken Marians and Dr. Mike Overholtzer. They created a unique and inspirational environment that made all of this possible.

Thank you to my previous mentors, Dr. Burt Goldberg, Dr. Jane Carlton, Dr. Brian Dynlacht, and Dr. Irma Sánchez for their guidance and support throughout the years. Their patience, belief in my capabilities, and love of science provided me with the confidence and experience I needed to pursue doctoral training.

Lastly, I would like to thank my family for their unconditional love and support throughout my doctoral training. I could not and would not have done this without them.

TABLE OF CONTENTS

LIST OF TABLES

Supplementary Tables

LIST OF FIGURES

LIST OF ABBREVIATIONS

5'-FSBA: 5'-*p*-fluorosulfonylbenzoyl adenosine

$A_{1,2A,2B,3}$: adenosine receptor $A_{1,2A,2B,3}$

AA: arachidonic acid

ABPP: Activity based protein profiling

ADP: adenosine 5'-diphosphate

AdoR: N^6-biotinylated-8-azido-adenosine probe

AKT-PH: AKT-pleckstrin homology domain

AMP: adenosine 5'-monophosphate

AMPK: AMP-activated protein kinase

AMP-PNP: β-γ-Imidoadenosine 5'-triphosphate

AP: alkaline phosphatase

ATP: adenosine 5'-triphosphate

ATPγS: adenosine-5'-O-(3-thio-triphosphate)

CBS: cystathionine-β-synthase

CD: cluster of differentiation

CD44: CD44 antigen

CD73: ecto-5'-nucleotidase

cGMP: cyclic guanosine monophosphate

cPLA2: cytosolic phospholipase A_2

CRISPR: Clustered regularly interspaced short palindromic repeats

DAMP: damage-associated molecular pattern

DORN1: Does not Respond to Nucleotides 1

Dpf: days post fertilization

E3: zebrafish embryo medium

EC: endothelial cell

EGFR: epidermal growth factor receptor

E-NPP: ecto-nucleotide pyrophosphatase/phosphodiesterase phosphatases

E-NTPDases: ecto-nucleoside triphosphate diphosphohydrolases

FAS: Fas receptor; tumor necrosis factor receptor superfamily member 6

$G_{i,q,s}$: G protein alpha subunit i, q, or s

GO: Gene Ontology

GPCR: G protein-coupled receptor

GPI: glycosylphosphatidylinositol

GTP: guanosine 5'-triphosphate

IMPDH: inosine 5'-monophosphate dehydrogenase

KO: knockout

LC-MS/MS: liquid chromatography tandem mass spectrometry

mipATP: minimally invasive photoaffinity ATP

MS: mass spectrometry

NAD: nicotinamide adenine dinucleotide

NADPH: nicotinamide adenine dinucleotide phosphate

NDP: nucleoside diphosphate

NMP: nucleoside monophosphate

NO: nitric oxide

NOS: nitric oxide synthase

NTP: nucleoside triphosphate

NTPase: nucleoside-triphosphatase

$P2Y_{1-14}$: P2Y receptor subtype 1-14

$P2X_{1-7}$: P2X receptor subtype 1-7

PAL: photoaffinity labeling

PFK: phosphofructokinase

PGI_2: prostaglandin I2

P_i: orthophosphate

PIV: particle image velocimetry

PP_i: pyrophosphate

PYG: glycogen phosphorylase

RNP: ribonucleoprotein

SAR: structure activity relationship

SD: standard deviation

SEM: standard error of the mean

sGC: soluble guanylyl cyclase

sgRNA: single guide RNA

SILAC: Stable Isotope Labeling with Amino acids in Cell culture

TAMRA: tetramethylrhodamine

UDP: uridine 5'-diphosphate

UTP: uridine 5'-triphosphate

UV: Ultraviolet

WT: wildtype

CHAPTER 1 Introduction

Adenosine 5'-triphosphate (ATP) is the universal source of free energy in biological systems and has been termed the "energy currency" of the cell. The energy harvested from ATP is critical for all life including humans who typically consume ~40 kg (88 lbs.) of ATP in 24 hours (Berg et al., 2007). The ATP nucleotide consists of an adenine, ribose, and triphosphate moiety. The triphosphate contains two high energy phosphoanhydride bonds that liberate a large amount of free energy when ATP is hydrolyzed to adenosine diphosphate (ADP) and orthophosphate (P_i) (~50 kJ mol^{-1} in typical cellular conditions) (Figure 1.1A). This high energy is a result of greater resonance and hydration of ADP and P_i, and electrostatic repulsion within the triphosphate of ATP. Otherwise unfavorable biological reactions are made possible when coupled to ATP hydrolysis. Hydrolysis drives critical cell processes such as motility, transport, and biosynthesis. Besides its pivotal role as an energy source, ATP is a building block for nucleic acids and an important metabolite in cell signaling. In cell signaling mechanisms, ATP can function 1) catalytically as a cosubstrate to drive enzyme-mediated signaling, such as in phosphorylation by protein kinases or 2) non-catalytically as an allosteric regulator or ligand that modulates protein function by binding interactors at regulatory or orthosteric sites, such as in energy sensing proteins like AMP-activated protein kinase (AMPK) and in extracellular signaling through cell surface ATP receptors, respectively (Figure 1.1B).

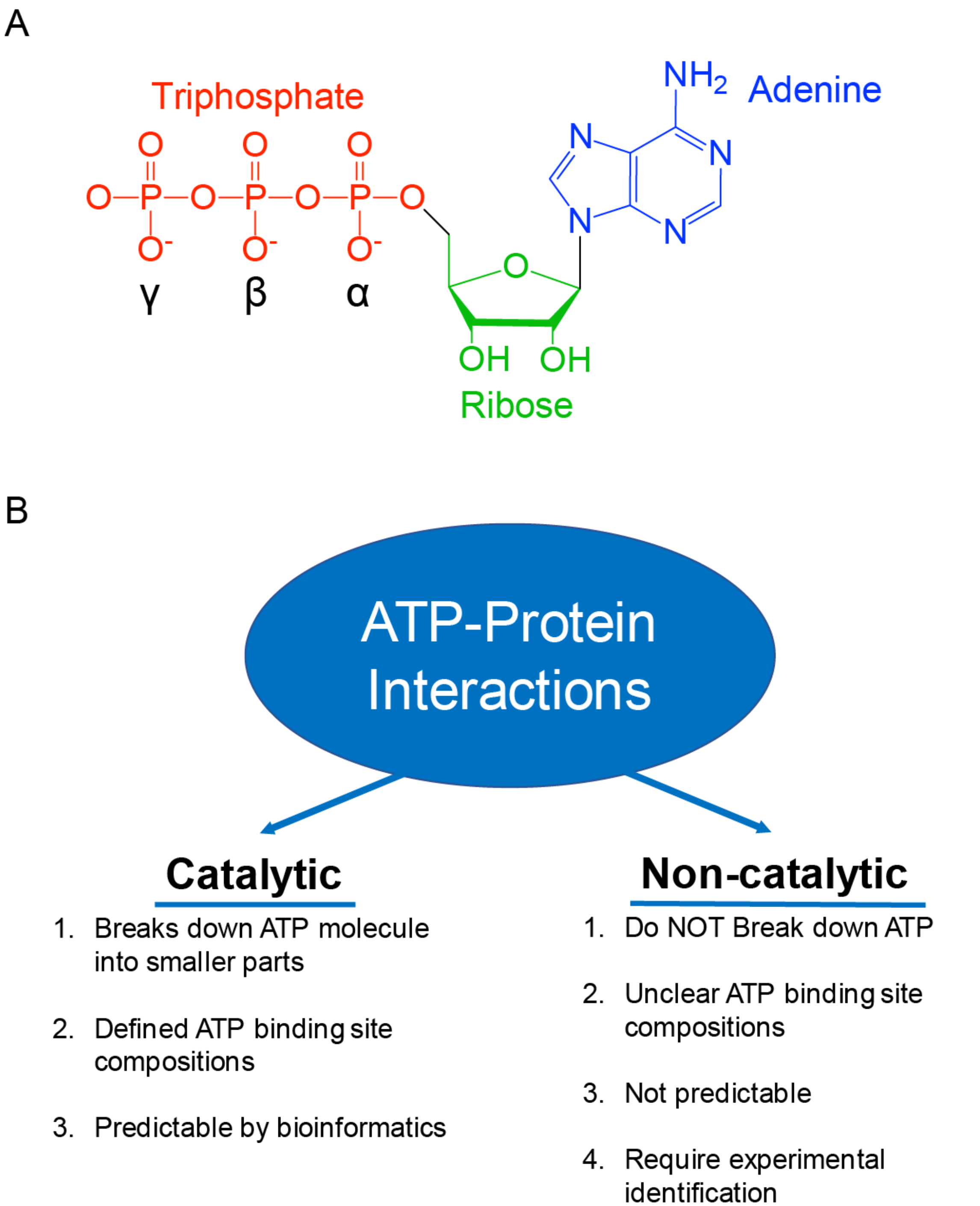

Figure 1.1. Adenosine 5'-triphosphate (ATP) interacts with proteins catalytically or non-catalytically.
(A) The ATP molecule consists of three essential components: the adenine base (blue), ribose sugar (green), and triphosphate chain (red). The triphosphate chain consists of α, β, and γ phosphates (labeled in black). (B) ATP interacts reversibly with proteins in essentially two ways: catalytically as a cosubstrate at the active sites of enzymes or non-catalytically as an allosteric effector or ligand at regulatory and orthosteric sites, respectively.

Catalytic ATP interactors modulate cell signaling through well characterized ATP-binding domains

Kinases are enzymes that catalyze the reversible transfer of a phosphoryl group from a bound cosubstrate ATP molecule to a separate molecular substrate in a process known as phosphorylation. Phosphorylation is the most common means of covalent modification in the cell with ~30% of all eukaryotic proteins being phosphorylated (Berg et al., 2007). The addition of a phosphoryl group modulates protein activity through changes in electrostatic charge which can alter protein structure and binding partners. Protein kinases are the largest enzyme family in mammals, consisting of 518 members which is approximately 1.7% of all human genes (Manning et al., 2002), and are involved in almost all signal transduction pathways. Their dysregulation contributes to the pathogenesis of many illnesses making therapeutic intervention of protein kinases highly sought after with currently 48 FDA approved small molecule inhibitors (Roskoski, 2019).

Kinases and other enzymes that bind and hydrolyze ATP contain highly conserved ATP-binding domains such as the P-loop NTPase fold (Ramakrishnan et al., 2002; Walker et al., 1982), protein kinase glycine rich loop (Taylor and Kornev, 2011), the ATP-grasp fold (Galperin and Koonin, 1997), and the Bergerat fold (Bergerat et al., 1997; Dutta and Inouye, 2000). The P-loop NTPase fold is the most commonly occurring ATP-binding domain in the proteome. In fact, it is the most prevalent of all domains found in most organisms (~18% and ~11% of all genes encoded by bacteria and eukaryotes, respectively) (Koonin et al., 2000). Catalytic ATP binding proteins can typically be identified by computational

prediction methods using sequence and structure homology to these known ATP-binding domains (Chauhan et al., 2009; Hu et al., 2018; Yu et al., 2013)

Non-catalytic ATP interactions regulate cell signaling

While ATP is mostly known for regulating protein function in cell signaling through its activity as the predominant phosphodonor in phosphorylation, it also regulates signaling as a non-substrate effector through non-catalytic protein interactions. Proteins that are functionally regulated through non-catalytic binding to ATP and/or its hydrolysis products (ADP, AMP, and adenosine) are well studied and documented as key regulators of physiological processes such as inflammation and metabolism. The compositions of non-catalytic regulatory ATP-binding sites deviate from the conventional catalytic binding sites, such as the P-Loop NTPase fold. Unlike catalytic ATP-binding sites, sequence and structural characteristics of non-catalytic ATP-binding sites are inconsistent and unclear, such as in the ATP binding sites of cell surface P2 receptors. The vague compositions of these sites prohibit their identification through computational prediction, restricting elucidation only through experimental methods.

Cystathionine-β-synthase (CBS) domain containing proteins

Some non-catalytic regulatory ATP-binding sites are well conserved, most notably the cystathionine-β-synthase (CBS) domain. The CBS domain is a sequence motif of ~60 amino acids in length that exists in proteins in all organisms. CBS domains are found either in pairs or quads with each pair tightly associated

as a dimer and referred to as a Bateman domain (Bateman, 1997). This domain was originally identified in a group of proteins found in the archaebacteria *Methanococcus jannaschii* (Bateman, 1997). Bateman first noted that this same domain exists in the human cystathionine-β-synthase protein in the region where mutations lead to the disease homocystinuria (Kluijtmans et al., 1996). CBS domains were also found to exist in a diversity of proteins in humans including four copies in the γ subunit of AMPK, two copies in inosine 5'-monophosphate dehydrogenase (IMPDH), and two copies on the intracellular c-terminus of members of the CLC family of chloride channels. The function of the CBS domain remained elusive at the time of its discovery; however, its importance in normal protein regulation was highlighted by findings that mutations in the CBS domains of proteins attributed to hereditary diseases. For example, mutations cause retinitis pigmentosa (IMPDH1), hypertrophic cardiomyopathy with Wolff-Parkinson-White syndrome (AMPK), congenital myotonia (CLC1), idiopathic generalized epilepsy (CLC2), Bartter syndrome (CLCKB) and more (Bowne et al., 2002; Gollob et al., 2001; Haug et al., 2003; Konrad et al., 2000; Pusch, 2002).

AMPK is activated by metabolic stresses that result in a fall in cellular ATP concentration and subsequent rise in AMP by directly sensing the AMP/ATP ratio. Kinase activity results in subsequent cellular ATP conservation through the activation of catabolic and downregulation of anabolic pathways (Hardie et al., 2012). AMPK is a heterotrimer composed of a catalytic α subunit and regulatory β and γ subunits. In 2000, it was discovered that the γ subunit isoforms of AMPK function as energy sensors by binding AMP and ATP. This was discovered using

the synthetic AMP analog 8-azido-[^{32}P]AMP to label purified AMPK subunits in the absence and presence of excess unlabeled AMP competitor (Cheung et al., 2000). Following up this work in 2004, Scott and colleagues discovered that the paired CBS domains were the allosteric binding sites for ATP and AMP. This study went on to further show that other proteins such as IMPDH2 and CLC2 bind and are regulated by ATP at the CBS domains (Scott et al., 2004). Thus, CBS domain containing proteins can act as sensors of cellular energy.

Other energy sensing, allosteric ATP binders

Cell homeostasis requires a balance between ATP consumption and generation, making cellular levels of ATP and its hydrolysis products well suited to act as standards for cellular energy status. Besides CBS domain containing proteins like AMPK, cells take advantage of ATP and its hydrolysis products as allosteric modulators of critical metabolic regulators like phosphofructokinase (PFK) and glycogen phosphorylase (PYG). PFK isoforms catalyze the first committing step of glycolysis and PYG catalyzes the breakdown of glycogen to glucose-1-phosphate for glycolysis. PFK and PYG isoforms are inhibited by ATP or activated by AMP at regulatory sites depending on cellular energy status (AMP/ATP ratio). These regulatory nucleotide binding sites do not contain conventional catalytic ATP binding motifs.

Proteins that regulate cell nucleotide pools are functionally modulated through non-catalytic binding of ATP. For example, cytosolic 5'-nucleotidase II (NT5C2) which is a regulator of ATP and GTP pools through catalyzing the

dephosphorylation of 6-hydroxypurine monophosphates is allosterically activated by dATP and ATP during states of high energy through poorly characterized, non-catalytic, ATP binding sites (Walldén et al., 2007).

Cell surface extracellular ATP and nucleotide receptors

Extracellular ATP and other nucleotides activate cell surface "purinergic" receptors in animals and plants. Purinergic ATP receptors consist of families of P2Y G protein-coupled receptors (GPCRs) and P2X ligand-gated cation channels. A detailed description of the mechanisms and physiological relevance of extracellular ATP and nucleotide signaling is provided later in this chapter. Here, I wish to note that purinergic receptors bear no sequence homology to catalytic ATP binding proteins, and their ATP-binding sites do not contain conventional ATP-binding motifs. Mutational analyses have been performed to identify critical amino acids in P2 receptor ATP binding; however, these ATP-binding sites remain mostly unresolved (Erb et al., 1995; Jiang et al., 2000). The first molecular identification of a P2 receptor was done experimentally through expression cloning coupled to Ca^{2+} responses to exogenous ATP as a functional readout (Lustig et al., 1993). Sequence homology methods were applied to further uncover the molecular identities of P2 receptor subtypes after this initial discovery.

Similar to animals, plant cells respond to extracellular nucleotides by increases in cytosolic Ca^{2+}; however, plants do not express proteins with homology to animal extracellular nucleotide receptors. Recently, an ATP receptor in plants (DORN1) was identified through a forward genetic screen of *Arabidopsis* that used

Ca^{2+} signaling as a functional readout (Choi et al., 2014). There is no classic ATP binding motif nor similarity to animal purinergic receptors in the extracellular portion of DORN1 that binds to ATP. Intriguingly, ATP binds DORN1 at an extracellular lectin domain that is typically characterized to bind carbohydrates (Cho et al., 2017).

Recent work in the Niethammer lab described that ATP released at injury sites triggers epithelial wound closure in larval zebrafish (Gault et al., 2014). The ATP receptor that triggers wound closure remains elusive. The pharmacological agonist and antagonist profiles of the receptor do match any known animal purinergic receptor. This may be due to phylogenetic differences in the pharmacologic profiles of these receptors (Abbracchio et al., 2006); however, it is possible that a yet to be identified ATP receptor that, similar to DORN1, bears no sequence identity to known P2 receptors plays a role in zebrafish wound closure.

Biochemical profiling of ATP binding proteins

The fundamental role of ATP in cell function signifies the importance of identifying a complete repertoire of ATP binders in order to understand cell biology. ATP binds to a diverse number of proteins with unrelated structures and sequences (~60 families of proteins interact with ATP) (Kuttner et al., 2003). Importantly, not all identified ATP-binding sites have characteristic motifs and remain structurally unsolved (Traut, 1994). This implies the existence of proteins with yet to be characterized ATP-binding sites for which computational prediction methods, relying on sequence or structural homology, will not be able to identify

(Chauhan et al., 2009; Hu et al., 2018). These uncharacterized ATP-binding sites must first be identified experimentally.

Over the last few decades, a variety of studies have utilized biochemical approaches with functionalized nucleotide baits to identify ATP interactors. These approaches are powerful because they describe direct physical interactions. This section will describe past and current biochemical techniques that have been utilized to identify ATP binding proteins and their limitations.

Affinity chromatography with immobilized ATP

In the 1970's, the drive to characterize enzymes and their properties prompted the development of tools for their isolation. Because ATP and other nucleotides were already known to play roles in enzymatic reactions as substrates, cofactors, and allosteric modulators, enzymologists decided that immobilizing nucleotides to resins such as agarose through covalent interactions would allow for the isolation of enzymes from complex proteomic mixtures by affinity chromatography. Initial attempts immobilized ATP to resins through linkages at different parts of the molecule; however, the majority of nucleotide resins were linked to ATP at the adenine base, specifically at the N^6 and C8 positions (Figure 1.2A) (Barry and O'Carra, 1973; Berglund and Eckstein, 1972; Larsson and Mosbach, 1971; Lindberg and Mosbach, 1975; Trayer et al., 1974). These initial studies with nucleotide immobilized resins successfully purified active enzymes for subsequent characterization. The rapid growth of interest in protein kinases and the insight gained from structural studies indicated that ATP binding at the kinase

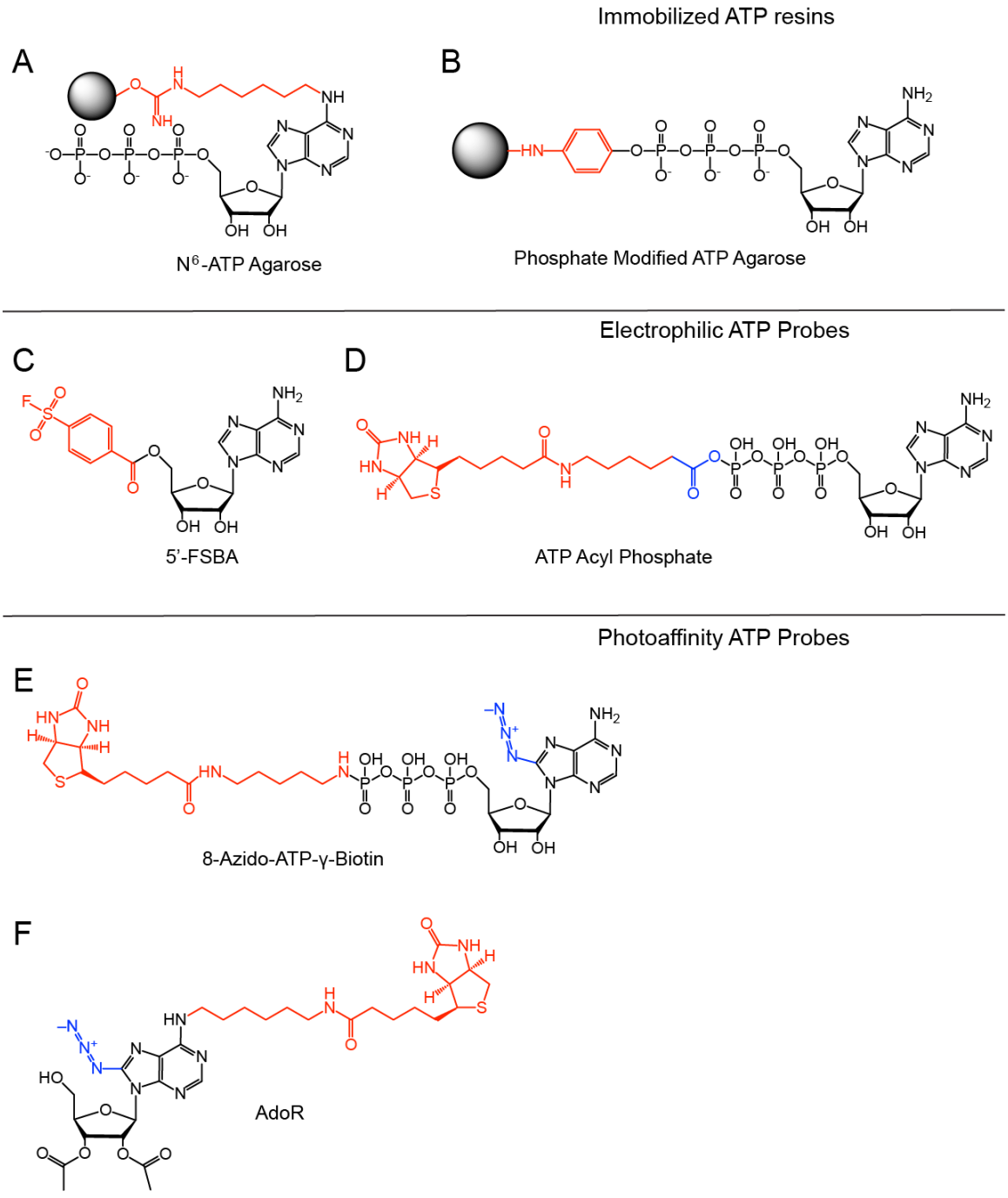

Figure 1.2. Biochemical tools to profile ATP binding proteins in complex proteomes (A, B) ATP resins functionalized at the N^6 amino (A) and γ phosphate (B) used to enrich enzymes by affinity chromatography. Red, additional groups added to parent ATP to link to agarose bead. Grey sphere, agarose bead. (C) 5'-FSBA. Red, functional addition including the electrophilic sulfonyl fluoride moiety. (D) ATP acyl phosphate. Red, biotin addition. Blue, electrophilic acyl phosphate group. (E, F) Photoaffinity ATP probes: 8-Azido-ATP-γ-Biotin (E) and AdoR (Mahajan et al., 2015) (F). Red, biotin addition. Blue, photoreactive azide moiety.

catalytic pocket relied on protein interactions with the N^6 amino of ATP (Hanks et al., 1988; Knighton et al., 1991; Taylor et al., 1992). This prompted the use of ATP resins immobilized at the γ phosphate that would circumvent interference with kinase-ATP binding (Figure 1.2B) (Haystead et al., 1993). In later years, the development and spread of mass spectrometry (MS) based proteomics allowed for the identification of nucleotide binding proteins from complex proteomes using immobilized ATP resins; however, only a few studies have used this approach to profile ATP binders (Graves et al., 2002; Ito et al., 2006; Lee et al., 2013).

Activity based protein profiling (ABPP) of ATP binding proteins

Activity based protein profiling (ABPP) methods are widely used chemical proteomic strategies to identify small molecule targets and screen for enzyme functionality in native proteomes and complex proteomic mixtures. ABPP relies on chemical probes designed to interact with and covalently link to a specific family of proteins. Specificity is achieved by targeting conserved mechanistic or structural features of the protein family of interest. ABPP probes are made of three main components: (1) a target binding parent molecule, (2) a reactive group that covalently links the probe to bound targets, and (3) a reporter tag that allows for downstream target enrichment and subsequent identification by mass spectrometry.

Two classes of probes are generally used: (1) probes with electrophilic reactive groups that react covalently upon interaction with conserved nucleophilic residues in the active site of a family of enzymes and (2) probes that contain a

photoreactive group that covalently labels proximate residues of probe interactors upon UV exposure (also known as photoaffinity labeling (PAL)) (Cravatt et al., 2008). Covalent linkage is advantageous because (1) non-covalent interactions may not survive downstream affinity purification processes which can lead to false negatives, (2) stable covalent interactions allow for harsh purification strategies to remove background false positives, and (3) covalent interactions allow for probes to report on direct physical interactions.

An assortment of reporter tags can be added to ABPP probes including biotin, fluorophores, and terminal alkynes or azides that can be conjugated to biotin or fluorophore reporter tags via click chemistry after covalent linkage to targets.

Functionalized ATP probes have been used to identify ATP interactors from complex proteomic mixtures (Figure 1.2 C-F) (Hanoulle et al., 2006; Mahajan et al., 2015; Patricelli et al., 2007). Typical electrophilic ABPP probes target the active sites of enzymes that form intermediate adducts with target substrates through conserved hypernucleophilic amino acid residues in the catalytic site. For example, the catalytic serine and cysteine of serine and cysteine hydrolases, respectively. Intermediate adducts are not commonly formed during interactions between ATP and catalytic binders. For example, kinases catalyze the direct transfer of a phosphate group to a substrate (Cravatt et al., 2008). Nonetheless, the first ABPP probe used to profile ATP binding proteins was an ATP analog functionalized with an electrophilic group. This electrophilic ATP analog, 5'-*p*-fluorosulfonylbenzoyl adenosine (5'-FSBA), employed a similar but not identical approach to other electrophilic ABPP probes (Figures 1.2C). 5'-FSBA contains a 5' electrophilic

sulfonyl fluoride moiety located in a position analogous to the γ phosphate of unmodified ATP (Colman, 1983). Nucleophilic amino acids in ATP binding sites are capable of forming covalent adducts with 5'-FSBA through elimination of the fluoride upon interaction (Figure 1.3A); however, 5'-FSBA has many drawbacks as a competent ATP ABPP probe. 5'-FSBA does not have a reporter tag for downstream protein identification and, unlike unmodified ATP, is uncharged, subsequently binding nucleotide binding proteins with weak affinity (Cravatt et al., 2008). One study developed a proteomics method using 5'-FSBA to identify ATP binding proteins in Jurkat cell lysates; however, no groups have utilized this method since, most likely due to its complexity and the development of better and easier to use probes such as acyl phosphate ATP probes (Hanoulle et al., 2006; Patricelli et al., 2007).

In 2007, Patricelli and colleagues developed a novel electrophilic acyl phosphate ATP probe in order to screen complex proteomic mixtures for kinase functionality and profile the selectivity of kinase inhibitors (Figure 1.2D) (Patricelli et al., 2007). Structural knowledge of the ATP-binding sites of kinases informed probe development (Zheng et al., 1993). Kinase ATP-binding pockets contain at least one highly conserved lysine residue (with a positively charged ε amino group) that is in close proximity to the β and γ phosphates of a bound ATP molecule. Additionally, ATP's γ phosphate protrudes out of the kinase ATP binding pocket and is solvent accessible, indicating that terminal phosphate additions would not disrupt ATP-kinase binding. Acyl phosphates are known to be particularly reactive with amino groups, such as the ε amino group of a lysine residue and are stable in

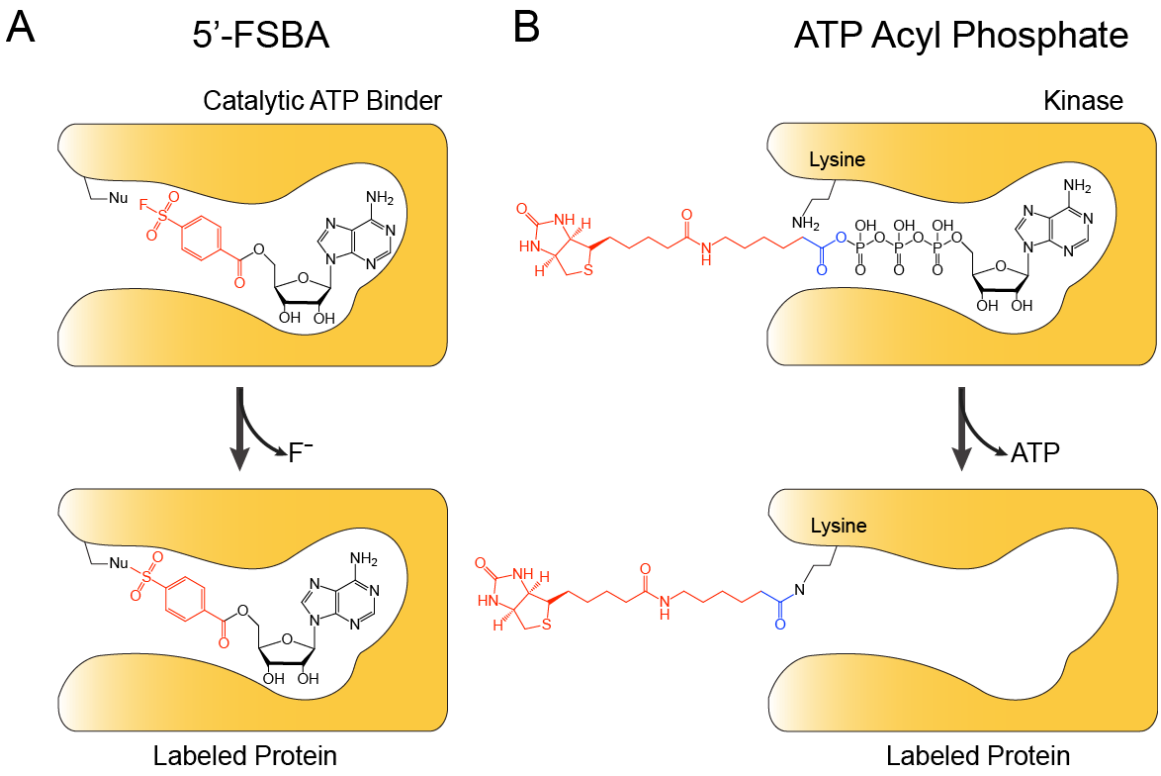

Figure 1.3. Labeling of catalytic ATP binding proteins by electrophilic ATP probes
(A) Mechanism of protein target labeling by 5'-FSBA. A nucleophilic residue in the ATP binding site of a catalytic ATP-binding protein forms a covalent adduct with 5'-FSBA through the elimination of a fluoride. (B) Mechanism of protein target labeling by ATP acyl phosphate probes. A positively charged ε amino group from a highly conserved lysine residue in the catalytic ATP-binding pockets of protein kinases acts as a nucleophile toward the carbonyl carbon of the reactive acyl phosphate group. The biotin moiety is covalently linked to the protein kinase and the ATP scaffold is released by C-O bond cleavage.

aqueous environments. Taking advantage of this structural knowledge, a novel probe containing a biotin reporter tag attached to an acyl phosphate group that is linked to the γ phosphate of an ATP scaffold was produced. The mechanism of labeling is (1) the probe binds kinases through its ATP scaffold, (2) the amine nitrogen of the conserved lysine attacks the carbonyl carbon of the reactive acyl phosphate, and (3) the ATP scaffold is released by C–O bond cleavage (Figure 1.3B). This results in the covalent attachment of the biotin moiety to the kinase lysine residue through an amide bond, allowing for downstream protein identification through streptavidin enrichment and MS analysis. Patricelli and colleagues proved that the acyl phosphate ATP probe was capable of enriching protein kinases through the predicted conserved lysine residues. Additionally, other classes of nucleotide binding proteins were labeled by the probe including other ATPases, GTPases, and nicotinamide adenine dinucleotide (NAD)-binding proteins. Acyl phosphate ATP probes have since become the most popular ABPP method to profile nucleotide binding proteins, particularly kinases. Studies have utilized the probe to profile nucleotide binding proteins in multiple species and profile kinase inhibitor selectivity in native proteomes (Adachi et al., 2014; McAllister et al., 2013; Patricelli et al., 2011; Villamor et al., 2013; Wolfe et al., 2013; Xiao et al., 2013a). Some of these studies were even able to identify novel ATP binding proteins and their ATP binding sites (Adachi et al., 2014; Xiao et al., 2013b)

Acyl phosphate ATP probes provide an excellent method to analyze families of ATP binding proteins; however, the site (γ phosphate) and properties of the

attached biotin-acyl phosphate functional group biases its interaction profile (Mahajan et al., 2015). Limitations come from (1) the dependence on a conserved lysine residue that is in close proximity to and coordinates with the β and γ phosphates of a bound ATP and (2) the 5'-terminal phosphate additions of the reactive acyl phosphate and biotin groups can interfere with binding to proteins with nucleotide binding sites that differ from kinases. Importantly, non-catalytic ATP-binding proteins such as P2 receptors have altered specificities for differentially modified ATP derivatives (Burnstock et al., 1994). There is a need for complementary biochemical approaches utilizing functionalized ATP probes that are not reliant on conventional ATP-binding site compositions and are functionalized at positions other than the γ phosphate in order to obtain a more complete repertoire of ATP-binding proteins.

Photoreactive ATP ABPP probes have also been developed. A photoaffinity ATP derivative functionalized with a photoreactive azido at the C8 and a biotin reporter tag linked to the γ phosphate by a phosphoramide bond (8-azido-ATP-γ-biotin) was used to characterize purified proteins (synaptic vesicle protein 2 (SV2) and SV2-related protein (SVOP)) as adenine nucleotide binders (Yao and Bajjalieh, 2008, 2009) (Figure 1.2E).

A novel photoaffinity adenosine probe (termed AdoR) functionalized solely at the adenine base was developed to screen for nucleotide binding proteins on a proteome-wide scale (Figure 1.2F) (Mahajan et al., 2015). AdoR is functionalized with a biotin reporter tag at the N^6 amino and a photoreactive azide at the C8. The adenine location and photoreactive functionalization avoid the biases introduced

by electrophilic γ-phosphate modified probes. AdoR was capable of enriching for nucleotide binding proteins from whole cell extracts, with 111 out of the top 150 proteins isolated (74%) being nucleotide binding proteins. Enriched nucleotide binding proteins consisted of heat shock proteins, T-complex proteins, and elongation factors. Besides IMPDH2, there does not seem to be an enrichment of non-catalytic allosteric ATP binders by AdoR, including an absence of extracellular nucleotide receptors. Additionally, almost no protein kinases were enriched (1 out of the top 50 enriched proteins). The profile of nucleotide binding proteins enriched by AdoR is most likely explained by the vast abundance of these protein families in the cell. Additionally, the overall lack of protein kinases may be attributed to their selectivity for ATP over adenosine and also the disruption of key intermolecular interactions by perturbation of the adenine base. Structural insights and structure activity relationship (SAR) studies indicate that the N^6 amino is essential for ATP binding in the kinase catalytic pocket and that hydrophobic additions at this position disrupt ATP-kinase binding (Shah et al., 1997; Taylor et al., 1992; Zheng et al., 1993). The large hydrophobic N^6 biotin most likely blocked AdoR interactions with kinases.

Bulky hydrophobic functional additions to small molecules, such as the biotin reporter tag on AdoR, can alter target binding by sterically interfering with physiological protein interactions and/or enabling non-physiological interactions resulting in unfavorable false negative and false positive hits in ABPP profiling. We wished to develop a compact, minimally interfering photoaffinity ATP probe in order to limit the biases inherent with these bulky hydrophobic additions.

Minimally invasive ABPP probes

A competent ABPP photoaffinity probe retains biological activity; therefore, photoreactive and reporter tag additions should minimally modulate physiological protein-probe interactions. Furthermore, functionalized probes should retain cell permeability, thus allowing for target protein profiling within native cell environments (live cells, not cell extracts) (Shi et al., 2011; Su et al., 2013).

Recent photoaffinity labeling strategies have preferentially utilized probes functionalized with (1) a photoreactive alkyl diazirine in combination with (2) a terminal alkyne handle amenable to reporter tag conjugation via click chemistry. These additions are sterically compact, minimally perturb biological activity, and allow for cell permeability while retaining functionality.

The alkyl diazirine, nearly isosteric to a methyl group, is the smallest photoreactive group used in photoaffinity labeling studies (Figure 1.4A). Other than its compact size, alkyl diazirine has ideal properties in comparison to other photoreactive groups such as benzophenone and azide. Upon UV irradiation, diazirine generates a reactive carbene that rapidly forms a covalent bond with a proximal target molecule through insertion into C–C, C–H, O–H, and other X–H (X = heteroatom) bonds (Dubinsky et al., 2012). In the absence of a nearby target the activated carbene is rapidly quenched through reaction with H_2O molecules in aqueous solutions, minimizing nonspecific labeling (Mackinnon and Taunton, 2009). Additionally, alkyl diazirines are stable at room temperature, ambient light,

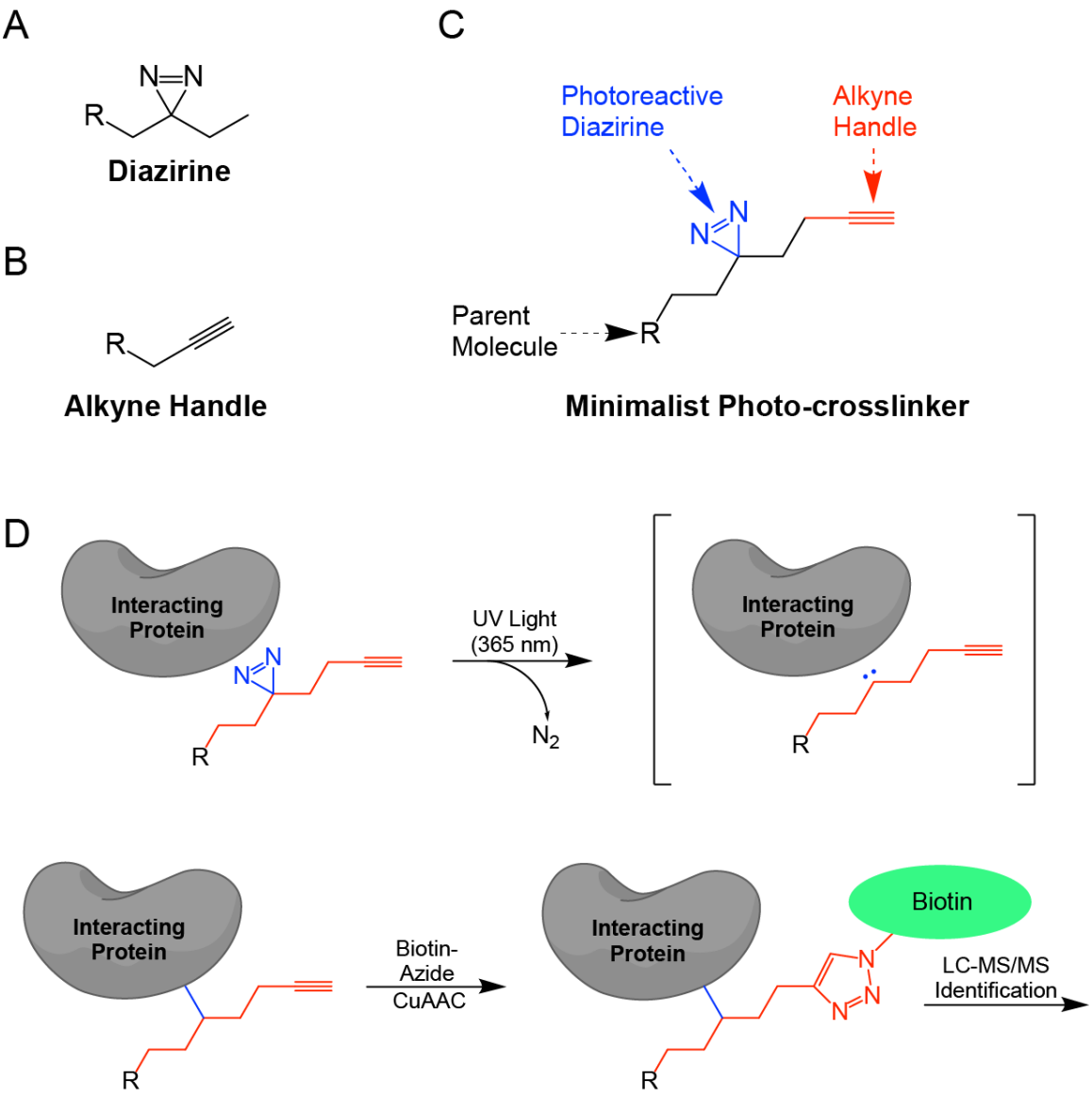

Figure 1.4. Protein profiling with minimally invasive ABPP probes
(A) Molecular structure of photoreactive alkyl diazirine. (B) Molecular structure of a terminal alkyne handle. (C) Molecular structure of a minimalist photo-crosslinker containing both the photoreactive diazirine for covalent linkage to target proteins and alkyne handle which is amenable to azide reporter tag conjugation via Cu(I) catalyzed click chemistry. (D) Mechanism of protein target labeling by a small molecule probe functionalized with a minimalist photo-crosslinker. Step 1: the probe is added to a complex proteomic mixture or onto live cells and incubated for a defined period. Step 2: The sample is irradiated with UV light (365 nm), generating a reactive carbene that rapidly forms a covalent bond with a proximal target molecule or is rapidly quenched through interaction with H_2O molecules. Step 3: an azide containing reporter tag (biotin) is conjugated to probe-protein complexes via Cu(I) catalyzed click chemistry.

both acidic and basic conditions, and are activated at long UV wavelengths (~355 nm) that reduce damage to biological systems (Dubinsky et al., 2012).

A terminal alkyne handle allows for the conjugation to azide containing reporter tags, such as a biotin or fluorophore, via Cu(I) catalyzed click chemistry after the probe has interacted with and covalently linked to targets (Figure 1.4B) (Best, 2009). This avoids the protein–probe interaction perturbations during labeling caused by bulky hydrophobic reporters like biotin. Like alkyl diazirine, terminal alkynes are sterically small and cell permeable. Terminal alkynes (and azides) are not found on endogenous molecules in cells and are biologically inert. They do not specifically interact with biological molecules found in native cells or cell extracts, thus making the click reaction bioorthogonal. Additionally, the 1,2,3-triazole linkage formed between the probe and reporter tag after the click reaction is chemically inert against oxidation, reduction, and hydrolysis under acidic and basic conditions (Haldón et al., 2015).

The combination of alkyl diazirine and terminal alkyne additions for photoaffinity labeling based proteomic profiling was pioneered by the Yao group in 2011 (Shi et al., 2011). Since then, multiple groups have taken advantage of this method to profile binders of endogenous small molecules such as cholesterol (Hulce et al., 2013) and fatty acids (Niphakis et al., 2015), kinase inhibitors (Li et al., 2013; Shi et al., 2012) and other synthetic small molecules (Parker et al., 2017a, 2017b).

In 2013, the Yao group developed a chemical handle that contains both the alkyl diazirine and terminal alkyne groups connected by a short aliphatic chain

(Figure 1.4C) (Li et al., 2013). Termed a “minimalist” clickable photo-crosslinker, this single addition handle functionalizes the parent small molecule as a photoaffinity probe with the minimal amount of structural perturbation (Figure 1.4D). This initial 2013 study successfully utilized kinase inhibitors functionalized with minimalist linkers to profile targets in live cells using proteomics. Other groups have since taken advantage of minimalist photo-crosslinkers to profile targets of small molecules and also in fragment-based ligand discovery (Galmozzi et al., 2018; Gao et al., 2018; Lang et al., 2019; Li et al., 2018; Parker et al., 2017b; Wang et al., 2019). The minimalist photo-crosslinker is even now commercially available through Sigma-Aldrich due to its rise in popularity.

The success of minimalist photo-crosslinkers encourages the extension of this approach to proteomic profiling of other bioactive small molecules. ATP based ABPP probes have been successfully used in profiling ATP and other nucleotide binders. Unfortunately, the current available set of ATP probes are biased towards identifying catalytic ATP binding sites and/or contain bulky hydrophobic additions that can modulate ATP–protein interactions. A novel ATP probe functionalized with a minimalist photo-crosslinker can be a valuable tool to profile allosteric ATP binding proteins that lack classic ATP binding motifs and contain undescribed ATP binding sites.

Extracellular ATP signaling and metabolism

Purinergic signaling mechanisms

Besides its role as the essential metabolite that drives biological processes within cells, ATP also acts as an extracellular ligand in plants and animals. Extracellular purines (ATP, ADP, and adenosine) and pyrimidines (UTP and UDP) are critical signaling molecules in variety of physiological contexts. Biological effects of extracellular nucleosides and nucleotides were first discovered by Drury and Szent-Györgyi in 1929 when they reported that adenosine and other adenine compounds isolated from animal organ extracts slowed heart rate, lowered arterial blood pressure, and dilated blood vessels when injected intravenously into animals (Drury and Szent-Györgyi, 1929). Gillespie followed up this study in 1934 with the first SAR analysis of extracellular adenine nucleotides, showing for the first time that ATP and adenosine have different potencies in eliciting physiological effects such as vasodilation (Gillespie, 1934). In the following decades, countless studies have followed up on these initial reports to demonstrate that extracellular nucleosides and nucleotides are important signaling molecules in a variety of physiological processes such as neurotransmission, muscle contraction, inflammation and immunity, and cardiovascular function (Burnstock, 1972; Burnstock et al., 1970; Chen et al., 2006; Cronstein et al., 1983, 1992; Deaglio et al., 2007; Elliott et al., 2009; Holton, 1959; Holton and Holton, 1954; Ralevic and Burnstock, 1998).

In the 1970's Burnstock presented the "purinergic hypothesis" suggesting that extracellular ATP acts as a neurotransmitter at purine specific receptors in nonadrenergic, noncholinergic (NANC) transmission to smooth muscle in the gut and bladder (Burnstock, 1972; Burnstock et al., 1970). In 1978, Burnstock first

classified two types of purinergic receptors as being specific for adenosine or ATP/ADP which he termed P1 and P2 receptors, respectively (Burnstock and G. A., 1978). The classification was based in part on the potencies of activation by ATP and its hydrolysis products on a biological response and also the ability to activate adenylate cyclase, which was specific for adenosine and not ATP. In the years following Burnstock's initial propositions, studies identified and confirmed the existence of different subtypes of P1 and P2 receptors (Brake et al., 1994; van Calker et al., 1979; Gordon, 1986; Hollopeter et al., 2001; Londos et al., 1980; Lustig et al., 1993; Valera et al., 1994; Webb et al., 1993). Two different types of P2 receptors were identified: ligand-gated cation channels and GPCRs (Benham and Tsien, 1987; Ralevic and Burnstock, 1998). In 1994, these receptor subtypes were classified as P2X (ligand-gated cation channels) or P2Y (GPCRs) based on the molecular structures of the cloned receptors and further divided numerically by subtype ($P2X_n$ and $P2Y_n$) (Abbracchio and Burnstock, 1994; Ralevic and Burnstock, 1998).

Presently, it is widely accepted that extracellular nucleotides and nucleosides can evoke vital biological signaling by activation of cell surface receptors (Figure 1.5). There is evidence for four subtypes of P1 or adenosine receptors which are all GPCRs: A_1, A_{2A}, A_{2B}, and A_3. The A_{2A} and A_{2B} receptors couple to and activate G_s while A_1 and A_3 receptors activate G_i (Figure 1.5) (Fredholm et al., 2001). Seven ionotropic P2X receptor isoforms ($P2X_{1-7}$) have been cloned and characterized. P2X receptors share ~30-50% sequence homology at the peptide level and form homo- or heterotrimeric channels

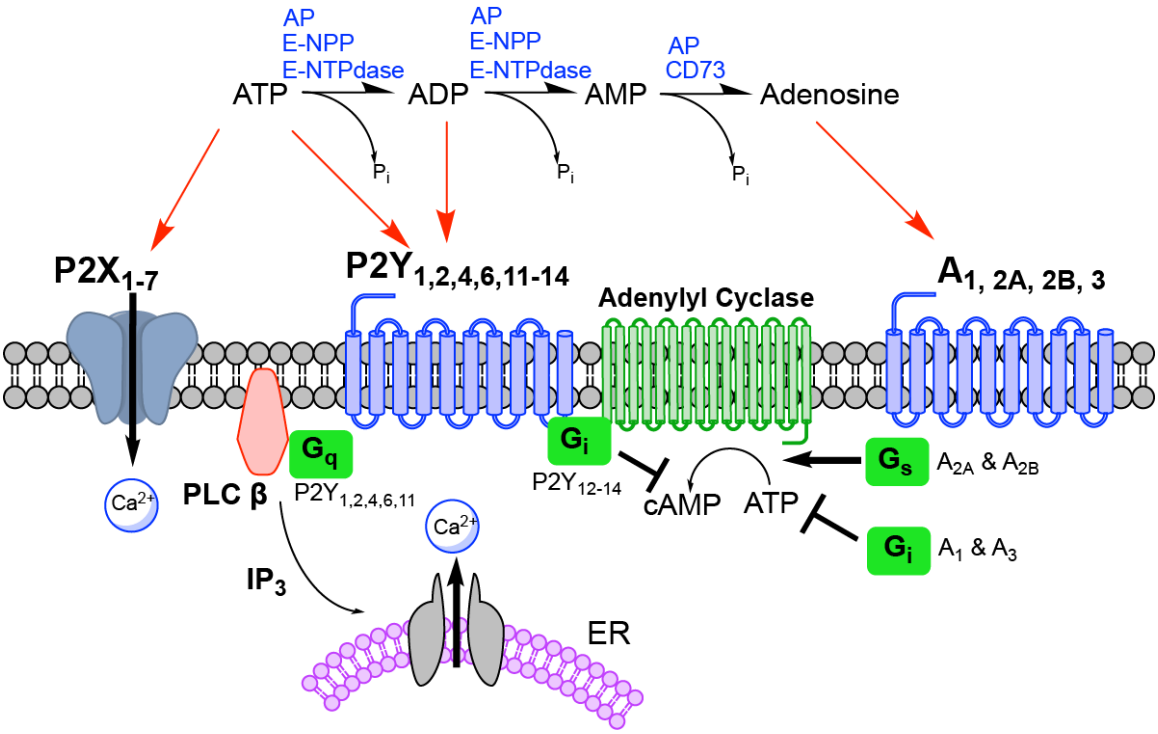

Figure 1.5. Purinergic signaling and extracellular nucleotide metabolism. Extracellular ATP and its hydrolysis products are ligands for cell surface purinergic receptors. Binding to extracellular ATP activates P2X ligand gated channels and a variety of P2Y G protein-coupled receptors ($P2Y_{2,4,11}$) resulting in an increase in cytosolic calcium levels through an influx of extracellular calcium or the release of intracellular calcium stores, respectively. The ATP hydrolysis products ADP and adenosine are ligands for P2Y receptor subtypes ($P2Y_{1,12,13}$) and P1 receptors ($A_{1,2A,2B,3}$), respectively. A_{2A} and A_{2B} adenosine activated GPCRs are coupled to G_s and activate adenylyl cyclase to produce the second messenger cAMP from intracellular ATP. $P2Y_{12\text{-}14}$ subtypes and A_1 and A_3 adenosine activated GPCRs are coupled to and activate G_i which inhibits adenylyl cyclase. Extracellular nucleotides are rapidly hydrolyzed in the interstitial space by four different families of cell surface ectonucleotidases: ecto-nucleoside triphosphate diphosphohydrolases (E-NTPDases), ecto-5'-nucleotidase (CD73, also known as NT5E), ecto-nucleotide pyrophosphatase/phosphodiesterases (E-NPPs), and alkaline phosphatases (APs).

depending on the subtype (Burnstock, 2007). P2X channels undergo conformational changes upon simultaneous activation by three molecules of ATP, subsequently allowing for the influx of Na^+ and Ca^{2+}, and efflux of K^+ (Figure 1.5) (Kawate et al., 2009; Khakh and North, 2006; Surprenant and North, 2009). Eight metabotropic P2Y receptors ($P2Y_1$, $P2Y_2$, $P2Y_4$, $P2Y_6$, $P2Y_{11}$, $P2Y_{12}$, $P2Y_{13}$, and $P2Y_{14}$) have been cloned and characterized to be accepted as P2 family members. P2Y receptors are further classified into two subgroups based on sequence identity, the presence of amino acid motifs critical for ligand binding, and selectivity of G protein coupling. $P2Y_1$, $P2Y_2$, $P2Y_4$, $P2Y_6$ and $P2Y_{11}$ are considered one group and share ~35-52% amino acid sequence homology, a Q/K-X-X-R ligand binding motif in transmembrane domain 7 (TM7), and preferentially activate G_q to raise cytosolic Ca^{2+} levels by phospholipase activity (although $P2Y_{11}$ can also activate G_s) (Figure 1.5). The second group includes the $P2Y_{12\text{-}14}$ receptors which share ~47-48% sequence homology, a K-E-X-X-L motif in TM7, and activate G_i (Figure 1.5) (Abbracchio et al., 2006; Idzko et al., 2014).

While the natural agonists of P1 and P2X receptors are only reported to be adenosine and ATP, respectively, P2Y receptors display broad endogenous ligand profiles that differ depending on the P2Y subtype. For example, some P2Y receptors are potently activated by nucleoside diphosphates (NDPs) such as $P2Y_1$ and $P2Y_{12}$ receptors which are preferentially activated by ADP. Other P2Y receptors are activated by nucleoside triphosphates (NTPs) such as the $P2Y_2$ and $P2Y_4$ receptors which can be activated by ATP or UTP. Additionally, P2Y subtypes can be activated by purines (ATP or ADP) and/or pyrimidines (UTP or UDP).

Extracellular nucleotide metabolism by ectonucleotidases

Plasma membrane proteins that contain extracellular nucleotidase catalytic domains, or ectonucleotidases, rapidly hydrolyze extracellular nucleotides down to nucleosides in the interstitial space. The hydrolysis of nucleotides by ectonucleotidases has not been demonstrated to provide energy to drive biological processes and primarily functions to control the availability of ligands to P1 and P2 receptors.

Similar to purinergic receptors, multiple families and subtypes of ectonucleotidases exist that have differential preferences for nucleotide substrates. The four main families of ectonucleotidases are the ecto-nucleoside triphosphate diphosphohydrolases (E-NTPDases), ecto-5'-nucleotidase (CD73, also known as NT5E), ecto-nucleotide pyrophosphatase/phosphodiesterases (E-NPPs), and alkaline phosphatases (APs) (Figure 1.5). These enzymes typically have distinct patterns of tissue and cell type distribution and therefore can contribute to different physiological and pathological processes dependent on purinergic signaling.

The involvement of E-NPPs and APs in purinergic signaling is not well characterized. There are seven E-NPP paralogs (NPP1-7) with broad substrate specificity that are capable of hydrolyzing phosphodiester and pyrophosphate bonds; however, only NPP1-3 are capable of hydrolyzing extracellular nucleotides (Goding et al., 2003). APs are glycosylphosphatidylinositol (GPI)-anchored enzymes with four known human isoenzymes that have broad substrate specificities for various phosphomonoesters and phosphate containing

compounds such as nucleotides and PP_i (Yegutkin, 2008). Importantly, APs are the only ectonucleotidases that can hydrolyze nucleotide triphosphates directly to nucleosides (e.g., ATP → adenosine) (Ciancaglini et al., 2010).

The major regulators of extracellular nucleotide metabolism and purinergic signaling are the E-NTPDases and CD73. E-NTPDases are capable of hydrolyzing NTPs and/or NDPs to NMPs in the presence of Ca^{2+} and Mg^{2+} (Yegutkin, 2008). These enzymes can act in concert with GPI-anchored CD73, which specifically hydrolyzes NMPs into nucleosides that then activate P1 receptors or are taken up by cells through specific nucleoside transporters (Knapp et al., 2012). Multiple E-NTPDase subtypes with varying properties have been reported in vertebrates such as humans and zebrafish, including eight subtypes (E-NTPDase1-8) in mammals. Four of these subtypes are cell surface enzymes (E-NTPDase1-3, and 8) (Bigonnesse et al., 2004; Kaczmarek et al., 1996; Maliszewski et al., 1994). E-NTPDase 5 and 6 are intracellular but have been shown to be secreted upon heterologous expression (Braun et al., 2000; Mulero et al., 1999). E-NTPDase 4 and 7 are intracellularly located, facing the lumen of cytoplasmic organelles. Homology-based searches have identified zebrafish orthologs of human E-NTPDase1-6, and 8 (*entpd1-6* and *8*) (Rosemberg et al., 2010). Similar to P2 receptors, E-NTPDase paralogs have varying substrate specificities. For example, E-NTPDase1-2 have a preference for adenine nucleotides and E-NTDPDase5-6 prefer NDPs; however, ADP is a poor substrate (Braun et al., 2000; Zimmermann et al., 2012). Additionally E-NTPDases have varying rates of nucleotide hydrolysis which can effect purinergic signaling in tissues (Kukulski et al., 2005). E-

NTPDase2-8 sequentially hydrolyze ATP to ADP and then finally AMP, resulting in the accumulation of ADP intermediates and promotion of signaling through ADP receptors such as $P2Y_1$ and $P2Y_{12}$. E-NTPDase1 (also known as CD39) directly hydrolyzes ATP to AMP and acts in concert with CD73 to promote adenosine formation and activation by P1 receptors.

The CD39/CD73 hydrolysis axis is extremely important in regulating immunity and inflammation by controlling ATP-mediated proinflammatory and adenosine-mediated anti-inflammatory functions of immune cells (Antonioli et al., 2013; Deaglio et al., 2007). There has been a recent rise of interest in immunosuppressive adenosine rich microenvironments generated by CD39/CD73 and their potential roles in the generation and progression of tumors (Allard et al., 2017). CD39 and CD73 are highly expressed on regulatory T cells (Tregs) and adenosine generated through the activity of these enzymes has been shown to be a critical player in the immunosuppressive activity of Tregs through the paracrine activation of P1 receptors on effector T cells (Deaglio et al., 2007).

Purinergic signaling in acute inflammation and wound healing

Signaling by extracellular nucleotides is well documented to influence a variety of fundamental physiological and also pathological processes in animals. The following section will describe some of the documented regulatory functions of extracellular nucleotide signaling in acute inflammatory responses and wound healing, focusing on non-bleeding tissue injuries. Acute inflammation consists of the immediate (within seconds to minutes) detection and first responses to tissue

damage and pathogen infiltration that occur independent of transcription and is characterized by leukocyte infiltration of injury sites. Tissues other than immune cells, including epithelial cells and endothelial cells, are also able to detect and immediately respond to damage and play critical roles in inflammation and wound healing.

Damage triggered nucleotide release mechanisms

Cells have high steady-state concentrations of intracellular ATP (5-10 mM) compared to extracellular ATP (~10 nM) under basal conditions (Schwiebert and Zsembery, 2003). ATP cannot freely cross intact membranes; however, in response to physical or chemical stress, ATP is released into the interstitial space either passively from lysing cells as a damage-associated molecular pattern (DAMP) or it is actively secreted by non-lytic mechanisms from intact cells (Enyedi and Niethammer, 2015).

Given the high concentration of ATP within the cytosol, any cell can act as a potential source of lytic release of ATP; however, previous studies have demonstrated a variety of non-lytic ATP release mechanisms upon cell stress that are active depending on cell and stress types. The two major types of non-lytic ATP release are (1) exocytosis via ATP-filled granules or vesicles and (2) ATP conductance through large pore ATP-permeable channels (Figure 1.6). Vesicular ATP release is well documented in neuroendocrine cells which store and release ATP along with other neurotransmitters at high concentrations in chromaffin

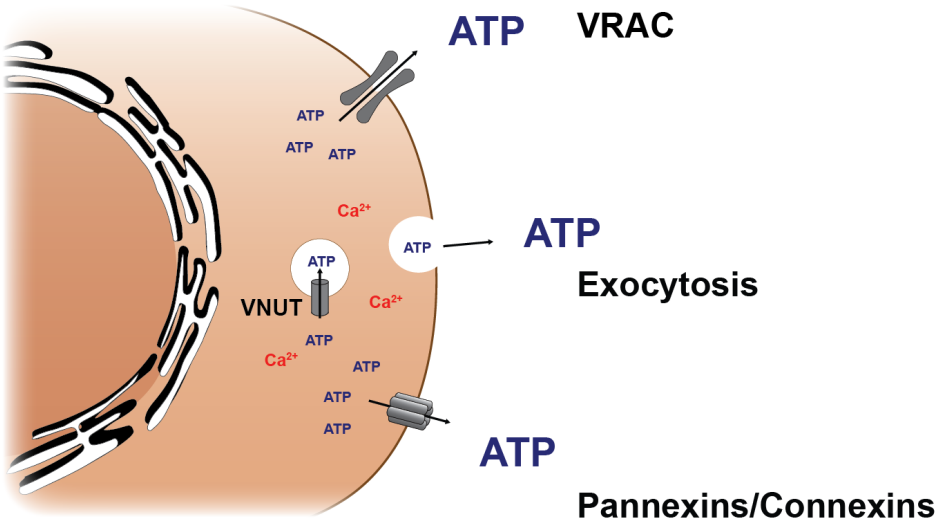

Figure 1.6. Mechanisms of ATP secretion from live cells.
ATP is actively secreted by live cells in response to chemical and physical stress. A variety of non-lytic ATP release mechanisms have been reported including exocytosis via ATP-filled granules or conductance through large pore channels such as pannexin and connexin hemichannels or volume regulated anion channels (VRAC). VNUT, vesicular nucleotide transporter (also known as SLC17A9) transports intracellular nucleotides into vesicles.

granules during synaptic transmission and in platelets that release ATP and ADP from platelet-granules upon activation (Gordon, 1986; Kahner et al., 2006). Additionally, ATP has been shown to be released via exocytosis of ATP-filled vesicles upon mechanical stimulation of cells such as in endothelial cells during shear stress (Bodin and Burnstock, 2001; Sathe et al., 2011). ATP conductance through large pore channels upon cellular stress has been shown to be mediated by various molecular mechanisms depending on cell type and context. Studies have demonstrated non-lytic ATP conductance via Pannexin channels in cells undergoing apoptosis (Chekeni et al., 2010), unpaired connexin hemichannels upon mechanical stimulation and drops in extracellular Ca^{2+} levels (Cotrina et al., 1998), and also volume-regulated large-conductance anion channels (also called maxi anion channels) upon cell swelling (Sabirov et al., 2001).

Extracellular nucleotide regulation of leukocyte activity

Extracellular nucleotide signaling upon tissue injury can influence leukocyte function in the early stages of inflammation. Recruitment of neutrophils to injury sites is one of the first responses to tissue injury and occurs within minutes without *de novo* protein synthesis. Autocrine activation of $P2Y_2$ and A_3 receptors promote the amplification of chemotactic signals induced by formylated peptides and other damage signals (Chen et al., 2006, 2010). Additionally, the paracrine activation of neutrophil A_1 receptors promotes attachment to activated endothelial cells after injury in order to promote transmigration near injury sites (Cronstein et al., 1992).

Extracellular nucleotides can also promote anti-inflammatory actions in neutrophils through adenosine activation of the A_{2A} receptor. Critically, A_{2A} receptor activation can inhibit the generation of superoxide anion and hydrogen peroxide (known as the oxidative burst) by activated neutrophils and decrease neutrophil adhesion to endothelium (Cronstein et al., 1983, 1987, 1992; Fredholm et al., 1996).

Wound induced extracellular nucleotide release also modulates the functions of phagocytic macrophages and microglia. Inflammatory signal induced ATP release promotes macrophage chemotaxis toward the initial signal by autocrine activation of $P2Y_2$, $P2Y_{12}$, and unspecified P1 receptor(s) (Kronlage et al., 2010). Caspase dependent Pannexin 1 mediated ATP and UTP release from apoptotic cells acts as a critical 'find me' signal by paracrine activation of the $P2Y_2$ receptor to promote phagocytic macrophage clearance (Chekeni et al., 2010; Elliott et al., 2009). Local CNS injury is accompanied by nucleotide release that activates the $P2Y_{12}$ receptor on microglia to induce chemotaxis to the site of injury (Haynes et al., 2006).

Purinergic signaling through extracellular ATP has also been shown to modulate eosinophil and dendritic cell function upon tissue damage and after allergen exposure, notably during asthmatic lung inflammation (Idzko et al., 2007; Kobayashi et al., 2010; Müller et al., 2010; Sáez et al., 2017). Autocrine extracellular ATP signaling amplifies eosinophil and dendritic cell chemotaxis to damage sites and increases cytokine production.

Extracellular nucleotides mediate epithelial wound closure in vitro and in vivo

Extracellular nucleotide release upon tissue damage has been demonstrated to modulate epithelial cell functions during wound healing. Epithelial barriers protect internal tissues from the noxious external environment in order to maintain internal homeostasis (Enyedi and Niethammer, 2015). Epithelial injury and barrier breach can result in damage cues such as cell lysis, unconstrained epithelial edges, and compartmental mixing that lead to lytic and non-lytic ATP release at injury sites which can subsequently modulate local epithelial cells through paracrine and autocrine signaling. A variety of studies have demonstrated that extracellular ATP released from lysed and/or stressed cells can stimulate epithelial cell migration and 'wound closure' *in vitro* using cell culture models of wound healing, such as in monolayer scratch wounds and transwell migration (Block and Klarlund, 2008; Boots et al., 2009; Boucher et al., 2007, 2010; Klepeis et al., 2004; Sham et al., 2013; Weinger et al., 2005; Yin et al., 2007). ATP mediated epithelial cell migration in cell culture has been demonstrated to be dependent on the activation of the $P2Y_2$ receptor and subsequent transactivation of the epidermal growth factor receptor (EGFR). Transactivation occurs through $P2Y_2$ activation of phospholipase D and NADPH oxidases which subsequently trigger EGF shedding by metalloproteinases and phosphorylation of EGFR by activated kinases such as Src.

Past work in the Niethammer lab has shown that wound induced ATP release can stimulate epithelial cell migration and subsequent wound closure *in vivo* (Gault et al., 2014). Epithelial barrier breach in zebrafish larvae tail fins results

in the exposure of internal tissues (~270-300 mOsm, the common extracellular tonicity of vertebrates) to the freshwater environment (~10 mOsm). Compartmental mixing with the hypotonic environment triggers mechanical cell stress through cell swelling and subsequent non-lytic secretion of ATP at injury sites. Extracellular ATP triggers rapid lamellipodia-mediated basal epithelial cell migration toward wound edges. Importantly, pharmacologic inhibition of ectonucleotidases and genetic inhibition of zebrafish E-NTPDase3 (*entpd3*) increased the range and duration of wound-induced epithelial cell migration. Additionally, application of cytoplasmic levels (5 mM) of exogenous ATP could reconstitute epithelial cell migration at injury sites in the absence of a transepithelial osmotic gradient.

The potential role of P2 receptors in hypotonicity induced epithelial wound closure remains unclear. Treatment of larvae with the pan P2 receptor antagonist Suramin did not perturb epithelial cell migration (Gault et al., 2014). Unlike ATP, the known $P2Y_2$ receptor agonists ATPγS and UTPγS could not reconstitute basal cell migration in the absence of a transepithelial osmotic gradient. In fact, the agonist profile of hypotonicity mediated wound closure in zebrafish diverges from all known P2 receptors.

While this is contradictory to past reports of *in vitro* models of mammalian wound closure, phylogenetic variations in P2Y receptor agonist specificity are commonly reported in even closely related species (Abbracchio et al., 2006; Bogdanov et al., 1998; Kennedy et al., 2000; von Kügelgen, 2006; Qi et al., 2001; Shen et al., 2004) For example, ATP and UTP are equipotent at the human $P2Y_2$ receptor; however, UTP is a significantly more potent agonist compared to ATP at

the porcine $P2Y_2$ receptor despite high sequence homology at the protein level (84%). This indicates the possibility that the zebrafish $P2Y_2$ receptor (48% identity to humans) differs in agonist specificity compared to mammalian isoforms.

It is important to note that the half-life of extracellular ATP in cell culture is on the order of minutes, while it is on the order of seconds to milliseconds *in vivo* (Orriss et al., 2009, 2013). It is possible that the extracellular nucleotide signaling mechanisms described *in vitro* may result from the artificially extended half-lives of nucleotides. Additionally, cell culture epithelial cell migration does not match the rapidness of epithelial wound closure in the zebrafish tail fin (5,000 μM puncture wounds close in ~20 min).

Purinergic signaling in the vasculature

Endothelial cells form a monolayer connected by adherens and tight junctions that internally line blood vessels in order to (1) maintain blood fluidity, (2) prevent leukocyte activation, (3) regulate blood vessel permeability, and (4) regulate perfusion to internal organs in uninjured tissues at rest (Pober and Sessa, 2007, 2014). In the acute inflammatory response, endothelial cells respond to damage released vasoactive autacoids by increasing local blood flow, recruiting and activating circulating leukocytes, and increasing permeability to release exudate into the interstitial space. This response has been termed type 1 activation and is initiated by ligands of GPCRs that activate G_q. G_q activation initiates Ca^{2+} signaling that can activate cytosolic phospholipase A_2 (cPLA2) and/or nitric oxide synthase 3 (NOS3; eNOS) resulting in the release of the potent vasodilators

prostaglandin I2 (prostacyclin or PGI_2) and nitric oxide (NO), respectively (Ignarro et al., 1987; Moncada et al., 1976).

Vascular responses to nucleotides, particularly changes in vascular tone, were the first physiological effects of extracellular nucleotides to be identified by by Drury and Szent-Györgyi in 1929 (Drury and Szent-Györgyi, 1929). Since then it has been shown that extracellular ATP, which is released from endothelial cells in response to mechanical stress or ATP activation, can act in an autocrine manner to activate Ca^{2+} signaling through $P2Y_1$ or $P2Y_2$ and trigger both PGI_2 and NO mediated vasodilation. (Bodin et al., 1991; Burnstock, 1999; Marrelli, 2001; Needham et al., 1987).

Adenosine is a more potent vasoactive molecule compared to ATP (Gillespie, 1934). The adenosine A_{2A} and A_{2B} receptors have been shown by a variety of studies to mediate vasodilation through activation of NOS (Belardinelli et al., 1998; Hein et al., 1999; Li et al., 1998; Olanrewaju and Mustafa, 2000; Smits et al., 1995). In contrast to purines, the pyrimidine nucleotides UTP and UDP have been demonstrated to trigger vasoconstriction, most likely through $P2Y_4$ and/or $P2Y_6$ activation (von Kügelgen et al., 1987; Matsumoto et al., 1997).

Perivascular nerves regulate vascular tone in concert with endothelial cells; however, endothelial activation by vasoactive autacoids is believed to be of greater significance in the response of blood vessels to local changes in the environment (Burnstock and Ralevic, 1994) while vascular tone regulation by perivascular nerves is believed to control blood flow throughout the whole organism. ATP released as a cotransmitter with noradrenaline from sympathetic nerves can

activate the $P2X_1$ receptor on vascular smooth muscle cells to induce vasoconstriction (Burnstock and Ralevic, 2014). Blood vessels are also innervated by sensory motor neurons that, upon mechanical stress or chemical irritation from the environment (antidromic conductance or axon reflex), can release ATP as a cotransmitter with calcitonin gene related peptide (CGRP). ATP can then act on vascular smooth muscle cells to induce vasoconstriction or vasodilation by $P2X_1$ or P2Y receptor activation, respectively (Holton, 1959; Holton and Holton, 1954; Westcott and Segal, 2013).

Zebrafish as a vertebrate model to study inflammation and wound healing

Zebrafish has emerged as an important vertebrate model system for studying acute inflammatory responses to tissue injury and infection (Enyedi et al., 2013; Gault et al., 2014; Huang and Niethammer, 2018; Niethammer et al., 2009; Stoddard et al., 2019), and also development and physiological processes of the vasculature (Fritsche et al., 2000; Gore et al., 2012; Isogai et al., 2001; Lawson and Weinstein, 2002). Zebrafish have both innate and adaptive immune systems that are highly similar to those in humans and other mammals (Trede et al., 2004). Adaptive immunity in zebrafish isn't fully functional until ~4 weeks post fertilization (Lam et al., 2004; Willett et al., 1999) allowing for the precise investigation of innate immune responses to injuries and pathogens in 2-3 days post fertilization (dpf) zebrafish larvae. Additionally, the molecular mechanisms driving the developing vasculature and the basic vascular plan of zebrafish larvae is highly similar to mammals (Gore et al., 2012; Isogai et al., 2001).

The thinness and optical transparency of zebrafish larvae in addition to numerous established transgenic reporter lines for a variety of immune (Ellett et al., 2011; Hall et al., 2007; Renshaw et al., 2006), epithelial (Gong et al., 2002; Reischauer et al., 2009), and also endothelial (Jin et al., 2005; Lawson and Weinstein, 2002) cell types allows for unique, noninvasive *in vivo* visual assessments of tissue and organ function and morphology by high-resolution intravital imaging techniques in studies of wound healing and innate inflammatory responses. Systematic imaging and analyses of these processes in mammalian models such as mice is problematic. Live imaging of internal tissues in mice typically requires the insertion of an imaging window which is inherently invasive and disturbs tissue homeostasis (Holtmaat et al., 2009). The difficulty in imaging methods results in a small number of animals imaged per experiment, lowering statistical confidence. Unlike mammalian model systems, zebrafish breed readily (about once a week) and can generate hundreds of progeny at a time. Embryos develop externally and innate immune responses can be imaged in the small, transparent 2-3 dpf larvae without invasive perturbations. This allows for live imaging of tissue functions at high numbers providing strong statistical confidence that is impossible to reach using mammalian model systems (Enyedi et al., 2013; Huang and Niethammer, 2018).

Genetic tools have established zebrafish as a powerful model to study human gene function and disease mechanisms. The available sequenced and annotated zebrafish genome has revealed that 70% of human genes have orthologs in zebrafish and more than 75% of human genes implicated in disease

have a counterpart in zebrafish (Howe et al., 2013; Schier, 2013). Ease of phenotypic analysis in a vertebrate has encouraged the wide use of zebrafish for large-scale forward genetic screens (Driever et al., 1996; Haffter et al., 1996). Additionally, antisense morpholino oligonucleotides allow for rapid and robust studies of gene function (Bill et al., 2009; Nasevicius and Ekker, 2000).

Clustered regularly interspaced short palindromic repeats (CRISPR)/Cas9-mediated gene disruption technology and its ease of use in the zebrafish has provided further advantage of utilizing the zebrafish model to study vertebrate gene function. Easy to follow, streamlined workflow for generating mutants has been developed by multiple groups and companies such as IDT™ (Integrated DNA Technologies) (Gagnon et al., 2014; Hwang et al., 2013). Additionally, several successful strategies using CRISPR/Cas9 for conducting phenotypic screens in F0 zebrafish have been developed and provide rapid and robust analysis of gene function (Hoshijima et al., 2019; Wu et al., 2018). The facility of obtaining the tools for genetic disruption (Cas9 and single guide RNA (sgRNA)) combined with the external fertilization and development of zebrafish, which allows for easy injection of Cas9-sgRNA ribonucleoprotein (RNP) complexes into single cell embryos, provides an unrivaled platform for analyzing genetic functions in vertebrates.

The small size of larvae, liquid environment, and large progeny size allow for the ease of use of pharmacologic inhibitors to study cellular processes. These advantages, in addition to the annotated and highly similar genome to humans, has provided a unique platform for pharmacologic interrogation of inflammatory

responses and also pharmacologic and toxicology screens (Hill et al., 2005; Niethammer et al., 2009; Zon and Peterson, 2005).

Aims

Unlike catalytic ATP binding proteins which contain conventional well-characterized ATP-binding sites such as P-loop NTPase domains, the compositions of non-catalytic allosteric ATP-binding sites are ill-defined, preventing their identification by computational prediction methods. The development of functionalized ATP ABPP probes coupled to MS-based protein identification has allowed researchers to biochemically profile ATP binding proteins and their binding sites from complex proteomic mixtures. Importantly, the site and type of functionalization of the probe can alter its chemical and physical properties relative to unmodified ATP and thus bias its protein interaction profile. Current functionalized ATP probes are either biased towards identifying ATP binders with conventional catalytic-ATP binding sites (Patricelli et al., 2007) or contain sterically bulky hydrophobic additions that can interfere with protein interactions (Mahajan et al., 2015; Yao and Bajjalieh, 2009). Recent advances in ABPP strategies suggest that an ATP probe functionalized with a minimalist photo-crosslinker can enable profiling of a wide spectrum of ATP interactors without the biases of currently available ATP probes. The aim of chapter 3 is to develop and describe a novel ATP probe functionalized with a minimalist photo-crosslinker which we called *minimally invasive photoaffinity ATP or mipATP*. We show that the N^6-modified mipATP probe can functionally mimic signaling triggered by non-

catalytic allosteric ATP interactions with cell surface receptors in cell culture and live tissues. Additionally, we show that mipATP can successfully bind and enrich both known and novel ATP binding proteins in a complex membrane proteome.

A drop in interstitial osmotic pressure triggers cell swelling and subsequent non-lytic secretion of ATP at injury sites in zebrafish larvae. Hypotonicity induced ATP release stimulates epithelial cell migration and subsequent wound closure *in vivo* (Gault et al., 2014). The identity of the ATP receptor that triggers wound closure is unknown and its pharmacological profile does not match that of a known mammalian P2 receptor. The aim of chapter 4 is to interrogate ATP mediated wound closure *in vivo* through functional genetic profiling of expressed P2 receptors and pharmacological profiling with an in-depth SAR analysis. We show that the known P2 receptors $P2Y_4$ and $P2Y_{11}$ may contribute to ATP-mediated wound closure; however, our data suggests that an unknown, potentially novel, ATP receptor contributes to epithelial wound closure *in vivo*. SAR analysis confirms that mipATP interacts with this receptor, indicating that further biochemical characterization may be able to uncover its identity.

Wound induced ATP release has been implicated in vascular responses to injury in higher vertebrates including humans and other mammals. Osmotically induced ATP release at injury sites may trigger the initial activation of the local vasculature in zebrafish larvae. The aim of chapter 5 is to characterize the mechanisms of vascular activation after injury using live zebrafish larvae as a model vertebrate system. We show that extracellular ATP and adenosine perfusion at injury sites can trigger rapid dilation of the local vasculature by activation of the

adenosine A_{2B} receptor; however, we find that these nucleotide ligands are not the endogenous molecules that initiate vasodilation after injury or they are coupled to other redundant vasoactive signals triggered by osmotic cues. We further show that vasodilation is triggered through cytosolic Ca^{2+} induced NO signaling and subsequent cyclic guanosine monophosphate (cGMP) generation.

CHAPTER 2 Materials and Methods

Chapter 3

Chemical synthesis of mipATP

Reagents for chemical reactions were purchased from Sigma-Aldrich without purification unless mentioned otherwise. 6-Chloropurine riboside-5'-triphosphate was purchased from BioLog Inc (Germany). Chemical reactions were carried out under argon atmosphere at the temperatures displayed by thermocouple or at ambient temperature unless described otherwise. NMR spectra were recorded on Bruker AVIII 600MHz spectrometers and reported with chemical shifts (ppm), multiplicities (s = singlet, d = doublet, t = triplet, q = quartet, p = pentet, m = multiplet, and br = broad), integration and coupling constants (*J* in Hz). Chemical shifts were recorded with residual proton peaks of deuterated solvents as references (residual ^{1}H of D_2O, 4.80 ppm). ^{1}H-NMR spectra were recorded at 24°C. ^{13}C-NMR spectra were recorded at 24°C. Mass spectra for compound characterization were collected by Waters Acuity SQD LC-MS with the mode of electron spray ionization (ESI).

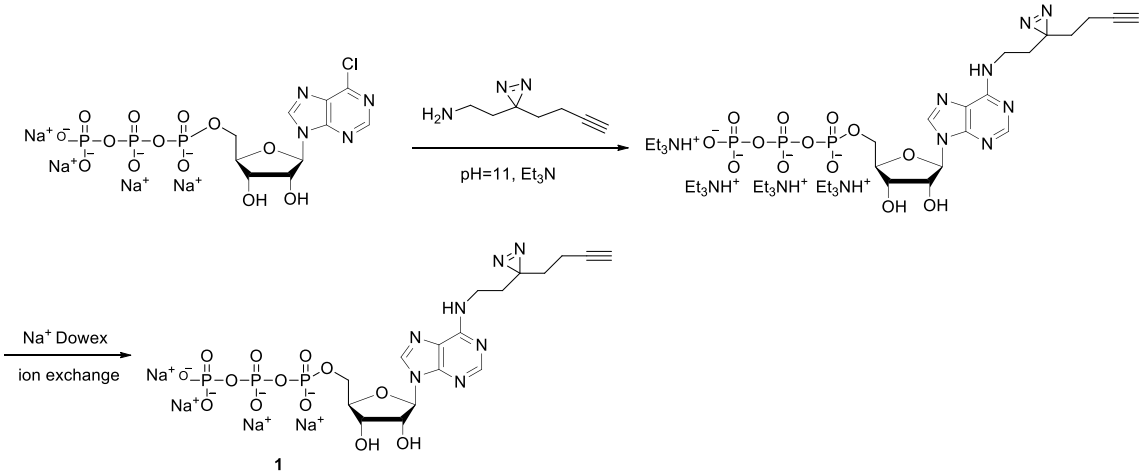

To a solution of 6-chloropurine riboside-5'-triphosphate (10 mg) in 5 mL buffer (pH = 11, triethylamine in water) was added 2-(3-(but-3-yn-1-yl)-3H-diazirin-3-yl)ethan-1-amine (4 mg) and the mixture was stirred at 40 °C under Ar. After the reaction was completed as indicated by LC-MS analysis, the resulting material was purified by reverse phase HPLC using a gradient of 20 mM triethylammonium bicarbonate (pH 7.4, acetic acid, 2% acetonitrile) solution and 100% acetonitrile. The product was lyophilized, dissolved in 2 mL water and passed through a 0.8 × 4.0 cm, (~ 3 g) column of Dowex AG50W-X8 (100-200 mesh, Na^+ form) cation-exchanged resin preequilibrated with two column volumes of water. The product was eluted with four column volumes of water and lyophilized to afford 4 mg of Compound **1**. Compound **1:** ^{1}H-NMR (D_2O): δ 8.46 (s, 1H), 8.24(s, 1H), 6.10 (d, 1H, *J* = 6.2 Hz), 4.77 (m, 1H), 4.56 - 4.54 (m, 1H), 4.37-4.36 (m, 1H), 4.25 (ddd, 1H, *J* = 2.70, 6.06, 12.00 Hz), 4.17 (dt, 1H, *J* = 2.85, 12.00 Hz), 3.44 (br, 2H), 2.21 (t, 1H, *J* = 2.52 Hz), 1.97 (dt, 2H, *J* = 2.52, 7.08 Hz), 1.87 (t, 2H, *J* = 6.60 Hz), 1.68 (t, 2H, *J* = 7.08 Hz); ^{13}C NMR (D_2O): 154.4, 152.7, 148.2, 139.3, 119.0, 86.4, 84.1, 84.0, 74.2, 70.4, 69.6, 65.2, 35.3, 31.4, 31.1, 27.7, 12.4. HRMS: calculated for $C_{17}H_{23}N_7O_{13}P_3$ ([M-H^+]) 626.0567, found 626.0588.

Plasmid construction and generation of stable cell lines

To create plasmids for transgenesis using the Tol2kit system (Kwan et al., 2007) the pME-QF2 (Addgene; 83307) (Ghosh and Halpern, 2016) entry clone was recombined with p5E-*krt4* (Gong et al., 2002) and p3E-polyA (Kwan et al., 2007) constructs into the pDestTol2CG2 backbone. The pDONR221-GCaMP6s-3xNLS

(Enyedi et al., 2016) entry clone was recombined with the p5E-*QUAS* (Addgene; 61374) (Ghosh and Halpern, 2016) and p3E-P2A-mKate2-3xNLS-polyA (Enyedi et al., 2016) constructs into the pDestTol2CmKate2 vector backbone.

For mammalian expression, MFSD5-FLAG (ENSG00000182544; Uniprot Isoform: Q6N075-1), CD44-V5 (ENSG00000026508), and CD44∆cytosol-V5 were subcloned from A549 cell cDNA into the pSBbi-Pur (Addgene; 60523) and pSB-CMV-MCS-Puro (Kowarz et al., 2015) transposon plasmids. The CD44-V5 construct encodes the full-length, predominant CD44 isoform (Uniprot Isoform: P16070-12) fused at the c-terminus to a V5 reporter tag. CD44∆cytosol-V5 encodes a truncated version of this CD44 isoform lacking the c-terminal 67 amino acids of the cytoplasmic domain (Jiang et al., 2002). A psBbi-GCaMP6s-3xNLS-P2A-mBeRFP-3xNLS-Puro plasmid was created by first subcloning a codon optimized gBlock® (IDT) containing the mBeRFP (Yang et al., 2013) coding sequence into the p3E-P2A-mKate2-3xNLS-polyA construct in order to create a *QUAS*:GCaMP6s-3xNLS-P2A-mBeRFP-3xNLS-polyA plasmid. Next, the GCaMP6s-3xNLS-P2A-mBeRFP-3xNLS sequence was subcloned into the pSBbi-Pur plasmid by NcoI and XbaI digestion.

For establishing stable A549 and HeLa cell lines expressing MFSD5-FLAG, and GCaMP6s-3xNLS-P2A-mBeRFP-3xNLS, cells were co-transfected with the pSBbi-Pur vector encoding the gene or reporter of interest and a vector encoding the SB100x *Sleeping Beauty* transposase at a 1:2 ratio (Izsvák et al., 2009). A549 and HeLa cells were subsequently grown in the presence of 1 μg mL^{-1} and 2 μg

mL^{-1} of puromycin, respectively, for 1 week. For transient expression, the vector encoding the gene of interest was transfected into A549 cells using the Lipofectamine 3000 reagent following the manufacturer's instructions.

Cell culture

A549 and HeLa cells were maintained in high-glucose DMEM supplemented with 10% (v/v) fetal bovine serum (FBS), penicillin (100 U mL^{-1}), streptomycin (100 µg mL^{-1}), and 2 mM L-alanyl-L-glutamine dipeptide (GlutaMAX™, ThermoFisher) in a 5% humidified CO_2 incubator at 37°C. For SILAC experiments, cell lines were passaged at least six times in SILAC DMEM (Thermofisher; #88364) lacking L-lysine and L-arginine and supplemented with 10% dialyzed FBS (Corning; #35071CV), P/S/Q (as above), and either L-arginine-$^{13}C_6{}^{15}N_4$ hydrochloride (87.8 µg mL^{-1}) (Cambridge Isotope Laboratories; #CNLM-539-H) and L-lysine-$^{13}C_6{}^{15}N_2$ dihydrochloride (181.2 µg mL^{-1}) (Cambridge Isotope Laboratories; #CNLM-291-H) or L-arginine hydrochloride (84 µg mL^{-1}) (Sigma; #A6969) and L-lysine monohydrate (131 µg mL^{-1}) (Sigma; #L9037).

Imaging calcium signals in A549 and HeLa cells by widefield fluorescence microscopy

A549 and HeLa cells stably expressing a GCaMP6s-3xNLS-P2A-mBeRFP-3xNLS reporter transgene were seeded into the wells of a black 96-well glass bottom plate (Cellvis; #P96-1.5H-N) at a density of $2x10^4$ cells per well 24 hrs before imaging. Before the experiment, cells were washed 2x with L-15 medium and equilibrated to 50 µL of L-15 medium for 30 min at RT. Images were acquired every 15 sec

from two different fields of view for a period of 22 min. During the experiment, 20 μM of ATP (Sigma; #A26209), ATPγS (Tocris; #4080), mipATP, AMP-PNP (Sigma; #A2647) or vehicle was added in 50 μL of L-15 to the well prior to the 2-min timepoint.

Images were captured at RT (~26°C) using NIS-Elements (Nikon) on an Eclipse Ti microscope (Nikon) equipped with a 20x Plan Apochromat NA 0.75 air objective lens, a Clara CCD camera (Andor), and a motorized stage. GCaMP6s fluorescence was excited with a LED light source (Lumencor) using a 475/28 bandpass filter together with a multispectral dichroic (59022 bs, Chroma), and acquired using a 525/50 emission filter (Chroma). mBeRFP fluorescence was excited using a 475/28 excitation filter combined with the previously mentioned dichroic and acquired using a 632/60 emission filter (Chroma).

Quantification of calcium signals in A549 and HeLa cells

Image processing and calcium signal analyses were performed with the MATLAB R2018a software. Nuclei (mBeRFP channel) are first identified and separated by watershed segmentation in individual frames and then the same nuclei are connected between consecutive frames, by looking for the nearest neighbor. The sum of GCaMP6s signal within individual nuclei was divided by that of mBeRFP signal to give a ratiometric measure of calcium.

Zebrafish procedures and generation of transgenic Lines

Casper background (White et al., 2008), wild-type and transgenic zebrafish larvae strains were maintained as described (Nüsslein-Volhard and Dahm, 2002) with the approval of the Institutional Animal Care and Use Committee (IACUC). Zebrafish larvae were raised in E3 medium (5 mM NaCL, 0.17 mM KCl, 0.33 mM $CaCl_2$, and 0.33 mM $MgSO_4$). For tail fin amputation assays 2.5-4 days post-fertilization (2.5-4 dpf) larvae were anaesthetized in E3 medium containing 0.2 mg mL^{-1} ethyl 3-aminobenzoate methanesulfonate (Sigma).

To generate transgenic lines, a solution containing 25-25 pg of *krt4*:QF2 or *QUAS*:GCaMP6s-3xNLS-P2A-mKate2-3xNLS plasmid and *in vitro* transcribed transposase mRNA was injected into the cytosol of one-cell stage Casper embryos. Injected larvae with mosaic cardiac EGFP or mKate2 expression were raised to sexual maturity and screened by crossing with wild-type fish to identify founders. F1 embryos were identified by cardiac EGFP or mKate2 expression and raised to sexual maturity. F1 TG(*krt4*:QF2) and TG(*QUAS*:GCaMP6s-3xNLS-P2A-mKate2-3xNLS) founders were crossed and F2 double transgenic TG(*krt4*:QF2; *QUAS*:GCaMP6s-3xNLS-P2A-mKate2-3xNLS) embryos were identified by epithelial expression of nuclear mKate2 and cardiac EGFP and then raised to sexual maturity. Experiments were performed on the progeny of F2 incross.

Spinning disk confocal imaging of calcium signals in zebrafish larvae

For amputation experiments, anesthetized 2.5-4 dpf TG(*krt4*:QF2; *QUAS*:GCaMP6s-3xNLS-P2A-mKate2-3xNLS) individual larvae were washed (3 x 1mL) with isotonic E3 (E3 medium supplemented with 140 mM NaCl) and

subjected to tail fin tip amputation using a needle knife (Fine Science Tools) in isotonic E3 on a glass dish. Tail fin amputated larvae were immobilized on a plastic dish by embedding in ~30 µL of 1% low-melting agarose dissolved in isotonic E3. After solidification, a strip of agarose (~10 µL) was removed along the amputated tail fin, and the sample was mounted on the microscope. 50 µL of isotonic E3 supplemented with 1 mM ATP (Sigma; #A26209), ATPγS (Tocris; #4080), mipATP, AMP-PNP (Sigma; #A2647), or vehicle was added to the sample on the imaging dish prior to the 2-minute timepoint.

Experiments were performed at RT (~26°C) on a Nikon Eclipse FN1 microscope equipped with a 25x Apochromat LWD NA 1.1 water immersion objective lens, a Yokogawa CSU-X1 Spinning Disk unit, an Andor iXon3 897 EMCCD camera, and 488 nm and 561 nm diode laser lines (Andor Revolution XD). GCaMP6s fluorescence was excited using the 488 nm laser line and emission was collected using a 535/20 bandpass filter (Chroma). mKate2 (mK2) fluorescence was excited using the 561 nm laser line and emission was collected using a 620/30 bandpass filter (Chroma). GCaMP6s and mK2 image acquisition was done simultaneously through triggered excitation and emission collection. Up to 30 Z-stack slices with a resolution of 3 µm were acquired per field of view with the NIS-Elements software (Nikon). Images were acquired every 10 sec for a period of 22 min.

Image processing and data analysis of nuclear calcium signals in zebrafish

Image processing and data analysis was performed as described in (Enyedi et al., 2016). Briefly, image processing tasks were performed with the open-source

program Fiji (Schindelin et al., 2012) and the Anaconda distribution of the Python programming language, using custom scripts, based on the pandas, SciPy, NumPy, and scikit-image libraries. To quantify nuclear Ca^{2+} signal intensity, background corrected and thresholded maximum intensity projection images of GCaMP6s and mK2 confocal time-lapse Z-stacks were generated and ratio images (GCaMP6s/mK2) were calculated using Fiji. The ratio value of every pixel was then remapped using a custom Python script, to express them as a function of binned distance (2 µm) from the moving wound margin. These spatiotemporal maps of the Ca^{2+} signals were then averaged over multiple experiments.

Cell membrane isolation

A549 cells were grown to confluency and washed 3x with ice-cold PBS. Cells were harvested in PBS with a cell lifter and pelleted by centrifugation at 250 x*g* for 5 min at 4°C. Cell pellets were resuspended in 4 volumes of ice-cold homogenization buffer (HB) (250 mM Sucrose, 20 mM HEPES pH 7.4, 1.5 mM $MgCl_2$) with EDTA-free protease inhibitors (Sigma; #11873580001) and pelleted by centrifugation at 1,100 x*g* for 10 min at 4°C. Pellets were resuspended in 3x ice-cold HB and the resuspended cells were homogenized by 10 passages through a 25G needle at 4°C. The homogenate was centrifuged at 1,000 x*g* for 10 min at 4°C and the pellets discarded (nuclei). The supernatant was centrifuged at 33,000 x*g* for 30 min at 4°C to obtain the crude membrane fraction. Membrane pellets were resuspended in binding buffer (BB) (150 mM NaCl, 20 mM HEPES pH 7.4, 2 mM $CaCl_2$, 2 mM $MgCl_2$, and EDTA-free protease inhibitors) and passaged 10x through a 25G

needle. Membranes were re-pelleted by centrifugation and resuspended in BB 1-3x. Membrane protein concentrations were determined by Pierce BCA assay (Thermo; #23227).

mipATP labeling of isolated membrane fractions

Isolated membranes at 1-2 mg mL^{-1} in BB were incubated with 10-50 μM of mipATP in a 96-well plate for 25-30 min at 4°C in the dark. For competition experiments, isolated membranes were first preincubated with the competitor compound for 10 min at 4°C in the dark prior to the addition of mipATP. Plates containing the samples were then placed on ice and UV-irradiated (365 nm) (Analytik Jena US; #95-0045-04) for 15 min a distance of 2 cm from the light source. Membranes were collected and resuspended in 10 volumes of ice-cold BB and centrifuged at 230,000 x*g* for 10 min at 4 °C. Supernatant was discarded, and the pellets were resuspended in BB and re-pelleted by centrifugation. Membrane pellets were snap frozen with liquid nitrogen or solubilized for downstream analysis.

mipATP labeling of intact cells

A549 cells were grown to confluency and washed 3x with ice-cold PBS. Cells were then detached from tissue culture dishes with 1 mM EDTA in PBS, pelleted by centrifugation at 250 x*g* for 5 min at 4°C, and sequentially washed 1x with ice-cold PBS and 1x with ice-cold HEPES-buffered extracellular medium (EC) (123 mM NaCl, 5 mM KCl, 1.8 mM $CaCl_2$, 0.9 mM $MgCl_2$, 0.9 mM $MgSO_4$, 2 mM $NaHCO_3$,

5 mM glucose, and 10 mM Na-HEPES ph 7.4). Cells were resuspended to ~2 x 10^7 cells mL^{-1} in EC and incubated with mipATP at the indicated concentrations in a well of a 24-well plate for 25-30 min at 4°C in the dark. For competition samples, cells were first preincubated with the competitor compound for 10 min at 4°C in the dark prior to the addition of mipATP. 24-well plates containing the samples were then placed on ice and UV-irradiated (365 nm) for 15 min. Cells were collected and resuspended in 10 volumes of ice-cold EC + EDTA-free protease inhibitors and pelleted by centrifugation at 250 x*g* for 5 min at 4°C. Cells were then washed in 10 volumes of ice-cold PBS + EDTA-free protease inhibitors and pelleted by centrifugation at 250 x*g* for 5 minutes at 4°C. Next, cells were resuspended in 3 volumes of ice-cold HB (250 mM Sucrose, 20 mM HEPES pH 7.4, 1.5 mM $MgCl_2$ + EDTA-free protease inhibitors) and homogenized by 10 passages through a 25G needle at 4°C. Homogenates were centrifuged at 1,000 x*g* for 10 min at 4°C and pellets (nuclei) were discarded. The supernatant was centrifuged at 100,000 x*g* for 1 hr at 4°C to and pellets were resuspended in ice-cold HB + EDTA-free protease inhibitors and re-pelleted by centrifugation. Supernatants were discarded, and the membranes were solubilized for downstream analysis and protein concentrations determined by Pierce BCA assay.

In-gel fluorescence analysis

Probe-crosslinked membranes (50 µg; determined by Pierce BCA assay) were solubilized in SDS lysis buffer (4% SDS, 150 mM NaCl, 50 mM TEA pH 7.4, EDTA-Free protease inhibitors) and brought to a final concentration of 1 mg mL^{-1} and

~0.5% SDS with SDS-free lysis buffer (150 mM NaCl, 50 mM TEA pH 7.4, EDTA-Free protease inhibitors). Solubilized membranes were reacted with a freshly premixed click chemistry reaction cocktail containing TAMRA-azide (25 μM, 10 mM stock in DMSO), tris(2-carboxyethyl)phosphine hydrochloride (TCEP) (1 mM, 50 mM freshly prepared in H_2O), tris[(1-benzyl-1H-1,2,3-triazol-4-yl)methyl]amine (TBTA) (100 μM, 1.7 mM in 20% DMSO/80% *tert*-butanol), and $CuSO_4$ (1 mM, 50 mM freshly prepared in H_2O) at a total reaction volume of 50 μL for 1 hr at RT in the dark. Reactions were terminated and protein precipitated by the sequential addition of 200 μL ice-cold MeOH, 50 μL ice-cold $CHCl_3$, and 150 μL of ice-cold H_2O. Samples were centrifuged at 15,000 x*g* for 10 min at 4°C and the aqueous phase was discarded. Proteins were washed (2 x 1 mL) with ice-cold MeOH and air-dried in the dark for ~10 min. Dried proteins were solubilized in 50 μL of 1x NuPAGE LDS Sample Buffer + Reducing Agent and incubated at 70°C for 10 min in the dark. Next, 25 μg of protein was loaded per gel lane for separation by SDS-PAGE using NuPAGE 4-12% Bis-Tris Protein Gels (Invitrogen). Gels were subsequently fixed in 50% MeOH, 10% acetic acid solution for 1 hr in the dark, washed with H_2O (3x for 20 min) in the dark and then imaged using GE Typhoon FLA 9500. Band intensity analysis (Figure 2) was performed using ImageQuant TL 8.1 software (GE Healthcare). For Figure 2B, values were fit to a One site – Specific binding curve using GraphPad Prism 8 software. Band intensity values were normalized to the maximum intensity value of each band (Bmax) as predicted by the fitted curve and these normalized values are displayed as “crosslinking efficiency” (Arguello et al., 2017). K_d and 95% CI values were determined using

the fitted curve on the GraphPad Prism 8 software. For Figures 2C-D, band intensity values were normalized to the intensity value of the non-competed band and displayed as “Signal Intensity (normalized units)”. Gels were stained with Coomassie Blue after fluorescence imaging.

Streptavidin isolation of mipATP-crosslinked proteins

mipATP-labeled membrane fractions (200-500 µg) were solubilized in SDS lysis buffer and brought to a final concentration of 0.5 mg mL^{-1} and 0.5% SDS with SDS-free lysis buffer. Next, samples were reacted with freshly premixed click chemistry reaction cocktail containing 100 µM biotin-azide, 1 mM TCEP, 100 µM TBTA, and 1 mM $CuSO_4$ for 1 hr at RT. Reactions were terminated and protein precipitated by the sequential addition of 4 volumes ice-cold MeOH, 1 volume ice-cold $CHCl_3$, and 3 volumes ice-cold H_2O or by the addition of 5 volumes of ice-cold MeOH and O/N incubation at -80°C. After protein precipitation, samples were centrifuged at 6,000 x*g* for 20 minutes at 4°C and the aqueous phase was discarded in order to isolate the precipitated proteins. The precipitated proteins were washed 2x with 5 mL of ice-cold MeOH and air-dried for ~10 min. Dried proteins are solubilized in SDS lysis buffer and then brought to a final concentration of 0.5 mg mL^{-1} and 0.4% SDS with SDS-free lysis buffer. Pre-washed (3x 1mL, of 0.4% SDS, 150 mM NaCl, 50 mM TEA pH 7.4) Streptavidin agarose (Pierce; #20357) was brought to a 50% bead slurry and 20 µL of bead slurry was added to each sample. Samples were incubated rotating for 2 hr at RT. Next, beads were centrifuged at 500 x*g* for 2 min at RT and washed with 0.4% SDS, 150 mM NaCL, 50 mM TEA pH 7.4 (4 x 1 mL).

Washing buffer was completely removed with an aspirator and beads were resuspended in 20 µL of 1x NuPAGE LDS Sample Buffer + Reducing Agent and incubated at 95°C for 10 min. Samples were vortexed and centrifuged at 20,000 x*g* for 1 min and subsequently separated by SDS-PAGE with NuPAGE 4-12% Bis-Tris Protein Gels.

Immunoblotting

Proteins were transferred onto a PVDF membrane at 100 V for 90 min at 4°C. Blots were then blocked with 5% nonfat dried milk in TBST (0.1% Tween-20 in TBS) for 1 hr at RT. Next, blots were probed with the following primary antibodies: anti-MRP1 (Cell Signaling; #14685S, 1:1,000), anti-CK1δ (Bethyl Laboratories; #A302-136A, 1:1,000), anti-CD44 (Cell Signaling; #3578S, 1:250 or 1:500), anti-FLAG M2 (Sigma; #F1804 1:2,500), anti-FAS (Abcam; #ab133619, 1:1,000) anti-V5 (Invitrogen; #R960-25, 1:2,000) in 5%-milk TBST O/N at 4°C or for 2 hr at RT. Membranes were washed with TBST (3 x 10 min) and incubated for 1 hr at RT with goat anti-rabbit (Cell Signaling; #7074, 1:5,000) or goat anti-mouse (Cell Signaling; #7076, 1:5,000) secondary antibody in 5%-milk TBST depending on the species of the primary antibody used. Membranes were washed with TBST (3 x 10 min) and visualized with Amersham ECL or ECL Select Western Blotting Detection Reagents (GE Healthcare). Chemiluminescence was detected using the ChemiDoc™ Touch Imaging System (Bio-Rad). For Figure 3.3 analysis, band intensity values were normalized to the intensity value of the UV-irradiated, no

competition band within the same blot using the Image Lab V 5.2 software (Bio-Rad) and displayed as “Signal Intensity (normalized units)”.

Sample preparation for label-free proteomic analysis

A549 cells were grown to confluency and a crude membrane fraction was isolated as described above (Cell membrane isolation) except that homogenization was performed by ~30 strokes in a Teflon Potter-Elvehjem homogenizer at 4°C in homogenization buffer (HB) consisting of 250 mM Sucrose, 30 mM Tris-HCl pH 7.4, EDTA-free protease inhibitors. The homogenate was centrifuged at 600 x*g* for 10 minutes at 4°C to remove nuclei. Membrane protein concentrations were determined by BCA assay and split into two equal 5 mg fractions in 2.5 mL (2 mg mL^{-1}) in Binding Buffer (150 mM NaCl, 25 mM HEPES pH 7.4, 2 mM $CaCl_2$, 2 mM $MgCl_2$ + EDTA-free protease inhibitors). ATP diluted in BB was added to a final of 2 mM to the competition sample while an equal volume of BB was added to the experimental sample and both samples were incubated at 4°C for 10 min. Next, mipATP was added to each sample to a final concentration of 20 μM and incubated at 4°C for 25 minutes in the dark. Samples were placed into separate wells of a pre-chilled 6-well plate on ice and UV-irradiated (365 nm) for 15 min. Next, samples were washed with 10 volumes of ice-cold BB + EDTA-free protease inhibitors and pelleted by centrifugation at 100,000 x*g* for 30 min at 4°C. Pellets were solubilized with SDS lysis buffer + EDTA-Free protease inhibitors and subsequently brought to a final concentration of 1 mg mL^{-1} and ~1% SDS with SDS-free lysis buffer + EDTA-Free protease inhibitors. Solubilized membranes

were reacted with freshly premixed click chemistry reaction cocktail containing 100 µM diazo biotin-azide (4 mM stock in DMSO) (Click Chemistry Tools; #1041), 1 mM TCEP, 100 µM TBTA, and 1 mM $CuSO_4$ at a total reaction volume of 5 mL for 1.5 hr at RT. Reactions were stopped by the addition of 5 volumes of ice-cold MeOH and placed overnight at -80°C for protein precipitation. Precipitated proteins were pelleted by centrifugation at 6,000 x*g* for 30 min at 4°C and subsequently washed with ice-cold MeOH (2 x 25 mL). The final MeOH wash was aspirated and the protein pellet was air-dried for ~10 min and subsequently solubilized in 6M Urea, 0.4% SDS in PBS pH 7.4. TCEP (10 mM) was added and samples were incubated at RT for 30 min. Next, iodoacetamide (20 mM) was added and samples were incubated in the dark at RT for 30 min. Samples were diluted to 0.5 mg mL^{-1} in 0.4% SDS, PBS pH 7.4 + EDTA-free protease inhibitors. Streptavidin agarose slurry (pre-washed 3x with 0.4% SDS, PBS pH 7.4 solution) was added at a final bed volume of 100 µL and the samples were incubated at RT rotating for 2 hrs. Next, the beads were pelleted by centrifugation at 1,000 x*g* for 5 min at RT and sequentially washed 3x with PBS + 0.4% SDS, pH 7.4 and 3x with PBS + 1% SDS, pH 7.4. Beads were transferred to a Protein LoBind tube (Eppendorf; # 022431081) and resuspended in elution buffer (50 mM $Na_2S_2O_4$ + 1% SDS in PBS, pH 7.4) for 1 hour at RT. Beads were then pelleted by centrifugation at 1,000 x*g* for 3 min and the eluate was transferred to a fresh LoBind tube. Beads were resuspended in fresh elution buffer and incubated again for 1 hr at RT. First and second eluates from the same sample were mixed, concentrated with an Ultracel ® -3K centrifugal filter (Amicon; #UFC500324), and

subsequently dried by speed-vac. Dried samples were resuspended in 25 µL of 1x NuPAGE LDS Sample Buffer + Reducing agent and separated on a 10% NuPAGE Bis-Tris Gel until the dye front entered ~2 cm into the gel. After Coomassie blue staining, four gel slices were excised for each sample and sent to the Harvard Medical School Taplin Mass Spectrometry Facility for analysis.

Sample preparation for SILAC proteomic analysis

Isotopically heavy and light A549 cells were grown to confluency and intact cells were labeled with 50 µM mipATP alone (experimental) or after 10 min preincubation with 5 mM ATP (competition) as described above (mipATP labeling of intact cells). For the "forward" experiment, isotopically heavy cells were labeled with mipATP alone and light cells were labeled with mipATP in the presence of the excess ATP competitor. Cell isotypes were switched for the "reverse" experiment. After mipATP labeling, membranes were isolated as described above except that cell homogenization was performed by ~30 strokes in a Teflon Potter-Elvehjem homogenizer at 4°C in homogenization buffer consisting of 250 mM Sucrose, 30 mM Tris-HCl pH 7.4, EDTA-Free protease inhibitors. The homogenate was centrifuged at 600 x*g* for 10 minutes at 4°C to remove nuclei. After isolation, membranes were solubilized in SDS-lysis buffer + EDTA-free protease inhibitors and protein concentrations were determined by BCA assay. 2.5 mg of each sample type was mixed 1:1 and the combined sample was brought to a final concentration of 1 mg mL^{-1} and ~1% SDS with SDS-free lysis buffer + EDTA-free protease inhibitors. The solubilized sample was reacted with a freshly premixed click

chemistry reaction cocktail containing 100 µM diazo biotin-azide, 1 mM TCEP, 100 µM TBTA, and 1 mM $CuSO_4$ at a total reaction volume of 5 mL for 1.5 hr at RT. Reactions were stopped and proteins were precipitated by the addition of 5 volumes of ice-cold MeOH as described in the label-free sample preparation. The dried protein pellet was solubilized in SDS lysis buffer + 10 mM EDTA + EDTA-Free protease inhibitors and brought to 1 mg mL^{-1} and 0.4% SDS with SDS-free lysis buffer + protease inhibitors. Streptavidin agarose slurry (pre-washed 3x with 150 mM NaCl, 0.4% SDS, 50 mM TEA pH 7.4) was added at a final bed volume of 100 µL and the samples were incubated at RT rotating for 2 hrs. The beads were pelleted by centrifugation at 1,000 x*g* for 5 min at RT and sequentially washed 4x with 150 mM NaCl, 0.4% SDS, 50 mM TEA pH 7.4 and then 3x with PBS + 1% SDS, pH 7.4. Proteins were eluted and samples were prepared for MS analysis as described in the sample preparation for the label-free proteomic analysis. Gel slices were excised and sent to the Harvard Medical School Taplin Mass Spectrometry Facility for analysis.

Protein sequence analysis by LC-MS/MS

Mass spectrometry analysis was performed by the Harvard Medical School Taplin Mass Spectrometry Facility. For the label-free samples, gel pieces were subjected to a modified in-gel trypsin digestion procedure (Shevchenko et al., 1996). Gel pieces were washed and dehydrated with acetonitrile for 10 min followed by removal of acetonitrile then completely dried by speed-vac. Next, gel pieces were rehydrated with 50 mM NH_4HCO_3 containing 12.5 ng $µl^{-1}$ modified sequencing-

grade trypsin (Promega) at 4ºC. After 45 min, the trypsin solution was removed and replaced with 50 mM NH_4HCO_3 to just cover the gel pieces. Samples were then placed in a 37ºC room O/N. Peptides were later extracted by removing the NH_4HCO_3 solution, followed by 1 wash with 50% acetonitrile, 1% formic acid solution and then dried by speed-vac. Samples were then stored at 4ºC until analysis. For SILAC experiments, gel bands were incubated with 1 mM DTT in 50 mM NH_4HCO_3 for 30 min at 60ºC. Next, the samples were cooled to RT and iodoacetamide was added to 5 mM. Samples were incubated at RT in the dark for 15 min and DTT (5 mM) was added to quench the reaction. Next, 5 ng μL^{-1} of sequence grade trypsin was added and samples were digested overnight at 37ºC. The samples were desalted by an in-house made desalting column the following day.

On the day of analysis, the samples were reconstituted in 5-10 µl of HPLC solvent A (2.5% acetonitrile, 0.1% formic acid). A nano-scale reverse-phase HPLC capillary column was created by packing 2.6 µm C18 spherical silica beads into a fused silica capillary (100 µm inner diameter x ~30 cm length) with a flame-drawn tip (Peng and Gygi, 2001). After equilibrating the column each sample was loaded via a Famos auto sampler (LC Packings) onto the column. A gradient was formed, and peptides were eluted with increasing concentrations of solvent B (97.5% acetonitrile, 0.1% formic acid).

As peptides eluted, they were subjected to electrospray ionization and then entered into an LTQ Orbitrap Velos Pro ion-trap mass spectrometer (Thermo). Peptides were detected, isolated, and fragmented to produce a tandem mass

spectrum of specific fragment ions for each peptide. Peptide sequences were determined by matching protein databases with the acquired fragmentation pattern by the software program, Sequest (Thermo) (Eng et al., 1994). For SILAC experiments, each dataset was searched with light and heavy parameters. For the heavy search, differential modifications on lysine (+8.0141988132 Da) and arginine (+10.0082685996 Da) were specified. All databases include a reversed version of all the sequences and the data was filtered to between a one and two percent peptide false discovery rate.

For label-free samples, carryover and common contaminants (human keratins and trypsin) were removed and peptides with a ΔCn value $\geq$ 0.08 and minimum XCorr values of 1.8, 2.0, 3.0, and 4.0 for single-, double-, triple-, and quadruple-charged spectra were retained. Next, identified proteins from the “Experimental” (20 μM mipATP alone) sample were compared to the proteins from the “Competition” (20 μM mipATP + 2 mM ATP) sample. The identified peptide intensity sum for each protein in both samples was calculated and the experimental to competition ratios were determined. Proteins with a peptide intensity sum ratio $\geq$ 4.5 were retained. Next, proteins with less than at least 1.5x more total peptides in the experimental sample compared to the competition were filtered out. Finally, proteins with at least 2 total peptides in the experimental sample were retained.

For SILAC samples, carryover and common contaminants were removed. For each protein, the median values of the identified isotypically ‘heavy’ peptide intensities and isotypically ‘light’ peptide intensities were determined. Next, for each screen, the sum value of the median ‘heavy’ peptide intensities and the sum

value of the median ‘light’ peptide intensities for all identified proteins were calculated. For the “forward” SILAC screen, the ratio of the sum of all ‘heavy’ signals to the sum of all ‘light’ signals was calculated to be 1.27. A “corrected median ‘light’ peptide intensity” for each identified protein was calculated by multiplying the median ‘light’ peptide intensity of the protein by 1.27. The final “forward” SILAC ratio of each identified protein is the ratio of the median ‘heavy’ peptide intensity to the “corrected median ‘light’ peptide intensity”. For the “reverse” SILAC screen, the ratio of the sum of all ‘light’ signals to the sum of all ‘heavy’ signals was calculated to be 1.13. A “corrected median ‘light’ peptide intensity” for each identified protein was determined by dividing the median ‘light’ peptide intensity of each identified protein by 1.13. The final “reverse” SILAC ratio of each identified protein is the ratio of the “corrected median ‘light’ peptide intensity” to the median ‘heavy’ peptide intensity. Next, for both “forward” and “reverse” SILAC experiments, only proteins represented by at least 3 total peptides were retained. Proteins identified in the “forward” and “reverse” SILAC screens were ranked as high confidence ATP-binders based on the value of their SILAC ratios, as described above. In each screen, proteins in the 90^{th} percentile based on SILAC ratios were identified and listed as high confidence ATP interactors. For Figure 3.5D, only proteins identified in both screens were retained and the Log_2 values of the median SILAC ratios were plotted.

For figure 3C, proteins enriched in each of the three proteomic screens were compared. Briefly, the 222 proteins identified as high confidence ATP binders in the label-free MS screen were compared to proteins found in the 90^{th} percentile of

the “forward” SILAC screen and proteins found in the 90th percentile of the “reverse” SILAC screen. Proteins found to be high confidence ATP binders in at least two of the three screens were identified (73 total). Next, we screened the 73 identified proteins for their frequency in the CRAPome database. Proteins found at a high frequency in the CRAPome (>5%) were filtered out. Next, the remaining unfiltered proteins were compared to lists of identified proteins from similar MS screens (Niphakis et al., 2015; Parker et al., 2017a). All proteins that were found in either of these screens were filtered out as low priority hits. The remaining unfiltered 32 proteins were considered high confidence mipATP binders.

ATPase activity detection

A549 cell membranes were isolated as described above. 100 µg of isolated membrane at a final of 1 mg mL^{-1} in BB (150 mM NaCl, 20 mM HEPES pH 7.4, 2 mM $CaCl_2$, 2 mM $MgCl_2$ + EDTA-free protease inhibitors) was incubated with 100 µM ATP for 30 min at 0, 4, or 37°C. For membrane protein-less samples, 100 µM ATP in BB was incubated for 30 min at the indicated temperature. ATPase activity detection was performed using the Luminescent ATP Detection Assay Kit (Abcam; #ab113849) following the manufacturer’s instructions. Luminescence counts from 10% of each sample were measured and ATP concentrations were quantified using an ATP standard curve.

Gene Ontology (GO) enrichment analysis

GO Molecular Function enrichment analysis was done using the PANTHER version 14.1 Overrepresentation Test (Mi et al., 2019). The GO Ontology database used was released on 2019-07-03. The reference gene list for each test used was the entire *Homo sapiens* gene list in the GO Ontology database. All p values were determined using Fisher's Exact Test and Bonferroni corrected.

Statistics

Data points represent mean ± SEM or mean ± SD as indicated in the figure legends. All p values have been derived by an unpaired two-tailed t test assuming unequal variances using Prism (Welch's t test) and MATLAB. Significance was assumed with *p<0.05; **p<0.005; ***p<0.0005; ****p<0.0001; *****p<0.00005.

Chapter 4

General zebrafish procedures

Casper background (White et al., 2008) wild-type and transgenic zebrafish larvae strains were maintained as described (2002)) with the approval of the Institutional Animal Care and Use Committee (IACUC). Zebrafish larvae were raised in E3 medium (5 mM NaCl, 0.17 mM KCl, 0.33 mM $CaCl_2$, and 0.33 mM $MgSO_4$). For wounding and tail fin tip amputation assays 2.5-4 dpf larvae were anesthetized in E3 medium containing 0.2 mg mL^{-1} ethyl 3-aminobenzoate methanesulfonate (tricaine, Sigma). The following previously described transgenic lines were used: TG(*krt4*:AKT-PH-GFP), TG(*krt4*:AKT-PH-mKate2), TG(*ΔNp63*:Gal4; *UAS*:GFP),

and TG(*hsp70l*:GCaMP6s-3xNLS-P2A-mKate2-3xNLS) (Enyedi et al., 2016; Gault et al., 2014).

Epidermal cell sorting and RNA purification for mRNA sequencing

Basal and suprabasal cell sorting was performed by disaggregating ~200 TG(*ΔNp63*:Gal4; *UAS*:GFP) and TG(*krt4*:PH-AKT-GFP; *krt4*:PH-AKT-mKate2) 2.5-3 dpf larvae, respectively, into single cell suspensions as described previously (Gault et al., 2014). Briefly, anesthetized larvae (0.2 mg mL^{-1} tricaine (Sigma)) were dissociated using Liberase TM (Roche) for 15 minutes at 32 °C and disrupted mechanically with a pestle. Cell suspensions were passed through a 40 μm nylon mesh and washed twice in FACs buffer and stained with DAPI to label damaged cells (centrifugation at 250 *g* for 5 min). Cell sorting of GFP+ basal and GFP+/mKate2+ suprabasal epithelial cells was performed by FACs (Aria III, BD) using 488 nm excitation and 530/30 nm emission wavelengths for GFP and 561 nm and 670/14 nm emission wavelengths for mKate2. RNA was isolated using the Quick-RNA™ Miniprep Kit (Zymo Research; R1054) according to the manufacturer's instructions. For whole larvae, 2.5-3 dpf Casper WT larvae were dissociated and RNA was isolated from the entire cell mixture. RNA samples were submitted to the MSKCC Genomics and Bioinformatics core facilities for mRNA sequencing analysis as previously described (Huang and Niethammer, 2018; Stoddard et al., 2019).

mRNA preparation, injection, and basal epidermal specific labeling

pCS2+ AKT-PH-GFP and pCS2+ AKT-PH-mKate2 (Gault et al., 2014) were linearized and *in vitro* transcribed using the mMessage mMachine SP6 kit according to the manufacturer's instructions (Invitrogen). 0.5-1 ng of *in vitro* transcribed mRNA was injected into the yolk of one-cell stage embryos to ubiquitously label plasma membranes for the *p2ry2*$^{-/-}$ and *p2ry11*$^{-/-}$ tissue motion experiments (Figure 4.7). Labeling of plasma membranes in the basal cell layer was achieved by mosaic expression of AKT-PH-mKate2 as previously described (Gault et al., 2014). Briefly, AKT-PH-mKate2 mRNA (0.5-1 ng) was injected into the yolk of 4-8 cell stage TG(*krt4*:AKT-PH-GFP) embryos. 2.5-3 dpf larvae with strong mosaic expression in the tail fin were selected for experiments.

Confocal imaging, laser wounding, and tail fin tip amputation

For UV-laser injury shifting experiments (Figures 4.2, 4.7-4.13), anesthetized 3 dpf TG(*krt4*:AKT-PH-GFP) or TG(*krt4*:AKT-PH-mKate2) transgenic larvae were first acclimated to isotonic (Iso) E3 medium (E3 medium supplemented with 140 mM NaCl) by three consecutive washes with 1 mL of Iso + tricaine. Next, larvae were embedded in 50-100 µL of 1% low-melting agarose dissolved in Iso medium. After solidification the samples were mounted on the microscope and wounds were induced by several quick successive laser pulses (3-4 pulses) using a microscope-mounted 435 nm UV MicroPoint laser (Andor). Laser cutting generated triangular wounds on the tip of the tail fin (Figure 4.2). Imaging started immediately after injury. After acquisition of the 9 minute 30 second timepoint, a bolus of hypotonic E3 (Hypo; normal E3 medium) or Iso medium supplemented with the indicated

concentration of compounds was added to the imaging dish (at least 10x agarose pad equivalent volume). 5 mM of nucleotide derivative was used for shifting experiments unless otherwise indicated. Images were acquired for another 30 minutes after the shift.

For tail fin tip amputation shifting experiments (Figure 4.5), anesthetized 3 dpf TG(*krt4*:AKT-PH-GFP) larvae were acclimated to Iso medium and tail fin tips were amputated with a needle knife (Fine Science Tools) on a glass petri dish. Next, larvae were embedded in 50-100 µL of 1% low-melting agarose dissolved in Iso medium. After solidification, samples were mounted on the microscope to begin imaging. After acquisition of the 2 minute 30 second timepoint, a bolus of Hypo or Iso medium was added to the imaging dish (at least 10x agarose pad equivalent volume). Images were acquired for another 30 minutes after the shift.

For Ca^{2+} imaging experiments (Figure 4.6), 2.5 dpf TG(*hsp70l*:GCaMP6s-3xNLS-P2A-mKate2-3xNLS) were first heat shocked at 37 °C for 2 hours to induce expression of the reporters and imaged 8-12 hours later. Just prior to laser wounding, anesthetized 3 dpf larvae were embedded in 50-100 µL of 1% low-melting agarose dissolved in Hypo medium. Wounding was induced with quick successive laser pulses (3-4) at ~1 min using a microscope-mounted 435 nm UV MicroPoint laser (Andor).

Experiments were performed at RT (~26°C) on a Nikon Eclipse FN1 microscope equipped with a 25x Apochromat LWD NA 1.1 water immersion objective lens, a Yokogawa CSU-X1 Spinning Disk unit, an Andor iXon3 897 EMCCD camera, and 488 nm and 561 nm diode laser lines (Andor Revolution XD). GCaMP6s and GFP

fluorescence were excited using the 488 nm laser line and emission was collected using a 535/20 bandpass filter (Chroma). mKate2 (mK2) fluorescence was excited using the 561 nm laser line and emission was collected using a 620/30 bandpass filter (Chroma). GCaMP6s and mK2 image acquisition was done simultaneously through triggered excitation and emission collection. Up to 30 Z-stack slices with a resolution of 3 μm were acquired per field of view with the NIS-Elements software (Nikon). Images were acquired every 30 sec for periods of 40 min and 33 min for the laser cut and tail fin amputation tissue motion experiments, respectively. For Ca^{2+} imaging experiments, images were acquired every 10 seconds for a period of 10 minutes.

Reagents

The following nucleoside and nucleotide derivatives were used at a final concentration of 5 mM in isotonic E3 medium unless otherwise stated in the text: ATP (Sigma; A26209), ATPγS (Tocris; 4080), AMP-PNP (Sigma; A2647), AMP-PCP (Sigma; M7510), ADPβS (Sigma; A8016), ADP (Sigma; A2754), BzATP (Sigma; B6396), AMP (Sigma; A1752), adenosine (Sigma, A9251), UTP (Sigma, U6625), 2-MeSADP (Tocris; 1624), 2-MeSATP (Tocris; 1062), AMP-CPP (Sigma; M6517), AP_4A (Sigma; D1262), CTP (Sigma; C1506), GTP (Sigma; G8877), ITP (Sigma; I0879), 3'-O-methyl-ATP (Trilink; N-1056), 2'-O-methyl-ATP (Trilink), 3'-dATP (Trilink; N-3001), N1-methyl-ATP (Trilink), 2-amino-ATP (Trilink), N^6-Methyl-Amino-ATP (Trilink; N-1083), N^6-Methyl-ATP (Trilink; N-1013), N^6-propargyl ATP (Jena; CLK-NU-001), N^6-benzyl ATP (Jena; NU-1196S), 6-AB-ATP (BIOLOG;

A074), 8-azido ATP (Trilink; N-1052), Puromycin-TP (Trilink; N-1022), 2'-O-Methyl-2-amino ATP (Trilink; N-1040).

Global velocimetry analysis

Velocimetry analysis of epithelial tissue motion was conducted as previously described (Gault et al., 2014). Briefly, confocal time-lapse stacks were z-projected (maximum-intensity projection), convoluted (3 × 3 × 1 matrix, Fiji "Convolve" command), background subtracted, and contrast enhanced in Fiji (Schindelin et al., 2012). Shifting experiments typically caused unspecific bulk movements of the specimens due to liquid addition. To eliminate velocity components caused by unspecific bulk movements, time-lapse stacks were registered ("StackReg→Rigid Body" command; Fiji) before analysis. Tissue velocities were measured by calculating particle motion between subsequent frames of the time lapse using MATLAB (R2014a, R2018a; MathWorks) with the open source PIV analysis software PIVlab v1.34 (developed by W. Thielicke and E.J Stamhuis). In brief, the program split each frame into 63 × 63 interrogation windows for which the respective displacement vectors between subsequent frames were calculated, yielding a 63 × 63 velocity vector matrix that was masked to eliminate regions of low image intensity. The magnitudes of the velocity vectors (|v|) in the unmasked field of view were averaged at each time frame to generate global velocity as a function of time.

Image processing and data analysis of nuclear Ca^{2+} signals in zebrafish larvae

Ca^{2+} signaling images were processed as previously described (Enyedi et al., 2016). Briefly, image processing tasks were performed in the open-source program Fiji and the Anaconda distribution of the Python programming language, using custom scripts, based on the pandas, SciPy, NumPy, and scikit-image libraries. To quantify nuclear Ca^{2+} signal intensity, confocal time-lapse stacks of GCaMP6s and mKate2 were z-projected (maximum-intensity projection), background corrected and thresholded in Fiji. Next, ratio images (GCaMP6s/mKate2) were calculated using Fiji. The ratio value of every pixel was then remapped using a custom Python script, to express them as a function of a binned distance (2 μm) from the moving wound margin. These spatiotemporal maps of the average Ca^{2+} signals were then averaged over multiple experiments.

Morpholino injections

One-cell stage larvae were injected with 2.3 nL of translation blocking morpholino (Gene Tools) diluted in water:

p2ry2.1 Tx MO: 5'-TCGTGATCCAGATATAGATACTTTC-3' (0.5 mM & 1 mM), *p2ry11* Tx MO: 5'-TGCATAAACTGTCGTTCTTCATCTC-3' (1 mM)

$p2ry2.1^{-/-}$ and $p2ry11^{-/-}$ (KO) zebrafish generation

Two *p2ry2.1* single guide RNAs (sgRNAs) targeting the following 20 base pair sequences, *p2ry2.1* gRNA1: 5'-ATTGGACCATCGCCAACACC-3' and *p2ry2.1* gRNA2: 5'-AGCACGACGGGCATTCGTCC-3', were selected from a predesigned list of *p2ry2.1* targeting sgRNA's generated by a propriety algorithm from

Integrated DNA Technologies (IDT) and were ordered as Alt-R® CRISPR-Cas9 crRNAs from IDT. The two *p2ry2.1* ALT-R® crRNAs and tracrRNA (IDT; #1072532) were solubilized in Nuclease Free IDTE pH 7.5 solution (IDT; #11-01-02-02) to final concentrations of 100 µM each. The solubilized *p2ry2.1* crRNAs were separately mixed with tracrRNA in IDT Nuclease Free Duplex Buffer (IDT; #11-01-03-01) to final concentrations of 3 µM each. The mixtures were subsequently heated at 95 °C for 5 minutes, removed from heat, and allowed to cool to RT on the bench top to form the gRNA solutions. ALT-R® S.p. Cas9 Nuclease (IDT; #1081058) was diluted to 1 mg mL^{-1} in 150 mM KCl, 20 mM HEPES pH 7.5 solution.

A *p2ry11* targeting sgRNA was generated using the protocol developed by Gagnon and colleagues (Gagnon et al., 2014). A 20 base pair *p2ry11* specific targeting sequence (5'-GGCAAATATATTGCCCAGCA-3') was selected using CHOPCHOP (https://chopchop.cbu.uib.no) (Labun et al., 2016). To generate a template for sgRNA transcription, a gene-specific oligonucleotide containing the SP6 (5'-ATTTAGGTGACACTATA-3') promoter sequence, the 20 base target sequence, and a complementary region was annealed to a constant oligonucleotide encoding the reverse complement of the tracrRNA tail. *p2ry11*-specific oligonucleotide: 5'-ATTTAGGTGACACTATAGGCAAATATATTGCCCAGCAGTTTTAGAGCTAGAAATAGCAAG-3', constant oligonucleotide: 5'-AAAAGCACCGACTCGGTGCCACTTTTTCAAGTTGATAACGGACTAGCCTTATTTTAACTTGCTATTTCTAGCTCTAAAAC-3'. After annealing the two oligonucleotides, the ssDNA overhangs were filled in with T4 DNA polymerase

(NEB), and the resulting sgRNA template was purified using a Qiaquick column. The sgRNA was transcribed using the MEGAscript™ SP6 kit (Invitrogen; AM1330), DNase treated, and precipitated with 3 M ammonium acetate/ 70% ethanol. The sgRNA was solubilized in H_2O (~200-400 ng μL^{-1}).

ALT-R® S.p. Cas9 Nuclease (IDT; #1081058) was diluted to 1 mg mL^{-1} in 150 mM KCl, 20 mM HEPES pH 7.5 solution. Prior to injection, Cas9-gRNA ribonucleoprotein (RNP) complexes were assembled by combining the gRNA and Cas9 protein solutions 1:1 (v/v), then incubating at 37 °C for 10 minutes and allowing the mixtures to cool to RT on the bench top. 2.3 nL of each Cas9-gRNA RNP complex solution was subsequently injected into the cytoplasm of one-cell stage *casper* zebrafish embryos and injected F0 larvae were grown to sexual maturity (2-3 months post fertilization). Individual F0 adults were crossed to wild type *casper* zebrafish and F1 progeny were collected. At 2-3 days post fertilization (dpf) genomic DNA (gDNA) was isolated from 4-6 individual F1 larvae for genotyping. Briefly, euthanized 2-3 dpf were separately suspended in 100 µL of 50 mM NaOH and incubated at 95 °C for 10 minutes. Samples were then cooled on ice, neutralized with 10 µL of 1 M Tris-HCl pH 8 and centrifuged at 16,000 *g* to remove debris.

The *p2ry2.1* and *p2ry11* sequences of interest were PCR amplified from the gDNA samples with the following primers designed using CHOPCHOP: *p2ry2.1* gRNA fwd: (5'-TGACACGCTCTACATCCTCACT-3'), *p2ry2.1* gRNA1 rev: (5'-GTTGAAGGTGGTTTCTTTCCAG-3'), *p2ry2.1* gRNA2 rev: (5'-ACCTGTTTATCCAGGTAGCGAA-3'), *p2ry11* gRNA fwd: (5'-

GTGCGTTAATTTAGCCAGTTCC-3'), *p2ry11* gRNA rev: (5'-TTATCTTTGCAAGAGACGCAAA-3'). Next, PCR products were incubated with a selected restriction enzyme (PflmI for *p2ry2.1* gRNA1, Mva1269I for *p2ry2.1* gRNA2, BseYI for *p2ry11* gRNA) for ~2 hours at 37 °C and then samples were separated by agarose gel electrophoresis. F1 heterozygous larvae were identified by the presence of three double stranded DNA products; *p2ry2.1* gRNA1: 768, 449, and 319 bp; *p2ry2.1* gRNA2: 594, 386, and 208 bp; *p2ry11* gRNA: 781, 440, and 341 bp. F1 homozygous wild type larvae were identified by the presence of only the two smaller restriction products, indicating complete digests of the amplified wild type alleles by the respective restriction enzymes. F0 KO founder adults were identified by the presence of F1 heterozygous progeny. Once an F0 KO founder adult was identified, the fish was again crossed to a wild type *casper*. At 3 dpf, progeny tail fin tips were amputated, and genomic DNA was isolated by suspending the tail fin tip in 20 µL of 50 mM NaOH then heating at 95 °C for 10 minutes. Samples were then cooled on ice, neutralized with 2 µL of 1 M Tris-HCl pH 8, and centrifuged at 16,000 *g* to remove debris. Genotyping was conducted by PCR amplification followed by restriction enzyme digest. Heterozygous F1 larvae were identified and grown to sexual maturity. F1 adults were tail fin clipped to isolate gDNA and the mutated alleles were sequenced by Sanger sequencing. For the *p2ry2.1* gRNAs, F1 heterozygous male and female adults containing the frameshift mutation of interest (2 bp deletion for gRNA1 and 4 bp deletion for gRNA2; see Figure 4.4) were crossed to generate F2 homozygous mutant *p2ry2.1* progeny (*p2ry2.1* $^{-/-}$). For Figure 4.7D an F1 *p2ry11*$^{+/-}$ male with a 2 bp deletion was

crossed with an F1 *p2ry11*$^{+/-}$ female with a 1 bp insertion and all animals were genotyped by PCR coupled to restriction enzyme digest after completion of imaging.

F0 crispant zebrafish generation

In F0 crispant experiments, two separate Cas9-gRNA RNPs targeting the gene of interest were mixed 1:1 (v/v) and 2.3 nL was injected into one-cell stage embryos. All sgRNAs used for crispant screens were designed by IDT and purchased as ALT-R® crRNAs. Cas9-gRNA RNPs were formed prior to injection as described above in "*p2ry2.1 and p2ry11 knockout zebrafish generation*". For *p2ry2.1* (Figure 4.7B), the above described sgRNAs were used. For *p2ry4* (Figure 4.9) and *p2rx1* (Figure 4.8) crispant experiments the following 20 bp target sequences were used: *p2ry4* sgRNA1: 5'-GAGGCCTTGGAAACCCAGTA-3', *p2ry4* sgRNA2: 5'-CGGACTAATCCTTAACTCTG-3', *p2rx1* sgRNA1: 5'-TGAATATGAGACTCCTCGGG-3', *p2rx1* sgRNA2: 5'-GGCGTTTTAGCCTACATCAT-3'.

The following primers were used for PCR analysis: *p2ry2.1* gRNA fwd, *p2ry2.1* gRNA2 rev, *p2ry4* gRNA fwd: 5'-TTCTGCCCGTTTCATATTCC-3', *p2ry4* gRNA rev: 5'-ACAGAGGACAACGCCAAAAG-3', *p2rx1* gRNA fwd: 5'-GGACGTCTCAAGAACACTGTGA-3', *p2rx1* gRNA rev: 5'-CATGCTCTGTTCAGTTTCTCGT-3'.

Statistics

All data points represent mean ± SEM of (n) number of biological replicates as indicated in the figure legends.

Chapter 5

General zebrafish procedures

Casper background (White et al., 2008) wild-type and transgenic zebrafish larvae strains were maintained as described (2002) with the approval of the Institutional Animal Care and Use Committee (IACUC). Zebrafish larvae were raised in E3 medium (5 mM NaCl, 0.17 mM KCl, 0.33 mM $CaCl_2$, and 0.33 mM $MgSO_4$). For wounding and tail fin tip amputation assays 2.5-4 dpf larvae were anesthetized in E3 medium containing 0.2 mg mL^{-1} ethyl 3-aminobenzoate methanesulfonate (tricaine, Sigma). The following previously described transgenic lines were used: TG(*krt4*:AKT-PH-GFP), and TG(*hsp70l*:GCaMP6s-3xNLS-P2A-mKate2-3xNLS) (Enyedi et al., 2016; Gault et al., 2014). The casper background TG(*flk*:RFP) reporter line was a gift from Dr. Richard M. White.

Confocal imaging

For UV laser injury experiments (Figure 5.1), anesthetized 3 dpf TG(*flk*:RFP; *krt4*:AKT-PH-GFP) transgenic larvae were immobilized on a plastic petri dish by embedding in ~50 µL of 1% low melting agarose dissolved in standard hypotonic E3 medium (Hypo) or isotonic E3 medium (Iso; E3 medium supplemented with 135 mM NaCl). UV-laser cut wounds were induced in the ventral tail fin fold under the caudal hematopoietic tissue with several quick successive pulses (3-4) using a microscope-mounted 435 nm UV MicroPoint laser (Andor).

For shifting experiments (Figures 5.2-5.5), anesthetized 3 dpf TG(*flk*:RFP) or heat shocked TG(*hsp70l*:GCaMP6s-3xNLS-P2A-mKate2-3xNLS) transgenic larvae were acclimated to Iso E3 medium and tail fin tips were amputated with a needle knife (Fine Science Tools) on a glass petri dish. Larvae were embedded in ~50 µL of 1% low-melting agarose dissolved in Iso medium, and for pharmacological inhibition experiments, supplemented with the indicated concentrations of inhibitor compounds. After solidification, samples were mounted on the microscope to begin imaging. At the 5 minute timepoint for vasodilation and 1 minute for Ca^{2+} signaling, a bolus of Hypo or Iso medium supplemented with the indicated concentration of compounds was added to the imaging dish (at least 10x agarose pad equivalent volume).

Confocal imaging was performed as described above in "Chapter 4: *Confocal imaging, laser wounding, and tail fin tip amputation"*. Up to 30 Z-stack slices with a resolution of 2 µm (vasodilation) or 3 µm (Ca^{2+} signaling) were acquired per field of view with the NIS-Elements software (Nikon). Images were acquired every 30 sec for periods of 40-45 min for vasodilation experiments and every 10 sec for periods of 20-25 min for Ca^{2+} signaling experiments.

Pharmacological treatments

Pharmacological inhibition was achieved by acclimating anesthetized larvae to Iso E3 (3 x 1 mL washes), amputating tail fin tips, then preincubating for 45-60 minutes in Iso E3 supplemented with the following compounds: 10, 50, and 100 µM ODQ (Tocris; 0880) or 100 µM suramin (Tocris; 1472). Mounting agarose and imaging

medium also contained the same concentration of the indicated compounds. 5 μM Arachidonic acid (Sigma; A3611), 5 mM ATP (Sigma; A26209), 5 mM UTP (Sigma; U6625), and 0.05 – 5 mM adenosine (Sigma; A9251) were added to Iso E3 shifting media and applied to the injured larvae at the indicated time of shift.

Zebrafish larvae vasodilation image processing and data analysis

For vasodilation imaging, confocal time-lapse stacks were z-projected (maximum-intensity projection), background subtracted, median filtered, and contrast enhanced in Fiji (Schindelin et al., 2012). Shifting experiments typically caused unspecific bulk movements of the specimens due to liquid addition. To eliminate unspecific bulk movements, time-lapse stacks were registered ("StackReg→Rigid Body" command; Fiji) before analysis.

2.5-3 dpf larvae have a small vessel (which will be referred to as the caudal vessel) that extends caudally from the caudal most end of the caudal artery (CA) as a single tube (Isogai et al., 2001). This vessel was used for analysis because its separation from other vessels allowed for precise diameter measurements without signal interference from other vessels. Also, this vessel is closest to the tail fin tip and can be accessed by the environmental medium during shifting experiments. The average caudal vessel diameter in pixels at each timepoint was calculated by averaging the diameter at 50-100 separate pixel length slices along the vessel using a custom MATLAB script (R2018a; MathWorks). For laser injury experiments, the "% change in vessel diameter" was obtained by calculating the percentage change in average vessel diameter at each timepoint compared to the

average vessel diameter at the first timepoint (Time = 0 min). For shifting experiments, the "% change in vessel diameter" was obtained by calculating the percentage change in average vessel diameter at each timepoint compared to the median average vessel diameter prior to the shift (the first 5 minutes of imaging). Percentage calculations were performed in Excel.

F0 crispant zebrafish generation

F0 crispant generation was conducted as described above in "Chapter 4: *F0 crispant zebrafish generation*". For *adora2aa, adora2b*, and *nos1* crispant experiments the following 20 bp target sequences were used: *adora2aa* sgRNA1: 5'-AGATACATGATCAGAGCCGG-3', *adora2aa* sgRNA2: 5'-CGCTTACAAGAGGGCCACAA-3', *adora2b* sgRNA1: 5'-GTACCAGAACGAAACAGGCC-3', *adora2b* sgRNA2: 5'-CACCAGCACATTACCGGCGA-3', *nos1* sgRNA1: 5'-ACGCGGGACTTCTCCTCAAT-3', and *nos1* sgRNA2: 5'-CCTTCCTATCGATGACCCTC-3.

The following primers were used for PCR analysis: *adora2aa* gRNA fwd: 5'-GTACAACAGCCTAGTAACCGGG-3', *adora2aa* gRNA rev: 5'-CCAAAATATGATAGCGGACGAT-3', *adora2b* gRNA fwd: 5'-TCTTTTGTCACTGGATGAGCAG-3', *adora2b* gRNA rev: 5'-ATATCTGTCTATGGCAACCGCT-3', *nos1* gRNA fwd: 5'-ACCTATCCTCTTCCTCCACTCC-3', *nos1* gRNA rev: 5'-GCATTAATGACATCCCTCACCT-3'.

mRNA sequencing analysis

mRNA sequencing results from Figures 5.3 and 5.5 are taken from the “Uninjected” samples from Huang et al., 2018. The “Uninjected” samples are mRNA from whole WT 3 dpf *casper* zebrafish larvae. The data was collected from three independent biological experiments. This data was retrieved from the Gene Expression Omnibus (GEO, NCBI) under the accession code GSE111528.

Statistics

All data points represent the mean ± SEM of (n) number of biological replicates as indicated in the figure legends.

CHAPTER 3 A photo-clickable ATP-mimetic reveals novel nucleotide interactors in the membrane proteome

Introduction

ATP drives cellular processes through the hydrolysis of its high energy phosphoanhydride bonds. ATP also acts non-catalytically at regulatory sites as an allosteric effector. Catalytic ATP-binding sites can be identified through highly conserved primary sequence and structural motifs, most notably the P-loop (Walker A) NTPase fold (Walker et al., 1982). There are also well-conserved allosteric ATP-binding sites, for instance, the cystathionine beta synthase domain found in AMP-activated protein kinase and inosine 5'-monophosphate dehydrogenase (Bateman, 1997; Zhang et al., 1999). Yet many non-catalytic ATP-binding sites follow unclear structural rules. For example, the ATP-binding sites of most G protein-coupled purinergic P2 receptors in animals remain unresolved because they lack classic ATP-binding motifs (Choi et al., 2014; Zhang et al., 2015, 2014). Such sites are difficult to predict by bioinformatics and must be experimentally identified. One example is the plant ATP receptor DORN1, which shows no sequence homology to known P2 receptors of animals (Choi et al., 2014). DORN1 was experimentally identified in a mutational screen that utilized Ca^{2+} responses as a functional readout for purinergic receptor activity.

However, in contrast to plants, about a dozen, known P2 receptors can trigger Ca^{2+} responses to ATP in animal cells. Identifying novel ATP receptors by gene perturbation and Ca^{2+} measurements amidst the large background of known

P2 receptors is challenging. In such situations, unbiased biochemical screens with functionalized ATP baits are a powerful tool, because they do not rely on pleiotropic functional readouts, and report on direct, physical interactions.

So far, different nucleotide resins and functionalized ATP probes have been used to identify ATP interactors from complex proteomes (Hanoulle et al., 2006; Ito et al., 2006; Mahajan et al., 2015; Patricelli et al., 2007). As previously discussed (Mahajan et al., 2015), site, size, and properties of the functional group(s) attached to ATP biases the interaction profile of the respective probe. Meaningful ATP-interaction profiles can only be expected if the probe design does not interfere with ATP's allosteric or enzymatic functions of interest. For example, N^6-modifications at the adenine base of ATP hinder probe-binding to protein kinase pockets, whereas modifications to ATP's γ-phosphate are well tolerated by kinases (Patricelli et al., 2007; Shah et al., 1997). Likewise, allosteric ATP-binders, such as P2 receptors, prefer certain ATP-modifications over others (Burnstock et al., 1994; Fischer et al., 1993). Large functional groups, such as biotin affinity tags (Mahajan et al., 2015), more likely alter ATP-binding than small ones; either by not fitting to small pockets, or by enabling non-physiological interactions through their additional hydrophobicity. By contrast, sterically compact additions containing a photo-crosslinking diazirine and a terminal alkyne allow for "click" chemistry-mediated conjugation with large affinity tags, such as biotin, after protein-probe complexes have formed. Thereby, the affinity tag cannot inhibit physiological nor promote non-physiological ATP interactions. Such probes are increasingly used in biochemical screens for small molecule targets (Li et al., 2013; Niphakis et al.,

2015; Parker et al., 2017a, 2017b), but have not yet been implemented to interrogate the ATP interactome.

This work describes the development and verification of a novel, minimally invasive photoaffinity ATP probe, mipATP, which mimics physiological signaling functions of extracellular, native ATP *in vitro* and *in vivo*, and specifically enriches for known and unknown ATP interacting proteins from membrane fractions of cultured A549 lung cancer cells.

Results

Design and verification of a novel, minimally invasive photoaffinity ATP probe

A subset of ATP-interacting membrane proteins, including P2Y purinergic receptors and various membrane transporters, are equally activated by, or even prefer N^6-substituted over native ATP (Burnstock et al., 1994; Fischer et al., 1993; Zhou et al., 2005). Their "N^6-tolerant" ATP binding sites structurally differ from classic protein kinase pockets (Shah et al., 1997), but except for P-loop motifs, they remain little characterized, and are thus hard to predict by bioinformatics. To systematically probe their abundancy, we functionalized ATP at its N^6 position with a sterically compact combination of a photoreactive diazirine and a terminal alkyne (Figure 3.1A). The linker stabilizes reversible protein-probe interactions by UV-crosslinking. Subsequent ligation with a biotin tag allows for affinity enrichment of ATP-protein complexes and protein identification by mass spectrometry (MS). Similar linkers were previously used to screen for fatty acid-protein interactions and targets of other small molecules (Li et al., 2013; Niphakis et al., 2015; Parker et al., 2017a, 2017b).

An important allosteric function of extracellular ATP is to trigger Ca^{2+} transients through G protein-coupled, purinergic receptor signaling (Garritsen et al., 1992; Lustig et al., 1993), which one can measure with genetically encoded biosensors, such as GCaMP6 (Chen et al., 2013). To confirm that our probe functionally reconstitutes allosteric interactions of native ATP, we measured ATP-induced Ca^{2+} transients in cells and animals. In A549 lung cancer cells and HeLa cells expressing a genetically encoded, nuclear-targeted GCaMP6 Ca^{2+} sensor,

addition of unmodified ATP and the N^6-modified probe to the cell supernatant led to similar Ca^{2+} transients (Figures 3.1B-E, & H), whereas the phosphate-modified ATP analogs ATPγS and AMP-PNP, caused little or no Ca^{2+} signaling (Figures 3.1B-C & F-H). *In vivo* experiments led to the same conclusion; when GCaMP6-expressing zebrafish larvae where perfused with ATP or its analogs through an open wound, the N^6-modified ATP probe evoked the same tissues patterns of Ca^{2+} fluxes as native ATP, while phosphate-modified analogs did not (Figure 3.2). We conclude that mipATP minimally interferes with ATP's allosteric ligand functions and is thus suited to search for underlying membrane protein interactions.

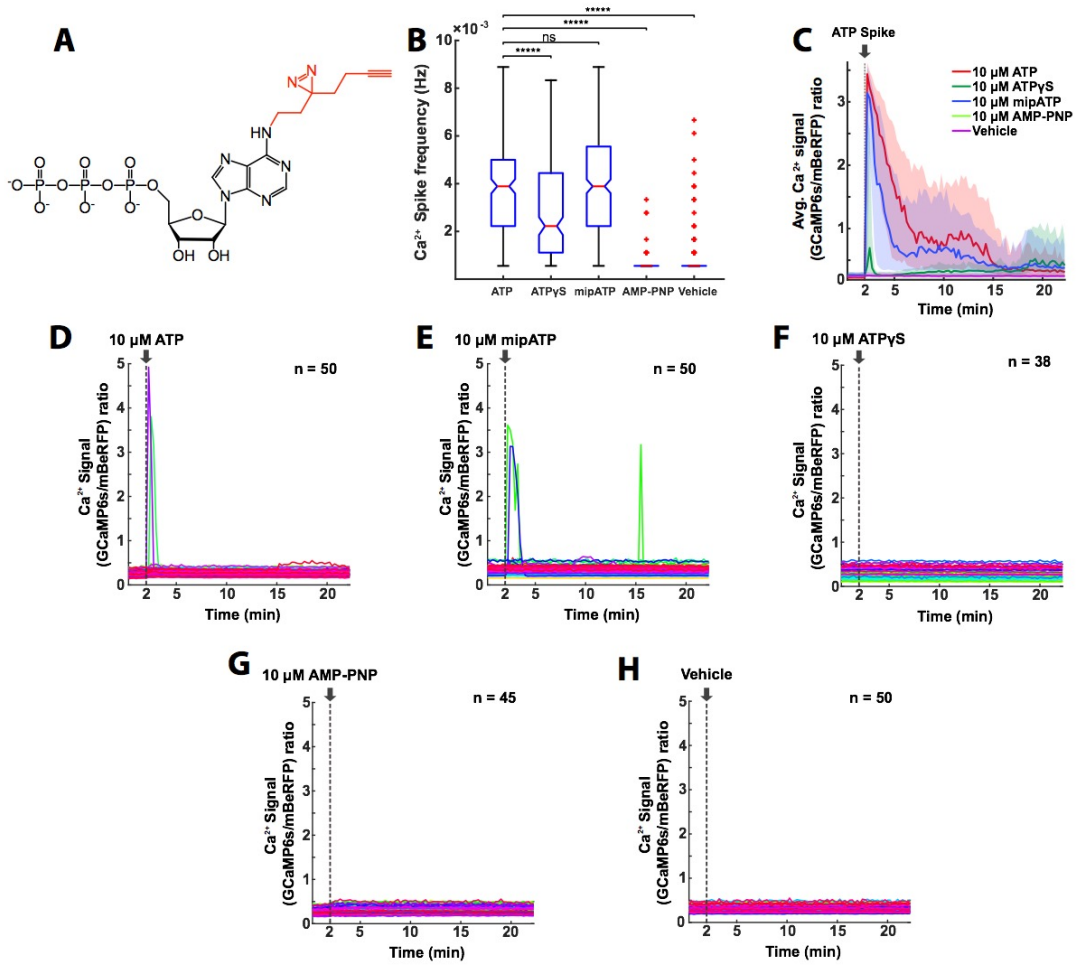

Figure 3.1. mipATP mimics ATP-triggered Ca^{2+} transients *in vitro*
(A) Structure of the minimally invasive photoaffinity ATP probe (mipATP). Minimalist photo-clickable handle highlighted in red. (B-C) Single cell measurements of extracellular ATP-mediated nuclear Ca^{2+} signals in HeLa cells expressing a nuclear targeted, ratiometric GCaMP6s transgene. (B) Boxplot indicating the median number of Ca^{2+} transients per cell over 20 minutes after exposure to 10 µM ATP or ATP derivative in HeLa cells expressing a GCaMP6s-3xNLS-P2A-mBeRFP-3xNLS transgene. Error bars extend to the most extreme datapoints. ***** $p < 0.00005$, unpaired t test. (C) Average Ca^{2+} signal of HeLa cells after exposure to 10 µM ATP or ATP analog as determined by the nuclear GCAMP6s/mBeRFP fluorescence ratio. Error bars indicate ± SEM of the following (n) number of cells per condition: ATP n=221, ATPγS n=198, mipATP n=336, AMP-PNP n=104, and Vehicle n=308. Data was compiled from at least two independent biological experiments for each nucleotide derivative. (D-H) Ca^{2+} transients from representative fields of A549 cells expressing genetically encoded GCaMP6s-3xNLS-P2A-mBeRFP-3xNLS after exposure to ATP or the indicated analog at 2 minutes into imaging. Each line represents the Ca^{2+} signal (GCaMP6s/mBeRFP ratio) of a single cell in the representative field of view over the time lapse. Fields are representative of at least three independent biological experiments for each nucleotide derivative.

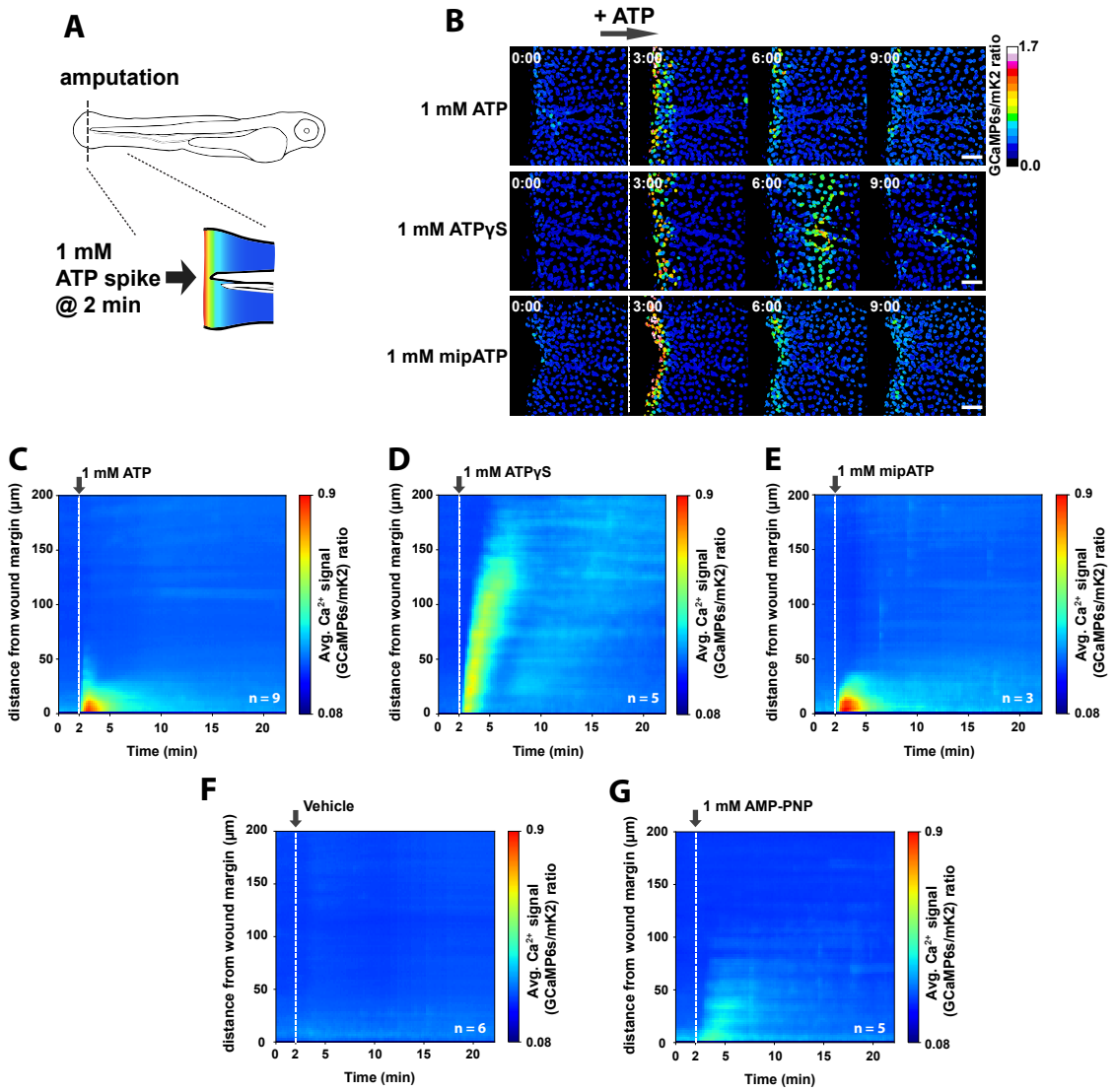

Figure 3.2. mipATP mimics ATP-triggered Ca^{2+} transients in live tissues
(A-B) Ratiometric imaging of ATP-mediated Ca^{2+} transients in zebrafish larvae tail fins. Left, scheme of experimental setup. Tail fin tips of 2.5-4 days post-fertilization (dpf) transgenic Ca^{2+} reporter zebrafish larvae TG(*krt4*:QF2; *QUAS*:GCaMP6s-3xNLS-P2A-mKate2-3xNLS) are amputated and a bolus of 1 mM ATP or ATP analog is applied to the injured larvae at 2 minutes into imaging. Right, ratiometric imaging of Ca^{2+} transients induced by perfusion of wounded tail fins with 1 mM ATP or ATP analog. Nuclear GCaMP6s signals are normalized by nuclear mK2 (mKate2) fluorescence. Scale bars, 50 μm. Time in minutes. (C-G) Average spatiotemporal Ca^{2+} signal profiles of the indicated number (n) of transgenic Ca^{2+} reporter larvae TG(*krt4*:QF2; *QUAS*:GCaMP6s-3xNLS-P2A-mKate2-3xNLS) after perfusion with 1 mM ATP or ATP analog at 2 minutes from the start of imaging.

mipATP competes with ATP for membrane protein binding

To test whether mipATP binds to ATP sites on proteins, we incubated total membrane fractions of A549 cells with varying concentrations of mipATP together or without competing, native ATP. Membrane bound ATPases rapidly hydrolyze ATP to generate ADP, AMP, and adenosine, which may complicate interpretation. Thus, experiments were performed at 4°C to suppress enzymatic (mip)ATP hydrolysis (Figure 3.3A).

After UV-crosslinking, membrane protein targets were conjugated to a fluorescent reporter tetramethylrhodamine (TAMRA) by click chemistry, separated by SDS-PAGE, and protein-linked mipATP complexes were visualized on the gel by fluorescence scanning (Figure 3.3B). UV-crosslinking was required for significant target enrichment, suggesting that the probe primarily reports on reversible ATP-protein interactions (Figure 3.3C). Binding was dose dependent, and densitometry analysis of representative gel bands approximated overall affinities in the low micromolar range (~5-20 μM), that is, within the physiological response range of known ATP receptors (Figure 3.3D) (Garritsen et al., 1992). Equimolar amounts of native ATP or ATPγS quenched mipATP-target interactions by half. Thus, mipATP binds target proteins with the same affinity as native ATP (Figures 3.3E-F).

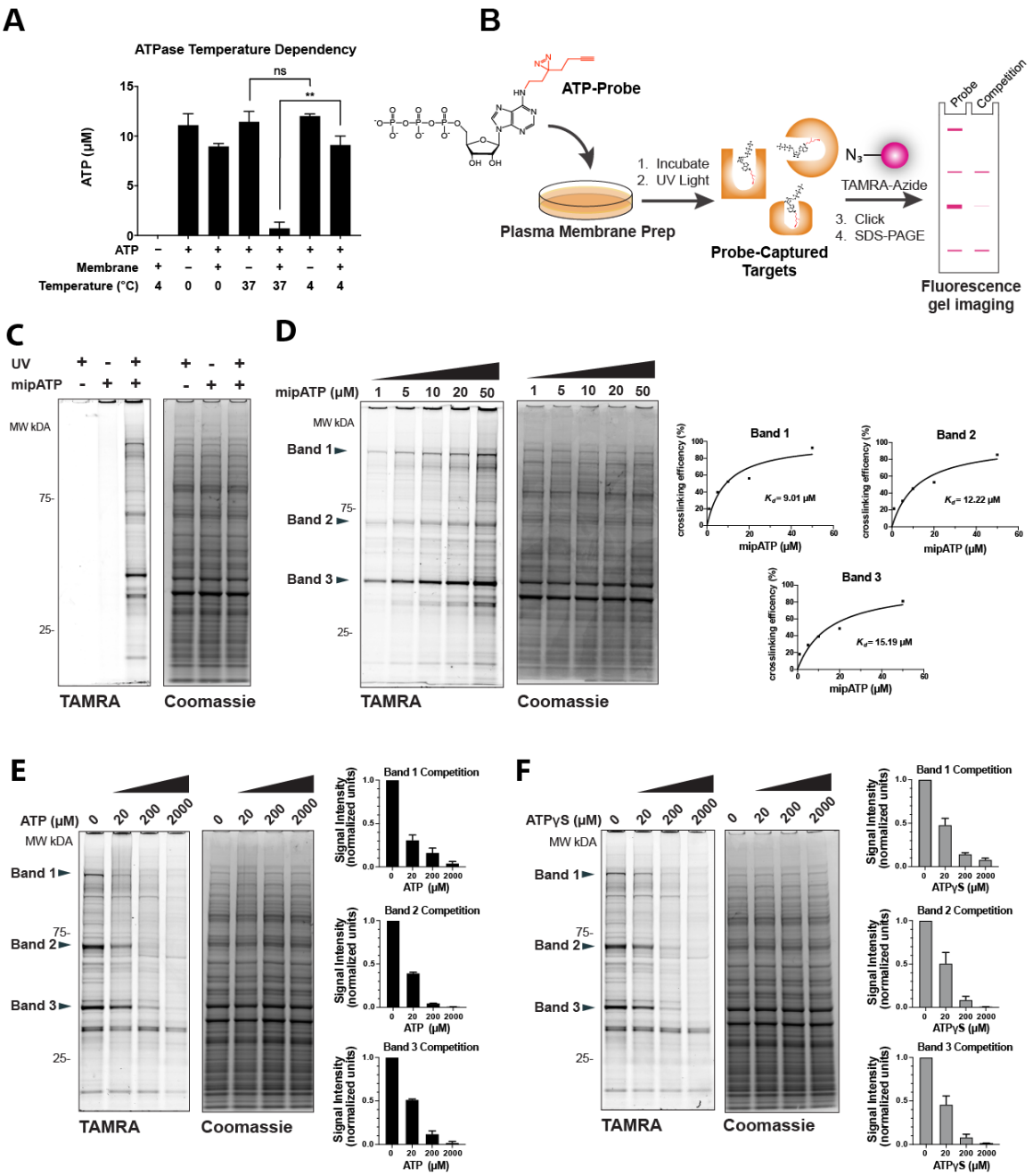

Figure 3.3. mipATP reversibly interacts with A549 cell membrane proteins
(A) 100 μM of exogenous ATP was incubated with A549 membranes at 0, 4, and 37°C and hydrolysis was monitored after 30 minutes. ATP was almost completely hydrolyzed after incubation with membranes at 37°C (n=3) while hydrolysis was stunted by incubation at 0°C and 4°C (n=2) in comparison. Values represent mean ± SEM. *p < 0.05, unpaired t-test. (B) Experimental schematic for labeling membrane fractions with mipATP for in-gel fluorescence analysis. (C) SDS-PAGE in-gel fluorescence scan and Coomassie stain of A549 cell membrane fractions incubated with 50 μM mipATP or vehicle and then exposed or not to 365 nm UV-irradiation prior to click chemistry with TAMRA-azide. Representative of two independent experiments. (D) Left panel, in-gel fluorescence scan and Coomassie stain of A549 membrane fractions incubated with increasing concentrations (1-50 μM) of mipATP. Samples were UV-irradiated prior to click chemistry with TAMRA-azide. Right

panel, analyses of photo-crosslinking efficiency of mipATP to the selected proteins based on TAMRA-fluorescence. K_d (95% CI); Band 1 K_d=9.01(0.72-82.57) μM, Band 2 K_d=12.22(0.83-164.6) μM, Band 3 K_d=15.19(1.35-265.9) μM. Representative of two independent experiments. (E-F) Left panels, in-gel fluorescence scans and Coomassie stains of A549 membrane fractions pre-incubated with increasing concentrations of unmodified ATP or ATPγS prior to treatment with 20 μM mipATP. Representative images are from two independent experiments. Right panels, analyses of selected protein (Bands 1-3) TAMRA-fluorescence intensities in the presence of the indicated amounts of ATP or ATPγS competitor normalized to the fluorescence intensity value of the band in the absence of the competitor. Values indicate the mean ± SEM of two independent experiments.

Label-free mass spectrometry (MS) profiles mipATP binders in isolated membrane fractions

The above results encouraged us to use mipATP to screen for N^6-tolerant ATP-interactors on membranes. First, we employed a label-free mass spectrometry (MS) strategy to search for protein interactors in total membrane fractions of homogenized A549 cells (Figure 3.4A). Second, we used "Stable Isotope Labeling with Amino acids in Cell culture" (SILAC) (Ong et al., 2002) MS to identify protein mipATP interactors on live A549 cells (Figure 3.5C). In both approaches, native ATP was used as competitive quencher of specific probe interactions.

Label-free MS revealed 222 specific ATP interactors in A549 total membrane fractions (Figures 3.4B-C and Table S1). According to Gene ontology (GO) and Uniprot database analyses, 123 of these proteins potentially recognize some structural element of the probe, e.g., its sugar, purine, or phosphate moiety (Ashburner et al., 2000; Mi et al., 2019; The Gene Ontology Consortium, 2019). The group contained 59 ATP, 26 DNA/RNA, 6 NAD^+/$NADP^+$, and 6 GTP binding proteins (Figure 3.4B). In addition, mipATP retrieved 99 previously unknown ATP binders.

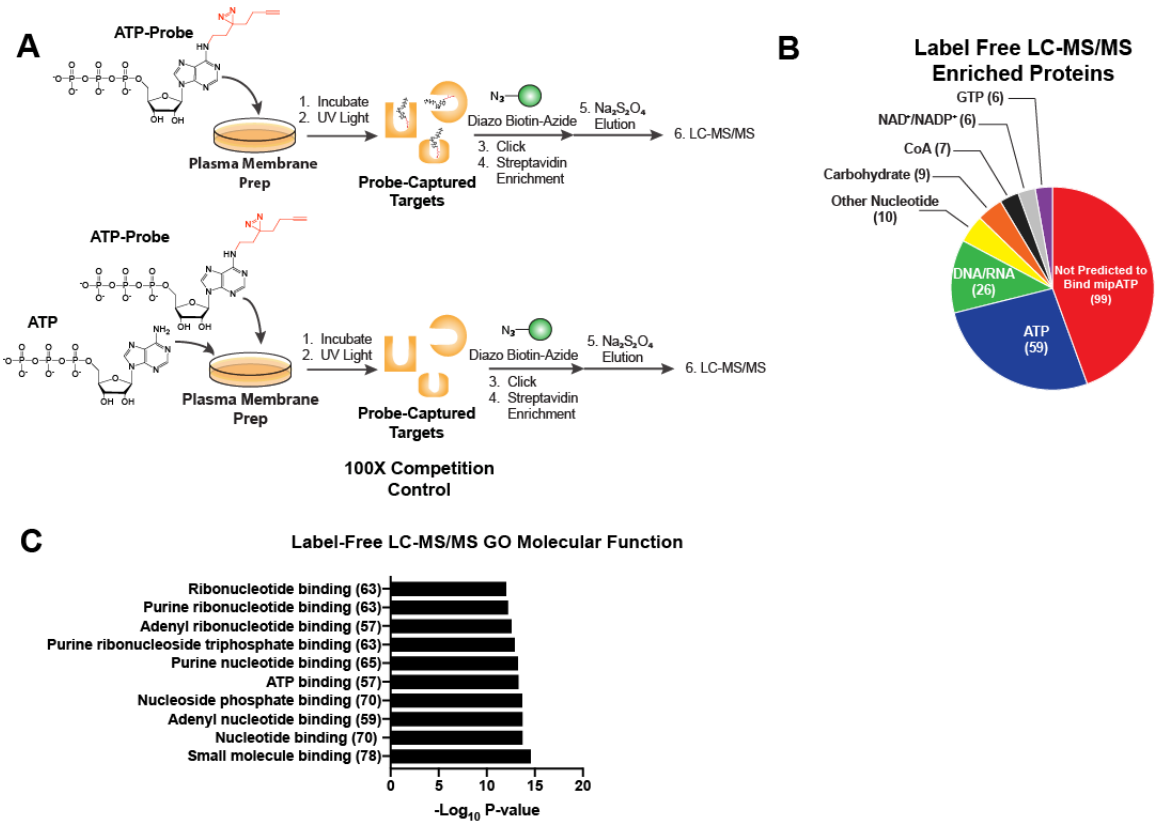

Figure 3.4. Label-free mass spectrometry profiles mipATP binders in isolated membrane fractions

(A) Experimental schematic for the identification of specific mipATP binders in A549 cell membrane fractions using label free LC/MS-MS analysis. A549 cell membranes were labeled with 20 μM mipATP alone or in the presence of excess (100x) ATP. Labeled proteins were conjugated to a biotin reporter via click chemistry, enriched by streptavidin agarose, and subsequently identified by LC-MS/MS. (B) Protein-mipATP interactions quenched by the presence of excess ATP were identified and classified by their predicted abilities to bind mipATP based on Gene Ontology (GO) and Uniprot Keyword analyses. Also see Table S1. (C) GO Molecular Function analysis of the enriched proteins shows that mipATP interacts with known nucleotide- and ATP-binding proteins. Analysis using PANTHER indicates the top ten GO Molecular Function terms from the enriched proteins as determined by Bonferroni corrected p-value (Ashburner et al., 2000; Mi et al., 2019; The Gene Ontology Consortium, 2019). Numbers in parenthesis indicate the number of mipATP-binding proteins in the respective category.

SILAC-based quantitative proteomics profiles mipATP binders on intact cells

To confirm and confine these hits with an orthogonal, quantitative SILAC MS approach, mipATP supplied in extracellular medium was UV-crosslinked onto intact A549 cells in suspension (Figure 3.5A-B). In a first, "forward" SILAC experiment, heavy isotope-labeled cells were probed with mipATP, whereas non-labeled cells were probed with mipATP and excess (100×) competing native ATP (Figure 3.5C). In a second, "reverse" SILAC experiment, the isotope labels were swapped between mipATP and mipATP + ATP samples (Li et al., 2012). We affinity-purified the crosslinked proteins from total A549 membrane fractions and combined them into one sample for ratiometric MS analysis. The resulting SILAC ratios are a measure of specific, that is, ATP-quenchable ATP-protein interactions. We ranked these ratios by percentile, and functionally classified hits within the 90^{th} percentile by functional clustering (Figures 3.5D-F and Table S2). The two inverted SILAC experiments overlapped on 47 likely ATP-binders, 32 of which were previously annotated to likely recognize some structural element of the probe. Those included 21 known ATP, 2 DNA/RNA, 4 NAD^+/$NADP^+$, and 1 GTP binding protein(s). 15 proteins were not previously described to bind to nucleotides (Figure 3.5D).

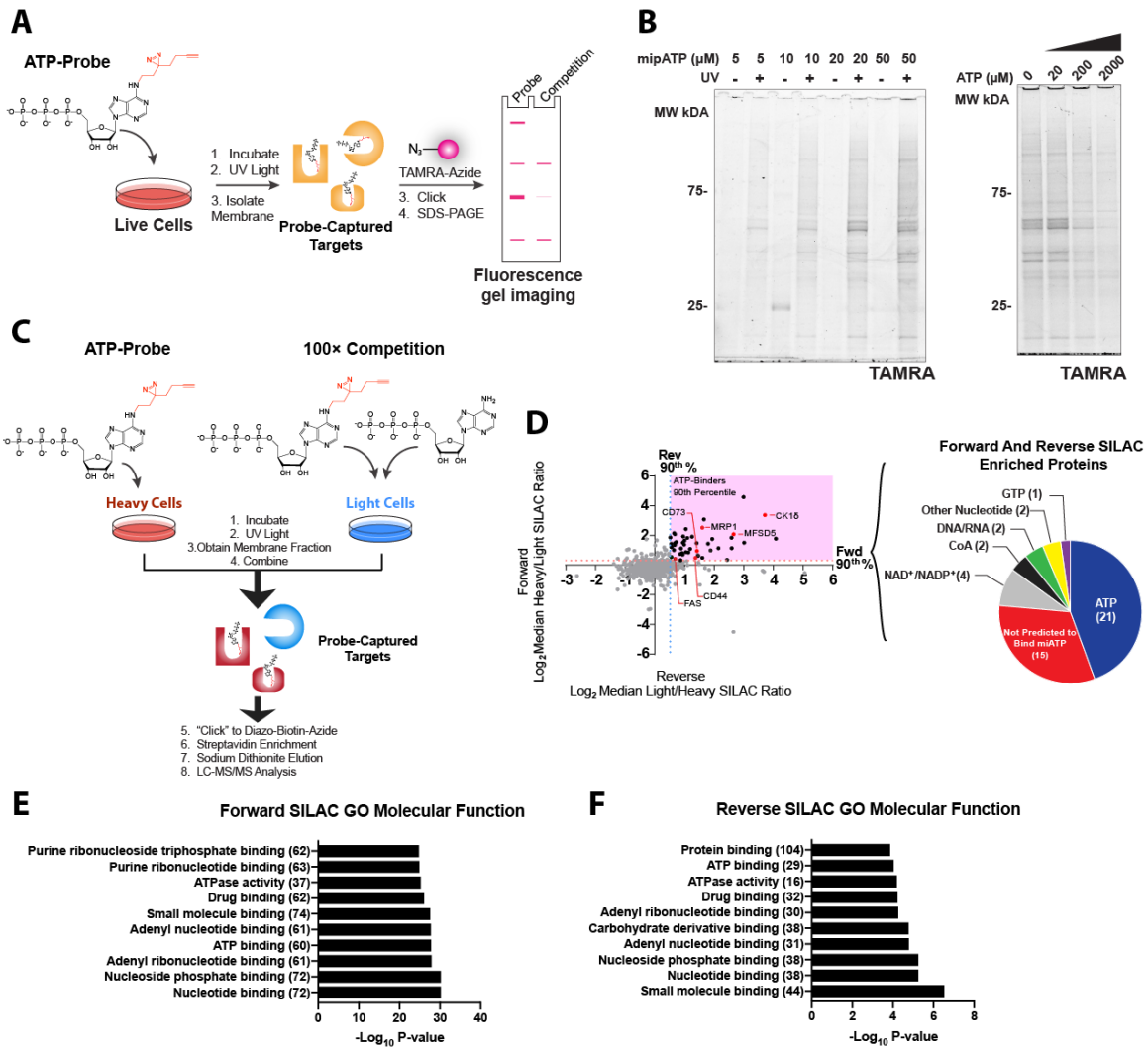

Figure 3.5. SILAC-based quantitative proteomics profiles mipATP binders on intact A549 cells

(A) Experimental schematic for labeling intact A549 cells with mipATP for in-gel fluorescence analysis. (B) Left, representative in-gel fluorescence scan of intact A549 cells incubated with increasing concentrations (5-50 μM) of mipATP. Samples were subsequently UV-irradiated or not prior to click chemistry with TAMRA-azide. 25 μg of each sample was loaded to the gel. Right, in-gel fluorescence scan of intact A549 cells pre-incubated (10 minutes) with increasing concentrations of ATP prior to treatment with 20 μM mipATP. Samples were UV-irradiated and subjected to click chemistry with TAMRA-azide. 25 μg of each sample was loaded to the gel. (C) Experimental schematic for the identification of mipATP binders on intact A549 cells using SILAC-based quantitative proteomics. (The forward screen is represented in the schematic). Isotopically labeled intact A549 cells were treated with 50 μM mipATP alone or in the presence of excess (100x) ATP and then UV-irradiated (365 nm). Probe labeled proteins were conjugated to a biotin reporter via click chemistry, enriched by streptavidin agarose, and identified by SILAC-based quantitative LC-MS/MS. Data are from two independent experiments (D) Protein-mipATP interactions quenched by the presence of excess ATP were identified by calculated SILAC ratios. Left, plot of the Log_2 values of the SILAC ratios for the proteins identified in the forward and reverse experiments. Proteins with SILAC

ratios in the 90th percentile of both the forward and reverse experiments are considered high confidence mipATP interactors and are located in the top right quadrant that is highlighted in a purple background. Also see Table S2. Right, classification of the high confidence mipATP interactors based on their predicted abilities to bind mipATP according to GO and Uniprot terms and keywords. The forward and reverse analyses are two independent biological experiments (E-F) GO Molecular Function analysis of proteins found in the 90th percentile of the forward and reverse SILAC experiments. Analysis using PANTHER indicates the top ten GO Molecular Function terms from the enriched proteins as determined by Bonferroni corrected p-value. Numbers in parenthesis indicate the number of mipATP-binding proteins in the respective category.

mipATP maps a novel ligand space in the membrane proteome

Combining all the data, 73 proteins showed ATP-quenchable mipATP-binding in at least two of the three MS experiments (label-free MS, forward & reverse SILAC) (Figure 3.6, Table S3). 47 of those were predicted ATP/nucleotide binders, leaving 26 previously unknown, potential novel ATP interactors. We ranked these hits according to their frequency of appearance in the Contaminant Repository for Affinity Purification (CRAPome), a database for common MS background artifacts (Mellacheruvu et al., 2013). Notably, 32 out of our 73 high confidence hits had previously come up in SILAC screens using different small molecule baits (Niphakis et al., 2015; Parker et al., 2017a). This might reflect some propensity of (mip)ATP to undergo pleiotropic target interactions. To focus on likely foreground interactors, we only selected candidates for further consideration that exhibited both a low CRAPome frequency (<5%) and that had not previously been retrieved by other small molecule baits. 32 high confidence candidates remained after this final filtering, among them 15 previously unknown, possible ATP interactors (Figure 3.6, Table S3). All unknown mipATP targets are plasma membrane proteins, most of them transporters of the SLC family (SLC35F2, SLC47A1, SLC19A3, SLC22A3, SLC12A9, SLC30A1, SLC12A2). During assembly of this manuscript, SLC19A1 was identified as immunogenic nucleotide transporter (Luteijn et al., 2019; Ritchie et al., 2019). In addition to SLCs, we found one putative iron-binding, cell surface protein (MELTF), and 5 signaling/adhesion molecules (FAS, CD44, CESLR1, PTGFRN, ITGA5) as likely ATP-interactors.

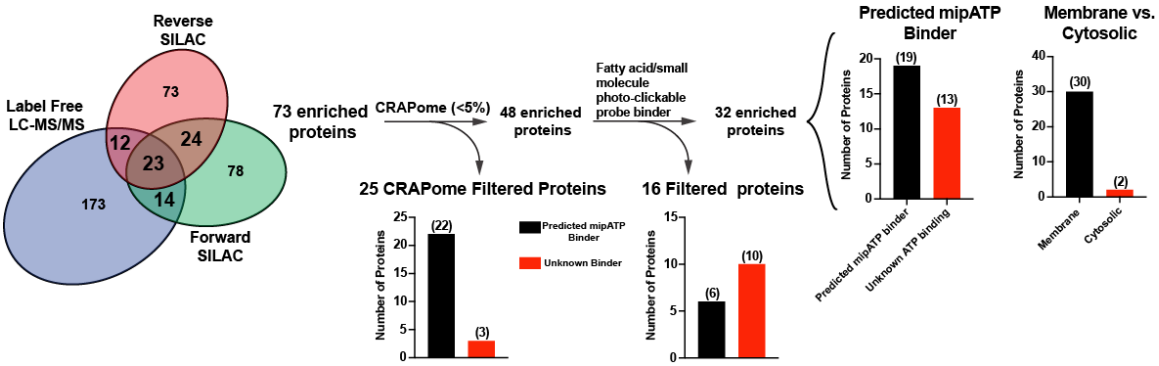

Figure 3.6. mipATP maps a novel ligand space in the membrane proteome
Left, 73 proteins were identified as high confidence mipATP interactors in at least two of three independent mass spectrometry experiments (Micallef and Rodgers, 2014). Proteins identified in (i) >5% of CRAPome database experiments and/or in (ii) similar proteomic studies using fatty acid and small molecule probes (Niphakis et al., 2015; Parker et al., 2017a) were eliminated as specific mipATP interactors resulting in 32 high confidence mipATP binders.

Select candidate validation

For proof-of-principle, we picked three known and three unknown ATP-interactors from our screens for Western blot validation.

MRP1 is a multi-specific ATP-binding Cassette (ABC) Transporter that uses ATP hydrolysis for catalyzing the efflux of organic ions, such as GSH and proinflammatory cysteinyl leukotriene C4, and other lipid mediators (Leier et al., 1994). Western blot analysis confirmed the UV-dependency and ATP-specificity of mipATP-MRP1 complex formation. Namely, competition with 10-fold excess native ATP and ATPγS blocked the mipATP-MRP1 interaction by ~40% and ~25%, respectively (Figure 3.7A). These results are in line with previous studies demonstrating that ABC transporters preferentially bind N^6-substituted ATP analogs over unmodified ATP (Zhou et al., 2005).

Casein kinase 1 delta (CK1δ) is a serine kinase involved in cell cycle regulation, DNA-damage signaling, and circadian rhythm (Behrend et al., 2000; Etchegaray et al., 2009; Knippschild et al., 1997). CK1δ associates with the plasma membrane (Stöter et al., 2005). Interestingly, longdaysin, a small molecule with a N^6-substituted purine (Hirota et al., 2010) binds and inhibits CK1δ. Casein kinase 1 alpha (CK1α), another a longdaysin target, also showed up in our screen. But due to its concomitant appearance in the CRAPome (>5% frequency) and a previous fatty acid interactor screen (Niphakis et al., 2015), we did not classify it as high confidence target. Western blot analysis confirmed the UV-dependency of CK1δ-mipATP complex formation, which was blocked by native ATP and ATPγS (Figure 3.7B).

Ecto-5'-nucleotidase (CD73) is a GPI-anchored cell surface enzyme that catalyzes the hydrolysis of extracellular AMP to adenosine. The latter is converted to inosine by adenosine deaminase, imported into cells by nucleoside transporters, or activates P1 G protein-coupled receptors (Antonioli et al., 2013; Knapp et al., 2012). Native ATP and N^6-substituded nucleotide derivatives (K_i's in nanomolar and picomolar range) inhibit CD73 activity (Bowman et al., 2019; Grondal and Zimmermann, 1987; Knapp et al., 2012), suggesting that it possesses N^6-tolerant ATP-binding sites. As expected, our Western blot analysis confirmed UV-dependent crosslinking of mipATP to CD73, and an excess of native ATP or ATPγS blocked mipATP-CD73 interactions (Figure 3.7C). Next, we set out to validate three interesting, unknown ATP targets from our screens.

CD44 is a cell surface adhesion receptor involved in a variety of biological processes including cell migration, lymphocyte activation and homing, and tumor progression and metastasis (DeGrendele et al., 1997; Günthert et al., 1991; Haynes et al., 1989; Liu et al., 2011). CD44 directly binds multiple ligands including hyaluronic acid, osteopontin, collagens, and matrix metalloproteinases (Aruffo et al., 1990; Katayama et al., 2005; Mori et al., 2002; Weber et al., 1996). However, direct interactions with ATP or other nucleotides have not been reported. Western blot analysis confirmed the UV-dependency of the CD44-mipATP interaction (Figure 3.7D). Competition with excess ATP or ATPγS, and to a lesser extent ADP, but not AMP or adenosine blocked CD44 binding to mipATP, highlighting the importance of the phosphate groups for CD44-mipATP binding. A truncated version of CD44 lacking its intracellular portion did not interact with mipATP

suggesting that CD44's nucleotide-binding site is located on the cytoplasmic side (Figure 3.7E).

The major facilitator superfamily domain-containing protein 5 (MFSD5) is an atypical solute carrier (SLC) localized to the plasma membrane. It mediates the cellular uptake of molybdate ions (Tejada-Jiménez et al., 2011). MFSD5 was enriched in all our proteomics experiments, but also appeared in preceding small molecule target screens (Niphakis et al., 2015; Parker et al., 2017a). Western blotting confirmed that recombinant MFSD5 directly binds to mipATP. The interaction was UV-dependent and almost completely abolished by excess ATP or ATPγS (Figure 3.7F). Various ATP hydrolysis products were also capable of blocking the interaction with an apparent rank-order of ATP>ADP>GTP≥UTP>AMP~adenosine~CTP, pointing to the importance of the phosphates and adenine base for MFSD5-ATP interactions (Figure 3.7G).

Intriguingly, our screen also enriched for the FAS receptor, a cell surface death receptor that triggers apoptosis upon ligation to the FAS ligand (FASL) (Itoh et al., 1991; Suda et al., 1993). To our knowledge, FAS is not known to directly bind ATP. But it is well-known that FAS-stimulated apoptosis depends on intracellular ATP, and extracellular ATP triggers apoptosis of various cell types (Gandelman et al., 2013; Leist et al., 1997; Li et al., 1997). Western blotting confirmed the UV-dependent labeling of FAS by mipATP. The interaction was blocked by excess ATP and ATPγS (Figure 3.7H), and to a lesser extent by ADP. By contrast, AMP or adenosine, or other nucleotide triphosphates with varying

bases (GTP, CTP, and UTP) had no effect. Again, this underlines the importance of ATP's phosphate and nucleic acid moieties for this interaction (Figure 3.7I).

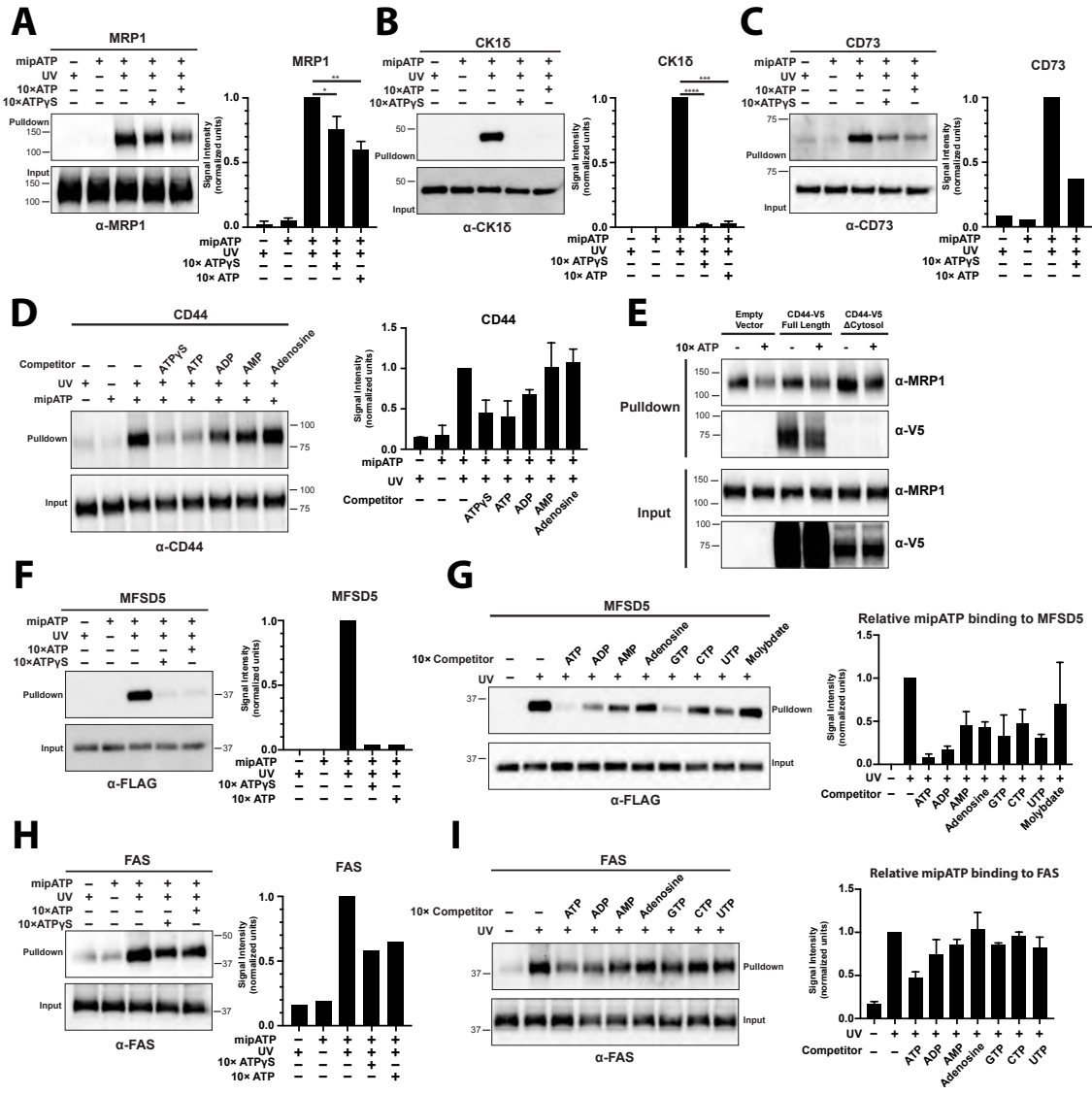

Figure 3.7. Select candidate validation of known and novel ATP interactors
(A) Left panel, A549 membrane fractions were treated with 10 μM mipATP after preincubation with 100 μM ATPγS or ATP competitor, UV-irradiated (365 nm), and mipATP-labeled proteins were conjugated to a biotin reporter by click chemistry with biotin-azide. Biotin-conjugated proteins were enriched with streptavidin agarose and separated by SDS-PAGE. MRP1–mipATP complexes and input from 5 μg of membrane protein extract were detected by Western blot with anti-MRP1. The exposure is representative of four independent experiments. Right panel, analysis of MRP1–mipATP complex signal intensities normalized to the intensity value of the complex in the absence of competition. *$p < 0.05$ and **$p < 0.005$, unpaired t test. Values represent mean ± SD from four independent experiments. (B) Left, enriched CK1δ–mipATP complexes and input from 5 μg of membrane protein extract were detected by Western blot with anti-CK1δ antibody. Representative of three independent experiments. Right, analyses of CK1δ–mipATP complex signal intensities. ***$p < 0.0005$ and ****$p < 0.0001$, unpaired t test. Values represent mean ± SD from three independent experiments. (C) Left, enriched CD73–mipATP complexes and input from 5 μg of membrane protein extract were detected

by Western blot with anti-CD73 antibody. Right panel, analyses of CD73–mipATP complex signal intensities. (D) Left, A549 membrane fractions were labeled with 10 μM mipATP in the presence of 100 μM of the indicated competitor. Western blot with anti-CD44 antibody detects biotin-conjugated CD44–mipATP complexes enriched with streptavidin agarose after biotin-azide click chemistry. 5 μg of membrane protein extract was used for input. Representative of two independent experiments. Right, analysis of CD44–mipATP complex signal intensity normalized to the intensity value of the complex in the absence of competition. Values represent mean ± SD from two independent experiments. (E) Membrane fractions of A549 cells transiently transfected to express CD44-V5 full length, or CD44-V5 with a truncated intracellular domain (ΔCytosol) were labeled with 10 μM mipATP in the presence of 100 μM ATP competitor. Western blot with anti-V5 and anti-MRP1 antibodies detect biotin-conjugated CD44–, and MRP–mipATP complexes enriched with streptavidin agarose after biotin-azide click chemistry respectively. 5 μg of membrane protein extract was used for input. (F) Membrane fractions of A549 cells stably expressing recombinant MFSD5-FLAG were labeled with 10 μM mipATP ± 100 μM of ATPγS or ATP. Western blot with anti-FLAG antibody detects biotin-conjugated MFSD5–mipATP complexes enriched after biotin-azide click chemistry. 5 μg of membrane protein extract was used for input. Right panel, analysis of MFSD5–mipATP complex signal intensity. (G) Left, MFSD5–mipATP complexes enriched in the presence of the indicated competitor. Right, analysis of MFSD5–mipATP complex signal intensity. Values represent mean ± SD from three independent experiments. (H) Left, FAS–mipATP complexes enriched in the presence of ATPγS or ATP competitor and input from 5 μg of membrane protein extract were detected by Western blot with anti-FAS antibody. Right, analysis of FAS–mipATP complex signal intensity. (I) Left, FAS–mipATP complexes enriched in the presence of the indicated nucleoside or nucleotide competitor. Values represent mean ± SD from three independent experiments.

Discussion

To identify small molecule targets, chemical proteomics have become an interesting alternative/complement to functional genomics. Such strategies have identified ATP-interacting proteins from human cell lines, plants, and parasitic organisms including *mycobacterium tuberculosis* (Adachi et al., 2014; Ansong et al., 2013; Mahajan et al., 2015; Patricelli et al., 2007; Villamor et al., 2013). To this end, ATP probes are commonly functionalized at the γ-phosphate, favoring the identification of enzymatic over allosteric ATP-binding sites, or contain physiologically invasive, bulky hydrophobic additions. To illuminate novel regions of the ATP-binding landscape, we thus developed and characterized mipATP, which contains a very compact, photo-clickable linker at the N^6 position of its adenine base (Li et al., 2013). Importantly, mipATP faithfully mimics allosteric signaling responses of extracellular ATP in cells and tissues, unlike commonly used γ-phosphate modified ATP derivatives, and is thus physiologically less invasive.

In this study, we focused on ATP-interacting membrane proteins. Besides the known panel of P2 receptors, those likely comprise additional unknown ATP-regulated signaling proteins. Underlining the robustness of our screen, most of our hits were previously known nucleotide-interacting membrane proteins such as transporters, ATPases, and others. Demonstrating mipATP explorative value, we identified and confirmed various novel ATP interactors in prominent cellular signaling pathways, such as the FAS receptor and CD44 (Haynes et al., 1989; Itoh et al., 1991).

For all tested targets, our experiments suggest binding affinities in the ~10-100 micromole range. Except for CD44, which we show to bind intracellular nucleotides, and CD73 that has no intracellular domain, the location of the nucleotide binding sites remains uncertain. If these sites were extracellular, they should be unoccupied under basal conditions, because extracellular steady state concentrations of nucleotides are extremely low (Schwiebert and Zsembery, 2003). Upon tissue damage, however, extracellular [ATP] may temporally rise into the micro- to millimolar range to support allosteric regulation or enzymatic activity. Conversely, if these sites were intracellular, they should always be occupied amidst millimolar cytoplasmic [ATP]. However, after severe homeostatic perturbation, for example, during cell death, low intracellular [ATP] levels will cause dissociation of micromolar affinity interactions. Surveillance of cytoplasmic nucleotide concentrations, for example, by AMPK or the apoptosome, crucially regulates energy metabolism or cell death decisions, respectively (Hardie et al., 2012; Li et al., 1997).

We were intrigued to find the FAS receptor among our high-confidence ATP interactors. Despite being at the top of the apoptotic cascade FAS' direct regulation by nucleotides is not reported. Our result raises the possibility that ATP directly regulates cell death fate decisions at the death receptor level.

The relative scarceness of multipass transmembrane proteins in our screen, specifically, G-protein coupled receptors was undesired but expected. The identification of highly hydrophobic intramembrane portions of transmembrane proteins by mass spectrometry is notoriously difficult, and tryptic lysine and

arginine residues in transmembrane domains are often sparse (Speers and Wu, 2007). Importantly, the failure of mipATP to enrich for P2 receptors in our screens unlikely resembles a lack of probe binding, as mipATP fully reconstitutes purinergic Ca^{2+} responses. Future protocol optimizations may be able to improve on GPCR enrichment.

It is possible that one or more of the candidates identified in our screens binds ATP as a ligand at an extracellular site(s). Such interactions may promote signaling that contributes to the Ca^{2+} responses observed in cells and tissues upon exposure to ATP and other nucleotides as in Figures 3.1 and 3.2. Previous studies have confirmed that Fas ligation to its ligand FasL triggers an IP_3-dependent increase in cytosolic Ca^{2+} (Khadra et al., 2011). This transient increase in cytosolic Ca^{2+} inhibits Fas-mediated apoptosis by blocking the initial apoptotic steps such as Fas binding to the Fas-associated death domain protein (FADD) and formation of the death-inducing signaling complex (DISC). Future experiments should determine if genetic perturbations of Fas have any effect on ATP-triggered Ca^{2+} responses in cells and tissues. It will also be interesting to determine whether or not ATP-dependent Ca^{2+} signaling blocks DISC formation similar to Fas binding to FasL.

In summary, we establish mipATP as a promising, non-invasive probe for exploring novel regions of the cellular ATP interactome.

CHAPTER 4 Genetic and pharmacologic characterization of nucleotide mediated epithelial wound closure in the larval zebrafish tail fin

Introduction

The epithelia of freshwater animals such as zebrafish, as well as the oral, esophageal, and possibly lung mucosa of land mammals, are constantly exposed to hypotonic fluid (Jayaraman et al., 2001a, 2001b; Joris et al., 1993). These epithelial barriers separate the interstitial fluid of the animal (~270-300 mOsm, the common extracellular tonicity of vertebrates) from the hypotonic environment (fresh water, ~10 mOsm; saliva, ~30 mOsm) (Joris et al., 1993). The tail fin fold of 2-4 day post fertilization (dpf) zebrafish larvae consists of a basal epithelial layer that is attached to a basal lamina and a suprabasal layer in which cells are connected by adherens- and tight- junctions to act as a permeability barrier (Figure 4.1A). When zebrafish larvae tail fin epithelium is wounded, internal tissues are exposed to the hypotonic freshwater environment resulting in a drop in interstitial osmolarity and subsequent epithelial wound closure (Figure 4.1B) (Gault et al., 2014). The drop in interstitial osmolarity swells the cells of internal tissues at the injury site, triggering non-lytic ATP release into the interstitial space (Figure 4.1C). ATP subsequently stimulates rapid wound closure through lamellipodia-mediated migration of basal epithelial cells (Figure 4.1D).

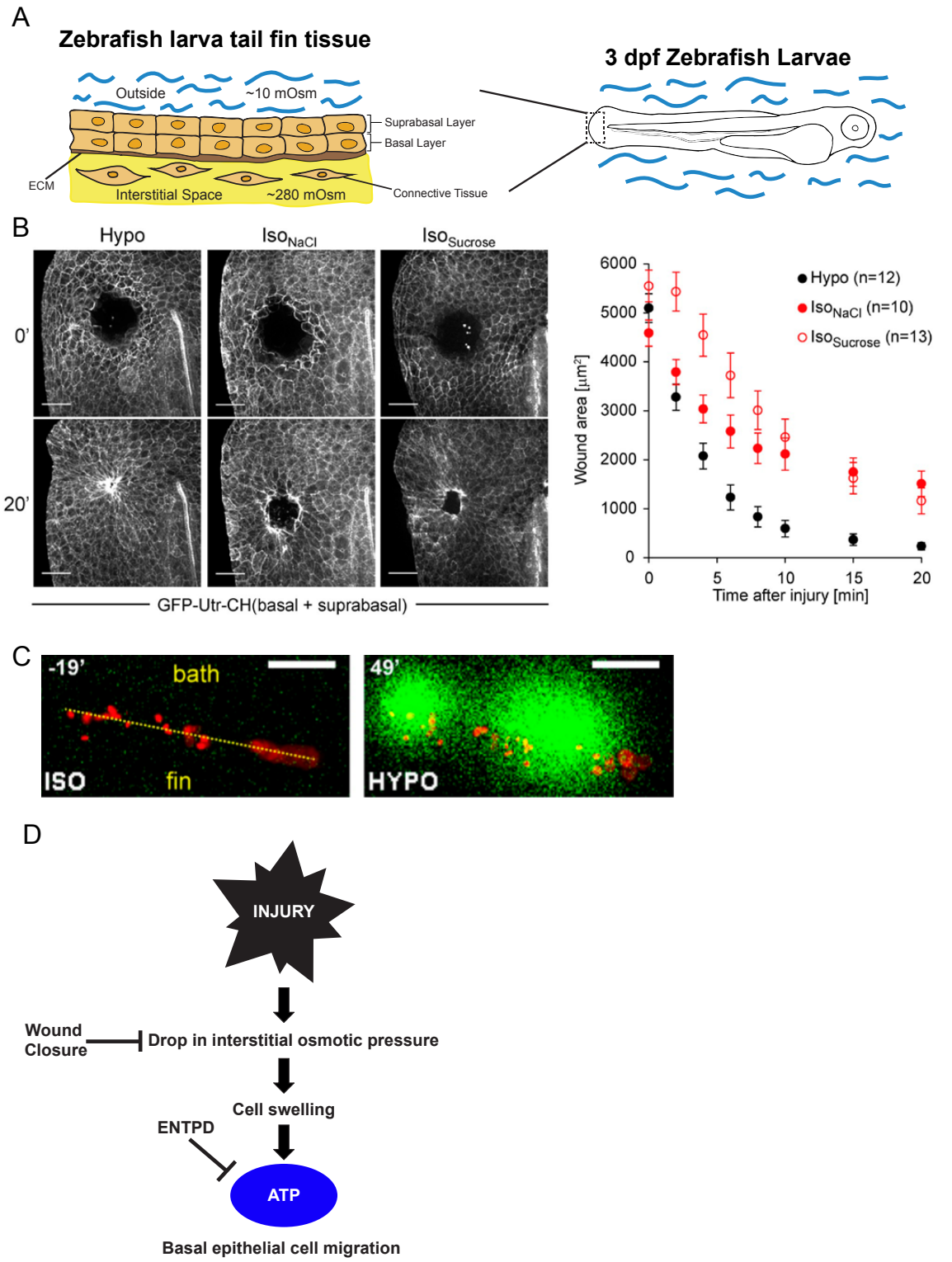

Figure 4.1. A drop in interstitial osmotic pressure triggers nucleotide dependent wound closure in zebrafish larvae

(A) Simplified architecture of the 3 day post fertilization (dpf) larval zebrafish epithelium. The double layered epithelium consists of the periderm or suprabasal layer connected to

the basal epidermis by adherens junctions and desmosomes. The epithelium separates the hypotonic freshwater environment (~10 mOsm) from the interstitial space (~270-300 mOsm). (B) Representative timelapse of larval zebrafish tail fin epithelium wounded in hypotonic medium (Hypo), or isotonic medium (Iso_{NaCl}, $Iso_{Sucrose}$). Epithelium is injured by UV-laser puncture at the start of imaging. Ubiquitous labeling of the actin cytoskeleton is achieved by embryo injection of *in vitro* transcribed mRNA encoding GFP-utrophin-calponin homology domain (GFP-Utr-CH). Scale bars, 50 μm. Figure from Gault et al., 2014. (C) ATP is released at the wound margin of an amputated tail fin after exposure to hypotonic medium (Hypo). Red, SYTOX orange fluorescence labels cells that were damaged during amputation. Green, luminescence from endogenous ATP reacting with firefly luciferase and luciferin that was supplemented in the bathing medium. Scale bars, 100 μm. Figure from Gault et al., 2014. (D) Proposed scheme of hypotonicity mediated epithelial wound closure in zebrafish larvae tail fins.

Cell swelling, and thus ATP secretion, is inhibited when the tail fin epithelium is wounded in a bathing solution that is isosmotic (normal E3 embryo medium + 140 mM NaCl) to the interstitial fluid, preventing basal epithelial cell migration and thus epithelial tissue movement (Figure 4.1B). Basal epithelial cell migration can be rescued by the exogenous application of cytoplasmic levels of ATP (5 mM) to the isotonic bathing solution (Figure 4.2A-B). Particle image velocimetry (PIV) analysis allows for direct, quantitative measurements of average global epithelial tissue velocity as a function of time after experimental perturbations such as the application of exogenous ATP to the wounded tissue in isotonic media (Figure 4.2C-D). The combination of basal cell lamellipodia formation and measurement of global epithelial tissue velocity by PIV, allows us to identify normal and perturbed tissue motion phenotypes upon exposure to hypotonicity or other stimulants. This work demonstrates the role of extracellular ATP as a mediator of rapid wound closure of wet epithelia *in vivo* (Gault et al., 2014).

A variety of studies have proposed that extracellular ATP mediates epithelial wound closure *in vitro* (Block and Klarlund, 2008; Boucher et al., 2010; Klepeis et al., 2004; Sham et al., 2013; Takada et al., 2014; Weinger et al., 2005). Activation of the $P2Y_2$ receptor mediates scratch wound healing in monolayers of epithelial cells in culture. $P2Y_2$ receptor activation is reported to induce epithelial cell migration by transactivation of the EGF receptor, possibly through the activation of phospholipase D and NADPH oxidases (Ratchford et al., 2010; Sham et al., 2013; Yin et al., 2007). However, the known $P2Y_2$ agonists ATPγS and

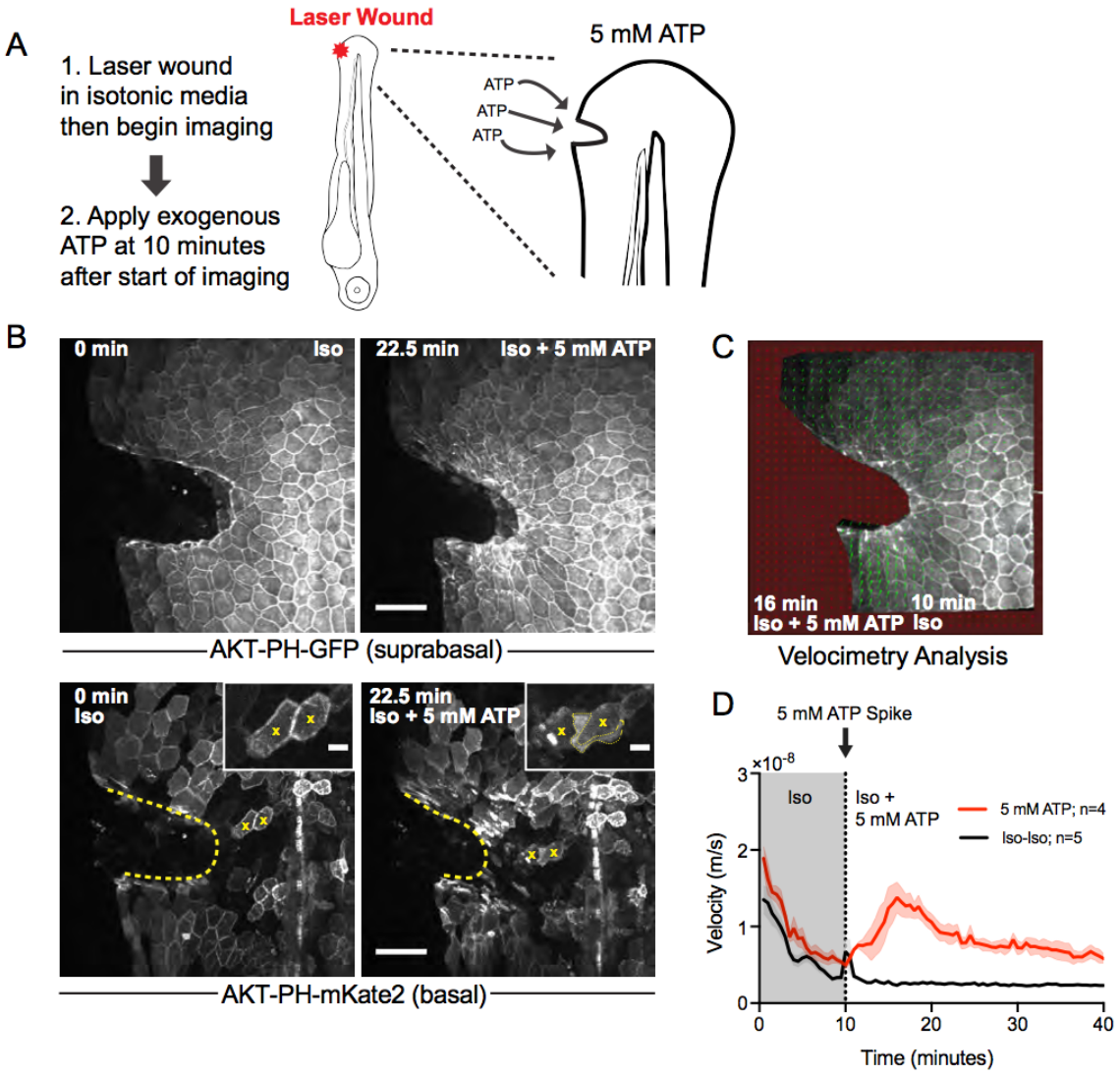

Figure 4.2. ATP reconstitutes basal cell migration and epithelial tissue motion in an isosmotic environment

(A) Schematic for wounding larval zebrafish tail fin epithelium with UV-laser pulses. Transgenic 3 dpf larvae expressing an AKT-pleckstrin homology domain-GFP reporter in the suprabasal epidermal layer (also known as TG(*krt4*:AKT-PH-GFP) larvae) with mosaic basal epithelial cell AKT-PH-mKate2 expression are acclimated to isotonic medium and injured by UV-laser. Imaging begins immediately after injury and a bolus of isotonic medium containing 5 mM nucleotide or nucleotide derivative is applied to the larva at 10 minutes into imaging. (B) Representative images of epithelial wound closure reconstitution by exogenous 5 mM ATP in a TG(*krt4*:AKT-PH-GFP) reporter larva with mosaic AKT-PH-mKate2 expression in basal cells through mRNA injection. Frames are from the start of imaging (0 min) and 12.5 minutes after ATP application (22.5 min from the start of imaging). Broken yellow line, wound margin. Inset, yellow x, representative cells developing lamellipodia (yellow dotted line) in response to exogenous ATP application. (C) Representative frame from PIV analysis (PIVlab, MATLAB) of epithelial tissue motion after application of exogenous ATP to a UV-wounded TG(*krt4*:AKT-PH-GFP) larva. The frame is from 6 minutes after ATP application (16 min from the start of imaging). Green

arrows are velocity vectors derived by comparing particle movements between subsequent frames. (D) Global PIV analysis of the indicated number of TG(*krt4*:AKT-PH-GFP) larvae. Larvae were subjected to UV-laser wounding in isotonic medium and a bolus of isotonic medium ± 5 mM ATP was added to the larvae at 10 minutes after wounding. Scale bars, 50 μm and 10 μm (inset). Time in minutes. Values indicate the mean velocity ± SEM of the indicated (n) number of larvae.

UTPγS could not rescue basal cell migration when applied to tail fins injured in an isotonic environment. Additionally, none of the ATP/UTP hydrolysis products, which are described agonists for the various P2Y and P2X receptor subtypes, were capable of inducing basal cell migration *in vivo*. Consequently, the agonist profile of the receptor mediating epithelial wound closure *in vivo* diverges from all known P2 receptors that have been described thus far (Table 4.1).

Mammalian isoforms have been predominantly used to determine P2 receptor pharmacological profiles. Notably, even closely related species homologs, such as the human and rat $P2Y_4$ receptors (~83% protein identity) or the human and dog $P2Y_{11}$ receptors (~70% protein identity), have different pharmacological profiles (Bogdanov et al., 1998; von Kügelgen, 2006; Qi et al., 2001). Phylogenetic variabilities of zebrafish P2 receptor pharmacology may explain the divergent agonist profile of basal cell migration. Using intravital microscopy and functional genetic screening, this chapter investigates a potential role for P2 receptors in extracellular ATP-mediated basal cell migration in larval zebrafish epithelium. We find that zebrafish isoforms of $P2Y_4$ and $P2Y_{11}$, but not $P2Y_2$, potentially play roles in hypotonicity mediated epithelial wound closure and thus extracellular ATP-triggered basal cell migration. This chapter further describes the pharmacological profile of epithelial wound closure through a comprehensive structure-activity relationship (SAR) analysis using known endogenous and synthetic P2 receptor agonists. The SAR analysis reveals a preference for N^6-modified ATP derivatives including the newly reported novel mipATP.

Agonist	Receptor (Mammals)
ATP*	$P2Y_1$, $P2Y_2$, $P2Y_4$, $P2Y_{11}$, $P2Y_{12}$, $P2X_1$, $P2X_2$, $P2X_3$, $P2X_4$, $P2X_5$, $P2X_6$, $P2X_7$
ADP^x	$P2Y_1$, $P2Y_6$, $P2Y_{12}$, $P2Y_{13}$
AMP^x	A_1
$Adenosine^x$	A1, A_{2A}, A_{2B}, A_3
UTP*	$P2Y_2$, $P2Y_4$, $P2Y_6$
UDP^x	$P2Y_6$, $P2Y_{14}$
$ATP\gamma S^x$	$P2Y_2$, $P2Y_{11}$, $P2X_2$, $P2X_5$
$UTP\gamma S^x$	$P2Y_2$, $P2Y_4$
$ADP\beta S^x$	$P2Y_1$, $P2Y_{11}$, $P2Y_{12}$, $P2Y_{13}$
$BzATP^x$	$P2Y_{11}$, $P2X_1$, $P2X_3$, $P2X_7$
3-PA-UDP^x	$P2Y_6$
$UDP\text{-Glucose}^x$	$P2Y_{14}$

Table 4.1. Known P2 receptor agonists screened to rescue larval zebrafish basal epithelial cell migration in an isotonic environment by Gault et al. 2014
The list of nucleotide ligands that have been tested for the ability to mediate basal cell migration in the larval zebrafish in isotonicity (Gault et al., 2014) and the purinergic receptors that they are characterized to bind and activate (based on mammalian isoforms). (*) indicates that the ligand elicits basal cell migration response. (^{x}) indicates that the ligand does not elicit basal cell migration response.

Results

Identification of P2 receptor subtypes expressed in larval zebrafish epidermis

Extracellular ATP and other adenine or uridine nucleotides can bind and activate purinergic receptors that include eight characterized metabotropic P2Y GPCRs and seven ionotropic P2X channel subtypes. To determine if any known purinergic receptor(s) plays a role in ATP-mediated basal cell migration in the larval zebrafish, we first aimed to identify P2 receptor expression levels and patterns in zebrafish larvae, with particular interest in those expressed in the ATP-responsive basal epithelial cells. To this end, we employed mRNA sequencing on 3 dpf zebrafish larvae basal epithelial cells isolated from the transgenic TG(*ΔNp63*:Gal4; *UAS*:GFP) reporter line (Reischauer et al., 2009). mRNA sequencing on whole larvae and ATP-unresponsive suprabasal epithelial cells isolated from double transgenic larvae expressing AKT-pleckstrin-homology domain-GFP (AKT-PH-GFP) and AKT-PH-mKate2 in the suprabasal epithelial layer from a *krt4* promoter (known as the TG(*krt4*:AKT-PH-GFP; *krt4*:AKT-PH-mKate2) reporter line) were conducted in parallel (Gong et al., 2002; Kwon et al., 2007). Basal and suprabasal epithelial cells showed varying P2 receptor expression profiles (Figure 4.3).

Moving forward with our functional screening, we initially focused on the P2Y receptors expressed in the ATP-responsive basal cells as high priority candidates because the activation of P2Y receptors, particularly $P2Y_2$, have been reported to mediate epithelial cell migration in previous studies.

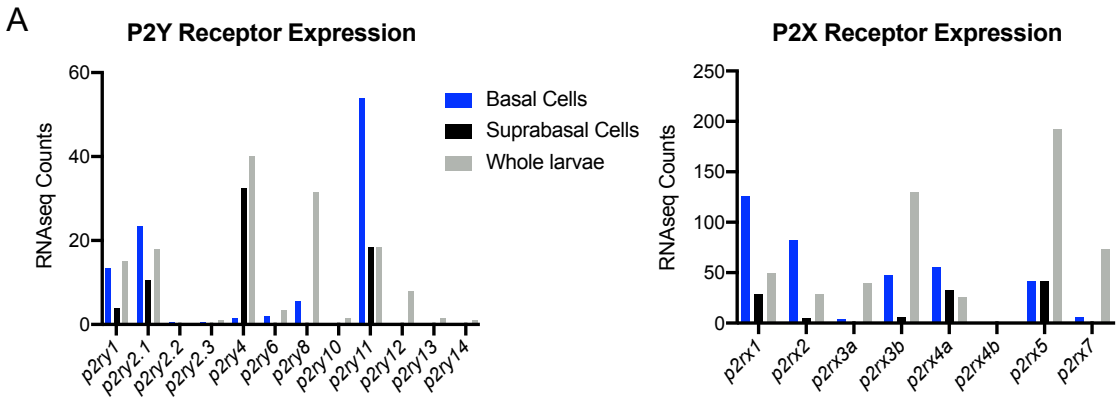

Figure 4.3. P2 receptor subtype expression in the larval zebrafish epidermis
Whole 3 dpf larvae, and basal and suprabasal epithelial cells isolated by FACS from dissociated 3 dpf TG(*ΔNp63*:Gal4; UAS:GFP) and TG(*krt4*:AKT-PH-GFP, *krt4*:AKT-PH-mKate2) reporter larvae, respectively, were subjected to mRNA-sequencing analysis. P2Y and P2X subtype expression levels in basal epithelial cells (blue), suprabasal epithelial cells (black), and whole larvae (gray). Values are average normalized mRNAseq counts from two independent experiments.

The P2Y receptor subtypes expressed in basal epithelial cells are *p2ry1* ($P2Y_1$), *p2ry2.1* ($P2Y_2$), and *p2ry11* ($P2Y_{11}$) (Figure 4.3A). Importantly, each of these genes is expressed at higher levels in basal compared to suprabasal epithelial cells. Vertebrate $P2Y_1$ receptors are mainly classified as ADP receptors involved in platelet aggregation (Hechler et al., 1998; Jin et al., 1998). ADP is not an agonist of basal cell migration in the zebrafish tail fin (Gault et al., 2014), and the pharmacological agonist profile of $P2Y_1$ does not include the ligands that are able to elicit basal cell migration (e.g. UTP and ATP) (Abbracchio et al., 2006; von Kügelgen and Hoffmann, 2016; Léon et al., 1997; Palmer et al., 1998).

UTP and ATP ligands are known to act equivalently as full agonists for the human ortholog of zebrafish P2ry2.1 ($P2Y_2$) (Abbracchio et al., 2006; von Kügelgen and Hoffmann, 2016). Additionally, a variety of studies have shown that activation of mammalian $P2Y_2$ receptors can mediate chemotaxis of multiple cell types, including epithelial cells in models of wound healing (Bagchi et al., 2005; Boucher et al., 2010; Kaczmarek et al., 2005; Klepeis et al., 2004; Wesley et al., 2007; Yin et al., 2007).

P2ry11 is the most abundant P2Y receptor expressed in 3 dpf zebrafish basal epithelial cells. ATP and UTP are both characterized as agonists of the mammalian isoforms of $P2Y_{11}$ (Abbracchio et al., 2006; White et al., 2003) and previous studies have indicated a role for $P2Y_{11}$ in chemotaxis (Alkayed et al., 2012). For these reasons, we decided to focus on *p2ry2.1* and *p2ry11*, but not *p2ry1*, as high priority candidates.

Analysis of p2ry2.1 and p2ry11 knockdown on zebrafish wound closure

Selective small molecule antagonists are not readily available for each purinergic receptor subtype. Additionally, the effective drug working concentrations for zebrafish larvae are typically higher than those used in cell culture or pure enzyme experiments for reasons including altered pharmacokinetics, target affinity, and epithelial permeability (Jelcic et al., 2017; Wittmann et al., 2015). Potential drug pleiotropy can result in off-target effects that lead to uncertainty in data. Thus, we decided against utilizing a small molecule inhibitor screen to perturb P2Y receptor function, avoiding the use of non-selective P2 receptor antagonists such suramin and PPADS, and other drugs reported to act as selective P2 receptor subtype antagonists in systems other than zebrafish (Beindl et al., 1996).

We employed orthogonal methods to genetically perturb *p2ry2.1* and *p2ry11* expression in order to characterize a potential role for P2Y receptors in larval zebrafish epithelial wound closure (Figure 4.4A and B). Initially, we used morpholino antisense oligos targeting *p2ry2.1* and *p2ry11* transcripts to knockdown expression of the target genes in 3 dpf larval zebrafish. Briefly, morpholinos are antisense oligos that specifically bind target mRNA transcripts with high affinity via complementary base pairing to block processes such as translation or splicing by steric hinderance resulting in a knockdown of expression of the targeted gene (Bill et al., 2009). Zebrafish P2Y receptors, like the vast majority of vertebrate GPCR's (~96% of total characterized vertebrate GPCR's), lack introns in their open reading frames (ORFs) (Gentles and Karlin, 1999).

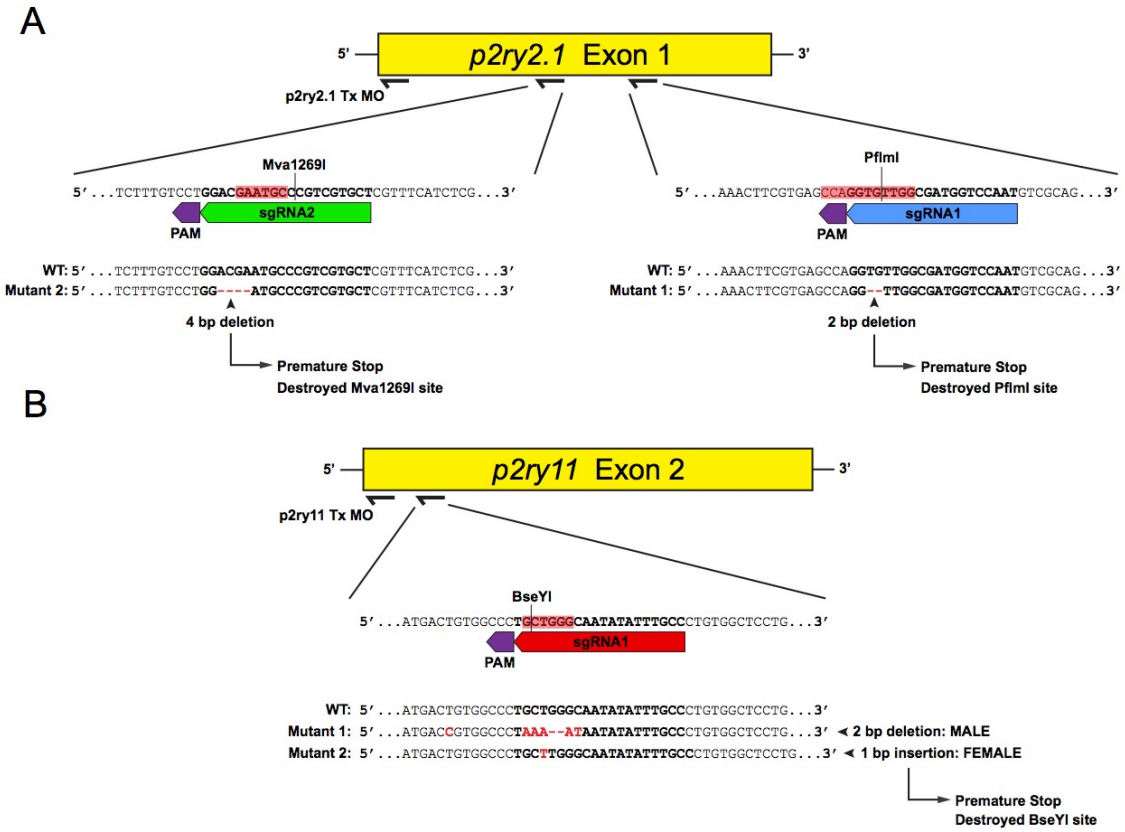

Figure 4.4. Genetic perturbations of *p2yr2.1* and *p2ry11* in zebrafish
(A) Schematic representation of the zebrafish *p2ry2.1* gene and the locations targeted for genetic perturbation by a translation blocking morpholino (p2ry2.1 Tx MO) and disruption by two Cas9-gRNA ribonucleoprotein (RNP) complexes made from single guide RNA's (sgRNA's) targeting different locations on the *p2ry2.1* coding sequence (CDS). The 20 base pair (bp) sgRNA targets and protospacer adjacent motif (PAM) sequences are indicated for sgRNA1 and 2. Restriction enzyme nucleotide recognition sites that are predicted to be destroyed by DNA repair mechanisms after Cas9-induced double strand breaks are highlighted in red with a black line between the bases of their predicted cut sites on the wild type sequence (Mva1269I and PflmI for sgRNA2 and sgRNA1, respectively). Two frameshift knockout (KO) lines, were generated through genomic disruption by injection of the separate Cas9-RNP complexes into one-cell stage embryos (a 4 bp deletion by Cas9-sgRNA2 and a 2 bp deletion by Cas9-sgRNA1 with destroyed Mva1269I and PflmI DNA recognition sites, respectively). (B) Schematic representation of the zebrafish *p2ry11* CDS and the locations targeted for genetic perturbation by a translation blocking morpholino (p2ry11 Tx MO) and disruption by a Cas9-gRNA ribonucleoprotein (RNP) complex. The 20 bp sgRNA target and PAM sequences are indicated. The DNA recognition site for the BseYI restriction enzyme (highlighted in red with a black line between the bases of the cut site) is predicted to be destroyed. Sequences of the mutant alleles of identified F1 *p2ry11*$^{+/-}$ male and female zebrafish are provided. These two F1 heterozygous animals were crossed to generate *p2ry11*$^{-/-}$ larvae for wound closure experiments.

Consequently, we designed and employed translation blocking morpholinos targeting *p2ry2.1* and *p2ry11* mRNA sequences within the 5' untranslated region (UTR) in order to knockdown expression of these genes in larvae and evaluate the effects on hypotonicity mediated epithelial wound closure (Figure 4.4A-B, Figure 4.5).

We initially evaluated the effect of gene knockdown on global epithelial tissue velocity changes triggered by hypotonicity. Transgenic TG(*krt4*:AKT-PH-GFP) larvae acclimated to isotonic medium had their tail fin tips amputated and were then exposed to excess hypotonic medium to trigger cell swelling and subsequent extracellular ATP-mediated wound closure (Figure 4.5A). Wound closure phenotypes were assessed by quantifying global epithelial tissue velocity after wound exposure to hypotonic or isotonic media using PIV analysis (Figure 4.5A). As expected, exposure of the open wound to excess hypotonic medium resulted in rapid epithelial wound closure that was quantified as a global increase in tissue velocity while exposure to isotonic media resulted in no quantifiable tissue motion (Figure 4.5B). Both *p2ry2.1* and *p2ry11* morphants displayed normal hypotonicity induced tissue motion phenotypes, suggesting morpholino based knockdown of either gene has no effect on epithelial wound closure or knockdown is insufficient to cause a phenotype (Figures 4.5A-D).

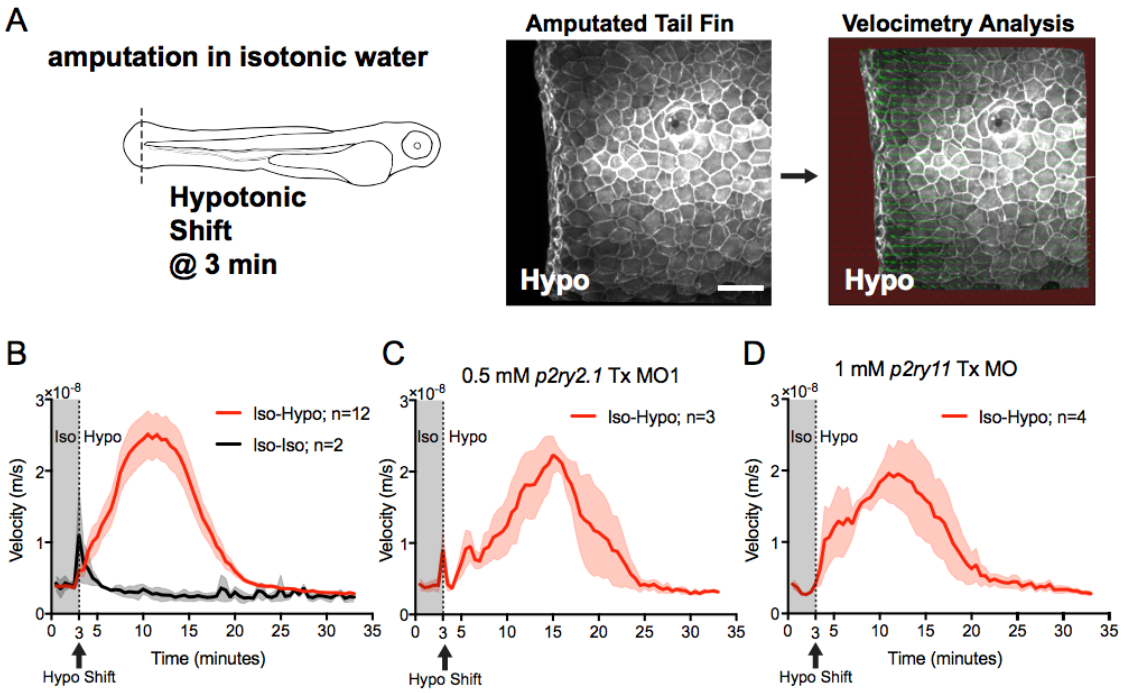

Figure 4.5. P2Y receptor morphants have a normal hypotonicity-mediated epithelial tissue motion phenotype

(A) Schematic for larval zebrafish tail fin tip amputation and epithelial tissue motion analysis by global PIV. 3 dpf TG(*krt4*:AKT-PH-GFP) tail fin tips are amputated in isotonic medium and wounded fish are subsequently exposed to hypotonic medium at 3 minutes into imaging. Representative frame from PIV analysis (PIVlab, MATLAB) of epithelial tissue motion after application of hypotonic medium to a tail fin amputated TG(*krt4*:AKT-PH-GFP) larva. Green arrows are velocity vectors derived by comparing particle movements between subsequent frames. (B) Global PIV analysis of the indicated number of TG(*krt4*:AKT-PH-GFP) larvae. Larvae were subjected to tail fin tip amputation in isotonic medium and a bolus of hypotonic or isotonic medium was added to the larvae at 3 minutes after the start of imaging. (C) Global PIV analysis of the indicated number of TG(*krt4*:AKT-PH-GFP) larvae with translation blocking morpholino-mediated knockdown of *p2ry2.1* mRNA (*p2ry2.1* Tx MO1) subjected to tail fin tip amputation in isotonic medium then subsequently exposed to hypotonic medium at 3 minutes into imaging. (D) Global PIV analysis of the indicated number of TG(*krt4*:AKT-PH-GFP) larvae with translation blocking morpholino-mediated knockdown of *p2ry11* mRNA (*p2ry11* Tx MO1) subjected to tail fin tip amputation in isotonic medium then subsequently exposed to hypotonic medium at 3 minutes into imaging. Scale bar 50 μm. Values indicate the mean velocity ± SEM of the indicated (n) number of larvae.

p2ry2.1 and p2ry11 are not essential for wound induced Ca^{2+} signaling

One of the initial responses to epithelial damage and mechanical cell stress, both *in vivo* and *in vitro*, is the propagation of intercellular Ca^{2+} waves (Enomoto et al., 1994; Enyedi et al., 2013; Frame and de Feijter, 1997; Hansen et al., 1993; Klepeis et al., 2001; Razzell et al., 2013; Yoo et al., 2012). In the injured larval zebrafish tail fin, osmotic cell swelling triggers Ca^{2+} waves and oscillations that are essential for the initial inflammatory response (Enyedi et al., 2013, 2016). P2Y receptor signaling has been shown to trigger damage induced Ca^{2+} waves and oscillations and promote wave propagation by stimulating further ATP secretion (Frame and de Feijter, 1997; Hansen et al., 1993; Klepeis et al., 2004; Praetorius and Leipziger, 2009).

$P2Y_2$ and $P2Y_{11}$, belong to the subfamily of P2Y GPCRs that couple to G_q to generate inositol 1,4,5-triphosphate (IP_3) and release Ca^{2+} from intracellular stores in the ER. Contribution of extracellular ATP signaling to the osmotically induced Ca^{2+} signals in the larval zebrafish would not be unexpected (Figure 4.6A). We tested if morpholino-mediated knockdown of *p2ry2.1* and/or *p2ry11* perturbed injury-induced Ca^{2+} signaling in larval zebrafish (Figure 4.6B). Perturbation(s) would suggest roles for these receptors in the injury response and also validate functional knockdowns of the targets. Both *p2ry2.1* and *p2ry11* morphants displayed normal Ca^{2+} signaling profiles after UV-laser mediated tail fin injury of larval transgenic zebrafish expressing a nuclear-targeted, genetically encoded GCaMP6s Ca^{2+} reporter (Figure 4.6C and D).

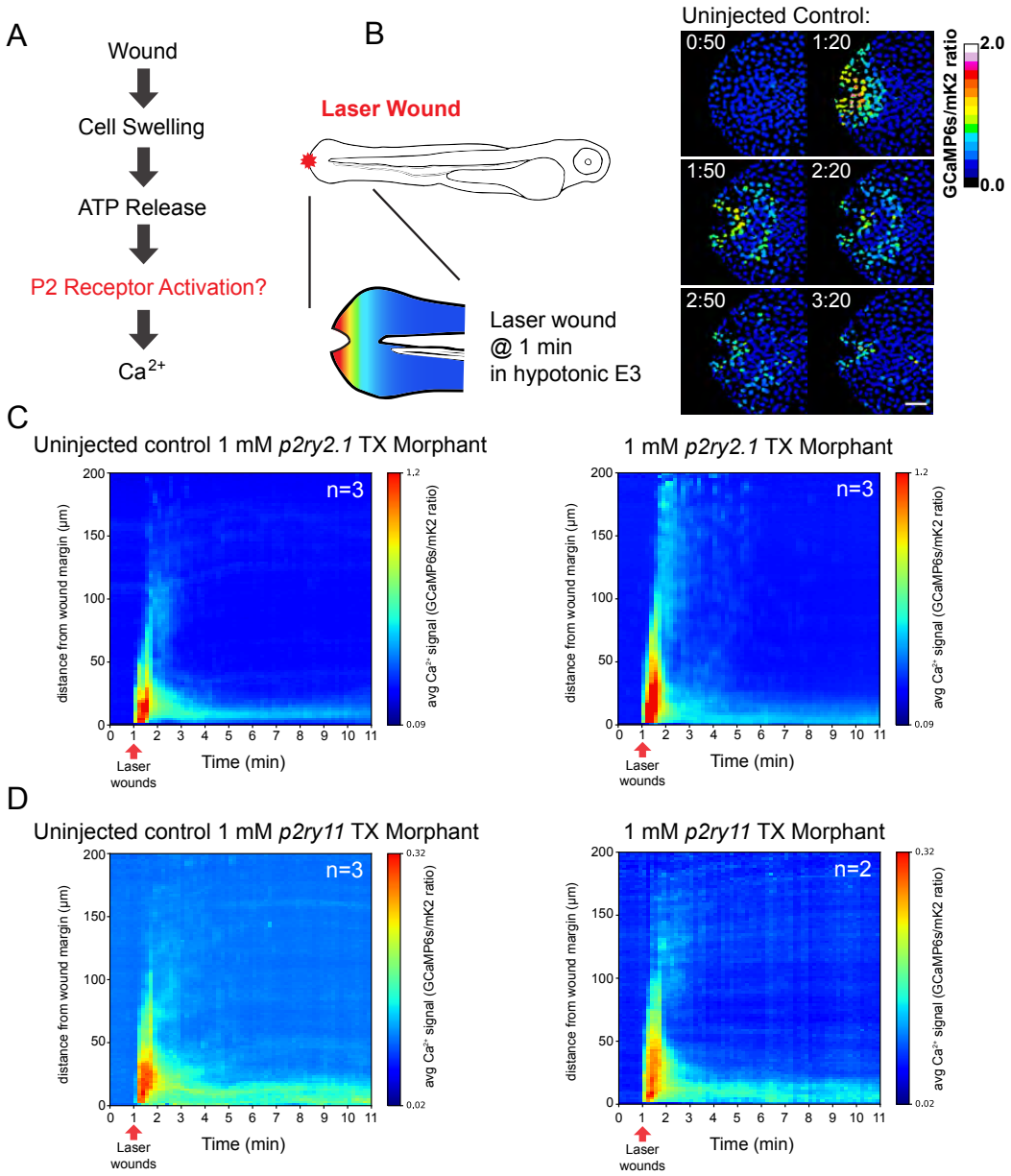

Figure 4.6. Wound-induced Ca^{2+} signaling is not mediated by P2ry2.1 or P2ry11 receptors in zebrafish larvae

(A) Working hypothesis for wound induced purinergic Ca^{2+} signaling. (B) Left: scheme of experimental setup. Right: ratiometric imaging of Ca^{2+} transients induced by UV-laser wounding at the tail fin tip of TG(*hsp70l*:GCaMP6s-3xNLS-P2A-mKate2-3xNLS) Ca^{2+} reporter larvae in hypotonic medium. Larvae are wounded by the UV-laser at 1 minute into imaging. Scale bar, 50 µm. (C) Averaged spatiotemporal Ca^{2+} signal profiles of the indicated (n) number of TG(*hsp70l*:GCaMP6s-3xNLS-P2A-mKate2-3xNLS) Ca^{2+} reporter larvae with translation blocking morpholino-mediated knockdown of *p2ry2.1* mRNA (*p2ry2.1* Tx MO1) and uninjected sibling controls. (D) Averaged spatiotemporal Ca^{2+} signal profiles of the indicated (n) number of TG(*hsp70l*:GCaMP6s-3xNLS-P2A-mKate2-3xNLS) Ca^{2+} reporter larvae with translation blocking morpholino-mediated knockdown of *p2ry11* mRNA (*p2ry11* Tx MO1) and uninjected sibling controls.

Combined, these data suggest either that (1) *p2ry2.1* and *p2ry11* are not essential for ATP-mediated epithelial tissue migration or Ca^{2+} signaling upon tissue injury and exposure to a hypotonic environment or (2) the translation blocking morpholinos were not efficient to functionally knockdown the targets of interest. Translation blocking morpholinos act by sterically blocking ribosome binding to the 5' UTR of targeted transcripts and therefore do not induce Nonsense-mediated mRNA decay (NMD) (Brogna and Wen, 2009). Consequently, P2ry2.1 and P2ry11 knockdown efficiencies cannot be assessed by quantifying transcript levels using RT-qPCR but only by (1) observing changes in protein levels with available antibodies or (2) co-injecting mRNA with the targeted 5' UTR of the gene of interest upstream of GFP or another reporter (Bill et al., 2009). Unfortunately, there are no available antibodies that are able to recognize P2ry2.1 or P2ry11 and so we decided on an orthogonal approach using CRISPR/Cas9 gene disruption to genetically perturb the targets of interest.

Genetic disruption of p2ry2.1 and p2ry11 suggests a potential role for p2ry11 in hypotonicity mediated epithelial migration

As an orthogonal approach to test which, if any, of these receptors is involved in wound closure, we generated frameshift knockout (KO) mutants using CRISPR/Cas9 for both (Figure 4.4A and B) (Gagnon et al., 2014). Importantly, motifs essential for extracellular nucleotide binding by P2Y receptors, the H-X-X-R/K and Q/K-X-X-R motifs in transmembrane domain 6 (TM6) and TM7, respectively, are destroyed in each mutant line (Erb et al., 1995; Jiang et al., 1997). *p2y2.1* homozygous mutant (*p2ry2.1*$^{-/-}$) zebrafish (Mutant 1, from gRNA1; Figure 4.4A) grew to larval and adult stages without obvious developmental phenotypes and were morphologically comparable to heterozygous (*p2ry2.1*$^{+/-}$) and wild type (*p2ry2.1*$^{+/+}$) siblings. Inbreeding of *p2y2.1*$^{+/-}$ fish results in the recovery of *p2ry2.1*$^{-/-}$ larvae (3 dpf) at ratios consistent with Mendelian inheritance. Among 36 siblings, 11 *p2ry2.1*$^{+/+}$ (30%), 19 *p2ry2.1*$^{+/-}$ (53%), and 6 *p2ry2.1*$^{-/-}$ (17%) were obtained. Importantly, a normal hypotonicity mediated tissue motion phenotype was observed in injured *p2ry2.1*$^{-/-}$ larvae ubiquitously expressing an AKT-PH-GFP reporter (Figure 4.7A).

Injection of a single Cas9-gRNA ribonucleoprotein (RNP) complex into one-cell stage embryos results in F0 fish that are genetic mosaics for wild-type and a variety of mutant alleles. These F0 fish have been termed “crispants”. More effective functional target disruption in F0 crispants can be achieved by co-injection of multiple redundant Cas9-gRNA RNP’s targeting the same gene (Burger et al., 2016; Hoshijima et al., 2019; Wu et al., 2018). In an orthogonal method to assess

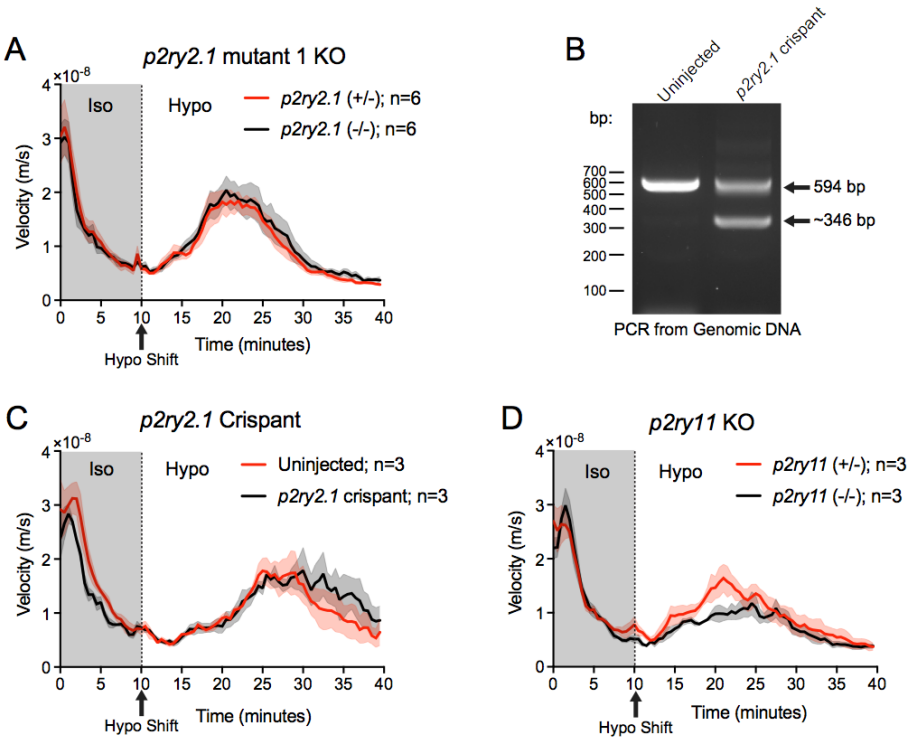

Figure 4.7. Hypotonicity-mediated tissue motion is normal in *p2ry2.1* knockout and crispant zebrafish larvae but perturbed in *p2ry11* knockout larvae

(A) PIV analysis of the indicated number of *p2ry2.1*$^{+/-}$ and *p2ry2.1*$^{-/-}$ larvae expressing ubiquitous plasma membrane GFP labeling (one-cell stage AKT-PH-GFP mRNA injection). Larvae were subjected to UV-laser wounding in isotonic medium and a bolus of hypotonic medium was added to the larvae at 10 min after injury. (B) Genomic DNA was isolated from 3 dpf *p2ry2.1* crispant larvae, and a portion of the *p2ry2.1* gene containing both Cas9-gRNA RNP target sites was PCR amplified and separated by agarose gel electrophoresis. The lane labeled "Uninjected" is a representative PCR product from gDNA of larvae that were not injected with Cas9-gRNA RNPs. The lane labeled "*p2ry2.1* crispant" is a representative image of the PCR amplification products from gDNA of larvae injected with both *p2ry2.1* Cas9-gRNA RNPs. The predicted wild type PCR product size is 594. The ~346 bp product is predicted to be amplified if the cut sites of the two Cas9-gRNA RNPs are fused by NHEJ, resulting in the loss of ~248 bp from the *p2ry2.1* exon. (C) PIV analysis of the indicated number of *p2ry2.1* crispant and uninjected sibling TG(*krt4*:AKT-PH-GFP) larvae. Larvae were subjected to UV-laser wounding in isotonic medium and a bolus of hypotonic medium was added to the larvae at 10 minutes after wounding. (D) PIV analysis of the indicated number of *p2ry11*$^{+/-}$ and *p2ry11*$^{-/-}$ exhibiting ubiquitous plasma membrane labeling (one-cell stage AKT-PH-GFP mRNA injection). Larvae were subjected to UV-laser wounding in isotonic medium and a bolus of hypotonic medium was added to the larvae at 10 min after injury. Values indicate the mean velocity ± SEM of the indicated (n) number of larvae.

p2ry2.1 function in larval epithelial wound closure, we generated *p2ry2.1* F0 crispants by co-injecting a 1:1 mixture of Cas9-gRNA RNPs made of gRNA1 and gRNA2 (Figure 4.4A). PCR amplification of the target followed by agarose gel electrophoresis demonstrated that crispant larvae displayed an ~248 bp truncated form of *p2ry2.1* that is predicted to form by Non-homologous end joining (NHEJ) at the DNA cut sites of the two Cas9-gRNA RNPs, confirming efficient target disruption (Figure 4.7B). TG(*krt4*:AKT-PH-mKate2) *p2ry2.1* crispants displayed the same hypotonicity mediated tissue motion phenotype as uninjected siblings (Figure 4.7C). Combined, these data suggest that *p2ry2.1* function is not essential for normal ATP-triggered epithelial wound closure in larvae.

p2ry11$^{-/-}$ zebrafish did not have any obvious developmental phenotypes at the larval stage (3 dpf) and were morphologically comparable to *p2ry11*$^{+/-}$ and *p2ry11*$^{+/+}$ siblings. Heterozygotes grown to adulthood were morphologically similar to wild-type adult zebrafish. *p2ry11*$^{-/-}$ larvae displayed a decreased range of epithelial tissue movement upon hypotonic exposure to injury sites compared to controls (Figure 4.7D). This suggests a potential role for *p2ry11* in larval zebrafish wound closure; however, more larvae, including *p2ry11*$^{+/+}$ siblings, will need to be tested and analyzed to increase confidence in this result.

p2rx1 is not essential for larval zebrafish epithelial wound closure

P2X ligand-gated ion channels are infrequently associated with nucleotide-mediated chemotaxis in comparison to P2Y GPCRs. However, P2X channel activation can trigger chemotaxis of certain cell types, such as in $P2X_1$ mediated neutrophil chemotaxis (Feng et al., 2015; Lecut et al., 2009; Sáez et al., 2017). P2rx1 is the most abundantly expressed P2 receptor in larval zebrafish basal epithelial cells, including P2Y GPCRs (Figure 4.3A). To assess for a functional role for P2rx1 in larvae epithelial wound closure, TG(*krt4*:AKT-PH-GFP) *p2rx1* crispant larvae were generated through co-injection of two Cas9-gRNA RNPs targeting *p2rx1* exon 1 (Figures 4.8A and B). UV laser injured *p2rx1* crispant animals displayed a hypotonicity mediated epithelial tissue motion phenotype similar to wild type uninjected sibling controls, suggesting that *p2rx1* is not essential for normal epithelial wound closure.

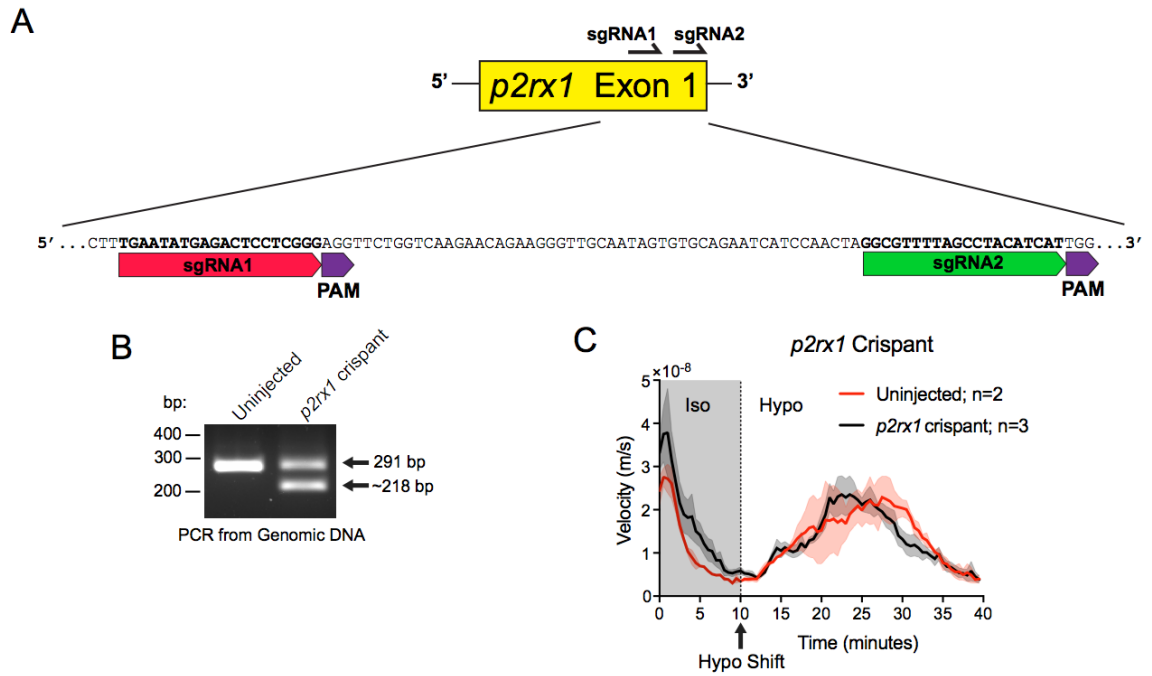

Figure 4.8. Hypotonicity-mediated tissue motion is normal in *p2rx1* crispant zebrafish larvae

(A) Schematic representation of exon 1 of the zebrafish *p2rx1* gene and the locations targeted for gene disruption by two Cas9-gRNA RNP complexes. The 20 base pair (bp) sgRNA targets and protospacer adjacent motif (PAM) sequences are indicated for sgRNA1 and 2. (B) Genomic DNA was isolated from 3 dpf *p2rx1* crispant larvae (larvae injected with both *p2rx1* Cas9-gRNA RNPs), and a portion of the *p2rx1* gene containing both RNP target sites was PCR amplified and separated by agarose gel electrophoresis. The lane labeled "Uninjected" is a representative PCR product from gDNA of larvae that were not injected with Cas9-gRNA RNPs. The lane labeled "*p2rx1* crispant" is a representative image of the PCR amplification products from gDNA of larvae injected with both *p2rx1* Cas9-gRNA RNPs. The predicted wild type PCR product size is 291 bp. The ~218 bp product is predicted to be amplified if the cut sites of the two Cas9-gRNA RNPs are fused by NHEJ, resulting in the loss of ~73 bp from *p2rx1* exon 1. (C) PIV analysis of the indicated number of *p2rx1* crispant and uninjected sibling TG(*krt4*:AKT-PH-GFP) larvae. Larvae were subjected to UV-laser wounding in isotonic medium and a bolus of hypotonic medium was added to the larvae at 10 minutes after wounding. Values indicate the mean velocity ± SEM of the indicated (n) number of larvae.

p2ry4 gene disruption perturbs nucleotide-mediated epithelial migration

Larval epithelial wound closure can be reconstituted by both ATP and UTP in an isotonic environment. $P2Y_2$ and $P2Y_4$ are the characterized UTP receptors in other species (Abbracchio et al., 2006; Bogdanov et al., 1998). Our data indicate that the predominant $P2Y_2$ isoform in basal epithelial cells does not play an essential role in epithelial wound closure, suggesting a potential role for $P2Y_4$. Interestingly, *p2ry4* is not expressed in the nucleotide-responsive basal epithelial cells but rather at high levels in unresponsive suprabasal epithelial cells (Figure 4.3A). A paracrine signaling mechanism may account for basal cell migration through the initial activation of $P2Y_4$ on suprabasal cells. We evaluated the efficiency of UTP to reconstitute closure of UV laser-mediated epithelial wounds in *p2ry4* crispant animals to test for a functional role for $P2Y_4$ in nucleotide-mediated wound closure. F0 genomic *p2ry4* disruption was achieved by the injection of two separate Cas9-sgRNA RNPs into one-cell stage TG(*krt4*:AKT-PH-mKate2) embryos (Figures 4.9A and B). *p2ry4* crispants had decreased duration and range of epithelial tissue movement in response to UTP (Figure 4.9C). This phenotype suggests *p2ry4* may play a role in hypotonicity mediated epithelial wound closure.

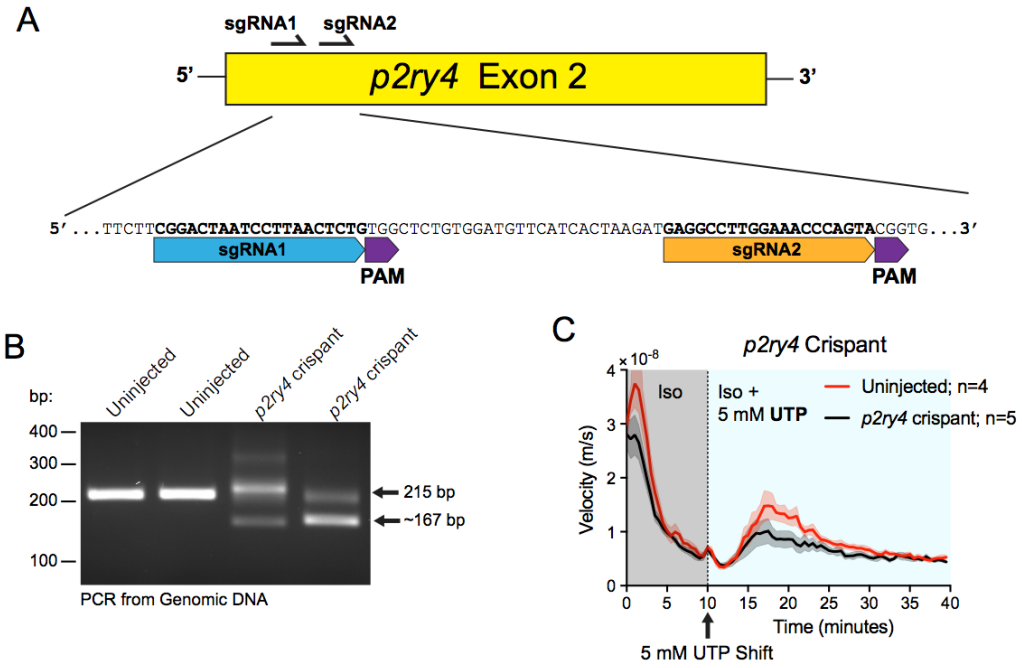

Figure 4.9. UTP-mediated tissue motion is perturbed in *p2ry4* crispant zebrafish larvae

(A) Schematic representation of the zebrafish *p2ry4* CDS and the locations targeted for genetic disruption by two Cas9-gRNA RNP complexes from sgRNA's. The 20 bp sgRNA targets and PAM sequences are indicated for sgRNA1 and 2. (B) Genomic DNA was isolated from 3 dpf *p2ry4* crispant larvae (larvae injected with both *p2ry4* Cas9-gRNA RNPs), and a portion of the *p2ry4* gene containing both RNP target sites was PCR amplified and separated by agarose gel electrophoresis. The lanes labeled "Uninjected" are representative PCR products from gDNA of larvae that were not injected with Cas9-gRNA RNPs. The lanes labeled "*p2ry4* crispant" are representative PCR amplification products from gDNA of larvae injected with both *p2ry4* Cas9-gRNA RNPs. The predicted wild type PCR product size is 215 bp. An ~167 bp product is predicted to be amplified if the cut sites of the two Cas9-gRNA RNPs are fused by NHEJ, resulting in the loss of ~48 bp from the *p2ry4* CDS. (C) PIV analysis of the indicated number of *p2ry4* crispant and uninjected sibling TG(*krt4*:AKT-PH-mK2) larvae. Larvae were subjected to UV-laser wounding in isotonic medium and a bolus of isotonic medium + 5 mM UTP was added to the larvae at 10 minutes after wounding. Values indicate the mean velocity ± SEM of the indicated (n) number of larvae.

Structure activity relationship (SAR) analysis of epithelial wound closure

Nucleotide agonist specificities of P2 receptor subtypes have been characterized in multiple species (Abbracchio et al., 2006; von Kügelgen and Hoffmann, 2016). Agonist profiling of larval zebrafish epithelial migration was previously performed by screening the abilities of a variety of nucleotide derivatives to reconstitute epithelial tissue movement in an isotonic environment; however, profiling was performed with only a limited number of ligands (Gault et al., 2014). Here, we expanded upon this initial screen by profiling additional nucleotide ligands for a more comprehensive SAR analysis to better characterize (1) the agonist profile of epithelial migration and (2) the ligand binding site of the receptor of interest. In general, we found that ATP and UTP derivatives with modifications at the triphosphate moiety could not reconstitute epithelial migration; however, derivatives with minor or even drastic modifications to the base, particularly to the adenine of ATP, were able to trigger basal cell migration and global increases in epithelial tissue velocity (Figures 4.10 and 4.11). Additional ligand screening revealed an agonist profile for basal cell migration that best resembles the profile of mammalian $P2Y_4$ receptor isoforms, which is in agreement with our genetic profiling (Table 4.2). The combination of genetic and pharmacological data suggests that the zebrafish $P2Y_4$ receptor potentially plays a role in triggering epithelial wound closure upon exposure to hypotonicity in zebrafish larvae.

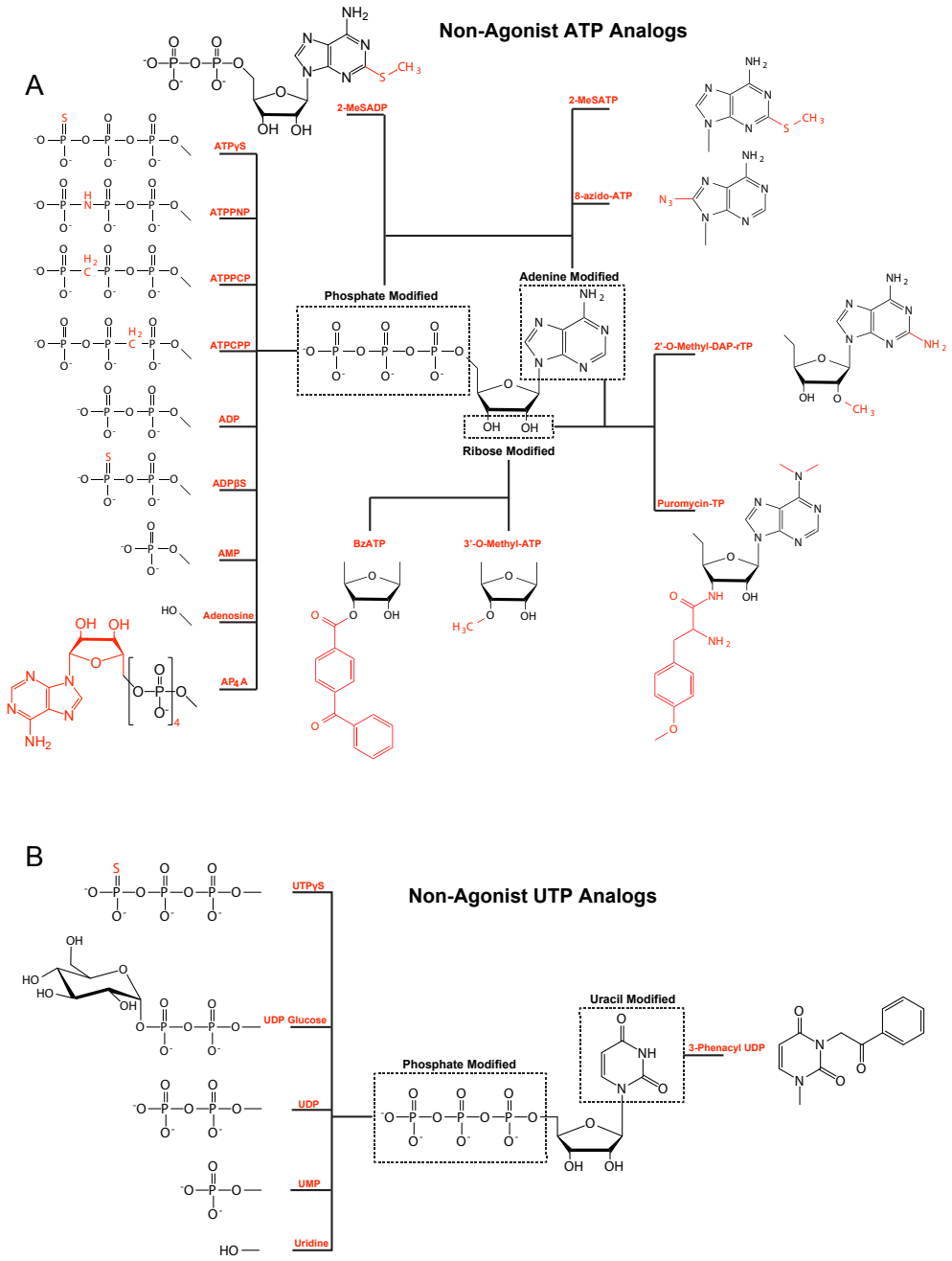

Figure 4.10. Nucleotide derivatives that cannot reconstitute epithelial wound closure

ATP (A) and UTP (B) derivates screened and failed to reconstitute epithelial wound closure when applied to wounded larval zebrafish tail fins in an isotonic environment. TG(*krt4*:AKT-PH-GFP) larvae expressing AKT-PH-mKate2 in basal cells (AKT-PH-mKate2 mRNA injected) were UV-laser wounded in isotonic medium, then shifted to isotonic medium containing 5 mM of the indicated compounds. Wound closure reconstitution was analyzed by PIV analysis and the ability of basal epithelial cells to generate lamellipodia in response to the applied ligand. Red structures indicate a deviation of the nucleotide derivative from natural ATP or UTP. This figure includes data generated from Gault et al., 2014.

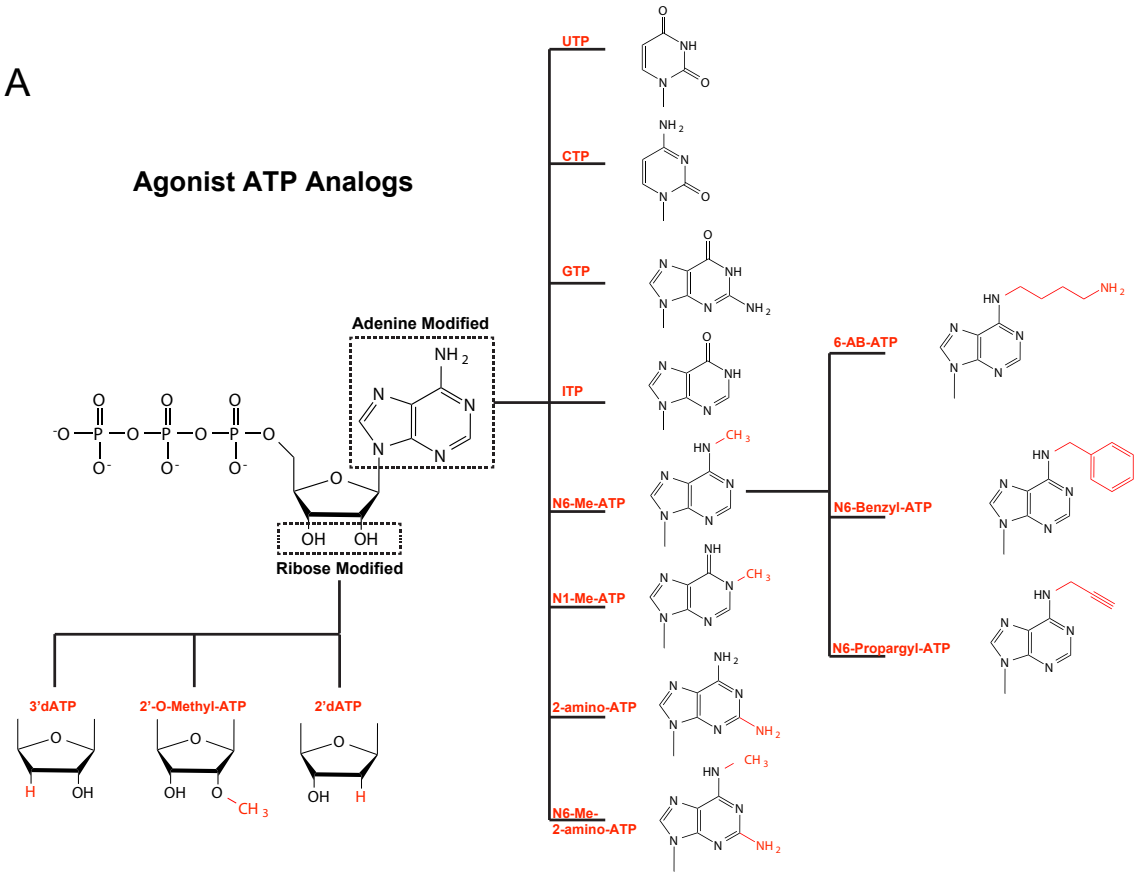

Figure 4.11. ATP derivatives that can reconstitute epithelial wound closure
ATP derivates screened that were able to reconstitute epithelial wound closure when applied to wounded larval zebrafish tail fins in an isotonic environment. TG(*krt4*:AKT-PH-GFP) expressing AKT-PH-mKate2 in basal cells (AKT-PH-mKate2 mRNA injected) were UV-laser wounded in isotonic medium, then shifted to isotonic medium containing 5 mM of the indicated compounds. Wound closure reconstitution was analyzed by PIV analysis and the ability of basal epithelial cells to generate lamellipodia in response to the applied ligand. Red structures indicate a deviation of the nucleotide derivate from ATP, except for UTP, CTP, GTP, and ITP for which the altered base remains in all black.

Receptor	Reported nucleotide agonist (Mammals)
$P2Y_1$	2-MeSADP^x, ADPβS^x, ADP^x, 2-MeSATP^x, **ATP***
$P2Y_2$	**UTP***, **ATP***, UTPγS^x, ATPγS^x, AP_4A^x
$P2Y_4$	**UTP***, **ATP***, UTPγS^x, AP_4A^x, **CTP***, **ITP***, **GTP***
$P2Y_6$	UDP^x, 3-PA-UDP^x, **UTP***, ADP^x
$P2Y_{11}$	ATPγS^x, BzATP^x, **ATP***, **UTP***, dATP^x ADPβS^x, 2-MeSADP^x, 2-MeSATP^x
$P2Y_{12}$	2-MeSADP^x, ADPβS^x, ADP^x
$P2Y_{13}$	ADP^x, 2-MeSADP^x, ADPβS^x, 2-MeSATP^x, **ATP***
$P2Y_{14}$	UDP^x, UDP-Glucose^x
$P2X_1$	BzATP^x, **ATP***, α,β-MeATP^x, β,γ-MeATP^x, 2-MeSATP^x
$P2X_2$	**ATP***, 2-MeSATP^x, ATPγS^x
$P2X_3$	**ATP***, 2-MeSATP^x, α,β-MeATP^x, BzATP^x
$P2X_4$	**ATP***, α,β-MeATP^x, **CTP***, 2-MeSATP^x
$P2X_5$	**ATP***, 2-MeSATP^x, ATPγS^x
$P2X_6$	No functional homomultimer
$P2X_7$	BzATP^x, **ATP***, 2-MeSATP^x

Table 4.2. Nucleotide ligands tested to rescue larval zebrafish epithelial wound closure in an isotonic environment and their known receptors
List of the nucleotide derivatives screened for the ability to reconstitute epithelial wound closure in larval zebrafish tail fins in an isotonic environment and the P2 receptors (mammalian isoforms) that they are documented to activate. Bold and underlined ligands with an asterisk (*) are agonists for basal epithelial cell migration in zebrafish larvae. Ligands with a (^{x}) cannot reconstitute basal epithelial cell migration.

N^6-substituted ATP derivatives reconstitute epithelial wound closure

The SAR analysis revealed that ATP derivatives with a hydrophobic addition at the N^6 amino are potent agonists for basal epithelial cell migration (Figure 4.11A). Interestingly, small hydrophobic N^6 additions, such as a methyl or propargyl, were even able to increase the duration and range of epithelial tissue motion compared to unmodified ATP at similar concentrations (Figure 4.12A, C, and D). N^6-modified derivatives with sterically larger additions were also able to reconstitute epithelial tissue motion; however, both the duration and range of motion were reduced in comparison to unmodified ATP (Figure 4.12 A, E and F). N^6-substituted ATP derivatives have been shown to activate P2Y, but not P2X, receptors in mammalian systems; however, no N^6-substituted ATP derivative is classified as a specific agonist for any P2Y receptor subtype (Fischer et al., 1993).

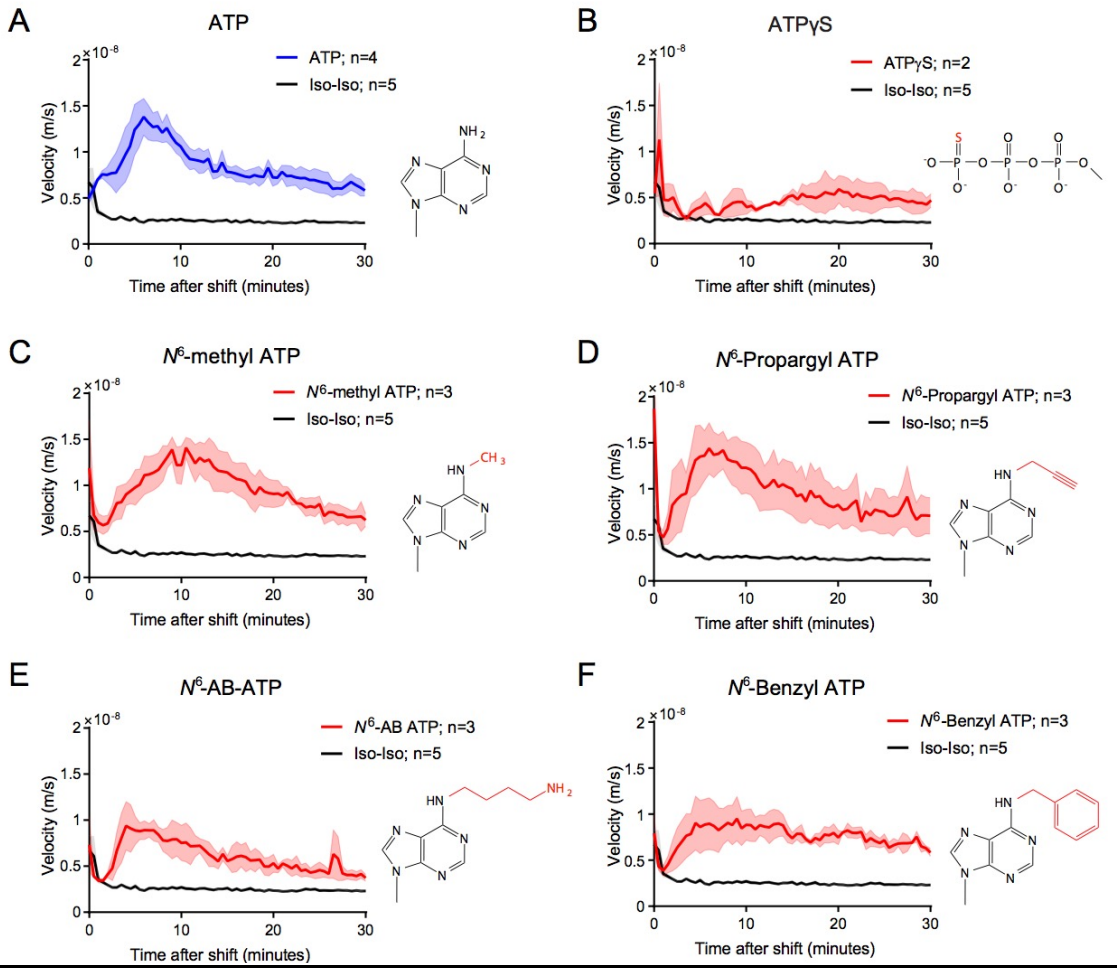

Figure 4.12. *N*^{6}-substituted ATP derivatives reconstitute epithelial tissue motion in the absence of a transepithelial osmotic gradient

(A-F) PIV analysis of the indicated number of TG(*krt4*:AKT-PH-GFP) larvae. Larvae were subjected to UV-laser wounding in isotonic medium and a bolus of isotonic medium ± 5 mM ATP or ATP derivative (7.5 mM *N*^{6} Benzyl ATP) was added to the larvae at 10 minutes after wounding. Note that PIV analysis does not include the initial 10 minute isotonic preincubation period (i.e, t = 0 minutes in the plot is 10 minutes after UV-laser injury and the start of imaging). Values indicate the mean velocity ± SEM of the indicated (n) number of larvae. Note, (A) is the same dataset as from Figure 4.2D and the Iso-Iso dataset is the same in all figures.

Minimally invasive photoaffinity ATP (mipATP) reconstitutes basal cell migration and epithelial tissue movement in the absence of a transepithelial osmotic gradient

The agonist profile of hypotonicity mediated epithelial wound closure diverges from all known P2 receptors. Genetic disruptions to *p2ry11* and *p2ry4* decrease the duration and range of nucleotide-mediated epithelial tissue motion compared to controls; however, it is a possible that a yet to be identified nucleotide receptor is the predominant mediator of epithelial wound closure in zebrafish larvae.

The SAR analysis suggests an ATP derivative that is fully functionalized at the N^6 amino would be able to interact with the receptor that triggers hypotonicity mediated epithelial wound closure. In chapter 3, I described the development and characterization of a minimally invasive photoaffinity ATP probe, mipATP, that is fully functionalized at the N^6 amino (Figure 4.13A). mipATP was able to reconstitute epithelial tissue motion and lamellipodia mediated basal cell migration in the absence of a transepithelial osmotic gradient, suggesting that this probe directly binds the nucleotide receptor of interest.

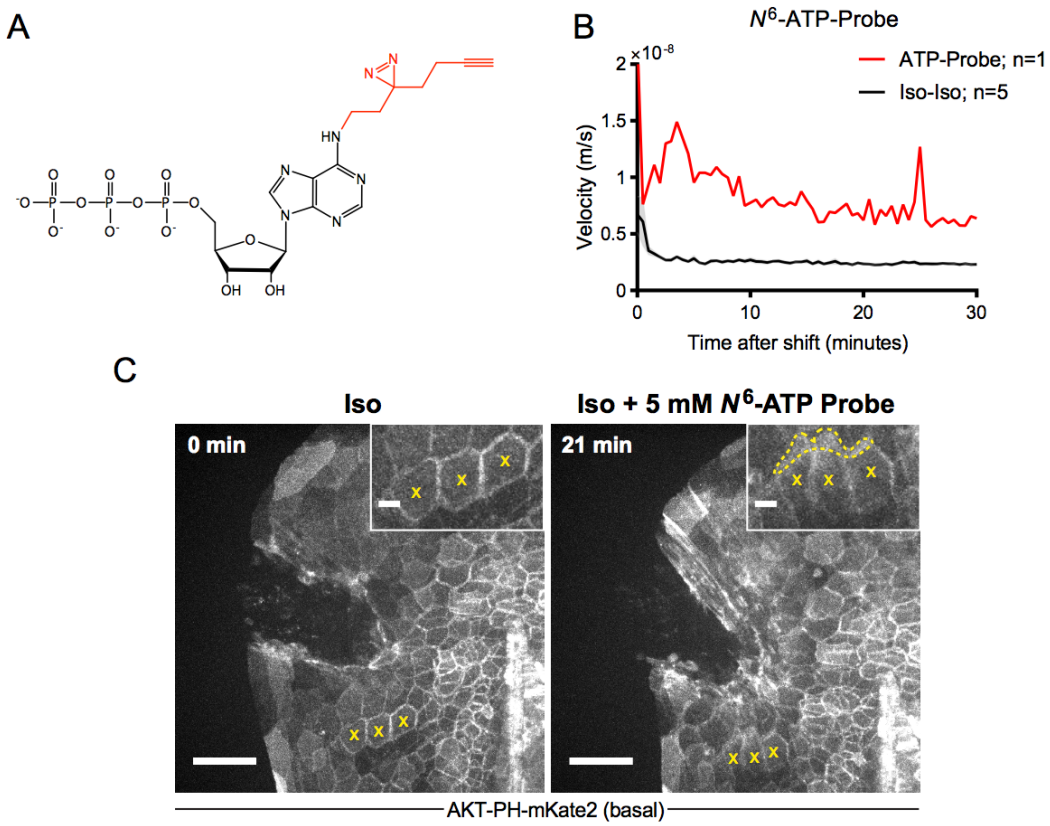

Figure 4.13. mipATP reconstitutes epithelial tissue motion and basal cell migration in the absence of a transepithelial osmotic gradient

(A) Molecular structure of the N^6-substituted photoaffinity ATP probe, mipATP. (B) PIV analysis of the indicated number of TG(*krt4*:AKT-PH-GFP) larvae. Larvae were subjected to UV-laser wounding in isotonic medium and a bolus of isotonic medium ± 5 mM mipATP was added to the larvae at 10 minutes after wounding. Note that PIV analysis does not include the initial 10 minute isotonic preincubation period (i.e, t = 0 minutes in the plot is 10 minutes after UV-laser injury and the start of imaging). Values indicate the mean velocity ± SEM of the indicated (n) number of larvae. Note, the Iso-Iso dataset is the same as in Figure 4.12. (C) Representative frames of epithelial wound closure reconstitution by exogenous 5 mM mipATP in a TG(*krt4*:AKT-PH-GFP) reporter larva with mosaic AKT-PH-mKate2 expression in basal cells through mRNA injection. Frames are from directly after UV-wounding (0 min) and 11 minutes after mipATP application (21 min after the start of imaging). Yellow x, representative cells developing lamellipodia (yellow dotted line, inset) in response to mipATP application. Scale bars, 50 μm and 10 μm (inset). Time in minutes.

Discussion

Using functional genetic perturbations and pharmacological profiling we demonstrated that zebrafish isoforms of $P2Y_4$ and $P2Y_{11}$ receptors, but not $P2Y_2$, potentially play roles in hypotonicity mediated epithelial wound closure in zebrafish larvae. Genetic disruptions of *p2ry11* and *p2ry4* revealed perturbed epithelial tissue motion phenotypes upon wound exposure to hypotonicity and exogenous nucleotides, respectively. The perturbed phenotypes displayed decreased duration and range of epithelial tissue movement. Further characterization of epithelial wound closure phenotypes in genetically perturbed larvae is required to better characterize the roles of $P2Y_{11}$ and $P2Y_4$. These future investigations should include, but not be limited to, evaluating a larger number of *p2ry11*$^{-/-}$ larvae and the effects of *p2ry4* genetic disruption on epithelial tissue motion upon wound exposure to hypotonicity. Additionally, the effects of simultaneous *p2ry11* and *p2ry4* gene disruption should be assessed due to reports of P2 receptor redundancy upon single gene knockout (Pochynyuk et al., 2008).

Disruption of *p2ry11* and *p2ry4* receptors alone did not completely abolish the ability of larvae to close epithelial wounds. This suggests that either *p2ry11* and *p2ry4* act in concert to trigger epithelial wound closure or that a separate, yet to be identified, ATP receptor(s) is additionally essential.

Our expanded SAR analysis uncovered a more detailed pharmacological agonist profile for epithelial wound closure. We revealed that ATP derivatives with small hydrophobic additions to the N^6 amino are equipotent to unmodified ATP in reconstituting epithelial wound closure. In the previous chapter we described a

minimally invasive photoaffinity ATP probe, termed mipATP, that allows for the enrichment and identification of conventional and novel ATP binding proteins in complex membrane proteomes. Intriguingly, mipATP is capable of reconstituting epithelial tissue movement in larval zebrafish in the absence of a transepithelial osmotic gradient. This suggests that mipATP can bind and potentially crosslink to the receptor(s) of interest, allowing for subsequent identification by LC-MS/MS. Future investigations utilizing mipATP to identify ATP binding proteins on intact zebrafish epithelial cells in culture or in isolated zebrafish cell membranes may be the optimal method for the identification of the receptor(s) of interest. It is possible that our previous mass spectrometry experiments (from Chapter 3) have enriched for the human ortholog of the receptor driving larval zebrafish wound closure. Future functional genetic screening of the selected candidates in zebrafish using crispant and/or morpholino based knockdown coupled to our established wound closure assays may shed light on the yet to be determined ATP receptor.

CHAPTER 5 Osmotic surveillance mediates rapid blood vessel dilation through nitric oxide signaling

Introduction

Acute inflammation is the first stage of wound repair, occurring within minutes after non-hemorrhaging tissue injury and is mainly characterized by the local recruitment of neutrophils to damage sites as the first line of defense to protect the internal tissues from environmental contaminants such as microbes (Gurtner et al., 2008). Before reaching the site of tissue injury, neutrophils must first escape circulation and transmigrate from blood vessels near the wounded tissue. Vascular endothelial cells (ECs) at rest do not interact with leukocytes, preventing their escape from circulation; however, injury activates ECs to promote neutrophil extravasation into wound sites (Pober and Sessa, 2007). EC activation results in leukocyte attachment by EC cell surface recruitment of P-selectin through exocytosis of Weibel-Palade bodies (WPBs) and by membrane association of platelet-activating factor (PAF) through the metabolism of newly generated arachidonic acid (AA) (Bonfanti et al., 1989; Lorant et al., 1991). Additionally, EC activation increases local blood flow and leukocyte number at vessels near the wounded tissue by vasodilation which is triggered by paracrine relaxation of vascular smooth muscle tone through EC dependent production of the potent vasodilators prostaglandin I_2 (prostacyclin or PGI_2) and nitric oxide (NO) (Ignarro et al., 1987; Moncada et al., 1976).

These initial EC responses to injury, termed type I activation, are rapid, occurring within seconds to minutes after tissue injury, and are independent of *de*

novo gene expression and protein synthesis (Pober and Sessa, 2007). Type I activation is triggered by recognition of damage signals and ligands including damage-associated molecular patterns (DAMPs), such as extracellular ATP, that activate GPCRs (Pober and Cotran, 1990). Inflammatory ligands can be released into the injured tissue by cell lysis and forms of non-lytic cell stress.

Epithelial damage triggers compartmental mixing resulting in subsequent displacement of tissues from their normal chemical and mechanical environments (Enyedi and Niethammer, 2015). The epithelia of freshwater animals such as zebrafish, as well as the oral, esophageal, and possibly lung mucosa of land mammals, are constantly exposed to hypotonic fluid (Jayaraman et al., 2001a, 2001b; Joris et al., 1993). These epithelial barriers separate the interstitial fluid (~270-300 mOsm, the common extracellular tonicity of vertebrates) from the hypotonic environment (fresh water, ~10 mOsm; saliva, ~30 mOsm) (Joris et al., 1993). Previously, we have shown that in a normal hypotonic environment, epithelial injury to zebrafish larvae results in a drop in interstitial osmotic pressure and subsequent cell swelling of internal tissues surrounding the injury site. Cell swelling triggers Ca^{2+} signaling and activates mechanosensitive cytosolic phospholipase A_2 (cPLA2) to release AA which rapidly recruits neutrophils to the injury site. Cell swelling also triggers non-lytic ATP secretion at injury sites which mediates epithelial wound closure through an unknown mechanism (Enyedi et al., 2013, 2016; Gault et al., 2014)

EC activation, particularly vasodilation, is initiated by Ca^{2+} signaling, extracellular nucleotides and nucleosides, and AA generation through activation of

cPLA2 in other systems (Egan and FitzGerald, 2006; Sessa, 2004; Smits et al., 1995). In this study, we asked if osmotic signaling mechanisms trigger a vascular response in acute inflammation in zebrafish larvae. We examined the potential involvement of osmotic surveillance in type I activation of ECs, focusing on vasodilation.

Results

Environmental hypotonicity triggers rapid vasodilation near epithelial injury sites in zebrafish larvae

To test for acute local vascular activation upon epithelial injury in larval zebrafish, we wounded 3 dpf larvae and observed the local vasculature using transgenic reporter lines and intravital time-lapse imaging. Double transgenic larvae with reporter labeled ECs (*flk*:RFP) (Jin et al., 2005) and suprabasal epithelial cells (*krt4*:AKT-PH-GFP) were injured by several pulses of a UV laser at the epithelial fold under the caudal hematopoietic tissue (Figure 5.1A). 2.5-3 dpf larvae have a small vessel that extends caudally from the caudal most end of the caudal artery (CA) (Figures 5.1A-D) (Isogai et al., 2001). This isolated vessel extends as a single tube, allowing for simple measurement of average vessel diameter changes upon injury, which we use as a proxy for vasodilation (Figure 5.1D) (Fritsche et al., 2000; Isogai et al., 2001). Blood vessel dilation occurred seconds after epithelial injury in zebrafish larvae, peaking between 15 to 20 minutes after injury at an ~30% increase in vessel diameter size compared to the vessel diameter at the moment of injury (Figure 5.1E). This is similar to mammals who have a peak vessel dilation at ~20 minutes after trauma (Stadelmann et al., 1998). Larval zebrafish blood vessels remain dilated at least 40 minutes after injury (Figure 5.1E). Further experiments need to be conducted to determine when/if vessels return to the same size prior to injury.

To test for a role of external tonicity in the vascular response to epithelial injury, we imaged ECs after UV laser wounding larvae acclimated to a bathing

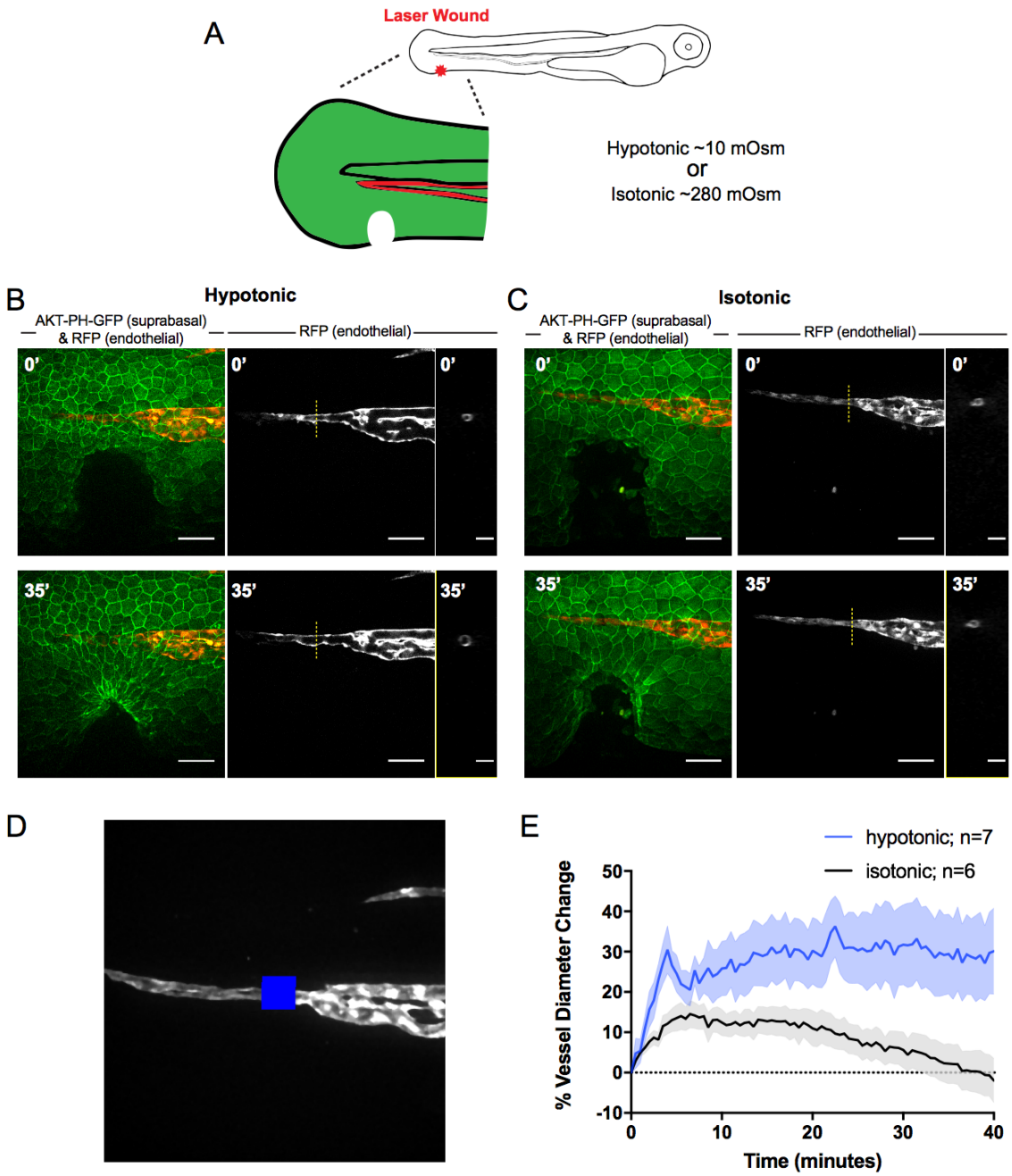

Figure 5.1. A drop in interstitial osmotic pressure mediates vasodilation after epithelial injury in zebrafish larvae

(A) Scheme of experimental set up. (B-C) Double transgenic 3 dpf larvae expressing a RFP reporter in endothelial cells and an AKT-pleckstrin homology domain-GFP reporter in the suprabasal epidermal layer (also known as TG(*flk*:RFP; *krt4*:AKT-PH-GFP) larvae) were injured at epithelium under the caudal hematopoietic tissue by UV-laser pulses in normal hypotonic medium ('hypotonic', containing 5 mM NaCl) or in medium that has been adjusted to the common extracellular tonicity of vertebrates (~270-300 mOsm) by the addition of 135 mM NaCl ('isotonic', containing 140 mM NaCl). Caudal endothelial and epithelial tissues were simultaneously imaged immediately after injury to monitor vascular

tone changes and wound closure. Representative frames are from immediately after injury (0') and 35 minutes after injury (35'). Broken yellow lines, sections of the caudal blood vessels visible in the orthogonal view (yz-plane). The orthogonal views (yz-plane) of the representative blood vessels show changes in blood vessel lumen area from immediately after injury (0') to 35 minutes after injury (35'). Scale bars, 50 μm and 25 μm in the orthogonal yz-plane images. (D) A custom MATLAB script measures the average diameter of the caudal blood vessel from 50 different slices throughout the 40 minute time-lapse. The average diameter is measured at each frame (30 seconds per frame) and subsequently normalized to the average vessel diameter measured immediately after injury (Time = 0'). Changes in vascular tone are then quantified as the percent change in average diameter of the caudal blood vessel compared to the average diameter immediately after injury (Time = 0') (E) Mean change in caudal blood vessel diameter over time after injury in hypotonic or isotonic medium. Error bars indicate SEM of indicated (n) number of larvae.

medium that had been adjusted to the ionic composition and tonicity of vertebrate interstitial fluid (isotonic medium; by the addition of NaCl). Vasodilation occurred after injury in isotonic medium; however, it was marginal in comparison to the vasodilation in normal hypotonic medium (Figure 5.1E). Vasodilation in isotonic medium occurred within seconds upon injury, peaking at ~5 minutes at a vessel diameter size increase of ~10% compared to ~30% in hypotonic medium (Figure 5.1E). Vessel diameter gradually returned to pre-injury size at ~40 minutes after injury (Figure 5.1E). This suggests that trauma mediated vasodilation depends on the osmotic difference between the freshwater environment and interstitial fluid of the fish, similar to the initial inflammatory response (Enyedi et al., 2013) and wound closure (Gault et al., 2014).

Isotonic inhibition of vasodilation can be rescued by exogenous adenine nucleotides

Next, we tested if isotonic inhibition of vasodilation was reversible. Isotonicity inhibits epithelial wound closure leaving wounds open and resulting in constant exposure of internal tissues to the bathing medium. Zebrafish larvae were acclimated to isotonic medium and tail fin tips were amputated to leave an open wound (Figure 5.2A). Injured larvae were mounted in isotonic agarose and imaged for 5 minutes prior to being exposed to a hypotonic bathing medium by application of a bolus of ~10x volume of hypotonic medium compared to the isotonic agarose pad (hypotonic shift) (Figure 5.2B). Hypotonic exposure triggered rapid vasodilation that peaked at an ~30% increase in diameter at ~25 minutes after application while a shift into a larger volume of isotonic medium had no vasodilatory effect (Figure 5.2C). These data suggest that vasodilation is reversibly inhibited by isotonicity and is triggered by a drop in interstitial osmotic pressure.

Osmotically induced AA and nucleotide release stimulate leukocyte migration to tail fin wounds and rapid wound closure, respectively (Enyedi et al., 2013; Gault et al., 2014). To test if AA and/or extracellular nucleotides could rescue isotonicity suppressed vasodilation, a bolus of isotonic medium containing AA or nucleotides was applied to tail fin tip amputated larvae in isotonic medium. A shift into 5 μM AA (enough to rescue leukocyte recruitment in isotonicity) induced a slight vasodilation within seconds after application that peaked within ~5 minutes after which the blood vessels began to constrict (Figure 5.2D). Vessels returned to normal size at ~15 minutes after AA application but vasoconstriction continued

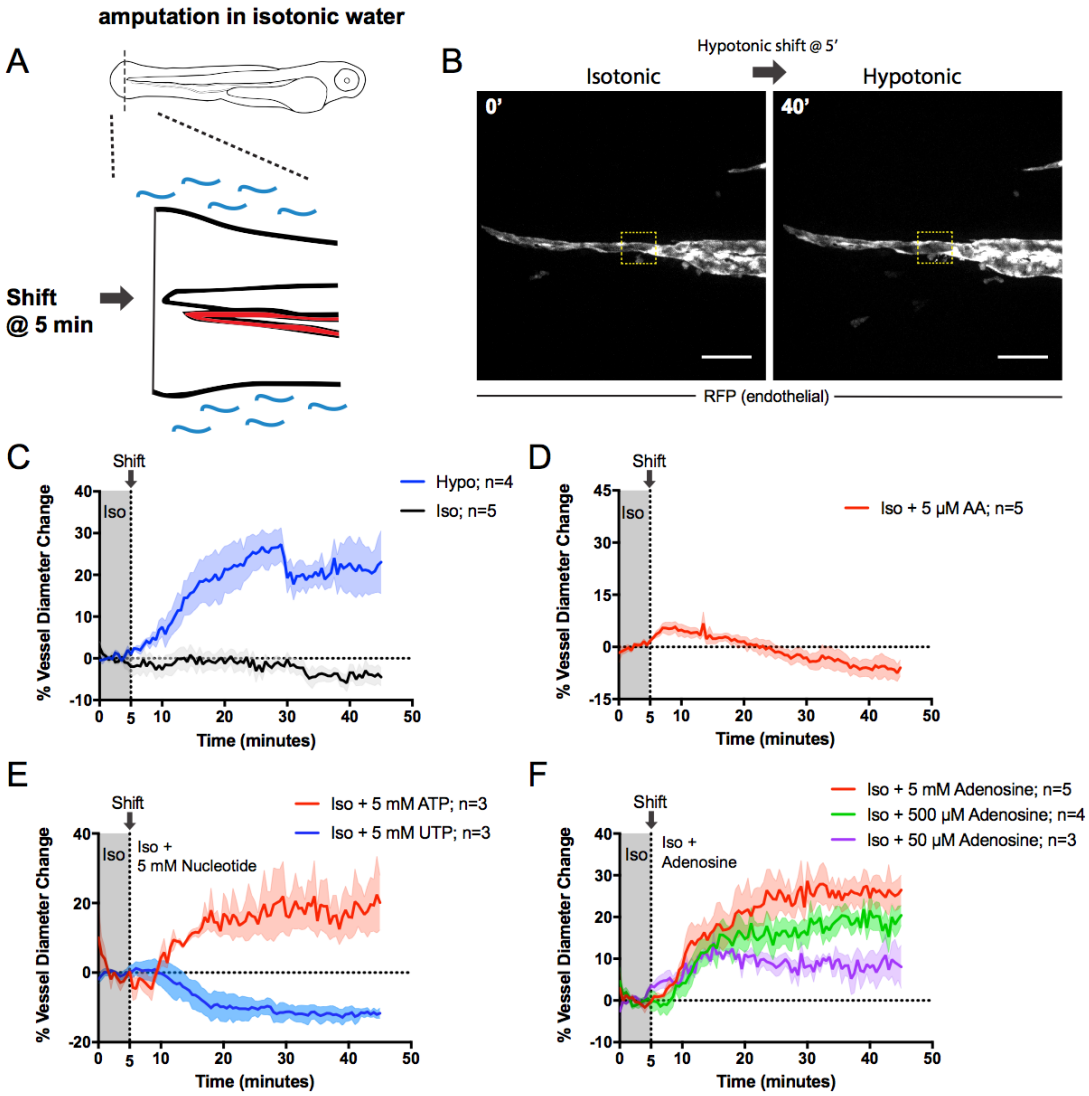

Figure 5.2. Adenine nucleotides reconstitute vasodilation in the absence of a transepithelial osmotic gradient

(A) Scheme of experimental setup. 3 dpf TG(*flk*:RFP) larvae are acclimated to isotonic medium, subjected to tail fin tip amputation, and mounted in isotonic agarose prior to imaging. At 5 minutes into imaging a bolus of ~10x the volume of the agarose pad of hypotonic medium or isotonic medium containing the indicated small molecule is applied to the mounted larva. The caudal blood vessel is then imaged for another 40 minutes after the shift into new medium. (B) Representative frames from an isotonic to hypotonic shift. Frames are from the start of imaging (0') and 35 minutes after the shift into hypotonic medium (40'). Broken yellow lines highlight the portion of the caudal blood vessel for which the average diameter is quantified over time. Time is in minutes. Scale bars, 50 µm. (C) Mean percent change in caudal blood vessel diameter as a function of time 5 minutes before and 40 minutes after a shift into normal hypotonic or isotonic embryo medium. The average caudal blood vessel diameter at each timepoint is normalized to the median average blood vessel diameter of the timepoints before the shift. Changes in vascular tone are then quantified as the percent change in average diameter of the caudal blood vessel compared to the median average diameter before the shift. (D) Mean percent change in

average caudal blood vessel diameter over time after a shift into isotonic medium containing 5 μM arachidonic acid (AA). (E) Mean percent changes in caudal blood vessel diameter over time after a shift into isotonic medium containing 5 mM ATP or 5 mM UTP. (F) Mean percent changes of caudal blood vessel diameter over time after shifts into isotonic medium containing the indicated concentrations of adenosine (50 μM, 500 μM, and 5 mM). Error bars indicate SEM of indicated (n) number of larvae.

with vessel diameters shrinking to ~90% of their original size (Figure 5.2D).

Similar to larval zebrafish wound closure (Gault et al., 2014), application of cytoplasmic levels (5 mM) of ATP rescued vasodilation in the absence of a transepithelial osmotic gradient (Figure 5.2E). Unlike in wound closure, UTP could not rescue vasodilation (Figure 5.2E). Similar to mammals, exposure to UTP induced rapid vasoconstriction, constricting vessels to ~85% of their original size (Figure 5.2E) (von Kügelgen et al., 1987). This suggests that isotonicity suppressed vasodilation and wound closure can be rescued in isotonic medium by extracellular ATP but through distinct mechanisms.

The half-life of extracellular nucleotides in intact tissues is short, ranging from seconds to milliseconds, due to rapid hydrolysis by extracellular nucleotidases such as ecto-NTP diphosphohydrolases (ENTPDases) (Gault et al., 2014; Yegutkin, 2008; Zimmermann et al., 2012). Adenosine, the product of complete hydrolysis of ATP, is a potent vasodilator in mammals through ligation to P1 GPCRs on ECs, specifically the A_{2A} and A_{2B} receptors (Burnstock and Ralevic, 2014; Smits et al., 1995). Similar to ATP, 5 mM of adenosine was able to reconstitute vasodilation in the absence of environmental hypotonicity (Figure 5.2F). Adenosine seemed to be a more potent vasodilator than ATP, increasing blood vessel diameter by ~25% compared to 20% (Figures 5.2E & F). Adenosine mediated vasodilation occurred in a concentration dependent manner, with as little as 50 μM capable of increasing vessel diameter size by ~10% (Figure 5.2F). These data suggest that extracellular ATP and adenosine can reconstitute

vasodilation in the absence of hypotonicity in larval zebrafish, but AA and UTP cannot.

Adenosine triggers vasodilation in zebrafish larvae by activating A_{2B} receptors

RNA sequencing revealed that 3 dpf zebrafish express the adenosine receptors *adora1b*, *adora2aa*, *adora2ab*, and *adora2b* at relatively similar levels (Figure 5.3A) (Huang and Niethammer, 2018). Mammalian orthologs of *adora2aa* (A_{2A}) and *adora2b* (A_{2B}) have been shown to mediate vasodilation in other systems (Belardinelli et al., 1998); therefore, we decided to genetically perturb these receptors to determine if they are involved in adenosine mediated vasodilation in zebrafish larvae. For *adora2aa* gene disruption, F0 crispant larvae were obtained by co-injection of two Cas9-RNPs targeting the coding sequence on exon 3 into the cytosol of one-cell stage TG(*flk*:RFP) embryos (Figure 5.3B). Simultaneous gDNA damage generated a truncated form of *adora2aa* in injected larvae (Figure 5.3C). Exogenous adenosine was capable of rescuing isotonicity suppressed vasodilation in *adora2aa* crispants, suggesting that vasodilation does not occur through A_{2A} activation (Figure 5.3D).

Next, crispant animals with a truncated *adora2b* coding sequence were generated by simultaneous Cas9-RNP injection into one-cell stage embryos (Figures 5.3E & F). Exogenous adenosine was not able to rescue vasodilation in *adora2b* crispant larvae in the absence of hypotoncity (Figure 5.3G). This suggests that induction of vasodilation by adenosine in the absence of a hypotonic environment is triggered by activation of the Adora2b (A_{2B}) receptor. Importantly, *adora2aa* and *adora2b* crispants grew to larval stages without obvious developmental phenotypes and were morphologically comparable to uninjected siblings.

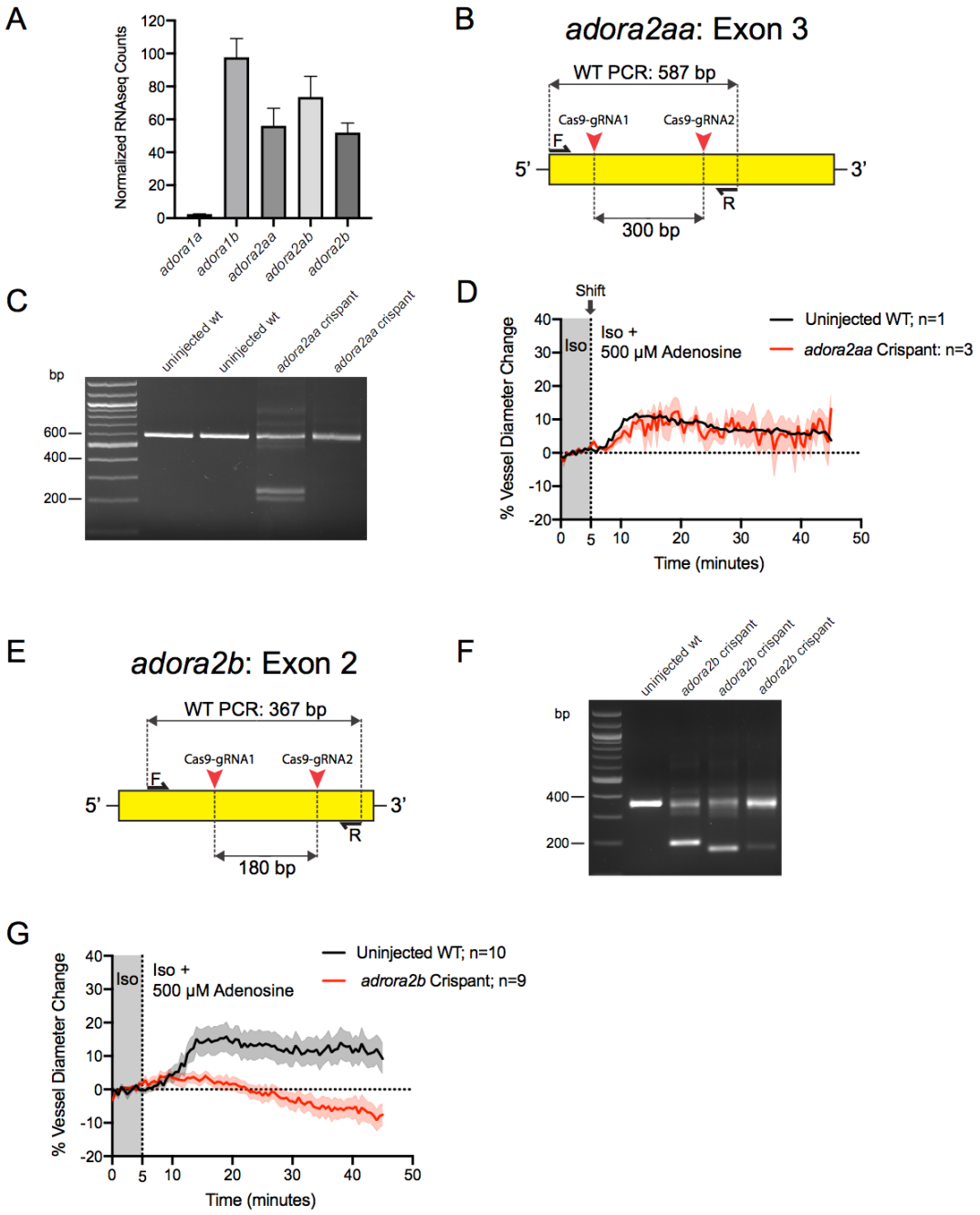

Figure 5.3. Exogenous adenosine reconstitutes vasodilation through the Adora2b (A_{2B}) receptor

(A) mRNA sequencing reveals the expression levels of extracellular adenosine receptors in 3 dpf wt *casper* zebrafish larvae. Data represents mean normalized mRNAseq counts ± SEM from three independent experiments (Huang and Niethammer, 2018). (B) Schematic representation of exon 3 of the zebrafish *adora2aa* gene and the locations targeted for gene disruption by two Cas9-gRNA RNP complexes. The Cas9-RNPs are predicted to cut the *adora2aa* coding sequence 300 bp apart, resulting in potential truncated gDNA after double-stranded DNA repair by non-homologous end joining

(NHEJ). Disrupted gDNA is monitored in 2-3 dpf larvae injected with the Cas9-RNPs (‘*adora2aa* crispants’) by PCR amplification of a gDNA region on exon 3 containing the two Cas9-RNP target sites. *Adora2aa* crispant animals are predicted to contain truncated PCR product (~300 bp less than the 587 bp WT product) compared to uninjected sibling controls (587 bp PCR product) signifying successful gene disruption. F and R indicate the locations on zebrafish gDNA of the forward and reverse PCR primers used for analysis, respectively. (C) Agarose gel electrophoresis analysis depicting representative amplified *adora2aa* gDNA PCR products from separate 3 dpf *adora2aa* crispant larvae (‘*adora2aa* crispant’) and uninjected sibling controls (‘uninjected wt’). (D) Mean percent changes in average caudal blood vessel diameter in tail fin tip amputated 3 dpf *adora2aa* crispants (‘*adora2aa* Crispant’) and uninjected sibling control (‘Uninjected WT’) before and after the application of isotonic medium containing 500 μM adenosine. (E) Schematic representation of exon 2 of the zebrafish *adora2b* gene and the locations targeted for gene disruption by two Cas9-RNPs. The Cas9-RNPs are predicted to cut the *adora2b* coding sequence 180 bp apart, resulting in potential truncated gDNA after NHEJ. *Adora2b* crispant larvae are predicted to have a truncated PCR product (~180 bp less than the 367 bp WT product) compared to uninjected sibling controls signifying successful gene disruption. F and R indicate the locations on zebrafish gDNA of the forward and reverse PCR primers used for analysis, respectively. (F) Agarose gel electrophoresis analysis depicting representative amplified *adora2b* gDNA products from separate 3 dpf *adora2b* crispant larvae (‘*adora2b* crispant’) and an uninjected sibling control (‘uninjected wt’). (G) Mean percent changes in average caudal blood vessel diameter in tail fin tip amputated 3 dpf *adora2b* crispants (‘*adora2b* Crispant’) and uninjected sibling controls (‘Uninjected WT’) before and after the application of isotonic medium containing 500 μM adenosine. Error bars indicate SEM of indicated (n) number of larvae.

Hypotonicity induced vasodilation is not solely triggered by extracellular nucleotides

To test if hypotonicity induced vasodilation occurs through extracellular adenosine activation of the Adora2b receptor, TG(*flk*:RFP) *adora2b* crispants were shifted into hypotonic medium after tail fin tip amputation in isotonic medium. Exposure to hypotonicity equally triggered vasodilation in *adora2b* crispants and uninjected siblings (Figure 5.4A). This suggests that adenosine is not the molecule or not the sole molecule that stimulates hypotonicity triggered vasodilation after epithelial injury in zebrafish larvae.

P2 purinergic ATP receptors have been shown to mediate vasodilation in other systems (Burnstock, 2017; Hopwood and Burnstock, 1987). Cytoplasmic levels of ATP were capable of triggering vasodilation in zebrafish larvae in the absence of a hypotonic environment (Figure 5.2E). Pre-incubation with Suramin, a compound used as a non-specific P2 receptor inhibitor, completely inhibited hypotonicity mediated vasodilation (Figure 5.4B). Suramin acts non-specifically at GPCRs, blocking association of G protein α and $\beta\gamma$ subunits (Beindl et al., 1996; Chung and Kermode, 2005). This suggests that hypotonicity mediated vasodilation occurs downstream of GPCR signaling; though not necessarily through P2 receptors. Next, we tested whether or not vasodilation triggered by exogenous ATP application occurs through extracellular hydrolysis to adenosine and subsequent activation of A_{2B}. We found that exogenous ATP was unable to trigger vasodilation in *adora2b* crispants in the absence of hypotonicity, suggesting that

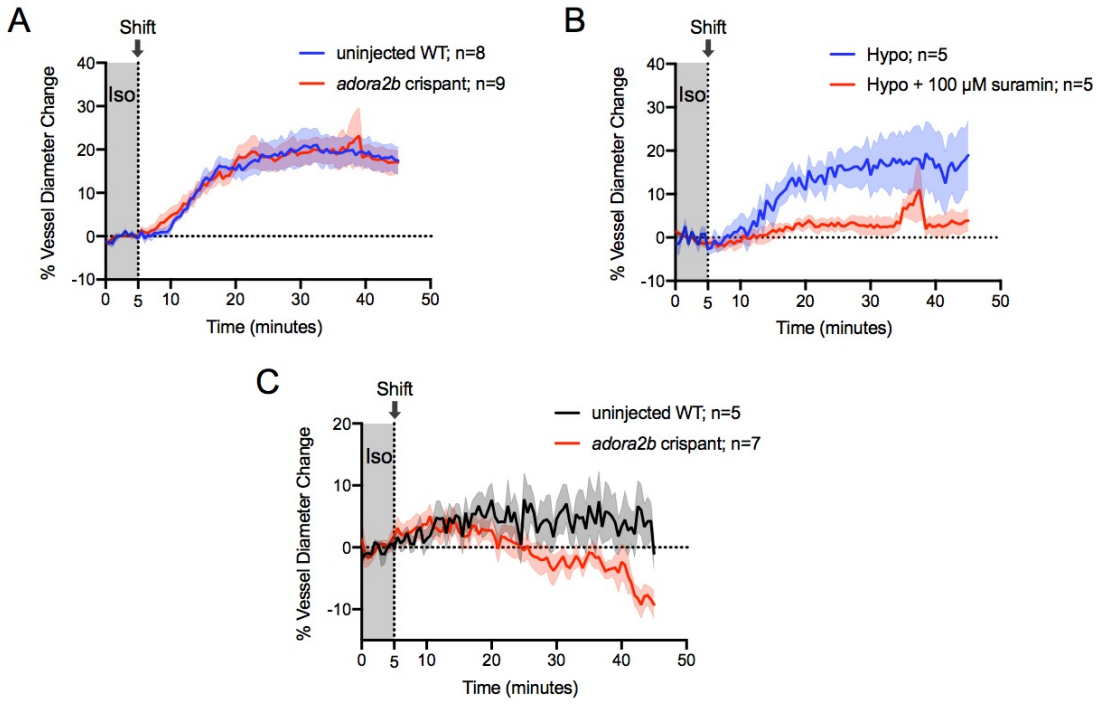

Figure 5.4. Extracellular adenine nucleotides are not essential for hypotonicity mediated vasodilation

(A) Mean percent change in average caudal blood vessel diameters over time in tail fin tip amputated 3 dpf *adora2b* crispants ('*adora2b* crispant') and uninjected sibling controls ('uninjected WT') after a shift from isotonic to hypotonic medium. The shift is at 5 minutes into imaging and imaging continues for an extra 40 minutes after the shift. Error bars indicate SEM of the indicated (n) number of larvae. (B) 3 dpf larvae are acclimated to isotonic medium, tail fin tip amputated, and subsequently incubated for 30 minutes in isotonic medium alone or containing 100 µM Suramin. Larvae are mounted in isotonic agarose with or without 100 µM Suramin and shifted into excess hypotonic medium with ('Hypo + 100 µM Suramin') or without ('Hypo') 100 µM Suramin at 5 minutes after the start of imaging. Mean percent changes in the caudal blood vessel diameter after the shift are calculated by normalizing the average vessel diameter at each timepoint to the median average vessel diameter in the frames prior to the shift. Error bars indicate SEM of indicated (n) number of larvae. (C) Mean percent change in average caudal blood vessel diameters over time in tail fin tip amputated 3 dpf *adora2b* crispants ('*adora2b* crispant') and uninjected sibling controls ('uninjected WT') after a shift from isotonic medium to isotonic medium containing 500 µM ATP. Error bars indicate SEM of indicated (n) number of larvae.

ATP triggers vasodilation through its hydrolysis to adenosine by ectonucleotidases and subsequent activation of A_{2B} (Figure 5.4C). Together these data suggest that vasodilation activated by exposure of internal tissues to the hypotonic environment after injury does not occur through extracellular nucleotides secreted upon cell swelling or that there are redundant osmotically triggered mechanism(s) coupled to nucleotide release that trigger vasodilation in concert.

cGMP production is essential to hypotonicity dependent vasodilation

In mammals, increases in cytosolic Ca^{2+} in ECs upon injury can activate endothelial nitric oxide synthase (eNOS) to generate the potent vasodilator nitric oxide (NO) that freely diffuses across membranes to activate NO-sensitive soluble guanylyl cyclase (sGC) in vascular smooth muscle cells (Figure 5.5A) (Russwurm and Koesling, 2004). Subsequent formation of intracellular cyclic guanosine monophosphate (cGMP) mediates vasodilation through activation of cGMP-dependent protein kinases (PKGs) (Francis et al., 2010; Zhao et al., 2015). Mammals possess three separate NOS isoforms, neuronal (nNOS; NOS1), inducible (iNOS; NOS2), and endothelial (eNOS; NOS3) with eNOS being most implicated in EC mediated vasodilation. Zebrafish possess a nNOS ortholog (*nos1*) and two orthologous isoforms of iNOS (*nos2a* and *nos2b*), but no distinct eNOS ortholog. 3 dpf zebrafish larvae express *nos1* and *nos2b*, with *nos1* being the most abundant NOS isoform (Figure 5.5B) (Huang and Niethammer, 2018).

To test if NOS plays a role in hypotonicity mediated vasodilation, we first confirmed that hypotonicity can induce transient increases in intracellular Ca^{2+} in transgenic larvae expressing a nuclear-targeted, genetically encoded GCaMP6s Ca^{2+} reporter (Figures 5.5C & D). Next, to verify vasodilation dependence on cGMP, we pharmacologically blocked cGMP formation with the highly selective sGC inhibitor ODQ. Incubation with ODQ completely inhibited hypotonicity triggered vasodilation at concentrations $\geq$ 50 μM, indicating a dependence on sGC activity and cGMP formation (Figure 5.5E).

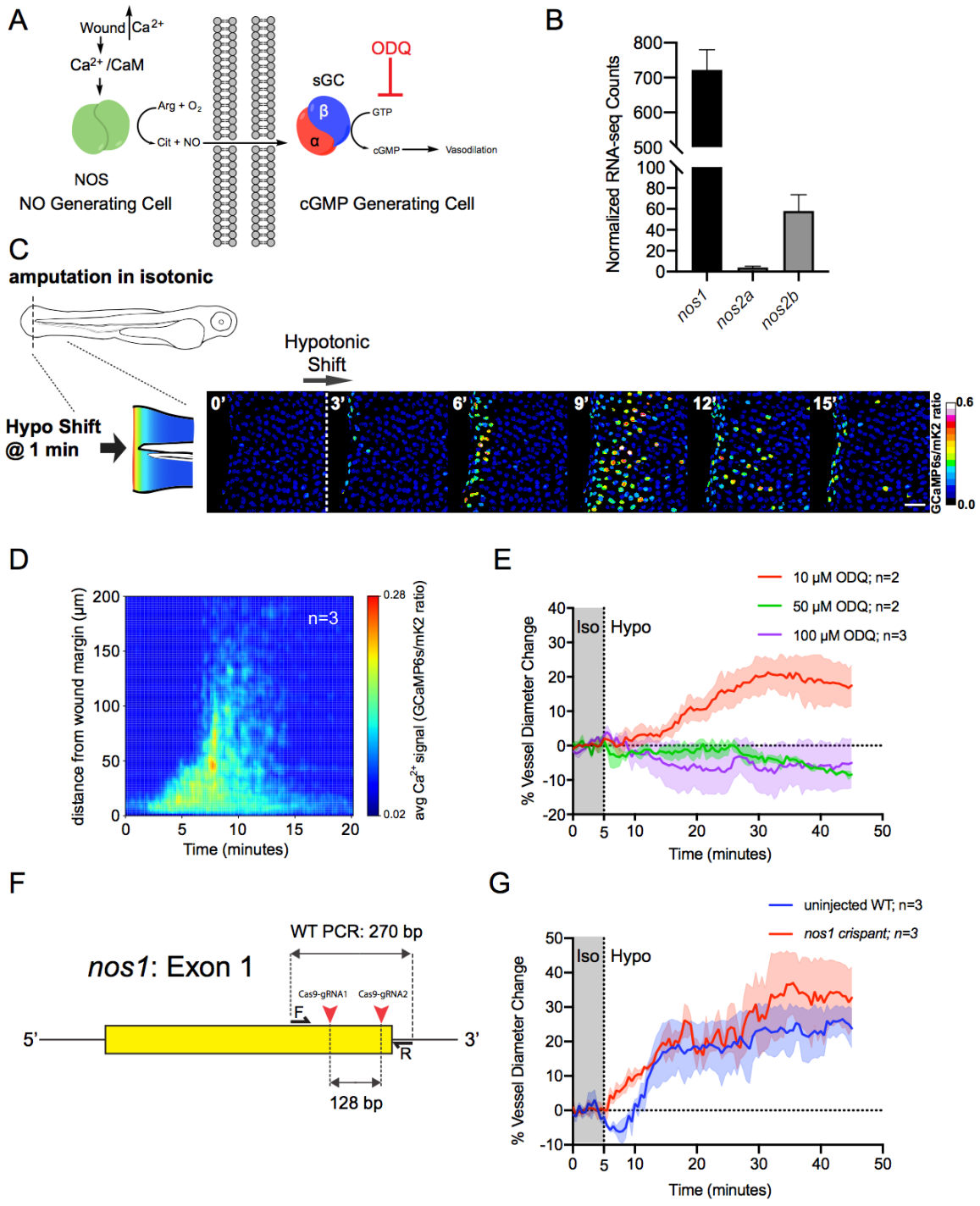

Figure 5.5. Hypotonicity triggers cGMP production to induce vasodilation after epithelial injury to zebrafish larvae

(A) Scheme of injury triggered nitric oxide (NO) production and subsequent cyclic guanosine monophosphate (cGMP) generation in neighboring tissues through paracrine signaling. The small molecule ODQ inhibits the production of cGMP through competitive inhibition of NO for soluble guanylyl cyclase (sGC). (B) mRNA sequencing reveals the expression levels of the known nitric oxide synthase (NOS) isoforms in 3 dpf wt *casper*

zebrafish larvae. Data represents mean normalized mRNAseq counts ± SEM from three independent experiments (Huang and Niethammer, 2018). (C) Left: Scheme of experimental setup. TG(*hsp70l*:GCaMP6s-3xNLS-P2A-mKate2-3xNLS) 3 dpf larvae are acclimated to isotonic medium, tail fin tip amputated, and mounted in isotonic agarose. Larvae are shifted to hypotonic medium at 1 minute into imaging. Right: Ratiometric imaging of Ca^{2+} transients evoked by a shift from an isotonic environment to a normal hypotonic environment. Nuclear GCaMP6s signals are normalized by nuclear mKate2 (mK2) fluorescence. Scale bar, 50 µM. (D) Average spatiotemporal Ca^{2+} signal profile of the indicated (n) number of transgenic Ca^{2+} reporter larvae TG(*hsp70l*:GCaMP6s-3xNLS-P2A-mKate2-3xNLS) after the shift into hypotonic medium. (E) Mean percent change in average caudal blood vessel diameter of TG(*flk*:RFP) larvae treated with the indicated concentrations of ODQ (10 µM, 50 µM, and 100 µM) after a shift from an isotonic to a normal hypotonic environment. (F) Schematic representation of exon 1 of the zebrafish *nos1* gene and the locations targeted for gene disruption by two Cas9-RNPs. The Cas9-RNPs are predicted to cut the *nos1* coding sequence 128 bp apart, resulting in potential truncated gDNA after NHEJ. *Nos1* crispant larvae are predicted to have a truncated PCR product (~128 bp less than the 270 bp WT product) compared to uninjected sibling controls signifying successful gene disruption. F and R indicate the locations on zebrafish gDNA of the forward and reverse PCR primers used for analysis, respectively. (D) Mean percent change in average caudal blood vessel diameter of tail fin tip amputated 3 dpf *nos1* crispants (‘*nos1* crispant’) and uninjected sibling controls (‘uninjected WT’) after a shift from an isotonic to a normal hypotonic environment. Error bars indicate SEM of indicated (n) number of larvae.

To determine the source of NO that activates sGC we genetically perturbed *nos1*, the most abundant NOS isoform in 3 dpf zebrafish larvae (Figure 5.5B). Two separate Cas9-RNPs targeting exon 1 of *nos1* were injected into the cytosol of one-cell stage TG(*flk*:RFP) embryos to generate F0 crispants with mosaic disruption of *nos1* (Figure 5.5F). *Nos1* crispant animals did not have perturbed hypotonicity mediated vasodilation, suggesting either that *nos1* is not involved in vasodilation or that a mosaic *nos1* knockout is not efficient enough to perturb *nos1* mediated vasodilation (Figure 5.5G).

Discussion

We have demonstrated that a signaling circuit triggered by a drop in interstitial osmotic pressure is the master regulator of injury induced vasodilation in zebrafish. Hypotonicity mediated vasodilation occurred at a similar timescale to injury induced vasodilation in mammals (Stadelmann et al., 1998). We did not image the larvae long enough to determine when or if blood vessels return to their original size prior to injury; however, vessel diameter began to constrict from peak size at around 40 minutes after injury. This same osmotic cue mediates wound detection by leukocytes through AA release and rapid wound closure through the secretion of nucleotides (Enyedi et al., 2013; Gault et al., 2014).

Extracellular adenosine triggered a concentration dependent rescue of vasodilation in the absence of a transepithelial osmotic gradient and was capable of triggering vasodilation to a similar extent as hypotonicity between concentrations of 0.5 and 5 mM (~20-25% increase in vessel diameter). Genetic disruption of *adora2b* mediated by embryo injection with multiple targeted Cas9-RNPs demonstrated that adenosine mediated vasodilation was solely dependent on the A_{2B} receptor. Similar to adenosine, extracellular ATP is capable of triggering vasodilation in larvae; however, this was dependent on the A_{2B} receptor and therefore most likely occurs through extracellular ATP hydrolysis to adenosine by ectonucleotidases in the interstitial space. Intriguingly, genetic disruption of *adora2b* had no effect on hypotonicity induced vasodilation, suggesting that adenosine, and therefore cell swelling triggered nucleotide secretion, does not mediate vasodilation in response to epithelial injury or that nucleotide signaling is

not the sole trigger for hypotonicity mediated vasodilation. Additionally, adenosine mediated vasodilation in larval zebrafish may be an important response in a yet to be determined context separate from the acute inflammatory response such as in response to shear stress caused by blood flow.

Osmotic cues trigger activation of cPLA2 and subsequent AA release upon epithelial injury in zebrafish larvae (Enyedi et al., 2013, 2016). Free AA can be sequentially converted by cyclooxygenases 1 and 2 (COX1 and COX2) to prostaglandin H2 (PGH_2), the first intermediate in the biosynthesis of prostanoids, and then by prostaglandin I2 synthase (PTGIS) to the potent vasodilator PGI_2, which has been shown to activate ECs in mammals (Egan and FitzGerald, 2006; Moncada et al., 1976; Rubin et al., 1982). PGH_2 can also be rapidly converted to the potent vasoconstrictor thromboxane A2 (TXA_2) by cells expressing thromboxane A synthase 1 (TBXAS1), most notably platelets (Egan and FitzGerald, 2006; Hamberg et al., 1975). The homeostatic balance of PGI_2 and TXA_2 plays a crucial role in vascular tone and imbalance in their production has been implicated in the pathology of cardiovascular disorders (Caughey et al., 2001; Oates et al., 1988). Bathing wounded zebrafish larvae in AA in an isotonic environment does not mimic the spatiotemporal release of AA triggered by hypotonicity at sites of injury. The cell permeability of AA allows for all cell types in the larvae to simultaneously take up free AA. The importance of cell type on AA metabolism indicates that this method is not optimal for testing the potential role of AA in hypotonicity mediated vasodilation. Further experiments utilizing genetic disruptions of the enzymes involved in the eicosanoid cascade including cPLA2,

COX1, COX2, and PTGIS will be conducted to identify a potential role for AA release in osmotically triggered vasodilation in zebrafish larvae.

NO is a potent vasodilator that is generated by NOS activation through injury induced Ca^{2+} signals. Exogenous sources of NO have previously been shown to trigger vasodilation in zebrafish larvae to a similar extent as exposure to hypotonicity (Fritsche et al., 2000). Incubation with non-selective NOS inhibitors prevented NO mediated vasodilation in these studies. Importantly, we have shown that hypotonicity triggers Ca^{2+} transients required for NOS activation. Additionally, treatment of zebrafish larvae with the highly selective small molecule inhibitor of sGC, ODQ, ablates hypotonicity mediated vasodilation, suggesting the requirement for cGMP production. These data implicate the involvement of NOS activation in larval zebrafish vasodilation; however, zebrafish do not have an obvious ortholog of the predominant NOS isoform involved in acute, injury triggered vasodilation in mammals, eNOS. Genetic disruption of the most highly expressed NOS isoform in zebrafish larvae, *nos1* (the zebrafish ortholog of mammalian nNOS), did not have observable effects on hypotonicity mediated vasodilation. Previous studies have concluded that zebrafish *nos2b* is the NOS isoform that generates NO upon wounding in larvae (Wittmann et al., 2015). Nos2b shares a myristoylation consensus site with mammalian eNOS isoforms (Lepiller et al., 2009), further suggesting that Nos2b is the NOS isoform most likely involved in hypotonicity mediated vasodilation in zebrafish larvae. Importantly, our transcriptional analysis confirms that *nos2b* is expressed in 3 dpf zebrafish larvae. Further experiments utilizing genetic disruption of *nos2b* will be able to shed light

on the importance of this gene and NO production in vasodilation triggered by hypotonicity.

Importantly, release of NO and PGI_2 has been reported to be coupled in mammalian ECs (de Nucci et al., 1988). Evolving two separate pathways for EC activation after injury may help to ensure that proper inflammatory processes take place through compensation in case one pathway is compromised. Our results indicate that nucleotide triggered vasodilation occurs through adenosine activation of A_{2B} receptors. Adenosine triggered vasodilation occurs through NO signaling in other systems (Smits et al., 1995). It is possible that secreted nucleotides contribute to NO signaling that is required for vasodilation after injury in the zebrafish larvae. Additionally, it is possible that PGI_2 generated from cPLA2 activation and AA release can compensate for nucleotide mediated vasodilation when A_{2B} receptor expression is disrupted in *adora2b* crispant animals. Again, further experiments with perturbations to the eicosanoid cascade, NOS family members, in addition to purinergic receptors including *adora2b* will help to clarify the mechanism of osmotically regulated vasodilation in the larval zebrafish.

It is important to note that our experiments reveal that a signal transduction mechanism is triggering hypotonicity induced vasodilation in larvae rather than changes in vascular oncotic pressure mediated by chemical changes of the interstitial fluid upon exposure to the hypotonic environment. This is confirmed by the experiments utilizing the non-specific GPCR inhibitor Suramin and the sGC inhibitor ODQ. Preincubation of zebrafish larvae with these small molecule

inhibitors ablated hypotonicity mediated vasodilation, suggesting roles for GPCR mediated Ca^{2+} signaling and cGMP production by paracrine NO signaling.

In addition to vasodilation, type I EC activation in acute inflammation is characterized by an increase in leukocyte recruitment and attachment to vessels near injury sites and leakage of plasma proteins (exudate) into the surrounding tissue. Here we have strictly shown that exposure to the hypotonic environment triggers vasodilation upon injury; however, whether these same osmotic cues directly influence leukocyte attachment and blood vessel permeability should not be ruled out. Transgenic larvae with fluorescent reporters marking leukocytes and BODIPY-based fluorescent dyes should be utilized in future investigations characterizing hypotonicity dependent leukocyte blood vessel attachment and vascular permeability, respectively (Enyedi et al., 2013; Huang and Niethammer, 2018; Stoletov et al., 2009).

Comparable transepithelial osmotic differences exist in the stratified linings of the human oral cavity and esophagus (Jayaraman et al., 2001a, 2001b; Joris et al., 1993). Further studies could determine the importance of osmotic surveillance in mammalian vasodilation and EC activation upon injury.

CHAPTER 6 Discussion

In the presented studies we developed and provided proof-of-principle for an original technique that revealed the existence of novel non-catalytic ATP binding proteins from complex membrane proteomes and investigated the mechanisms of allosteric nucleotide regulation of acute inflammation and wound healing in vertebrates *in vivo*.

Non-catalytic protein interactions with ATP and other nucleotides are critical in cell signaling processes that govern metabolism and inflammation. The identification of non-catalytic ATP binders is a challenging task because these proteins, such as P2 cell surface receptors, typically lack discernible ATP binding sites. In chapter 3, we wished to profile a more complete set of ATP binders in cell membranes, including the often-neglected non-catalytic ATP binding proteins, using a new technique that eludes the biases of current computational and experimental methods of ATP interactor identification. To do this, we developed a novel photoaffinity ATP probe functionalized at the N^6 amino with a minimalist photo-clickable handle which we have named *minimally invasive photoaffinity ATP* or *mipATP* (Li et al., 2013). Unlike previously developed ATP probes which have not been functionally characterized, we show that the minimal modifications to mipATP do not perturb its biological activity (Mahajan et al., 2015; Patricelli et al., 2007). Importantly, we confirmed that mipATP functionally reconstitutes allosteric interactions of native ATP *in vitro* and *in vivo*, suggesting its ability to target these families of proteins for proteomic identification.

We profiled mipATP binders in cell membranes through label-free and quantitative proteomics methods that allowed for the enrichment and identification of known catalytic and non-catalytic nucleotide binders such as the recently identified immunogenic nucleotide transporter SLC19A1 (Luteijn et al., 2019). Additionally, mipATP interacted with and enriched for multiple proteins that have not been characterized to bind ATP and lack conventional ATP binding sites. One novel target of interest enriched by mipATP is the Fas death receptor. Similar to P2 receptor ligation to extracellular ATP, Fas ligation to its ligand FasL triggers IP_3-dependent Ca^{2+} signals in a variety of cell types (Khadra et al., 2011). Whether or not direct interactions between ATP and Fas functionally contribute to extracellular ATP-triggered Ca^{2+} signaling in cells is not known. Future experiments that quantitatively assess ATP-mediated Ca^{2+} signaling in transgenic reporter cell lines and tissues with genetically perturbed Fas expression will be informative in clarifying the functional role of Fas-ATP interactions. Any divergence from a normal Ca^{2+} signaling response would suggest that Fas is most likely an extracellular ATP receptor. Both extra- and intracellular ATP levels have been shown to regulate apoptosis (Leist et al., 1997; Li et al., 1997). It is possible that extracellular ATP regulates cell death fate decisions through direct regulation of Fas.

Earlier in this dissertation, I highlighted the inherent biases of electrophilic acyl phosphate ATP probes, particularly their reliance on conserved residues at conventional ATP binding sites. Another caveat to the previous studies that used these probes is that they strictly profiled nucleotide binders only in whole cell extracts (Adachi et al., 2014; Patricelli et al., 2007; Xiao et al., 2013b, 2013a).

Membrane proteins comprise ~30% of eukaryotic open reading frames, however they are typically underrepresented in proteomic studies for a variety of reasons including inefficient extraction and solubilization methods due to their hydrophobicity, inefficient proteolytic digestion by trypsin due to a general lack of arginine and lysine residues, overall low abundance in comparison to soluble proteins (only 7.6% of total protein mass), and high amounts of post translational modifications (PTMs) such as glycosylation, particularly on plasma membrane proteins (Josic and Clifton, 2007; Vit and Petrak, 2017; Wiśniewski et al., 2009; Zhao et al., 2004). The poor compliance of membrane ATP binders may have prevented their identification in previous and our own ATP ABPP experiments, most likely through masking by abundant soluble ATP binding proteins such as chaperones. Our study is the first to utilize an ATP probe to profile nucleotide binders in a membrane proteome. Cell membranes contain various families of allosteric nucleotide binding proteins such as P2 receptors, the CLC family of chloride channels, nucleotide transporters, and possibly yet to be determined nucleotide receptors as hinted at through our studies of zebrafish wound closure. MipATP interacted with proteins not known to bind nucleotides, such as the FAS receptor, which may have not been identified by previous screens due to the described biases of the ATP probes used and also because these studies targeted solubilized proteomes.

In addition to membrane proteomes, in future studies we plan to employ mipATP for profiling ATP binders in other cellular compartments with an initial focus on the cytosol for which allosteric ATP-binding, energy sensing proteins such

as AMPK are located. The comprehensive screening of allosteric ATP binders in a variety of cellular compartments will help in the identification of a more complete repertoire of ATP binding proteins.

Diverse tissues and cell types display a variety of proteomic profiles, including the differential expression of ATP-binding proteins. Profiling mipATP targets in different sample types provides greater potential for discovery of yet to be characterized ATP-binding proteins. This is particularly true in cell and tissue types where ATP-mediated phenotypes are mechanistically unaccounted for.

Recently, our lab discovered that zebrafish larvae basal epithelial cells migrate in response to extracellular gradients of ATP and that the pharmacological profile of the receptor mediating this response is divergent from known P2 receptors (Gault et al., 2014). Initially, we believed that the lack of pharmacological correlation to P2 receptor signaling may be due to phylogenic differences in zebrafish P2 receptor pharmacology; however, this data may suggest the existence of an uncharacterized ATP receptor in zebrafish epithelial cells (Bogdanov et al., 1998). In chapter 4, we genetically screened for the functionality of expressed P2 receptors in ATP mediated epithelial cell migration in zebrafish larvae. To this end we employed targeted genetic knockdown by morpholinos and knockout by CRISPR/Cas9 in combination with tissue velocity analysis upon exposure to hypotonicity and extracellular nucleotides as a functional readout. Our results suggest that zebrafish isoforms of $P2Y_{11}$ and $P2Y_4$ may play roles in ATP mediated epithelial wound closure; however, neither of these genes was found to be essential.

While compensatory mechanisms may account for the retained ability of larvae with a single P2 receptor genetic perturbation to close wounds, the genetic data in combination with an exhaustive SAR analysis do not make a strong case for a P2 receptor subtype as the main mediator of ATP triggered epithelial migration *in vivo*. Again, it is important to note that epithelial migration in cell culture does not match the speed of migration in zebrafish larvae and the half-life of extracellular ATP in cell culture is on the order of minutes, while it is on the order of seconds to milliseconds *in vivo* (Orriss et al., 2009, 2013). The relatively slow epithelial cell migration mediated by P2 receptor signaling *in vitro* may rely on this artificially extended half-life of nucleotides.

It would not be unexpected if a yet to be identified ATP receptor, unrelated to P2 receptors, is the essential mediator of epithelial cell migration and wound closure in zebrafish larvae. The recently identified DORN1 receptor, which lacks sequence homology to P2 receptors and other ATP-binding proteins, is an example of such a receptor (Choi et al., 2014). The lack of a high-throughput assay to analyze wound closure phenotypes in zebrafish larvae rules out receptor identification through forward genetic screening (it takes over 1 hour to characterize wound closure in a single larva using current techniques). As stated earlier, cell culture models cannot faithfully recapitulate the rapid epithelial wound closure observed *in vivo*; therefore, cell culture migration phenotypes are not reliable functional readouts for rapid wound closure triggered by ATP. For these reasons, biochemical screening with functionalized ATP probes provides the best avenue for the identification of ATP receptors that mediate rapid *in vivo* cell

migration. Importantly, we found that rapid cell migration in zebrafish larvae can be reconstituted by mipATP when endogenous ATP release is suppressed by isotonicity. Future mipATP proteomic profiling of zebrafish larvae cell membranes coupled to functional target analysis by gene perturbation and tissue velocity analysis may permit the biochemical identification and characterization of the ATP receptor driving epithelial wound closure *in vivo*. It is possible that our proteomic screens with mipATP (Chapter 3) may have enriched for the human ortholog of the ATP receptor that drives zebrafish basal epithelial cell migration. Assessing the potential function of these identified novel ATP interactors in zebrafish wound closure can be easily addressed through morpholino and/or CRISPR-mediated genetic perturbations of zebrafish orthologs coupled to wound closure assays. Additionally, the mRNA-seq analysis of zebrafish larvae epithelium (Figure 4.1) will identify which (if any) candidates are expressed in the ATP-responsive basal epithelial cells. Such candidates would be considered the highest priority.

In addition to epithelial wound closure, in chapter 5 we show that secreted nucleotides may play prominent roles in the vascular response to non-bleeding epithelial injuries during acute inflammation in zebrafish larvae. Upon local chemical and physical environmental perturbations, ATP and adenosine released from lysed and mechanically stressed cells can induce vasodilation in mammalian systems (Bodin et al., 1991; Smits et al., 1995). For the first time, we show that extracellular ATP and adenosine can trigger vasodilation in live zebrafish larvae when initial damage signals are suppressed by isotonic bathing. Both ATP and adenosine triggered vasodilation are dependent upon the activation of the

adenosine Adora2b (A_{2B}) receptor, suggesting that adenosine is the active molecule and that ATP must first be hydrolyzed by ectonucleotidases to be functional. Surprisingly, genetic disruption of A_{2B} did not inhibit injury induced vasodilation in a normal hypotonic environment, suggesting that extracellular nucleotides may not be involved in injury triggered vasodilation in zebrafish larvae.

A variety of studies have shown that mechanistically divergent vasodilators are typically coupled and can act in a redundant manner, where one can fully regulate vasodilation when the other is compromised (Hellsten et al., 2012; de Nucci et al., 1988). We have previously shown that hypotonicity mediated AA release from injury sites triggers leukocyte recruitment to epithelial injuries in zebrafish larvae (Enyedi et al., 2013). The released AA after injury can act as a source for PGI_2 generation to trigger vasodilation in concert with extracellular nucleotides and may be able to completely take over vasodilation duties when the Adora2b receptor is compromised. Future studies will be conducted that employ combined genetic perturbations to simultaneously disrupt nucleotide and prostaglandin signaling pathways in zebrafish larvae.

Together, these studies highlight the critical role of ATP as a non-catalytic allosteric effector and ligand in cell signaling and encourage further investigations of these mechanisms. Our revelation of novel ATP interactors suggests the current understanding of ATP interaction mechanisms is incomplete. The complete set of ATP binding proteins and consequences of allosteric ATP signaling remains to be uncovered through the implementation of original ideas and experimental methods.

APPENDIX

Table S1. Label-Free LC-MS/MS Identified mipATP targets

Uniprot Accession	Gene Symbol	Protein Name	mipATP alone intensity/ ATP competition intensity	Total peptides mipATP alone/ Total peptides ATP competition
Q04656	ATP7A	Copper-transporting ATPase 1	N/A	N/A
P48730	CSNK1D	Casein kinase I isoform delta	N/A	N/A
P01031	C5	Complement C5	N/A	N/A
P48729	CSNK1A1	Casein kinase I isoform alpha	N/A	N/A
Q02818	NUCB1	Nucleobindin-1	N/A	N/A
Q9BPW8	NIPSNAP1	Protein NipSnap homolog 1	N/A	N/A
Q13438	OS9	Protein OS-9	N/A	N/A
P00813	ADA	Adenosine deaminase	N/A	N/A
Q9NQE9	HINT3	Histidine triad nucleotide-binding protein 3	N/A	N/A
P19474	TRIM21	E3 ubiquitin-protein ligase TRIM21	N/A	N/A
Q9BSD7	NTPCR	Cancer-related nucleoside-triphosphatase	N/A	N/A
Q86UL3	AGPAT6	Glycerol-3-phosphate acyltransferase 4	N/A	N/A
Q96FL8	SLC47A1	Multidrug and toxin extrusion protein 1	N/A	N/A
O60779	SLC19A2	Thiamine transporter 1	N/A	N/A
Q96I59	NARS2	Probable asparagine--tRNA ligase, mitochondrial	N/A	N/A
P38919	EIF4A3	Eukaryotic initiation factor 4A-III	N/A	N/A
Q9BVG8	KIFC3	Kinesin-like protein KIFC3	N/A	N/A
O00442	RTCA	RNA 3'-terminal phosphate cyclase	N/A	N/A
P18077	RPL35A	60S ribosomal protein L35a	N/A	N/A

O95816	BAG2	BAG family molecular chaperone regulator 2	N/A	N/A
Q9UNM6	PSMD13	26S proteasome non-ATPase regulatory subunit 13	N/A	N/A
P40937	RFC5	Replication factor C subunit 5	N/A	N/A
Q86TM6	SYVN1	E3 ubiquitin-protein ligase synoviolin	N/A	N/A
Q9BVK6	TMED9	Transmembrane emp24 domain-containing protein 9	N/A	N/A
P26368	U2AF2	Splicing factor U2AF 65 kDa subunit	N/A	N/A
Q8NBU5	ATAD1	ATPase family AAA domain-containing protein 1	N/A	N/A
P51398	DAP3	28S ribosomal protein S29, mitochondrial	N/A	N/A
Q96AQ6	PBXIP1	Pre-B-cell leukemia transcription factor-interacting protein 1	N/A	N/A
B7ZAQ6	GPR89A	Golgi pH regulator A	N/A	N/A
Q96T60	PNKP	Bifunctional polynucleotide phosphatase/kinase	N/A	N/A
Q9NS69	TOMM22	Mitochondrial import receptor subunit TOM22 homolog	N/A	N/A
P13747	HLA-E	HLA class I histocompatibility antigen, alpha chain E	N/A	N/A
O00461	GOLIM4	Golgi integral membrane protein 4	N/A	N/A
Q495W5	FUT11	Alpha-(1,3)-fucosyltransferase 11	N/A	N/A
Q96S66	CLCC1	Chloride channel CLIC-like protein 1	N/A	N/A
O15091	KIAA0391	Mitochondrial ribonuclease P protein 3	N/A	N/A
Q8N8N7	PTGR2	Prostaglandin reductase 2	N/A	N/A
Q96RQ1	ERGIC2	Endoplasmic reticulum-Golgi intermediate compartment protein 2	N/A	N/A
Q9BZD2	SLC29A3	Equilibrative nucleoside transporter 3	N/A	N/A
Q9BQ69	MACROD1	O-acetyl-ADP-ribose deacetylase MACROD1	N/A	N/A
O60361	NME2P1	Putative nucleoside diphosphate kinase	N/A	N/A
P62306	SNRPF	Small nuclear ribonucleoprotein F	N/A	N/A
O14657	TOR1B	Torsin-1B	N/A	N/A

P11169	SLC2A3	Solute carrier family 2, facilitated glucose transporter member 3	N/A	N/A
Q86VR7	VSIG10L	V-set and immunoglobulin domain-containing protein 10-like	N/A	N/A
P54577	YARS	Tyrosine--tRNA ligase, cytoplasmic	N/A	N/A
P43155	CRAT	Carnitine O-acetyltransferase	N/A	N/A
Q6IAA8	LAMTOR1	Ragulator complex protein LAMTOR1	N/A	N/A
P46821	MAP1B	Microtubule-associated protein 1B	N/A	N/A
Q9ULF5	SLC39A10	Zinc transporter ZIP10	N/A	N/A
P41440	SLC19A1	Folate transporter 1	N/A	N/A
O75822	EIF3J	Eukaryotic translation initiation factor 3 subunit J	N/A	N/A
P62249	RPS16	40S ribosomal protein S16	N/A	N/A
Q96Q45	TMEM237	Transmembrane protein 237	N/A	N/A
O00139	KIF2A	Kinesin-like protein KIF2A	N/A	N/A
A3KMH1	VWA8	von Willebrand factor A domain-containing protein 8	N/A	N/A
P98088	MUC5AC	Mucin-5AC	N/A	N/A
P07602	PSAP	Prosaposin	N/A	N/A
P51809	VAMP7	Vesicle-associated membrane protein 7	N/A	N/A
Q9UHW9	SLC12A6	Solute carrier family 12 member 6	N/A	N/A
Q5JPH6	EARS2	Probable glutamate--tRNA ligase, mitochondrial	N/A	N/A
Q6P587	FAHD1	Acylpyruvase FAHD1, mitochondrial	N/A	N/A
O75323	GBAS	Protein NipSnap homolog 2	N/A	N/A
Q10471	GALNT2	Polypeptide N-acetylgalactosaminyltransferase 2	N/A	N/A
Q68CR1	SEL1L3	Protein sel-1 homolog 3	N/A	N/A
Q9H5Z1	DHX35	Probable ATP-dependent RNA helicase DHX35	N/A	N/A
O95881	TXNDC12	Thioredoxin domain-containing protein 12	N/A	N/A
Q6ZMJ2	SCARA5	Scavenger receptor class A member 5	N/A	N/A

O75531	BANF1	Barrier-to-autointegration factor	N/A	N/A
P35249	RFC4	Replication factor C subunit 4	N/A	N/A
Q9ULC3	RAB23	Ras-related protein Rab-23	N/A	N/A
O94979	SEC31A	Protein transport protein Sec31A	N/A	N/A
Q8NBL1	POGLUT1	Protein O-glucosyltransferase 1	N/A	N/A
Q9BQL6	FERMT1	Fermitin family homolog 1	N/A	N/A
Q8TBZ3	WDR20	WD repeat-containing protein 20	N/A	N/A
Q8NBJ7	SUMF2	Sulfatase-modifying factor 2	N/A	N/A
P55735	SEC13	Protein SEC13 homolog	N/A	N/A
P60903	S100A10	Protein S100-A10	N/A	N/A
Q96B45	C10orf32	UPF0693 protein C10orf32	N/A	N/A
Q9BX95	SGPP1	Sphingosine-1-phosphate phosphatase 1	N/A	N/A
P10606	COX5B	Cytochrome c oxidase subunit 5B, mitochondrial	N/A	N/A
Q9H813	TMEM206	Transmembrane protein 206	N/A	N/A
P33947	KDELR2	ER lumen protein-retaining receptor 2	N/A	N/A
Q9BZ68	FRMD8P1	Putative FERM domain-containing protein FRMD8P1	N/A	N/A
P04004	VTN	Vitronectin	N/A	N/A
Q10588	BST1	ADP-ribosyl cyclase/cyclic ADP-ribose hydrolase 2	187.5	5
Q8N752	CSNK1A1L	Casein kinase I isoform alpha-like	185.7142857	11
Q03519	TAP2	Antigen peptide transporter 2	93.47826087	16
O75821	EIF3G	Eukaryotic translation initiation factor 3 subunit G	52	2
P49368	CCT3	T-complex protein 1 subunit gamma	45.23809524	5.708333333
Q13423	NNT	NAD(P) transhydrogenase, mitochondrial	43.18181818	10
Q9UP95	SLC12A4	Solute carrier family 12 member 4	35.625	5.5
Q96TA2	YME1L1	ATP-dependent zinc metalloprotease YME1L1	34.69387755	1.5
Q9HD20	ATP13A1	Manganese-transporting ATPase 13A1	29.33333333	4.375

Q93084	ATP2A3	Sarcoplasmic/endoplasmic reticulum calcium ATPase 3	28.69565217	5
Q9UMX5	NENF	Neudesin	28.51851852	5.333333333
Q6N075	MFSD5	Molybdate-anion transporter	26.92307692	6
P50991	CCT4	T-complex protein 1 subunit delta	26.08695652	3.586206897
P43307	SSR1	Translocon-associated protein subunit alpha	24.76190476	2
O15260	SURF4	Surfeit locus protein 4	23.91304348	5
O60266	ADCY3	Adenylate cyclase type 3	22.72727273	2
P00403	MT-CO2	Cytochrome c oxidase subunit 2	22.44897959	4
Q04941	PLP2	Proteolipid protein 2	22.30769231	2
Q14257	RCN2	Reticulocalbin-2	22.22222222	1.833333333
Q9H6R6	ZDHHC6	Palmitoyltransferase ZDHHC6	20.60606061	3
O43852	CALU	Calumenin	20	4.666666667
P06576	ATP5B	ATP synthase subunit beta, mitochondrial	20	2.666666667
Q8NBX0	SCCPDH	Saccharopine dehydrogenase-like oxidoreductase	19.56521739	3.142857143
Q99832	CCT7	T-complex protein 1 subunit eta	16.92307692	3.317073171
Q9UIW2	PLXNA1	Plexin-A1	16.90140845	2
O95302	FKBP9	Peptidyl-prolyl cis-trans isomerase FKBP9	16.66666667	6
Q32P28	LEPRE1	Prolyl 3-hydroxylase 1	16.25	3.5
Q9NTK5	OLA1	Obg-like ATPase 1	15.83333333	2
Q8IV08	PLD3	Phospholipase D3	15.55555556	3.8
Q9NUM4	TMEM106B	Transmembrane protein 106B	14.61538462	4
Q03518	TAP1	Antigen peptide transporter 1	14.28571429	2.368421053
Q9BZQ6	EDEM3	ER degradation-enhancing alpha-mannosidase-like protein 3	13.84615385	4
P78371	CCT2	T-complex protein 1 subunit beta	13.69863014	4.12195122
P53990	IST1	IST1 homolog	13.33333333	3

P24390	KDELR1	ER lumen protein-retaining receptor 1	12.90322581	3
P53985	SLC16A1	Monocarboxylate transporter 1	12.63157895	2.5
Q08211	DHX9	ATP-dependent RNA helicase A	11.80327869	2.941176471
P48723	HSPA13	Heat shock 70 kDa protein 13	11.60714286	3
P80303	NUCB2	Nucleobindin-2	11.28205128	4
O14681	EI24	Etoposide-induced protein 2.4 homolog	10.77922078	2
Q9BRR6	ADPGK	ADP-dependent glucokinase	10.66666667	4
Q14728	MFSD10	Major facilitator superfamily domain-containing protein 10	10.52631579	2
P25705	ATP5A1	ATP synthase subunit alpha, mitochondrial	10.45454545	2.111111111
Q9H173	SIL1	Nucleotide exchange factor SIL1	10.35714286	3
Q96PY5	FMNL2	Formin-like protein 2	10.31746032	2
P30837	ALDH1B1	Aldehyde dehydrogenase X, mitochondrial	10	2.333333333
P35611	ADD1	Alpha-adducin	9.56043956	2.333333333
Q6P1A2	LPCAT3	Lysophospholipid acyltransferase 5	9.5	1.6
P62495	ETF1	Eukaryotic peptide chain release factor subunit 1	9.253731343	6
P05067	APP	Amyloid beta A4 protein	8.780487805	3
Q9UJZ1	STOML2	Stomatin-like protein 2, mitochondrial	8.636363636	2.333333333
Q08477	CYP4F3	Docosahexaenoic acid omega-hydroxylase CYP4F3	8.333333333	1.5
P38571	LIPA	Lysosomal acid lipase/cholesteryl ester hydrolase	8.285714286	4
Q15166	PON3	Serum paraoxonase/lactonase 3	8.275862069	2.833333333
Q8IXU6	SLC35F2	Solute carrier family 35 member F2	8.275862069	2
P20839	IMPDH1	Inosine-5'-monophosphate dehydrogenase 1	8.181818182	3
O75718	CRTAP	Cartilage-associated protein	8.166666667	3.5
Q9NZ01	TECR	Very-long-chain enoyl-CoA reductase	8	2.333333333
O95425	SVIL	Supervillin	7.956989247	1.5
P61221	ABCE1	ATP-binding cassette sub-family E member 1	7.887323944	2

P38435	GGCX	Vitamin K-dependent gamma-carboxylase	7.631578947	2.333333333
Q6NZI2	PTRF	Polymerase I and transcript release factor	7.619047619	4.333333333
O43615	TIMM44	Mitochondrial import inner membrane translocase subunit TIM44	7.604166667	2
P41219	PRPH	Peripherin	7.6	2
P13688	CEACAM1	Carcinoembryonic antigen-related cell adhesion molecule 1	7.575757576	2
O60658	PDE8A	High affinity cAMP-specific and IBMX-insensitive 3',5'-cyclic phosphodiesterase 8A	7.5	2.25
Q16822	PCK2	Phosphoenolpyruvate carboxykinase [GTP], mitochondrial	7.446808511	2.5
P31948	STIP1	Stress-induced-phosphoprotein 1	7.272727273	1.5
Q70UQ0	IKBIP	Inhibitor of nuclear factor kappa-B kinase-interacting protein	7.24137931	2
P35580	MYH10	Myosin-10	7.142857143	2.106060606
O75907	DGAT1	Diacylglycerol O-acyltransferase 1	7.083333333	2
P36776	LONP1	Lon protease homolog, mitochondrial	7.058823529	1.666666667
O15427	SLC16A3	Monocarboxylate transporter 4	6.875	1.7
P04844	RPN2	Dolichyl-diphosphooligosaccharide--protein glycosyltransferase subunit 2	6.857142857	1.636363636
Q9P2J5	LARS	Leucine--tRNA ligase, cytoplasmic	6.829268293	3
Q9Y2H6	FNDC3A	Fibronectin type-III domain-containing protein 3A	6.666666667	3
P16070	CD44	CD44 antigen	6.6	3.75
P53680	AP2S1	AP-2 complex subunit sigma	6.6	3
P48643	CCT5	T-complex protein 1 subunit epsilon	6.4	3.117647059
Q8NE71	ABCF1	ATP-binding cassette sub-family F member 1	6.285714286	7
P55010	EIF5	Eukaryotic translation initiation factor 5	6.086956522	2
Q9P2B2	PTGFRN	Prostaglandin F2 receptor negative regulator	6.052631579	3.571428571
Q9UGT4	SUSD2	Sushi domain-containing protein 2	6	2

P21291	CSRP1	Cysteine and glycine-rich protein 1	6	2
Q9H6U8	ALG9	Alpha-1,2-mannosyltransferase ALG9	6	2
Q9NZB2	FAM120A	Constitutive coactivator of PPAR-gamma-like protein 1	5.916666667	2
O00400	SLC33A1	Acetyl-coenzyme A transporter 1	5.890410959	2.666666667
O14983	ATP2A1	Sarcoplasmic/endoplasmic reticulum calcium ATPase 1	5.862068966	1.794117647
Q8N1S5	SLC39A11	Zinc transporter ZIP11	5.833333333	2
P28472	GABRB3	Gamma-aminobutyric acid receptor subunit beta-3	5.789473684	4
Q9NP58	ABCB6	ATP-binding cassette sub-family B member 6, mitochondrial	5.774647887	1.625
Q13884	SNTB1	Beta-1-syntrophin	5.757575758	3
Q9UIQ6	LNPEP	Leucyl-cystinyl aminopeptidase	5.757575758	2.0625
Q93034	CUL5	Cullin-5	5.714285714	3
O75390	CS	Citrate synthase, mitochondrial	5.625	2.333333333
Q7KZI7	MARK2	Serine/threonine-protein kinase MARK2	5.571428571	2
Q9UBS4	DNAJB11	DnaJ homolog subfamily B member 11	5.567010309	1.5
Q9BXP2	SLC12A9	Solute carrier family 12 member 9	5.538461538	2.25
P61353	RPL27	60S ribosomal protein L27	5.538461538	2
O00767	SCD	Acyl-CoA desaturase	5.535714286	4
Q96FN4	CPNE2	Copine-2	5.454545455	2
P61764	STXBP1	Syntaxin-binding protein 1	5.454545455	2
P08648	ITGA5	Integrin alpha-5	5.428571429	2.5
Q9ULQ1	TPCN1	Two pore calcium channel protein 1	5.411764706	1.666666667
Q8N163	CCAR2	Cell cycle and apoptosis regulator protein 2	5.384615385	2
P33527	ABCC1	Multidrug resistance-associated protein 1	5.333333333	1.695035461
P35749	MYH11	Myosin-11	5.294117647	6.75
Q15293	RCN1	Reticulocalbin-1	5.272727273	1.75

Q99735	MGST2	Microsomal glutathione S-transferase 2	5.268817204	2
P26373	RPL13	60S ribosomal protein L13	5.2	1.5
Q9HCP0	CSNK1G1	Casein kinase I isoform gamma-1	5.172413793	2
Q2PZI1	DPY19L1	Probable C-mannosyltransferase DPY19L1	5.15625	2
Q96JQ2	CLMN	Calmin	5	4
Q9GZT3	SLIRP	SRA stem-loop-interacting RNA-binding protein, mitochondrial	5	3
P54619	PRKAG1	5'-AMP-activated protein kinase subunit gamma-1	5	3
P0DMN0	SULT1A4	Sulfotransferase 1A4	5	2
Q9BYX7	POTEKP	Putative beta-actin-like protein 3	5	2
P20337	RAB3B	Ras-related protein Rab-3B	4.916666667	2
P12236	SLC25A6	ADP/ATP translocase 3	4.897959184	3
Q15008	PSMD6	26S proteasome non-ATPase regulatory subunit 6	4.888888889	2
Q13232	NME3	Nucleoside diphosphate kinase 3	4.88372093	2
K7EM38	ACTG1	Actin, cytoplasmic 2 (Fragment)	4.875	2
P46459	NSF	Vesicle-fusing ATPase	4.848484848	2.083333333
P62191	PSMC1	26S protease regulatory subunit 4	4.823529412	2
Q9NXW2	DNAJB12	DnaJ homolog subfamily B member 12	4.819277108	5
Q12907	LMAN2	Vesicular integral-membrane protein VIP36	4.782608696	1.8
Q13948	CUX1	Protein CASP	4.722222222	2
P17987	TCP1	T-complex protein 1 subunit alpha	4.6875	1.8
P16615	ATP2A2	Sarcoplasmic/endoplasmic reticulum calcium ATPase 2	4.657534247	1.744680851
P68363	TUBA1B	Tubulin alpha-1B chain	4.634146341	3
Q7Z478	DHX29	ATP-dependent RNA helicase DHX29	4.615384615	2.5
P49257	LMAN1	Protein ERGIC-53	4.615384615	2.25
Q9NZJ7	MTCH1	Mitochondrial carrier homolog 1	4.615384615	2

Q9UHB6	LIMA1	LIM domain and actin-binding protein 1	4.6	2
A6NEC2	NPEPPSL1	Puromycin-sensitive aminopeptidase-like protein	4.545454545	1.75
Q8NCA5	FAM98A	Protein FAM98A	4.516129032	2
P11310	ACADM	Medium-chain specific acyl-CoA dehydrogenase, mitochondrial	4.5	1.5

Table S1. Label-free LC-MS/MS identified mipATP targets

Proteomic data for mipATP targets identified in isolated A549 cell membranes. Related to Figure 3.4. Proteins were classified as high confidence mipATP binders based on their total peptide sum intensity (≥4.5) and total peptide number (≥1.5) ratios in the 'Experimental' sample (20 μM mipATP) compared to the 'Competition' (20 μM mipATP + 2 mM ATP) sample. Total peptide sum intensity and total peptide number ratios are given for the high confidence mipATP targets. (N/A) signifies that no representative peptides were identified for the indicated protein in the 'Competition' sample.

Table S2. High confidence mipATP targets - combined SILAC 90th percentile

Uniprot Accession	Gene Symbol	Protein Name	Forward (H/L) SILAC Ratio	Reverse (L/H) SILAC Ratio
Q9BZV2	SLC19A3	Thiamine transporter 2	24.00	7.95
P48730	CSNK1D	Casein kinase I isoform delta	10.39	13.12
P46459	NSF	Vesicle-fusing ATPase	8.46	3.15
P33527	ABCC1	Multidrug resistance-associated protein 1	5.74	3.03
O43306	ADCY6	Adenylate cyclase type 6	5.39	2.07
P09543	CNP	2',3'-cyclic-nucleotide 3'-phosphodiesterase	4.45	1.57
Q6N075	MFSD5	Molybdate-anion transporter	4.26	6.30
Q12905	ILF2	Interleukin enhancer-binding factor 2	4.23	1.60
O15439	ABCC4	Multidrug resistance-associated protein 4	3.82	1.94
P50991	CCT4	T-complex protein 1 subunit delta	3.78	2.39
P55011	SLC12A2	Solute carrier family 12 member 2	3.65	1.44
Q9NUT2	ABCB8	ATP-binding cassette sub-family B member 8, mitochondrial	3.60	6.01
Q9HD20	ATP13A1	Manganese-transporting ATPase 13A1	3.57	2.14
Q9UMX5	NENF	Neudesin	3.46	16.94
Q03518	TAP1	Antigen peptide transporter 1	3.40	3.83
Q08211	DHX9	ATP-dependent RNA helicase A	3.14	2.00
P49368	CCT3	T-complex protein 1 subunit gamma	2.94	1.65
O75751	SLC22A3	Solute carrier family 22 member 3	2.86	8.07
Q04656	ATP7A	Copper-transporting ATPase 1	2.86	1.93
P78371	CCT2	T-complex protein 1 subunit beta	2.80	2.66
Q92887	ABCC2	Canalicular multispecific organic anion transporter 1	2.78	1.59

Q13011	ECH1	Delta(3,5)-Delta(2,4)-dienoyl-CoA isomerase, mitochondrial	2.72	3.48
Q12965	MYO1E	Unconventional myosin-Ie	2.70	1.46
Q9UG63	ABCF2	ATP-binding cassette sub-family F member 2	2.61	1.99
Q99832	CCT7	T-complex protein 1 subunit eta	2.56	1.60
P35580	MYH10	Myosin-10	2.33	1.48
Q02818	NUCB1	Nucleobindin-1	2.32	1.47
P41440	SLC19A1	Reduced folate transporter	2.21	6.03
P30837	ALDH1B1	Aldehyde dehydrogenase X, mitochondrial	2.20	4.42
O15438	ABCC3	Canalicular multispecific organic anion transporter 2	2.19	1.84
Q13423	NNT	NAD(P) transhydrogenase, mitochondrial	2.14	2.28
Q15629	TRAM1	Translocating chain-associated membrane protein 1	2.02	1.56
B7ZKQ9	SCARB1	Scavenger receptor class B member 1	1.99	3.68
P21589	NT5E	5'-nucleotidase	1.94	2.68
Q8NBX0	SCCPDH	Saccharopine dehydrogenase-like oxidoreductase	1.83	2.06
P49419	ALDH7A1	Alpha-aminoadipic semialdehyde dehydrogenase	1.80	2.19
P07099	EPHX1	Epoxide hydrolase 1	1.76	1.89
Q9H0D6	XRN2	5'-3' exoribonuclease 2	1.68	1.81
Q16822	PCK2	Phosphoenolpyruvate carboxykinase [GTP], mitochondrial	1.63	1.92
Q9NYQ6	CELSR1	Cadherin EGF LAG seven-pass G-type receptor 1	1.58	2.74
P55786	NPEPPS	Puromycin-sensitive aminopeptidase	1.53	2.75
P08582	MELTF	Melanotransferrin	1.46	1.47
Q9Y6M5	SLC30A1	Zinc transporter 1	1.41	3.03
P16070	CD44	CD44 antigen	1.40	2.59
P25445	FAS	Tumor necrosis factor receptor superfamily member 6	1.35	1.61
Q10588	BST1	ADP-ribosyl cyclase/cyclic ADP-ribose hydrolase 2	1.28	5.41
Q9NZ01	TECR	Very-long-chain enoyl-CoA reductase	1.26	1.83

Table S2. High confidence mipATP targets - combined SILAC 90th percentile

SILAC ratios for high confidence mipATP targets identified by mipATP labeling of intact A549 cells. Related to Figure 3.5. Data represent SILAC ratios from the 'forward' and 'reverse' datasets. In the forward experiment, isotopically heavy cells were labeled with mipATP alone (50μM mipATP) and isotopically light cells were labeled with mipATP in the presence of excess unmodified ATP (50μM mipATP + 5 mM ATP). Isotope labels were swapped in the reverse experiment. High confidence mipATP targets are found in the 90^{th} percentile (based on SILAC ratio) of both the forward and reverse screens. (L) and (H) signify isotopically light and heavy median peptide intensities, respectively.

Table S3. Filtered high confidence mipATP targets

Uniprot Accession	Gene Symbol	Protein Name	Transmembrane	Known Binding					
				ATP	GTP	NAD/NADP	DNA/RNA	Nucleotide	CoA
Q03518	TAP1	Antigen peptide transporter 1	Yes	X					
P48730	CSNK1D	Casein kinase I isoform delta	–	X					
Q04656	ATP7A	Copper-transporting ATPase 1	Yes	X					
P33527	ABCC1	Multidrug resistance-associated protein 1	Yes	X					
O60266	ADCY3	Adenylate cyclase type 3	Yes	X					
Q03519	TAP2	Antigen peptide transporter 2	Yes	X					
Q9NP58	ABCB6	ATP-binding cassette sub-family B member 6, mitochondrial	Yes	X					
O43306	ADCY6	Adenylate cyclase type 6	Yes	X					
O15439	ABCC4	Multidrug resistance-associated protein 4	Yes	X					
Q9NUT2	ABCB8	ATP-binding cassette sub-family B member 8, mitochondrial	Yes	X					
Q92887	ABCC2	Canalicular multispecific organic anion transporter 1	Yes	X					
Q12965	MYO1E	Unconventional myosin-Ie	–	X					
O15438	ABCC3	Canalicular multispecific organic anion transporter 2	Yes	X					
P21589	NT5E	5'-nucleotidase	–	X					
Q10588	BST1	ADP-ribosyl cyclase/cyclic ADP-ribose hydrolase 2	–			X		X	
O60658	PDE8A	High affinity cAMP-specific and IBMX-insensitive 3',5'-cyclic phosphodiesterase 8A	–					X	

Q6NZI2	CAVIN1	Caveolae-associated protein 1	–				X		
O15427	SLC16A3	Monocarboxylate transporter 4	Yes				X		
P41440	SLC19A1	Reduced folate transporter	Yes					X	
Q9BXP2	SLC12A9	Solute carrier family 12 member 9	Yes						
Q8IXU6	SLC35F2	Solute carrier family 35 member F2	Yes						
Q96FL8	SLC47A1	Multidrug and toxin extrusion protein 1	Yes						
Q9BZV2	SLC19A3	Thiamine transporter 2	Yes						
P55011	SLC12A2	Solute carrier family 12 member 2	Yes						
O75751	SLC22A3	Solute carrier family 22 member 3	Yes						
Q9Y6M5	SLC30A1	Zinc transporter 1	Yes						
P08648	ITGA5	Integrin alpha-5	Yes						
Q9P2B2	PTGFRN	Prostaglandin F2 receptor negative regulator	Yes						
Q9NYQ6	CELSR1	Cadherin EGF LAG seven-pass G-type receptor 1	Yes						
P25445	FAS	Tumor necrosis factor receptor superfamily member 6	Yes						
P16070	CD44	CD44 antigen	Yes						
P08582	MELTF	Melanotransferrin	–						

Table S3. Filtered high confidence mipATP targets
Related to Figure 3.6. Proteins identified as high confidence mipATP targets in at least two of the three orthogonal mass spectrometry screens are listed and classified by nucleotide binding capability.

BIBLIOGRAPHY

Abbracchio, M.P., and Burnstock, G. (1994). Purinoceptors: are there families of P2X and P2Y purinoceptors? Pharmacol. Ther. *64*, 445–475.

Abbracchio, M.P., Burnstock, G., Boeynaems, J.-M., Barnard, E.A., Boyer, J.L., Kennedy, C., Knight, G.E., Fumagalli, M., Gachet, C., Jacobson, K.A., et al. (2006). International Union of Pharmacology LVIII: update on the P2Y G protein-coupled nucleotide receptors: from molecular mechanisms and pathophysiology to therapy. Pharmacol. Rev. *58*, 281–341.

Adachi, J., Kishida, M., Watanabe, S., Hashimoto, Y., Fukamizu, K., and Tomonaga, T. (2014). Proteome-wide discovery of unknown ATP-binding proteins and kinase inhibitor target proteins using an ATP probe. J. Proteome Res. *13*, 5461–5470.

Alkayed, F., Kashimata, M., Koyama, N., Hayashi, T., Tamura, Y., and Azuma, Y. (2012). P2Y11 purinoceptor mediates the ATP-enhanced chemotactic response of rat neutrophils. J Pharmacol Sci *120*, 288–295.

Allard, B., Longhi, M.S., Robson, S.C., and Stagg, J. (2017). The ectonucleotidases CD39 and CD73: Novel checkpoint inhibitor targets. Immunol. Rev. *276*, 121–144.

Ansong, C., Ortega, C., Payne, S.H., Haft, D.H., Chauvignè-Hines, L.M., Lewis, M.P., Ollodart, A.R., Purvine, S.O., Shukla, A.K., Fortuin, S., et al. (2013). Identification of widespread adenosine nucleotide binding in Mycobacterium tuberculosis. Chem. Biol. *20*, 123–133.

Antonioli, L., Pacher, P., Vizi, E.S., and Haskó, G. (2013). CD39 and CD73 in immunity and inflammation. Trends Mol. Med. *19*, 355–367.

Arguello, A.E., DeLiberto, A.N., and Kleiner, R.E. (2017). RNA Chemical Proteomics Reveals the N6-Methyladenosine (m6A)-Regulated Protein-RNA Interactome. J. Am. Chem. Soc. *139*, 17249–17252.

Aruffo, A., Stamenkovic, I., Melnick, M., Underhill, C.B., and Seed, B. (1990). CD44 is the principal cell surface receptor for hyaluronate. Cell *61*, 1303–1313.

Ashburner, M., Ball, C.A., Blake, J.A., Botstein, D., Butler, H., Cherry, J.M., Davis, A.P., Dolinski, K., Dwight, S.S., Eppig, J.T., et al. (2000). Gene ontology: tool for the unification of biology. The Gene Ontology Consortium. Nat. Genet. *25*, 25–29.

Bagchi, S., Liao, Z., Gonzalez, F.A., Chorna, N.E., Seye, C.I., Weisman, G.A., and Erb, L. (2005). The P2Y2 nucleotide receptor interacts with alphav integrins to activate Go and induce cell migration. J. Biol. Chem. *280*, 39050–39057.

Barry, S., and O'Carra, P. (1973). A simple general method for the preparation of "6-immobilized" analogues of AMP, ATP, NAD and of other adenine-containing compounds for affinity chromatography. FEBS Lett. *37*, 134–139.

Bateman, A. (1997). The structure of a domain common to archaebacteria and the homocystinuria disease protein. Trends Biochem. Sci. *22*, 12–13.

Behrend, L., Stöter, M., Kurth, M., Rutter, G., Heukeshoven, J., Deppert, W., and

Knippschild, U. (2000). Interaction of casein kinase 1 delta (CK1delta) with post-Golgi structures, microtubules and the spindle apparatus. Eur. J. Cell Biol. *79*, 240–251.

Beindl, W., Mitterauer, T., Hohenegger, M., Ijzerman, A.P., Nanoff, C., and Freissmuth, M. (1996). Inhibition of receptor/G protein coupling by suramin analogues. Mol. Pharmacol. *50*, 415–423.

Belardinelli, L., Shryock, J.C., Snowdy, S., Zhang, Y., Monopoli, A., Lozza, G., Ongini, E., Olsson, R.A., and Dennis, D.M. (1998). The A2A adenosine receptor mediates coronary vasodilation. J. Pharmacol. Exp. Ther. *284*, 1066–1073.

Benham, C.D., and Tsien, R.W. (1987). A novel receptor-operated Ca2+-permeable channel activated by ATP in smooth muscle. Nature *328*, 275–278.

Berg, J.M., Tymoczko, J.L., and Stryer, L. (2007). Biochemistry: Sixth Edition. (W.H. Freeman and Company).

Bergerat, A., de Massy, B., Gadelle, D., Varoutas, P.C., Nicolas, A., and Forterre, P. (1997). An atypical topoisomerase II from Archaea with implications for meiotic recombination. Nature *386*, 414–417.

Berglund, O., and Eckstein, F. (1972). Synthesis of ATP- and dATP-substituted sepharoses and their application in the purification of phage-T4-induced ribonucleotide reductase. Eur. J. Biochem. *28*, 492–496.

Best, M.D. (2009). Click chemistry and bioorthogonal reactions: unprecedented selectivity in the labeling of biological molecules. Biochemistry *48*, 6571–6584.

Bigonnesse, F., Lévesque, S.A., Kukulski, F., Lecka, J., Robson, S.C., Fernandes, M.J.G., and Sévigny, J. (2004). Cloning and characterization of mouse nucleoside triphosphate diphosphohydrolase-8. Biochemistry *43*, 5511–5519.

Bill, B.R., Petzold, A.M., Clark, K.J., Schimmenti, L.A., and Ekker, S.C. (2009). A primer for morpholino use in zebrafish. Zebrafish *6*, 69–77.

Block, E.R., and Klarlund, J.K. (2008). Wounding sheets of epithelial cells activates the epidermal growth factor receptor through distinct short- and long-range mechanisms. Mol. Biol. Cell *19*, 4909–4917.

Bodin, P., and Burnstock, G. (2001). Evidence that release of adenosine triphosphate from endothelial cells during increased shear stress is vesicular. J. Cardiovasc. Pharmacol. *38*, 900–908.

Bodin, P., Bailey, D., and Burnstock, G. (1991). Increased flow-induced ATP release from isolated vascular endothelial cells but not smooth muscle cells. Br. J. Pharmacol. *103*, 1203–1205.

Bogdanov, Y.D., Wildman, S.S., Clements, M.P., King, B.F., and Burnstock, G. (1998). Molecular cloning and characterization of rat P2Y4 nucleotide receptor. Br. J. Pharmacol. *124*, 428–430.

Bonfanti, R., Furie, B.C., Furie, B., and Wagner, D.D. (1989). PADGEM (GMP140) is a component of Weibel-Palade bodies of human endothelial cells. Blood *73*, 1109–1112.

Boots, A.W., Hristova, M., Kasahara, D.I., Haenen, G.R.M.M., Bast, A., and van der Vliet, A. (2009). ATP-mediated activation of the NADPH oxidase DUOX1 mediates airway epithelial responses to bacterial stimuli. J. Biol. Chem. *284*, 17858–17867.

Boucher, I., Yang, L., Mayo, C., Klepeis, V., and Trinkaus-Randall, V. (2007). Injury and nucleotides induce phosphorylation of epidermal growth factor receptor: MMP and HB-EGF dependent pathway. Exp. Eye Res. *85*, 130–141.

Boucher, I., Rich, C., Lee, A., Marcincin, M., and Trinkaus-Randall, V. (2010). The P2Y2 receptor mediates the epithelial injury response and cell migration. Am. J. Physiol. Cell Physiol. *299*, C411-21.

Bowman, C.E., da Silva, R.G., Pham, A., and Young, S.W. (2019). An exceptionally potent inhibitor of human CD73. Biochemistry.

Bowne, S.J., Sullivan, L.S., Blanton, S.H., Cepko, C.L., Blackshaw, S., Birch, D.G., Hughbanks-Wheaton, D., Heckenlively, J.R., and Daiger, S.P. (2002). Mutations in the inosine monophosphate dehydrogenase 1 gene (IMPDH1) cause the RP10 form of autosomal dominant retinitis pigmentosa. Hum. Mol. Genet. *11*, 559–568.

Brake, A.J., Wagenbach, M.J., and Julius, D. (1994). New structural motif for ligand-gated ion channels defined by an ionotropic ATP receptor. Nature *371*, 519–523.

Braun, N., Fengler, S., Ebeling, C., Servos, J., and Zimmermann, H. (2000). Sequencing, functional expression and characterization of rat NTPDase6, a nucleoside diphosphatase and novel member of the ecto-nucleoside triphosphate diphosphohydrolase family. Biochem. J. *351 Pt 3*, 639–647.

Brogna, S., and Wen, J. (2009). Nonsense-mediated mRNA decay (NMD) mechanisms. Nat. Struct. Mol. Biol. *16*, 107–113.

Burger, A., Lindsay, H., Felker, A., Hess, C., Anders, C., Chiavacci, E., Zaugg, J., Weber, L.M., Catena, R., Jinek, M., et al. (2016). Maximizing mutagenesis with solubilized CRISPR-Cas9 ribonucleoprotein complexes. Development *143*, 2025–2037.

Burnstock, G. (1972). Purinergic nerves. Pharmacol. Rev. *24*, 509–581.

Burnstock, G. (1999). Release of vasoactive substances from endothelial cells by shear stress and purinergic mechanosensory transduction. J. Anat. *194 (Pt 3)*, 335–342.

Burnstock, G. (2007). Physiology and pathophysiology of purinergic neurotransmission. Physiol. Rev. *87*, 659–797.

Burnstock, G. (2017). Purinergic signaling in the cardiovascular system. Circ. Res. *120*, 207–228.

Burnstock, and G. A. (1978). A basis for distinguishing two types of purinergic receptor. Cell Membrane Receptors for Drugs and Hormone: A Multidisciplinary Approach.

Burnstock, G., and Ralevic, V. (1994). New insights into the local regulation of

blood flow by perivascular nerves and endothelium. Br J Plast Surg *47*, 527–543.

Burnstock, G., and Ralevic, V. (2014). Purinergic signaling and blood vessels in health and disease. Pharmacol. Rev. *66*, 102–192.

Burnstock, G., Campbell, G., Satchell, D., and Smythe, A. (1970). Evidence that adenosine triphosphate or a related nucleotide is the transmitter substance released by non-adrenergic inhibitory nerves in the gut. Br. J. Pharmacol. *40*, 668–688.

Burnstock, G., Fischer, B., Hoyle, C.H.V., Maillard, M., Ziganshin, A.U., Brizzolara, A.L., von Isakovics, A., Boyer, J.L., Harden, T.K., and Jacobson, K.A. (1994). Structure Activity Relationships for Derivatives of Adenosine-5'-Triphosphate as Agonists at P(2) Purinoceptors: Heterogeneity Within P(2X) and P(2Y) Subtypes. Drug Dev Res *31*, 206–219.

van Calker, D., Müller, M., and Hamprecht, B. (1979). Adenosine regulates via two different types of receptors, the accumulation of cyclic AMP in cultured brain cells. J. Neurochem. *33*, 999–1005.

Caughey, G.E., Cleland, L.G., Penglis, P.S., Gamble, J.R., and James, M.J. (2001). Roles of cyclooxygenase (COX)-1 and COX-2 in prostanoid production by human endothelial cells: selective up-regulation of prostacyclin synthesis by COX-2. J. Immunol. *167*, 2831–2838.

Chauhan, J.S., Mishra, N.K., and Raghava, G.P.S. (2009). Identification of ATP binding residues of a protein from its primary sequence. BMC Bioinformatics *10*, 434.

Chekeni, F.B., Elliott, M.R., Sandilos, J.K., Walk, S.F., Kinchen, J.M., Lazarowski, E.R., Armstrong, A.J., Penuela, S., Laird, D.W., Salvesen, G.S., et al. (2010). Pannexin 1 channels mediate "find-me" signal release and membrane permeability during apoptosis. Nature *467*, 863–867.

Chen, T.-W., Wardill, T.J., Sun, Y., Pulver, S.R., Renninger, S.L., Baohan, A., Schreiter, E.R., Kerr, R.A., Orger, M.B., Jayaraman, V., et al. (2013). Ultrasensitive fluorescent proteins for imaging neuronal activity. Nature *499*, 295–300.

Chen, Y., Corriden, R., Inoue, Y., Yip, L., Hashiguchi, N., Zinkernagel, A., Nizet, V., Insel, P.A., and Junger, W.G. (2006). ATP release guides neutrophil chemotaxis via P2Y2 and A3 receptors. Science *314*, 1792–1795.

Chen, Y., Yao, Y., Sumi, Y., Li, A., To, U.K., Elkhal, A., Inoue, Y., Woehrle, T., Zhang, Q., Hauser, C., et al. (2010). Purinergic signaling: a fundamental mechanism in neutrophil activation. Sci. Signal. *3*, ra45.

Cheung, P.C., Salt, I.P., Davies, S.P., Hardie, D.G., and Carling, D. (2000). Characterization of AMP-activated protein kinase gamma-subunit isoforms and their role in AMP binding. Biochem. J. *346 Pt 3*, 659–669.

Cho, S.-H., Nguyen, C.T., Choi, J., and Stacey, G. (2017). Molecular mechanism of plant recognition of extracellular ATP. Adv. Exp. Med. Biol. *1051*, 233–253.

Choi, J., Tanaka, K., Cao, Y., Qi, Y., Qiu, J., Liang, Y., Lee, S.Y., and Stacey, G. (2014). Identification of a plant receptor for extracellular ATP. Science *343*, 290–

294.

Chung, W.-C., and Kermode, J.C. (2005). Suramin disrupts receptor-G protein coupling by blocking association of G protein alpha and betagamma subunits. J. Pharmacol. Exp. Ther. *313*, 191–198.

Ciancaglini, P., Yadav, M.C., Simão, A.M.S., Narisawa, S., Pizauro, J.M., Farquharson, C., Hoylaerts, M.F., and Millán, J.L. (2010). Kinetic analysis of substrate utilization by native and TNAP-, NPP1-, or PHOSPHO1-deficient matrix vesicles. J. Bone Miner. Res. *25*, 716–723.

Colman, R.F. (1983). Affinity labeling of purine nucleotide sites in proteins. Annu. Rev. Biochem. *52*, 67–91.

Cotrina, M.L., Lin, J.H., Alves-Rodrigues, A., Liu, S., Li, J., Azmi-Ghadimi, H., Kang, J., Naus, C.C., and Nedergaard, M. (1998). Connexins regulate calcium signaling by controlling ATP release. Proc. Natl. Acad. Sci. USA *95*, 15735–15740.

Cravatt, B.F., Wright, A.T., and Kozarich, J.W. (2008). Activity-based protein profiling: from enzyme chemistry to proteomic chemistry. Annu. Rev. Biochem. *77*, 383–414.

Cronstein, B.N., Kramer, S.B., Weissmann, G., and Hirschhorn, R. (1983). Adenosine: a physiological modulator of superoxide anion generation by human neutrophils. J. Exp. Med. *158*, 1160–1177.

Cronstein, B.N., Kubersky, S.M., Weissmann, G., and Hirschhorn, R. (1987). Engagement of adenosine receptors inhibits hydrogen peroxide (H2O2-) release by activated human neutrophils. Clin Immunol Immunopathol *42*, 76–85.

Cronstein, B.N., Levin, R.I., Philips, M., Hirschhorn, R., Abramson, S.B., and Weissmann, G. (1992). Neutrophil adherence to endothelium is enhanced via adenosine A1 receptors and inhibited via adenosine A2 receptors. J. Immunol. *148*, 2201–2206.

Deaglio, S., Dwyer, K.M., Gao, W., Friedman, D., Usheva, A., Erat, A., Chen, J.-F., Enjyoji, K., Linden, J., Oukka, M., et al. (2007). Adenosine generation catalyzed by CD39 and CD73 expressed on regulatory T cells mediates immune suppression. J. Exp. Med. *204*, 1257–1265.

DeGrendele, H.C., Estess, P., and Siegelman, M.H. (1997). Requirement for CD44 in activated T cell extravasation into an inflammatory site. Science *278*, 672–675.

Driever, W., Solnica-Krezel, L., Schier, A.F., Neuhauss, S.C., Malicki, J., Stemple, D.L., Stainier, D.Y., Zwartkruis, F., Abdelilah, S., Rangini, Z., et al. (1996). A genetic screen for mutations affecting embryogenesis in zebrafish. Development *123*, 37–46.

Drury, A.N., and Szent-Györgyi, A. (1929). The physiological activity of adenine compounds with especial reference to their action upon the mammalian heart. J. Physiol. (Lond.) *68*, 213–237.

Dubinsky, L., Krom, B.P., and Meijler, M.M. (2012). Diazirine based photoaffinity labeling. Bioorg. Med. Chem. *20*, 554–570.

Dutta, R., and Inouye, M. (2000). GHKL, an emergent ATPase/kinase superfamily. Trends Biochem. Sci. *25*, 24–28.

Egan, K., and FitzGerald, G.A. (2006). Eicosanoids and the vascular endothelium. Handb Exp Pharmacol 189–211.

Ellett, F., Pase, L., Hayman, J.W., Andrianopoulos, A., and Lieschke, G.J. (2011). mpeg1 promoter transgenes direct macrophage-lineage expression in zebrafish. Blood *117*, e49-56.

Elliott, M.R., Chekeni, F.B., Trampont, P.C., Lazarowski, E.R., Kadl, A., Walk, S.F., Park, D., Woodson, R.I., Ostankovich, M., Sharma, P., et al. (2009). Nucleotides released by apoptotic cells act as a find-me signal to promote phagocytic clearance. Nature *461*, 282–286.

Eng, J.K., McCormack, A.L., and Yates, J.R. (1994). An approach to correlate tandem mass spectral data of peptides with amino acid sequences in a protein database. J Am Soc Mass Spectrom *5*, 976–989.

Enomoto, K., Furuya, K., Yamagishi, S., Oka, T., and Maeno, T. (1994). The increase in the intracellular Ca2+ concentration induced by mechanical stimulation is propagated via release of pyrophosphorylated nucleotides in mammary epithelial cells. Pflugers Arch. *427*, 533–542.

Enyedi, B., and Niethammer, P. (2015). Mechanisms of epithelial wound detection. Trends Cell Biol. *25*, 398–407.

Enyedi, B., Kala, S., Nikolich-Zugich, T., and Niethammer, P. (2013). Tissue damage detection by osmotic surveillance. Nat. Cell Biol. *15*, 1123–1130.

Enyedi, B., Jelcic, M., and Niethammer, P. (2016). The Cell Nucleus Serves as a Mechanotransducer of Tissue Damage-Induced Inflammation. Cell *165*, 1160–1170.

Erb, L., Garrad, R., Wang, Y., Quinn, T., Turner, J.T., and Weisman, G.A. (1995). Site-directed mutagenesis of P2U purinoceptors. Positively charged amino acids in transmembrane helices 6 and 7 affect agonist potency and specificity. J. Biol. Chem. *270*, 4185–4188.

Etchegaray, J.-P., Machida, K.K., Noton, E., Constance, C.M., Dallmann, R., Di Napoli, M.N., DeBruyne, J.P., Lambert, C.M., Yu, E.A., Reppert, S.M., et al. (2009). Casein kinase 1 delta regulates the pace of the mammalian circadian clock. Mol. Cell. Biol. *29*, 3853–3866.

Feng, J.-F., Gao, X.-F., Pu, Y.-Y., Burnstock, G., Xiang, Z., and He, C. (2015). P2X7 receptors and Fyn kinase mediate ATP-induced oligodendrocyte progenitor cell migration. Purinergic Signal *11*, 361–369.

Fischer, B., Boyer, J.L., Hoyle, C.H., Ziganshin, A.U., Brizzolara, A.L., Knight, G.E., Zimmet, J., Burnstock, G., Harden, T.K., and Jacobson, K.A. (1993). Identification of potent, selective P2Y-purinoceptor agonists: structure-activity relationships for 2-thioether derivatives of adenosine 5'-triphosphate. J. Med. Chem. *36*, 3937–3946.

Frame, M.K., and de Feijter, A.W. (1997). Propagation of mechanically induced

intercellular calcium waves via gap junctions and ATP receptors in rat liver epithelial cells. Exp. Cell Res. *230*, 197–207.

Francis, S.H., Busch, J.L., Corbin, J.D., and Sibley, D. (2010). cGMP-dependent protein kinases and cGMP phosphodiesterases in nitric oxide and cGMP action. Pharmacol. Rev. *62*, 525–563.

Fredholm, B.B., Zhang, Y., and van der Ploeg, I. (1996). Adenosine A2A receptors mediate the inhibitory effect of adenosine on formyl-Met-Leu-Phe-stimulated respiratory burst in neutrophil leucocytes. Naunyn Schmiedebergs Arch. Pharmacol. *354*, 262–267.

Fredholm, B.B., IJzerman, A.P., Jacobson, K.A., Klotz, K.N., and Linden, J. (2001). International Union of Pharmacology. XXV. Nomenclature and classification of adenosine receptors. Pharmacol. Rev. *53*, 527–552.

Fritsche, R., Schwerte, T., and Pelster, B. (2000). Nitric oxide and vascular reactivity in developing zebrafish, Danio rerio. Am. J. Physiol. Regul. Integr. Comp. Physiol. *279*, R2200-7.

Gagnon, J.A., Valen, E., Thyme, S.B., Huang, P., Akhmetova, L., Pauli, A., Montague, T.G., Zimmerman, S., Richter, C., and Schier, A.F. (2014). Efficient mutagenesis by Cas9 protein-mediated oligonucleotide insertion and large-scale assessment of single-guide RNAs. PLoS One *9*, e98186.

Galmozzi, A., Parker, C.G., Kok, B.P., Cravatt, B.F., and Saez, E. (2018). Discovery of modulators of adipocyte physiology using fully functionalized fragments. Methods Mol. Biol. *1787*, 115–127.

Galperin, M.Y., and Koonin, E.V. (1997). A diverse superfamily of enzymes with ATP-dependent carboxylate-amine/thiol ligase activity. Protein Sci. *6*, 2639–2643.

Gandelman, M., Levy, M., Cassina, P., Barbeito, L., and Beckman, J.S. (2013). P2X7 receptor-induced death of motor neurons by a peroxynitrite/FAS-dependent pathway. J. Neurochem. *126*, 382–388.

Gao, J., Mfuh, A., Amako, Y., and Woo, C.M. (2018). Small molecule interactome mapping by photoaffinity labeling reveals binding site hotspots for the nsaids. J. Am. Chem. Soc. *140*, 4259–4268.

Garritsen, A., Zhang, Y., and Cooper, D.M. (1992). Purinergic receptor regulation of signal transduction in NCB-20 cells. Mol. Pharmacol. *41*, 743–749.

Gault, W.J., Enyedi, B., and Niethammer, P. (2014). Osmotic surveillance mediates rapid wound closure through nucleotide release. J. Cell Biol. *207*, 767–782.

Gentles, A.J., and Karlin, S. (1999). Why are human G-protein-coupled receptors predominantly intronless? Trends Genet. *15*, 47–49.

Ghosh, A., and Halpern, M.E. (2016). Transcriptional regulation using the Q system in transgenic zebrafish. Methods Cell Biol. *135*, 205–218.

Gillespie, J.H. (1934). The biological significance of the linkages in adenosine triphosphoric acid. J. Physiol. (Lond.) *80*, 345–359.

Goding, J.W., Grobben, B., and Slegers, H. (2003). Physiological and pathophysiological functions of the ecto-nucleotide pyrophosphatase/phosphodiesterase family. Biochimica et Biophysica Acta (BBA) - Molecular Basis of Disease *1638*, 1–19.

Gollob, M.H., Seger, J.J., Gollob, T.N., Tapscott, T., Gonzales, O., Bachinski, L., and Roberts, R. (2001). Novel PRKAG2 mutation responsible for the genetic syndrome of ventricular preexcitation and conduction system disease with childhood onset and absence of cardiac hypertrophy. Circulation *104*, 3030–3033.

Gong, Z., Ju, B., Wang, X., He, J., Wan, H., Sudha, P.M., and Yan, T. (2002). Green fluorescent protein expression in germ-line transmitted transgenic zebrafish under a stratified epithelial promoter from keratin8. Dev. Dyn. *223*, 204–215.

Gordon, J.L. (1986). Extracellular ATP: effects, sources and fate. Biochem. J. *233*, 309–319.

Gore, A.V., Monzo, K., Cha, Y.R., Pan, W., and Weinstein, B.M. (2012). Vascular development in the zebrafish. Cold Spring Harb. Perspect. Med. *2*, a006684.

Graves, P.R., Kwiek, J.J., Fadden, P., Ray, R., Hardeman, K., Coley, A.M., Foley, M., and Haystead, T.A.J. (2002). Discovery of novel targets of quinoline drugs in the human purine binding proteome. Mol. Pharmacol. *62*, 1364–1372.

Grondal, E.J., and Zimmermann, H. (1987). Purification, characterization and cellular localization of 5'-nucleotidase from Torpedo electric organ. Biochem. J. *245*, 805–810.

Günthert, U., Hofmann, M., Rudy, W., Reber, S., Zöller, M., Haussmann, I., Matzku, S., Wenzel, A., Ponta, H., and Herrlich, P. (1991). A new variant of glycoprotein CD44 confers metastatic potential to rat carcinoma cells. Cell *65*, 13–24.

Gurtner, G.C., Werner, S., Barrandon, Y., and Longaker, M.T. (2008). Wound repair and regeneration. Nature *453*, 314–321.

Haffter, P., Granato, M., Brand, M., Mullins, M.C., Hammerschmidt, M., Kane, D.A., Odenthal, J., van Eeden, F.J., Jiang, Y.J., Heisenberg, C.P., et al. (1996). The identification of genes with unique and essential functions in the development of the zebrafish, Danio rerio. Development *123*, 1–36.

Haldón, E., Nicasio, M.C., and Pérez, P.J. (2015). Copper-catalysed azide-alkyne cycloadditions (CuAAC): an update. Org. Biomol. Chem. *13*, 9528–9550.

Hall, C., Flores, M.V., Storm, T., Crosier, K., and Crosier, P. (2007). The zebrafish lysozyme C promoter drives myeloid-specific expression in transgenic fish. BMC Dev. Biol. *7*, 42.

Hamberg, M., Svensson, J., and Samuelsson, B. (1975). Thromboxanes: a new group of biologically active compounds derived from prostaglandin endoperoxides. Proc. Natl. Acad. Sci. USA *72*, 2994–2998.

Hanks, S.K., Quinn, A.M., and Hunter, T. (1988). The protein kinase family: conserved features and deduced phylogeny of the catalytic domains. Science *241*, 42–52.

Hanoulle, X., Van Damme, J., Staes, A., Martens, L., Goethals, M., Vandekerckhove, J., and Gevaert, K. (2006). A new functional, chemical proteomics technology to identify purine nucleotide binding sites in complex proteomes. J. Proteome Res. *5*, 3438–3445.

Hansen, M., Boitano, S., Dirksen, E.R., and Sanderson, M.J. (1993). Intercellular calcium signaling induced by extracellular adenosine 5'-triphosphate and mechanical stimulation in airway epithelial cells. J. Cell Sci. *106 (Pt 4)*, 995–1004.

Hardie, D.G., Ross, F.A., and Hawley, S.A. (2012). AMPK: a nutrient and energy sensor that maintains energy homeostasis. Nat. Rev. Mol. Cell Biol. *13*, 251–262.

Haug, K., Warnstedt, M., Alekov, A.K., Sander, T., Ramírez, A., Poser, B., Maljevic, S., Hebeisen, S., Kubisch, C., Rebstock, J., et al. (2003). Mutations in CLCN2 encoding a voltage-gated chloride channel are associated with idiopathic generalized epilepsies. Nat. Genet. *33*, 527–532.

Haynes, B.F., Telen, M.J., Hale, L.P., and Denning, S.M. (1989). CD44 — A molecule involved in leukocyte adherence and T-cell activation. Immunol. Today *10*, 423–428.

Haynes, S.E., Hollopeter, G., Yang, G., Kurpius, D., Dailey, M.E., Gan, W.-B., and Julius, D. (2006). The P2Y12 receptor regulates microglial activation by extracellular nucleotides. Nat. Neurosci. *9*, 1512–1519.

Haystead, C.M., Gregory, P., Sturgill, T.W., and Haystead, T.A. (1993). Gamma-phosphate-linked ATP-sepharose for the affinity purification of protein kinases. Rapid purification to homogeneity of skeletal muscle mitogen-activated protein kinase kinase. Eur. J. Biochem. *214*, 459–467.

Hechler, B., Léon, C., Vial, C., Vigne, P., Frelin, C., Cazenave, J.P., and Gachet, C. (1998). The P2Y1 receptor is necessary for adenosine 5'-diphosphate-induced platelet aggregation. Blood *92*, 152–159.

Hein, T.W., Belardinelli, L., and Kuo, L. (1999). Adenosine A(2A) receptors mediate coronary microvascular dilation to adenosine: role of nitric oxide and ATP-sensitive potassium channels. J. Pharmacol. Exp. Ther. *291*, 655–664.

Hellsten, Y., Nyberg, M., Jensen, L.G., and Mortensen, S.P. (2012). Vasodilator interactions in skeletal muscle blood flow regulation. J. Physiol. (Lond.) *590*, 6297–6305.

Hill, A.J., Teraoka, H., Heideman, W., and Peterson, R.E. (2005). Zebrafish as a model vertebrate for investigating chemical toxicity. Toxicol. Sci. *86*, 6–19.

Hirota, T., Lee, J.W., Lewis, W.G., Zhang, E.E., Breton, G., Liu, X., Garcia, M., Peters, E.C., Etchegaray, J.-P., Traver, D., et al. (2010). High-throughput chemical screen identifies a novel potent modulator of cellular circadian rhythms and reveals CKIα as a clock regulatory kinase. PLoS Biol. *8*, e1000559.

Hollopeter, G., Jantzen, H.M., Vincent, D., Li, G., England, L., Ramakrishnan, V., Yang, R.B., Nurden, P., Nurden, A., Julius, D., et al. (2001). Identification of the platelet ADP receptor targeted by antithrombotic drugs. Nature *409*, 202–207.

Holtmaat, A., Bonhoeffer, T., Chow, D.K., Chuckowree, J., De Paola, V., Hofer,

S.B., Hübener, M., Keck, T., Knott, G., Lee, W.-C.A., et al. (2009). Long-term, high-resolution imaging in the mouse neocortex through a chronic cranial window. Nat. Protoc. *4*, 1128–1144.

Holton, P. (1959). The liberation of adenosine triphosphate on antidromic stimulation of sensory nerves. J. Physiol. (Lond.) *145*, 494–504.

Holton, F.A., and Holton, P. (1954). The capillary dilator substances in dry powders of spinal roots; a possible role of adenosine triphosphate in chemical transmission from nerve endings. J. Physiol. (Lond.) *126*, 124–140.

Hopwood, A.M., and Burnstock, G. (1987). ATP mediates coronary vasoconstriction via P2x-purinoceptors and coronary vasodilatation via P2y-purinoceptors in the isolated perfused rat heart. Eur. J. Pharmacol. *136*, 49–54.

Hoshijima, K., Jurynec, M.J., Klatt Shaw, D., Jacobi, A.M., Behlke, M.A., and Grunwald, D.J. (2019). Highly Efficient CRISPR-Cas9-Based Methods for Generating Deletion Mutations and F0 Embryos that Lack Gene Function in Zebrafish. Dev. Cell *51*, 645–657.e4.

Howe, K., Clark, M.D., Torroja, C.F., Torrance, J., Berthelot, C., Muffato, M., Collins, J.E., Humphray, S., McLaren, K., Matthews, L., et al. (2013). The zebrafish reference genome sequence and its relationship to the human genome. Nature *496*, 498–503.

Hu, J., Li, Y., Zhang, Y., and Yu, D.-J. (2018). ATPbind: Accurate Protein-ATP Binding Site Prediction by Combining Sequence-Profiling and Structure-Based Comparisons. J. Chem. Inf. Model. *58*, 501–510.

Huang, C., and Niethammer, P. (2018). Tissue damage signaling is a prerequisite for protective neutrophil recruitment to microbial infection in zebrafish. Immunity *48*, 1006–1013.e6.

Hulce, J.J., Cognetta, A.B., Niphakis, M.J., Tully, S.E., and Cravatt, B.F. (2013). Proteome-wide mapping of cholesterol-interacting proteins in mammalian cells. Nat. Methods *10*, 259–264.

Hwang, W.Y., Fu, Y., Reyon, D., Maeder, M.L., Tsai, S.Q., Sander, J.D., Peterson, R.T., Yeh, J.-R.J., and Joung, J.K. (2013). Efficient genome editing in zebrafish using a CRISPR-Cas system. Nat. Biotechnol. *31*, 227–229.

Idzko, M., Hammad, H., van Nimwegen, M., Kool, M., Willart, M.A.M., Muskens, F., Hoogsteden, H.C., Luttmann, W., Ferrari, D., Di Virgilio, F., et al. (2007). Extracellular ATP triggers and maintains asthmatic airway inflammation by activating dendritic cells. Nat. Med. *13*, 913–919.

Idzko, M., Ferrari, D., and Eltzschig, H.K. (2014). Nucleotide signalling during inflammation. Nature *509*, 310–317.

Ignarro, L.J., Buga, G.M., Wood, K.S., Byrns, R.E., and Chaudhuri, G. (1987). Endothelium-derived relaxing factor produced and released from artery and vein is nitric oxide. Proc. Natl. Acad. Sci. USA *84*, 9265–9269.

Isogai, S., Horiguchi, M., and Weinstein, B.M. (2001). The vascular anatomy of the developing zebrafish: an atlas of embryonic and early larval development. Dev.

Biol. *230*, 278–301.

Ito, J., Heazlewood, J.L., and Millar, A.H. (2006). Analysis of the soluble ATP-binding proteome of plant mitochondria identifies new proteins and nucleotide triphosphate interactions within the matrix. J. Proteome Res. *5*, 3459–3469.

Itoh, N., Yonehara, S., Ishii, A., Yonehara, M., Mizushima, S., Sameshima, M., Hase, A., Seto, Y., and Nagata, S. (1991). The polypeptide encoded by the cDNA for human cell surface antigen Fas can mediate apoptosis. Cell *66*, 233–243.

Izsvák, Z., Chuah, M.K.L., Vandendriessche, T., and Ivics, Z. (2009). Efficient stable gene transfer into human cells by the Sleeping Beauty transposon vectors. Methods *49*, 287–297.

Jayaraman, S., Song, Y., and Verkman, A.S. (2001a). Airway surface liquid osmolality measured using fluorophore-encapsulated liposomes. J. Gen. Physiol. *117*, 423–430.

Jayaraman, S., Song, Y., Vetrivel, L., Shankar, L., and Verkman, A.S. (2001b). Noninvasive in vivo fluorescence measurement of airway-surface liquid depth, salt concentration, and pH. J. Clin. Invest. *107*, 317–324.

Jelcic, M., Enyedi, B., Xavier, J.B., and Niethammer, P. (2017). Image-Based Measurement of H2O2 Reaction-Diffusion in Wounded Zebrafish Larvae. Biophys. J. *112*, 2011–2018.

Jiang, H., Peterson, R.S., Wang, W., Bartnik, E., Knudson, C.B., and Knudson, W. (2002). A requirement for the CD44 cytoplasmic domain for hyaluronan binding, pericellular matrix assembly, and receptor-mediated endocytosis in COS-7 cells. J. Biol. Chem. *277*, 10531–10538.

Jiang, L.H., Rassendren, F., Surprenant, A., and North, R.A. (2000). Identification of amino acid residues contributing to the ATP-binding site of a purinergic P2X receptor. J. Biol. Chem. *275*, 34190–34196.

Jiang, Q., Guo, D., Lee, B.X., Van Rhee, A.M., Kim, Y.C., Nicholas, R.A., Schachter, J.B., Harden, T.K., and Jacobson, K.A. (1997). A mutational analysis of residues essential for ligand recognition at the human P2Y1 receptor. Mol. Pharmacol. *52*, 499–507.

Jin, J., Daniel, J.L., and Kunapuli, S.P. (1998). Molecular basis for ADP-induced platelet activation. II. The P2Y1 receptor mediates ADP-induced intracellular calcium mobilization and shape change in platelets. J. Biol. Chem. *273*, 2030–2034.

Jin, S.-W., Beis, D., Mitchell, T., Chen, J.-N., and Stainier, D.Y.R. (2005). Cellular and molecular analyses of vascular tube and lumen formation in zebrafish. Development *132*, 5199–5209.

Joris, L., Dab, I., and Quinton, P.M. (1993). Elemental composition of human airway surface fluid in healthy and diseased airways. Am. Rev. Respir. Dis. *148*, 1633–1637.

Josic, D., and Clifton, J.G. (2007). Mammalian plasma membrane proteomics. Proteomics *7*, 3010–3029.

Kaczmarek, E., Koziak, K., Sévigny, J., Siegel, J.B., Anrather, J., Beaudoin, A.R., Bach, F.H., and Robson, S.C. (1996). Identification and characterization of CD39/vascular ATP diphosphohydrolase. J. Biol. Chem. *271*, 33116–33122.

Kaczmarek, E., Erb, L., Koziak, K., Jarzyna, R., Wink, M.R., Guckelberger, O., Blusztajn, J.K., Trinkaus-Randall, V., Weisman, G.A., and Robson, S.C. (2005). Modulation of endothelial cell migration by extracellular nucleotides: involvement of focal adhesion kinase and phosphatidylinositol 3-kinase-mediated pathways. Thromb. Haemost. *93*, 735–742.

Kahner, B.N., Shankar, H., Murugappan, S., Prasad, G.L., and Kunapuli, S.P. (2006). Nucleotide receptor signaling in platelets. J. Thromb. Haemost. *4*, 2317–2326.

Katayama, Y., Hidalgo, A., Chang, J., Peired, A., and Frenette, P.S. (2005). CD44 is a physiological E-selectin ligand on neutrophils. J. Exp. Med. *201*, 1183–1189.

Kawate, T., Michel, J.C., Birdsong, W.T., and Gouaux, E. (2009). Crystal structure of the ATP-gated P2X(4) ion channel in the closed state. Nature *460*, 592–598.

Kennedy, C., Qi, A.D., Herold, C.L., Harden, T.K., and Nicholas, R.A. (2000). ATP, an agonist at the rat P2Y(4) receptor, is an antagonist at the human P2Y(4) receptor. Mol. Pharmacol. *57*, 926–931.

Khadra, N., Bresson-Bepoldin, L., Penna, A., Chaigne-Delalande, B., Ségui, B., Levade, T., Vacher, A.-M., Reiffers, J., Ducret, T., Moreau, J.-F., et al. (2011). CD95 triggers Orai1-mediated localized Ca2+ entry, regulates recruitment of protein kinase C (PKC) β2, and prevents death-inducing signaling complex formation. Proc. Natl. Acad. Sci. USA *108*, 19072–19077.

Khakh, B.S., and North, R.A. (2006). P2X receptors as cell-surface ATP sensors in health and disease. Nature *442*, 527–532.

Klepeis, V.E., Cornell-Bell, A., and Trinkaus-Randall, V. (2001). Growth factors but not gap junctions play a role in injury-induced Ca2+ waves in epithelial cells. J. Cell Sci. *114*, 4185–4195.

Klepeis, V.E., Weinger, I., Kaczmarek, E., and Trinkaus-Randall, V. (2004). P2Y receptors play a critical role in epithelial cell communication and migration. J. Cell Biochem. *93*, 1115–1133.

Kluijtmans, L.A., Boers, G.H., Stevens, E.M., Renier, W.O., Kraus, J.P., Trijbels, F.J., van den Heuvel, L.P., and Blom, H.J. (1996). Defective cystathionine beta-synthase regulation by S-adenosylmethionine in a partially pyridoxine responsive homocystinuria patient. J. Clin. Invest. *98*, 285–289.

Knapp, K., Zebisch, M., Pippel, J., El-Tayeb, A., Müller, C.E., and Sträter, N. (2012). Crystal structure of the human ecto-5'-nucleotidase (CD73): insights into the regulation of purinergic signaling. Structure *20*, 2161–2173.

Knighton, D.R., Zheng, J.H., Ten Eyck, L.F., Ashford, V.A., Xuong, N.H., Taylor, S.S., and Sowadski, J.M. (1991). Crystal structure of the catalytic subunit of cyclic adenosine monophosphate-dependent protein kinase. Science *253*, 407–414.

Knippschild, U., Milne, D.M., Campbell, L.E., DeMaggio, A.J., Christenson, E.,

Hoekstra, M.F., and Meek, D.W. (1997). p53 is phosphorylated in vitro and in vivo by the delta and epsilon isoforms of casein kinase 1 and enhances the level of casein kinase 1 delta in response to topoisomerase-directed drugs. Oncogene *15*, 1727–1736.

Kobayashi, T., Kouzaki, H., and Kita, H. (2010). Human eosinophils recognize endogenous danger signal crystalline uric acid and produce proinflammatory cytokines mediated by autocrine ATP. J. Immunol. *184*, 6350–6358.

Konrad, M., Vollmer, M., Lemmink, H.H., van den Heuvel, L.P., Jeck, N., Vargas-Poussou, R., Lakings, A., Ruf, R., Deschênes, G., Antignac, C., et al. (2000). Mutations in the chloride channel gene CLCNKB as a cause of classic Bartter syndrome. J. Am. Soc. Nephrol. *11*, 1449–1459.

Koonin, E.V., Wolf, Y.I., and Aravind, L. (2000). Protein fold recognition using sequence profiles and its application in structural genomics. Adv. Protein Chem. *54*, 245–275.

Kowarz, E., Löscher, D., and Marschalek, R. (2015). Optimized Sleeping Beauty transposons rapidly generate stable transgenic cell lines. Biotechnol. J. *10*, 647–653.

Kronlage, M., Song, J., Sorokin, L., Isfort, K., Schwerdtle, T., Leipziger, J., Robaye, B., Conley, P.B., Kim, H.-C., Sargin, S., et al. (2010). Autocrine purinergic receptor signaling is essential for macrophage chemotaxis. Sci. Signal. *3*, ra55.

von Kügelgen, I. (2006). Pharmacological profiles of cloned mammalian P2Y-receptor subtypes. Pharmacol. Ther. *110*, 415–432.

von Kügelgen, I., and Hoffmann, K. (2016). Pharmacology and structure of P2Y receptors. Neuropharmacology *104*, 50–61.

von Kügelgen, I., Häussinger, D., and Starke, K. (1987). Evidence for a vasoconstriction-mediating receptor for UTP, distinct from the P2 purinoceptor, in rabbit ear artery. Naunyn Schmiedebergs Arch. Pharmacol. *336*, 556–560.

Kukulski, F., Lévesque, S.A., Lavoie, E.G., Lecka, J., Bigonnesse, F., Knowles, A.F., Robson, S.C., Kirley, T.L., and Sévigny, J. (2005). Comparative hydrolysis of P2 receptor agonists by NTPDases 1, 2, 3 and 8. Purinergic Signal *1*, 193–204.

Kuttner, Y.Y., Sobolev, V., Raskind, A., and Edelman, M. (2003). A consensus-binding structure for adenine at the atomic level permits searching for the ligand site in a wide spectrum of adenine-containing complexes. Proteins *52*, 400–411.

Kwan, K.M., Fujimoto, E., Grabher, C., Mangum, B.D., Hardy, M.E., Campbell, D.S., Parant, J.M., Yost, H.J., Kanki, J.P., and Chien, C.-B. (2007). The Tol2kit: a multisite gateway-based construction kit for Tol2 transposon transgenesis constructs. Dev. Dyn. *236*, 3088–3099.

Kwon, Y., Hofmann, T., and Montell, C. (2007). Integration of phosphoinositide- and calmodulin-mediated regulation of TRPC6. Mol. Cell *25*, 491–503.

Labun, K., Montague, T.G., Gagnon, J.A., Thyme, S.B., and Valen, E. (2016). CHOPCHOP v2: a web tool for the next generation of CRISPR genome engineering. Nucleic Acids Res. *44*, W272-6.

Lam, S.H., Chua, H.L., Gong, Z., Lam, T.J., and Sin, Y.M. (2004). Development and maturation of the immune system in zebrafish, Danio rerio: a gene expression profiling, in situ hybridization and immunological study. Developmental & Comparative Immunology *28*, 9–28.

Lang, W., Yuan, C., Zhu, B., Pan, S., Liu, J., Luo, J., Nie, S., Zhu, Q., Lee, J.-S., and Ge, J. (2019). Expanding the “minimalist” small molecule tagging approach to different bioactive compounds. Org. Biomol. Chem. *17*, 3010–3017.

Larsson, P.O., and Mosbach, K. (1971). Preparation of a NAD(H)-polymer matrix showing coenzyme function of the bound pyridine nucleotide. Biotechnol. Bioeng. *13*, 393–398.

Lawson, N.D., and Weinstein, B.M. (2002). In vivo imaging of embryonic vascular development using transgenic zebrafish. Dev. Biol. *248*, 307–318.

Lecut, C., Frederix, K., Johnson, D.M., Deroanne, C., Thiry, M., Faccinetto, C., Marée, R., Evans, R.J., Volders, P.G.A., Bours, V., et al. (2009). P2X1 ion channels promote neutrophil chemotaxis through Rho kinase activation. J. Immunol. *183*, 2801–2809.

Lee, J.-E., Park, J.-H., Moon, P.-G., and Baek, M.-C. (2013). Identification of differentially expressed proteins by treatment with PUGNAc in 3T3-L1 adipocytes through analysis of ATP-binding proteome. Proteomics *13*, 2998–3012.

Leier, I., Jedlitschky, G., Buchholz, U., Cole, S.P., Deeley, R.G., and Keppler, D. (1994). The MRP gene encodes an ATP-dependent export pump for leukotriene C4 and structurally related conjugates. J. Biol. Chem. *269*, 27807–27810.

Leist, M., Single, B., Castoldi, A.F., Kühnle, S., and Nicotera, P. (1997). Intracellular adenosine triphosphate (ATP) concentration: a switch in the decision between apoptosis and necrosis. J. Exp. Med. *185*, 1481–1486.

Léon, C., Hechler, B., Vial, C., Leray, C., Cazenave, J.-P., and Gachet, C. (1997). The $P2Y_1$ receptor is an ADP receptor antagonized by ATP and expressed in platelets and megakaryoblastic cells. FEBS Lett. *403*, 26–30.

Lepiller, S., Franche, N., Solary, E., Chluba, J., and Laurens, V. (2009). Comparative analysis of zebrafish nos2a and nos2b genes. Gene *445*, 58–65.

Li, J. m, Fenton, R.A., Wheeler, H.B., Powell, C.C., Peyton, B.D., Cutler, B.S., and Dobson, J.G. (1998). Adenosine A2a receptors increase arterial endothelial cell nitric oxide. J. Surg. Res. *80*, 357–364.

Li, P., Nijhawan, D., Budihardjo, I., Srinivasula, S.M., Ahmad, M., Alnemri, E.S., and Wang, X. (1997). Cytochrome c and dATP-dependent formation of Apaf-1/caspase-9 complex initiates an apoptotic protease cascade. Cell *91*, 479–489.

Li, W., Zhou, Y., You, W., Yang, M., Ma, Y., Wang, M., Wang, Y., Yuan, S., and Xiao, Y. (2018). Development of Photoaffinity Probe for the Discovery of Steviol Glycosides Biosynthesis Pathway in Stevia rebuadiana and Rapid Substrate Screening. ACS Chem. Biol. *13*, 1944–1949.

Li, X., Foley, E.A., Molloy, K.R., Li, Y., Chait, B.T., and Kapoor, T.M. (2012). Quantitative chemical proteomics approach to identify post-translational

modification-mediated protein-protein interactions. J. Am. Chem. Soc. *134*, 1982–1985.

Li, Z., Hao, P., Li, L., Tan, C.Y.J., Cheng, X., Chen, G.Y.J., Sze, S.K., Shen, H.-M., and Yao, S.Q. (2013). Design and synthesis of minimalist terminal alkyne-containing diazirine photo-crosslinkers and their incorporation into kinase inhibitors for cell- and tissue-based proteome profiling. Angew. Chem. Int. Ed. Engl. *52*, 8551–8556.

Lindberg, M., and Mosbach, K. (1975). Preparation of analogues of ATP, ADP and AMP suitable for binding to matrices and the enzymic interconversion of ATP and ADP in solid phase. Eur. J. Biochem. *53*, 481–486.

Liu, C., Kelnar, K., Liu, B., Chen, X., Calhoun-Davis, T., Li, H., Patrawala, L., Yan, H., Jeter, C., Honorio, S., et al. (2011). The microRNA miR-34a inhibits prostate cancer stem cells and metastasis by directly repressing CD44. Nat. Med. *17*, 211–215.

Londos, C., Cooper, D.M., and Wolff, J. (1980). Subclasses of external adenosine receptors. Proc. Natl. Acad. Sci. USA *77*, 2551–2554.

Lorant, D.E., Patel, K.D., McIntyre, T.M., McEver, R.P., Prescott, S.M., and Zimmerman, G.A. (1991). Coexpression of GMP-140 and PAF by endothelium stimulated by histamine or thrombin: a juxtacrine system for adhesion and activation of neutrophils. J. Cell Biol. *115*, 223–234.

Lustig, K.D., Shiau, A.K., Brake, A.J., and Julius, D. (1993). Expression cloning of an ATP receptor from mouse neuroblastoma cells. Proc. Natl. Acad. Sci. USA *90*, 5113–5117.

Luteijn, R.D., Zaver, S.A., Gowen, B.G., Wyman, S.K., Garelis, N.E., Onia, L., McWhirter, S.M., Katibah, G.E., Corn, J.E., Woodward, J.J., et al. (2019). SLC19A1 transports immunoreactive cyclic dinucleotides. Nature *573*, 434–438.

Mackinnon, A.L., and Taunton, J. (2009). Target Identification by Diazirine Photo-Cross-linking and Click Chemistry. Curr Protoc Chem Biol *1*, 55–73.

Mahajan, S., Manetsch, R., Merkler, D.J., and Stevens, S.M. (2015). Synthesis and evaluation of a novel adenosine-ribose probe for global-scale profiling of nucleoside and nucleotide-binding proteins. PLoS One *10*, e0115644.

Maliszewski, C.R., Delespesse, G.J., Schoenborn, M.A., Armitage, R.J., Fanslow, W.C., Nakajima, T., Baker, E., Sutherland, G.R., Poindexter, K., and Birks, C. (1994). The CD39 lymphoid cell activation antigen. Molecular cloning and structural characterization. J. Immunol. *153*, 3574–3583.

Manning, G., Whyte, D.B., Martinez, R., Hunter, T., and Sudarsanam, S. (2002). The protein kinase complement of the human genome. Science *298*, 1912–1934.

Marrelli, S.P. (2001). Mechanisms of endothelial P2Y(1)- and P2Y(2)-mediated vasodilatation involve differential [Ca2+]i responses. Am. J. Physiol. Heart Circ. Physiol. *281*, H1759-66.

Matsumoto, T., Nakane, T., and Chiba, S. (1997). UTP induces vascular responses in the isolated and perfused canine epicardial coronary artery via UTP-

preferring P2Y receptors. Br. J. Pharmacol. *122*, 1625–1632.

McAllister, F.E., Niepel, M., Haas, W., Huttlin, E., Sorger, P.K., and Gygi, S.P. (2013). Mass spectrometry based method to increase throughput for kinome analyses using ATP probes. Anal. Chem. *85*, 4666–4674.

Mellacheruvu, D., Wright, Z., Couzens, A.L., Lambert, J.-P., St-Denis, N.A., Li, T., Miteva, Y.V., Hauri, S., Sardiu, M.E., Low, T.Y., et al. (2013). The CRAPome: a contaminant repository for affinity purification-mass spectrometry data. Nat. Methods *10*, 730–736.

Mi, H., Muruganujan, A., Ebert, D., Huang, X., and Thomas, P.D. (2019). PANTHER version 14: more genomes, a new PANTHER GO-slim and improvements in enrichment analysis tools. Nucleic Acids Res. *47*, D419–D426.

Micallef, L., and Rodgers, P. (2014). eulerAPE: drawing area-proportional 3-Venn diagrams using ellipses. PLoS One *9*, e101717.

Moncada, S., Gryglewski, R., Bunting, S., and Vane, J.R. (1976). An enzyme isolated from arteries transforms prostaglandin endoperoxides to an unstable substance that inhibits platelet aggregation. Nature *263*, 663–665.

Mori, H., Tomari, T., Koshikawa, N., Kajita, M., Itoh, Y., Sato, H., Tojo, H., Yana, I., and Seiki, M. (2002). CD44 directs membrane-type 1 matrix metalloproteinase to lamellipodia by associating with its hemopexin-like domain. EMBO J. *21*, 3949–3959.

Mulero, J.J., Yeung, G., Nelken, S.T., and Ford, J.E. (1999). CD39-L4 is a secreted human apyrase, specific for the hydrolysis of nucleoside diphosphates. J. Biol. Chem. *274*, 20064–20067.

Müller, T., Robaye, B., Vieira, R.P., Ferrari, D., Grimm, M., Jakob, T., Martin, S.F., Di Virgilio, F., Boeynaems, J.M., Virchow, J.C., et al. (2010). The purinergic receptor P2Y2 receptor mediates chemotaxis of dendritic cells and eosinophils in allergic lung inflammation. Allergy *65*, 1545–1553.

Nasevicius, A., and Ekker, S.C. (2000). Effective targeted gene “knockdown” in zebrafish. Nat. Genet. *26*, 216–220.

Needham, L., Cusack, N.J., Pearson, J.D., and Gordon, J.L. (1987). Characteristics of the P2 purinoceptor that mediates prostacyclin production by pig aortic endothelial cells. Eur. J. Pharmacol. *134*, 199–209.

Niethammer, P., Grabher, C., Look, A.T., and Mitchison, T.J. (2009). A tissue-scale gradient of hydrogen peroxide mediates rapid wound detection in zebrafish. Nature *459*, 996–999.

Niphakis, M.J., Lum, K.M., Cognetta, A.B., Correia, B.E., Ichu, T.-A., Olucha, J., Brown, S.J., Kundu, S., Piscitelli, F., Rosen, H., et al. (2015). A Global Map of Lipid-Binding Proteins and Their Ligandability in Cells. Cell *161*, 1668–1680.

de Nucci, G., Gryglewski, R.J., Warner, T.D., and Vane, J.R. (1988). Receptor-mediated release of endothelium-derived relaxing factor and prostacyclin from bovine aortic endothelial cells is coupled. Proc. Natl. Acad. Sci. USA *85*, 2334–2338.

Nüsselein-Volhard, C., and Dahm, R. (2002). Zebrafish: A Practical Approach (Oxford University Press).

Oates, J.A., FitzGerald, G.A., Branch, R.A., Jackson, E.K., Knapp, H.R., and Roberts, L.J. (1988). Clinical implications of prostaglandin and thromboxane A2 formation (2). N. Engl. J. Med. *319*, 761–767.

Olanrewaju, H.A., and Mustafa, S.J. (2000). Adenosine A2A and A2B receptors mediated nitric oxide production in coronary artery endothelial cells. General Pharmacology: The Vascular System *35*, 171–177.

Ong, S.-E., Blagoev, B., Kratchmarova, I., Kristensen, D.B., Steen, H., Pandey, A., and Mann, M. (2002). Stable isotope labeling by amino acids in cell culture, SILAC, as a simple and accurate approach to expression proteomics. Mol. Cell Proteomics *1*, 376–386.

Orriss, I.R., Knight, G.E., Utting, J.C., Taylor, S.E.B., Burnstock, G., and Arnett, T.R. (2009). Hypoxia stimulates vesicular ATP release from rat osteoblasts. J. Cell Physiol. *220*, 155–162.

Orriss, I.R., Key, M.L., Hajjawi, M.O.R., and Arnett, T.R. (2013). Extracellular ATP released by osteoblasts is a key local inhibitor of bone mineralisation. PLoS One *8*, e69057.

Palmer, R.K., Boyer, J.L., Schachter, J.B., Nicholas, R.A., and Harden, T.K. (1998). Agonist action of adenosine triphosphates at the human P2Y1 receptor. Mol. Pharmacol. *54*, 1118–1123.

Parker, C.G., Kuttruff, C.A., Galmozzi, A., Jørgensen, L., Yeh, C.-H., Hermanson, D.J., Wang, Y., Artola, M., McKerrall, S.J., Josyln, C.M., et al. (2017a). Chemical proteomics identifies SLC25A20 as a functional target of the ingenol class of actinic keratosis drugs. ACS Cent. Sci. *3*, 1276–1285.

Parker, C.G., Galmozzi, A., Wang, Y., Correia, B.E., Sasaki, K., Joslyn, C.M., Kim, A.S., Cavallaro, C.L., Lawrence, R.M., Johnson, S.R., et al. (2017b). Ligand and Target Discovery by Fragment-Based Screening in Human Cells. Cell *168*, 527–541.e29.

Patricelli, M.P., Szardenings, A.K., Liyanage, M., Nomanbhoy, T.K., Wu, M., Weissig, H., Aban, A., Chun, D., Tanner, S., and Kozarich, J.W. (2007). Functional interrogation of the kinome using nucleotide acyl phosphates. Biochemistry *46*, 350–358.

Patricelli, M.P., Nomanbhoy, T.K., Wu, J., Brown, H., Zhou, D., Zhang, J., Jagannathan, S., Aban, A., Okerberg, E., Herring, C., et al. (2011). In situ kinase profiling reveals functionally relevant properties of native kinases. Chem. Biol. *18*, 699–710.

Peng, J., and Gygi, S.P. (2001). Proteomics: the move to mixtures. J Mass Spectrom *36*, 1083–1091.

Pober, J.S., and Cotran, R.S. (1990). The role of endothelial cells in inflammation. Transplantation *50*, 537–544.

Pober, J.S., and Sessa, W.C. (2007). Evolving functions of endothelial cells in

inflammation. Nat. Rev. Immunol. *7*, 803–815.

Pober, J.S., and Sessa, W.C. (2014). Inflammation and the blood microvascular system. Cold Spring Harb. Perspect. Biol. *7*, a016345.

Pochynyuk, O., Bugaj, V., Rieg, T., Insel, P.A., Mironova, E., Vallon, V., and Stockand, J.D. (2008). Paracrine regulation of the epithelial Na+ channel in the mammalian collecting duct by purinergic P2Y2 receptor tone. J. Biol. Chem. *283*, 36599–36607.

Praetorius, H.A., and Leipziger, J. (2009). ATP release from non-excitable cells. Purinergic Signal *5*, 433–446.

Pusch, M. (2002). Myotonia caused by mutations in the muscle chloride channel gene CLCN1. Hum. Mutat. *19*, 423–434.

Qi, A.D., Zambon, A.C., Insel, P.A., and Nicholas, R.A. (2001). An arginine/glutamine difference at the juxtaposition of transmembrane domain 6 and the third extracellular loop contributes to the markedly different nucleotide selectivities of human and canine P2Y11 receptors. Mol. Pharmacol. *60*, 1375–1382.

Ralevic, V., and Burnstock, G. (1998). Receptors for purines and pyrimidines. Pharmacol. Rev. *50*, 413–492.

Ramakrishnan, C., Dani, V.S., and Ramasarma, T. (2002). A conformational analysis of Walker motif A [GXXXXGKT (S)] in nucleotide-binding and other proteins. Protein Engineering Design and Selection *15*, 783–798.

Ratchford, A.M., Baker, O.J., Camden, J.M., Rikka, S., Petris, M.J., Seye, C.I., Erb, L., and Weisman, G.A. (2010). P2Y2 nucleotide receptors mediate metalloprotease-dependent phosphorylation of epidermal growth factor receptor and ErbB3 in human salivary gland cells. J. Biol. Chem. *285*, 7545–7555.

Razzell, W., Evans, I.R., Martin, P., and Wood, W. (2013). Calcium flashes orchestrate the wound inflammatory response through DUOX activation and hydrogen peroxide release. Curr. Biol. *23*, 424–429.

Reischauer, S., Levesque, M.P., Nüsslein-Volhard, C., and Sonawane, M. (2009). Lgl2 executes its function as a tumor suppressor by regulating ErbB signaling in the zebrafish epidermis. PLoS Genet. *5*, e1000720.

Renshaw, S.A., Loynes, C.A., Trushell, D.M.I., Elworthy, S., Ingham, P.W., and Whyte, M.K.B. (2006). A transgenic zebrafish model of neutrophilic inflammation. Blood *108*, 3976–3978.

Ritchie, C., Cordova, A.F., Hess, G.T., Bassik, M.C., and Li, L. (2019). SLC19A1 Is an Importer of the Immunotransmitter cGAMP. Mol. Cell *75*, 372–381.e5.

Rosemberg, D.B., Rico, E.P., Langoni, A.S., Spinelli, J.T., Pereira, T.C., Dias, R.D., Souza, D.O., Bonan, C.D., and Bogo, M.R. (2010). NTPDase family in zebrafish: Nucleotide hydrolysis, molecular identification and gene expression profiles in brain, liver and heart. Comp Biochem Physiol B, Biochem Mol Biol *155*, 230–240.

Roskoski, R. (2019). Properties of FDA-approved small molecule protein kinase inhibitors. Pharmacol. Res. *144*, 19–50.

Rubin, L.J., Groves, B.M., Reeves, J.T., Frosolono, M., Handel, F., and Cato, A.E. (1982). Prostacyclin-induced acute pulmonary vasodilation in primary pulmonary hypertension. Circulation *66*, 334–338.

Russwurm, M., and Koesling, D. (2004). NO activation of guanylyl cyclase. EMBO J. *23*, 4443–4450.

Sabirov, R.Z., Dutta, A.K., and Okada, Y. (2001). Volume-dependent ATP-conductive large-conductance anion channel as a pathway for swelling-induced ATP release. J. Gen. Physiol. *118*, 251–266.

Sáez, P.J., Vargas, P., Shoji, K.F., Harcha, P.A., Lennon-Duménil, A.-M., and Sáez, J.C. (2017). ATP promotes the fast migration of dendritic cells through the activity of pannexin 1 channels and P2X7 receptors. Sci. Signal. *10*.

Sathe, M.N., Woo, K., Kresge, C., Bugde, A., Luby-Phelps, K., Lewis, M.A., and Feranchak, A.P. (2011). Regulation of purinergic signaling in biliary epithelial cells by exocytosis of SLC17A9-dependent ATP-enriched vesicles. J. Biol. Chem. *286*, 25363–25376.

Schier, A.F. (2013). Genomics: Zebrafish earns its stripes. Nature *496*, 443–444.

Schindelin, J., Arganda-Carreras, I., Frise, E., Kaynig, V., Longair, M., Pietzsch, T., Preibisch, S., Rueden, C., Saalfeld, S., Schmid, B., et al. (2012). Fiji: an open-source platform for biological-image analysis. Nat. Methods *9*, 676–682.

Schwiebert, E.M., and Zsembery, A. (2003). Extracellular ATP as a signaling molecule for epithelial cells. Biochimica et Biophysica Acta (BBA) - Biomembranes *1615*, 7–32.

Scott, J.W., Hawley, S.A., Green, K.A., Anis, M., Stewart, G., Scullion, G.A., Norman, D.G., and Hardie, D.G. (2004). CBS domains form energy-sensing modules whose binding of adenosine ligands is disrupted by disease mutations. J. Clin. Invest. *113*, 274–284.

Sessa, W.C. (2004). eNOS at a glance. J. Cell Sci. *117*, 2427–2429.

Shah, K., Liu, Y., Deirmengian, C., and Shokat, K.M. (1997). Engineering unnatural nucleotide specificity for Rous sarcoma virus tyrosine kinase to uniquely label its direct substrates. Proc. Natl. Acad. Sci. USA *94*, 3565–3570.

Sham, D., Wesley, U.V., Hristova, M., and van der Vliet, A. (2013). ATP-mediated transactivation of the epidermal growth factor receptor in airway epithelial cells involves DUOX1-dependent oxidation of Src and ADAM17. PLoS One *8*, e54391.

Shen, J., Seye, C.I., Wang, M., Weisman, G.A., Wilden, P.A., and Sturek, M. (2004). Cloning, up-regulation, and mitogenic role of porcine P2Y2 receptor in coronary artery smooth muscle cells. Mol. Pharmacol. *66*, 1265–1274.

Shevchenko, A., Wilm, M., Vorm, O., and Mann, M. (1996). Mass Spectrometric Sequencing of Proteins from Silver-Stained Polyacrylamide Gels. Anal. Chem. *68*, 850–858.

Shi, H., Cheng, X., Sze, S.K., and Yao, S.Q. (2011). Proteome profiling reveals potential cellular targets of staurosporine using a clickable cell-permeable probe. Chem. Commun. *47*, 11306–11308.

Shi, H., Zhang, C.-J., Chen, G.Y.J., and Yao, S.Q. (2012). Cell-based proteome profiling of potential dasatinib targets by use of affinity-based probes. J. Am. Chem. Soc. *134*, 3001–3014.

Smits, P., Williams, S.B., Lipson, D.E., Banitt, P., Rongen, G.A., and Creager, M.A. (1995). Endothelial release of nitric oxide contributes to the vasodilator effect of adenosine in humans. Circulation *92*, 2135–2141.

Speers, A.E., and Wu, C.C. (2007). Proteomics of integral membrane proteins--theory and application. Chem. Rev. *107*, 3687–3714.

Stadelmann, W.K., Digenis, A.G., and Tobin, G.R. (1998). Physiology and healing dynamics of chronic cutaneous wounds. Am. J. Surg. *176*, 26S–38S.

Stoddard, M., Huang, C., Enyedi, B., and Niethammer, P. (2019). Live imaging of leukocyte recruitment in a zebrafish model of chemical liver injury. Sci. Rep. *9*, 28.

Stoletov, K., Fang, L., Choi, S.-H., Hartvigsen, K., Hansen, L.F., Hall, C., Pattison, J., Juliano, J., Miller, E.R., Almazan, F., et al. (2009). Vascular lipid accumulation, lipoprotein oxidation, and macrophage lipid uptake in hypercholesterolemic zebrafish. Circ. Res. *104*, 952–960.

Stöter, M., Bamberger, A.-M., Aslan, B., Kurth, M., Speidel, D., Löning, T., Frank, H.-G., Kaufmann, P., Löhler, J., Henne-Bruns, D., et al. (2005). Inhibition of casein kinase I delta alters mitotic spindle formation and induces apoptosis in trophoblast cells. Oncogene *24*, 7964–7975.

Su, Y., Ge, J., Zhu, B., Zheng, Y.-G., Zhu, Q., and Yao, S.Q. (2013). Target identification of biologically active small molecules via in situ methods. Curr. Opin. Chem. Biol. *17*, 768–775.

Suda, T., Takahashi, T., Golstein, P., and Nagata, S. (1993). Molecular cloning and expression of the Fas ligand, a novel member of the tumor necrosis factor family. Cell *75*, 1169–1178.

Surprenant, A., and North, R.A. (2009). Signaling at purinergic P2X receptors. Annu. Rev. Physiol. *71*, 333–359.

Takada, H., Furuya, K., and Sokabe, M. (2014). Mechanosensitive ATP release from hemichannels and Ca^{2+} influx through TRPC6 accelerate wound closure in keratinocytes. J. Cell Sci. *127*, 4159–4171.

Taylor, S.S., and Kornev, A.P. (2011). Protein kinases: evolution of dynamic regulatory proteins. Trends Biochem. Sci. *36*, 65–77.

Taylor, S.S., Knighton, D.R., Zheng, J., Ten Eyck, L.F., and Sowadski, J.M. (1992). Structural framework for the protein kinase family. Annu. Rev. Cell Biol. *8*, 429–462.

Tejada-Jiménez, M., Galván, A., and Fernández, E. (2011). Algae and humans share a molybdate transporter. Proc. Natl. Acad. Sci. USA *108*, 6420–6425.

The Gene Ontology Consortium (2019). The Gene Ontology Resource: 20 years and still GOing strong. Nucleic Acids Res. *47*, D330–D338.

Traut, T.W. (1994). Physiological concentrations of purines and pyrimidines. Mol. Cell. Biochem. *140*, 1–22.

Trayer, I.P., Trayer, H.R., Small, D.P., and Bottomley, R.C. (1974). Preparation of adenosine nucleotide derivatives suitable for affinity chromatography. Biochem. J. *139*, 609–623.

Trede, N.S., Langenau, D.M., Traver, D., Look, A.T., and Zon, L.I. (2004). The use of zebrafish to understand immunity. Immunity *20*, 367–379.

Valera, S., Hussy, N., Evans, R.J., Adami, N., North, R.A., Surprenant, A., and Buell, G. (1994). A new class of ligand-gated ion channel defined by P2x receptor for extracellular ATP. Nature *371*, 516–519.

Villamor, J.G., Kaschani, F., Colby, T., Oeljeklaus, J., Zhao, D., Kaiser, M., Patricelli, M.P., and van der Hoorn, R.A.L. (2013). Profiling protein kinases and other ATP binding proteins in Arabidopsis using Acyl-ATP probes. Mol. Cell Proteomics *12*, 2481–2496.

Vit, O., and Petrak, J. (2017). Integral membrane proteins in proteomics. How to break open the black box? J. Proteomics *153*, 8–20.

Walker, J.E., Saraste, M., Runswick, M.J., and Gay, N.J. (1982). Distantly related sequences in the alpha- and beta-subunits of ATP synthase, myosin, kinases and other ATP-requiring enzymes and a common nucleotide binding fold. EMBO J. *1*, 945–951.

Walldén, K., Stenmark, P., Nyman, T., Flodin, S., Gräslund, S., Loppnau, P., Bianchi, V., and Nordlund, P. (2007). Crystal structure of human cytosolic 5'-nucleotidase II: insights into allosteric regulation and substrate recognition. J. Biol. Chem. *282*, 17828–17836.

Wang, Y., Dix, M.M., Bianco, G., Remsberg, J.R., Lee, H.-Y., Kalocsay, M., Gygi, S.P., Forli, S., Vite, G., Lawrence, R.M., et al. (2019). Expedited mapping of the ligandable proteome using fully functionalized enantiomeric probe pairs. Nat. Chem. *11*, 1113–1123.

Webb, T.E., Simon, J., Krishek, B.J., Bateson, A.N., Smart, T.G., King, B.F., Burnstock, G., and Barnard, E.A. (1993). Cloning and functional expression of a brain G-protein-coupled ATP receptor. FEBS Lett. *324*, 219–225.

Weber, G.F., Ashkar, S., Glimcher, M.J., and Cantor, H. (1996). Receptor-ligand interaction between CD44 and osteopontin (Eta-1). Science *271*, 509–512.

Weinger, I., Klepeis, V.E., and Trinkaus-Randall, V. (2005). Tri-nucleotide receptors play a critical role in epithelial cell wound repair. Purinergic Signal *1*, 281–292.

Wesley, U.V., Bove, P.F., Hristova, M., McCarthy, S., and van der Vliet, A. (2007). Airway epithelial cell migration and wound repair by ATP-mediated activation of dual oxidase 1. J. Biol. Chem. *282*, 3213–3220.

Westcott, E.B., and Segal, S.S. (2013). Perivascular innervation: a multiplicity of roles in vasomotor control and myoendothelial signaling. Microcirculation *20*, 217–238.

White, P.J., Webb, T.E., and Boarder, M.R. (2003). Characterization of a Ca2+ response to both UTP and ATP at human P2Y11 receptors: evidence for agonist-specific signaling. Mol. Pharmacol. *63*, 1356–1363.

White, R.M., Sessa, A., Burke, C., Bowman, T., LeBlanc, J., Ceol, C., Bourque, C., Dovey, M., Goessling, W., Burns, C.E., et al. (2008). Transparent adult zebrafish as a tool for in vivo transplantation analysis. Cell Stem Cell *2*, 183–189.

Willett, C.E., Cortes, A., Zuasti, A., and Zapata, A.G. (1999). Early hematopoiesis and developing lymphoid organs in the zebrafish. Dev. Dyn. *214*, 323–336.

Wiśniewski, J.R., Zougman, A., and Mann, M. (2009). Combination of FASP and StageTip-based fractionation allows in-depth analysis of the hippocampal membrane proteome. J. Proteome Res. *8*, 5674–5678.

Wittmann, C., Reischl, M., Shah, A.H., Kronfuss, E., Mikut, R., Liebel, U., and Grabher, C. (2015). A Zebrafish Drug-Repurposing Screen Reveals sGC-Dependent and sGC-Independent Pro-Inflammatory Activities of Nitric Oxide. PLoS One *10*, e0137286.

Wolfe, L.M., Veeraraghavan, U., Idicula-Thomas, S., Schürer, S., Wennerberg, K., Reynolds, R., Besra, G.S., and Dobos, K.M. (2013). A chemical proteomics approach to profiling the ATP-binding proteome of Mycobacterium tuberculosis. Mol. Cell Proteomics *12*, 1644–1660.

Wu, R.S., Lam, I.I., Clay, H., Duong, D.N., Deo, R.C., and Coughlin, S.R. (2018). A rapid method for directed gene knockout for screening in G0 zebrafish. Dev. Cell *46*, 112–125.e4.

Xiao, Y., Guo, L., Jiang, X., and Wang, Y. (2013a). Proteome-wide discovery and characterizations of nucleotide-binding proteins with affinity-labeled chemical probes. Anal. Chem. *85*, 3198–3206.

Xiao, Y., Guo, L., and Wang, Y. (2013b). Isotope-coded ATP probe for quantitative affinity profiling of ATP-binding proteins. Anal. Chem. *85*, 7478–7486.

Yang, J., Wang, L., Yang, F., Luo, H., Xu, L., Lu, J., Zeng, S., and Zhang, Z. (2013). mBeRFP, an improved large stokes shift red fluorescent protein. PLoS One *8*, e64849.

Yao, J., and Bajjalieh, S.M. (2008). Synaptic vesicle protein 2 binds adenine nucleotides. J. Biol. Chem. *283*, 20628–20634.

Yao, J., and Bajjalieh, S.M. (2009). SVOP is a nucleotide binding protein. PLoS One *4*, e5315.

Yegutkin, G.G. (2008). Nucleotide- and nucleoside-converting ectoenzymes: Important modulators of purinergic signalling cascade. Biochim. Biophys. Acta *1783*, 673–694.

Yin, J., Xu, K., Zhang, J., Kumar, A., and Yu, F.-S.X. (2007). Wound-induced ATP

release and EGF receptor activation in epithelial cells. J. Cell Sci. *120*, 815–825.

Yoo, S.K., Freisinger, C.M., LeBert, D.C., and Huttenlocher, A. (2012). Early redox, Src family kinase, and calcium signaling integrate wound responses and tissue regeneration in zebrafish. J. Cell Biol. *199*, 225–234.

Yu, D.-J., Hu, J., Huang, Y., Shen, H.-B., Qi, Y., Tang, Z.-M., and Yang, J.-Y. (2013). TargetATPsite: a template-free method for ATP-binding sites prediction with residue evolution image sparse representation and classifier ensemble. J. Comput. Chem. *34*, 974–985.

Zhang, D., Gao, Z.-G., Zhang, K., Kiselev, E., Crane, S., Wang, J., Paoletta, S., Yi, C., Ma, L., Zhang, W., et al. (2015). Two disparate ligand-binding sites in the human P2Y1 receptor. Nature *520*, 317–321.

Zhang, K., Zhang, J., Gao, Z.-G., Zhang, D., Zhu, L., Han, G.W., Moss, S.M., Paoletta, S., Kiselev, E., Lu, W., et al. (2014). Structure of the human P2Y12 receptor in complex with an antithrombotic drug. Nature *509*, 115–118.

Zhang, R., Evans, G., Rotella, F.J., Westbrook, E.M., Beno, D., Huberman, E., Joachimiak, A., and Collart, F.R. (1999). Characteristics and crystal structure of bacterial inosine-5'-monophosphate dehydrogenase. Biochemistry *38*, 4691–4700.

Zhao, Y., Zhang, W., Kho, Y., and Zhao, Y. (2004). Proteomic analysis of integral plasma membrane proteins. Anal. Chem. *76*, 1817–1823.

Zhao, Y., Vanhoutte, P.M., and Leung, S.W.S. (2015). Vascular nitric oxide: Beyond eNOS. J Pharmacol Sci *129*, 83–94.

Zheng, J., Knighton, D.R., ten Eyck, L.F., Karlsson, R., Xuong, N., Taylor, S.S., and Sowadski, J.M. (1993). Crystal structure of the catalytic subunit of cAMP-dependent protein kinase complexed with MgATP and peptide inhibitor. Biochemistry *32*, 2154–2161.

Zhou, Z., Wang, X., Li, M., Sohma, Y., Zou, X., and Hwang, T.-C. (2005). High affinity ATP/ADP analogues as new tools for studying CFTR gating. J. Physiol. (Lond.) *569*, 447–457.

Zimmermann, H., Zebisch, M., and Sträter, N. (2012). Cellular function and molecular structure of ecto-nucleotidases. Purinergic Signal *8*, 437–502.

Zon, L.I., and Peterson, R.T. (2005). In vivo drug discovery in the zebrafish. Nat. Rev. Drug Discov. *4*, 35–44.